

Department of Experimental Pharmacology and Toxicology

Center for Experimental Medicine

University Medical Center Hamburg-Eppendorf

**Modeling of hypertrophic cardiomyopathy and assessment  
of gene therapy in human iPSC-derived cardiomyocytes**

**Cumulative dissertation**

with the aim of achieving the degree

Doctor of Natural Sciences

submitted to the Faculty of Biology, Mathematics, Informatics and Natural Sciences

University of Hamburg

by

Kamill Maksymilian Prondzynski

Hamburg 2017

1. Gutachterin: Prof. Dr. Lucie Carrier
  2. Gutachter: Prof. Dr. Thomas Dobner
- Disputation: 13.07.2018

Diese Doktorarbeit wurde von Januar 2015 bis Dezember 2017 am Institut für Experimentelle Pharmakologie und Toxikologie (Institutsdirektor: Prof. Dr. Thomas Eschenhagen) unter der Leitung von Prof. Dr. Lucie Carrier erarbeitet.

# Table of Contents

Prologue .....	6
1. Introduction .....	8
1.1 Hypertrophic cardiomyopathy (HCM) .....	8
1.1.1 The cardiac sarcomere .....	11
1.1.2 Cardiac myosin-binding protein C.....	14
1.1.3 $\alpha$ -Actinin 2 .....	16
1.1.4 Treatment of HCM .....	19
1.2 Human induced pluripotent stem cells .....	23
1.2.1 Disease modeling .....	26
1.3 Aim of this thesis .....	32
2. Material and methods .....	33
2.1 Material .....	33
2.1.1 Generation and analysis of a patient-specific hiPSC carrying a novel <i>ACTN2</i> mutation.....	33
2.2 Methods .....	33
2.2.1 Generation of an isogenic control cell line with CRISPR/Cas9 technology.....	33
2.2.2 Genotyping and off-target analysis using polymerase chain reaction.....	35
2.2.3 Sequencing of DNA .....	36
2.2.4 Analysis of contractile force in EHTs .....	36
3. Results.....	38
3.1 Evaluation of <i>MYBPC3</i> <i>trans</i> -splicing and gene replacement as therapeutic options in human iPSC-derived cardiomyocytes.....	38
3.2 Differentiation of cardiomyocytes and generation of human engineered heart tissue.....	60
3.3 Modeling of a novel <i>ACTN2</i> mutation (c.740C>T; p.Thr247Met) in hiPSC-CMs using an isogenic control cell line.....	84
3.3.1 Novel <i>ACTN2</i> mutation causes HCM .....	84
3.3.2 Generation of an isogenic control cell line using CRISPR/Cas9.....	84

3.3.3 HCM hiPSC-CMs exhibit hypertrophy in 2D .....	86
3.3.4 HCM EHTs exhibit hypercontractility and prolonged relaxation time .....	88
4. Discussion .....	90
4.1 hiPSC-CMs as a suitable tool for modeling of HCM.....	91
4.1.2 hiPSC-CMs as a suitable tool for evaluation of treatment options in HCM98	
4.1.3 Limitations of hiPSC-CMs for disease modeling.....	104
4.2 Implications for modeling <i>ACTN2</i> mutations associated with HCM.....	107
5. Conclusion.....	110
6. Bibliographie.....	111
7. Appendix.....	124
7.1 Materials .....	124
7.1.1 Antibodies.....	124
7.1.2 Bacterial strains .....	124
7.1.3 Chemicals.....	124
7.1.4 Consumable materials.....	124
7.1.5 Kits .....	124
7.1.6 Laboratory equipment.....	125
7.1.7 Enzymes.....	125
7.1.8 Oligonucleotides .....	125
7.2 List of abbreviations .....	127
Abstract .....	129
Zusammenfassung .....	130
Acknowledgments .....	131
English language certification .....	133
Authorship contribution .....	134
Eidesstattliche Erklärung .....	136

## Prologue

Science is a journey.

Just in the past decade major scientific discoveries were made based on journeys other scientists started or followed on. 100 years ago Albert Einstein predicted the existence of gravitational waves and in 2016 they have been detected (Einstein, 1916; Abbott et al., 2016). In the 1970's the standard model for particles was developed, which was proven by the detection of the Higgs Boson in 2013 (Atlas Collaboration, 2012). Those two discoveries proof that we know much more about natural forces on the cosmological scale and on the scale of particles then 300,000 years ago. This is the age that was estimated for the oldest known *Homo sapiens* fossil found 1961 in Morocco (Hublin et al., 2017). Of course we would not know about the evolution of humans nor the development of life-forms, as we understand them, without Charles Darwin (Darwin, 1872). Since then we try to uncover more and more about the domains of life, which seem sometimes as unknown and inaccessible as deep space and particle physics. But humans are inventive and produce tools that help them access this world. One of those journeys started with Antoni van Leeuwenhoek, who developed the first microscopes and is considered as one of the discoverers of microorganisms (Gest, 2004). Starting with his very rudimentary microscopes it is now possible to visualize biological components in cells with nanoscale resolution (Rust et al., 2006; Willig et al., 2007). Still, van Leeuwenhoek was one of the first persons, who saw what the smallest living units in our world were made of: Cells.

It took a few centuries until it was understood how cellular life is encoded. Watson and Crick predicted the DNA double Helix in 1953 and therewith the universal code that unifies all living things in our known world (Watson & Crick, 1953). Since then we try to solve the mysteries of DNA. We learned to read and write it (Sanger et al., 1975; Mullis & Faloona, 1987). We determined the smallest number of essential genes needed in a free-living organism, or created organisms with a complete artificial genome (Fraser et al., 1995; Gibson et al., 2010). We learned to reprogram cells and change their fates according to our needs (Takahashi et al., 2006; Takahashi et al., 2007). Now we have detailed protocols on how to modify single

nucleotides in the DNA and we can use those techniques to treat genetic diseases occurring in humans (Ran et al., 2013; Ma et al., 2017).

The research presented in this thesis will be in the context of the recent technological advances in cell biology, gene therapy and how those can be exploited for disease modeling of human inherited cardiomyopathies.

# 1. Introduction

## 1.1 Hypertrophic cardiomyopathy (HCM)

Hypertrophic cardiomyopathy (HCM) is a myocardial disease with a revised estimated prevalence of 1:200 in the general population that occurs equally in both sexes, yet with worse survival in women (Carrier et al., 2015; Olivotto et al., 2005; Geske et al., 2017). It is the most common Mendelian-inherited cardiomyopathy worldwide and is the main cause of sudden cardiac death (SCD) in individuals below the age of 35, particularly among young athletes (Maron, 2010; Maron et al., 1995; Ashrafian et al., 2007; Maron et al., 1996). Clinical manifestations of HCM are very variable in terms of disease development, age of onset and severity of symptoms (Richard et al., 2003). It is reported that many patients are asymptomatic with a normal life expectancy, some experience symptoms such as chest pain, vertigo, syncope and dyspnea, whereas others are in need for early heart transplantation, or die of SCD (Gersh et al., 2011; Maron et al., 2000; Richard et al., 2003; Moolman et al., 1997). This variety of clinical outcomes for HCM patients indicates that additional distinct modifiers must exist such as environmental factors and patient's life style choices. HCM is defined by hypertrophy, mainly seen in the left ventricle (LV) of the heart, chaotically-oriented cardiac myocytes, so called myocardial disarray, and interstitial fibrosis (Fig.1; Ho, 2010). HCM is diagnosed by echocardiography of the LV that enables to determine the LV wall thickness. If individuals exceed  $\geq 15$  mm in one or more segments of the LV, they are diagnosed with HCM (Gersh et al., 2011). In 70% of hospitalized HCM patients abnormal thickening of the LV leads to LV outflow obstruction, which is associated with normal systolic but impaired diastolic function (HOCM; Maron et al., 2006; Maron, 2002). If left untreated or undiagnosed disease progression can result in LV wall thinning, therefore to an enlargement of the left cavity. This is one of the main risk factors inducing irreversible heart failure and unexpected SCD (Maron et al., 2000). Furthermore, over 70% of HCM patients have electrocardiogram (ECG) abnormalities and 22% exhibit episodes of atrial fibrillation (Niimura et al., 1998; McLeod et al., 2009; Olivotto et al., 2001).



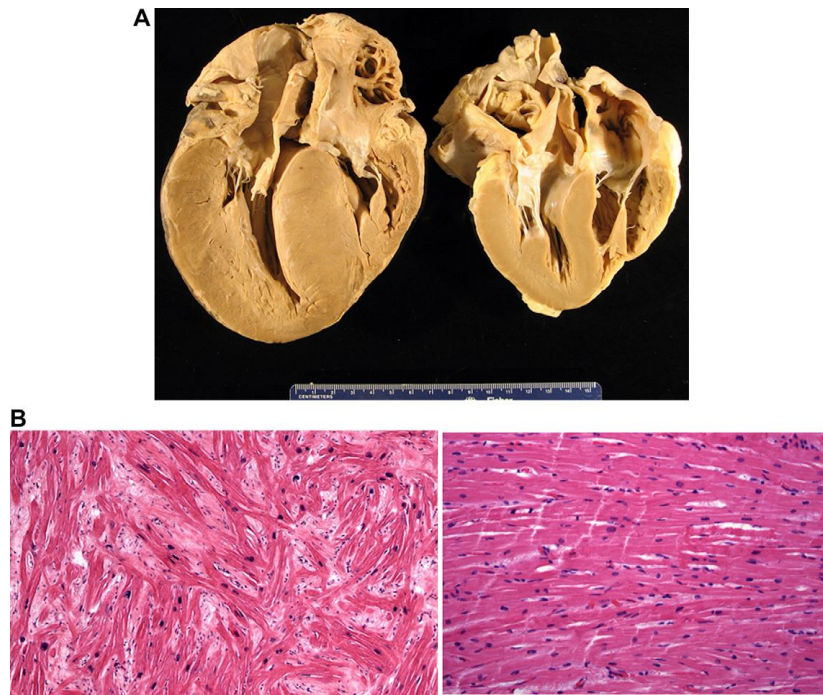


Figure 1: Pathological features of HCM. (A) Depicted are a HCM heart showing markedly increased left ventricular wall thickness (left) and a heart with normal cardiac morphology (right). (B) Histologic sections demonstrate myocyte disarray and increased myocardial fibrosis in HCM (left) when compared to a healthy heart (right). Images are at 10 x magnification (adapted from Ho, 2010).

Most cases of HCM are inherited in an autosomal-dominant pattern resulting in heterozygous mutation carriers (Richard et al., 2003). Individuals with homozygous mutations have a worse prognosis (Ho et al., 2000; Nanni et al., 2003; Wessels et al., 2015). Additionally, double and triple mutations have been reported in 3-5% of HCM patients, causing an even more severe progression of the disease (Girolami et al., 2010; Ingles et al., 2005). In the past years there have been reports on over 1,400 mutations in over 11 different genes, which have been identified as a potential cause for HCM (Fig. 2; Schlossarek et al., 2011; Friedrich et al., 2012; Maron et al., 2013). A large majority of known genes encode components of the sarcomere, which qualifies HCM as a “sarcomeropathy“. However, mutations in the *MYH7* gene, encoding cardiac  $\beta$ -myosin heavy chain ( $\beta$ -MHC) and in the *MYBPC3* gene, encoding cardiac myosin-binding protein C (cMyBP-C) account for 70% of all HCM cases (Richard et al., 2006; Maron et al., 2012). Mutations in the *MYBPC3* gene can range from a delayed onset and a mild hypertrophy to a high risk profile for SCD (Jarcho et al., 1998; Erdmann et al., 2001).

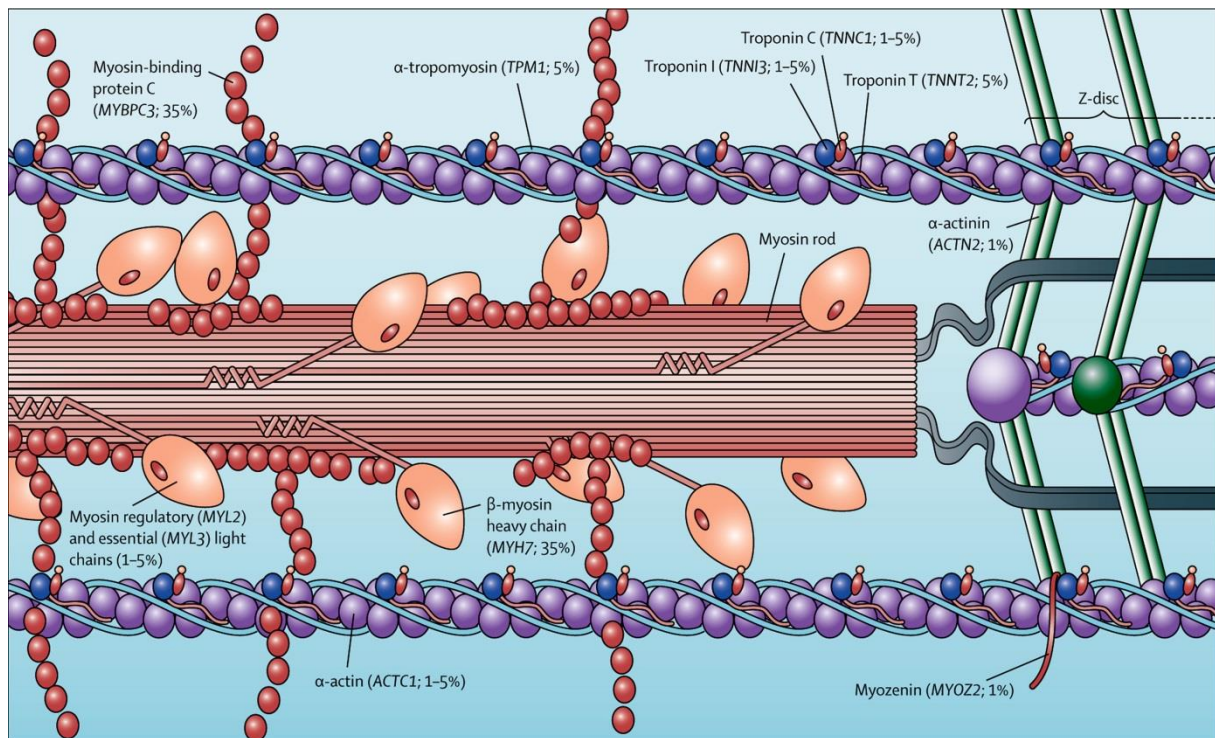


Figure 2: Location of sarcomeric genes known to cause HCM. Prevalence of every gene is shown in parentheses (data obtained from HCM patients with positive genotyping; adapted from Maron et al., 2013).

In fact, 20-30% of HCM mutation carriers do not reveal any cardiac symptoms, suggesting yet again that distinct modifiers must exist on molecular level, such as epigenetic signaling, microRNAs, gene polymorphisms or post-translational modifications (Marian, 2002; Richard et al., 2003; Richard et al., 2006; Schlossarek et al., 2011). As already stated, clinical outcomes of HCM are hard to predict mostly because pathogenic pathways leading to the disease are not fully understood. Several mechanisms have been described, such as deficits in energy homeostasis, altered calcium ( $\text{Ca}^{2+}$ ) cycling and sensitivity, disturbed stress sensing and microvascular dysfunction (Frey et al., 2012). Nevertheless, mutations in sarcomeric genes seem to trigger HCM. For this reason disturbed function of the sarcomere might be one of the key aspects in the pathological development of HCM.

### 1.1.1 The cardiac sarcomere

First observations of the sarcomere were accomplished by Antoni van Leeuwenhoek between 1674 and 1682 using his own manufactured microscopes (Martonosi, 2000). Leeuwenhoek was able to distinguish the basic organization of muscle fibers as an assembly of myofibrils that consist of myofilaments, which are further subdivided by sarcomeres, the smallest contractile units in the muscle. Based on those observations William Croone hypothesized that sarcomeres, at that time called “globules”, may serve as units of contraction. Today we know that Croone was right and over century’s scientists elucidated in detail structure and function of the sarcomere.

The sarcomere is composed of a variety of proteins, which fulfill different functions all aiming to facilitate contraction and relaxation. Two main groups of proteins are responsible for sarcomere shortening and therefore force development: thin filaments and thick filaments, mainly consisting of actin and myosin, respectively (Fig. 3).

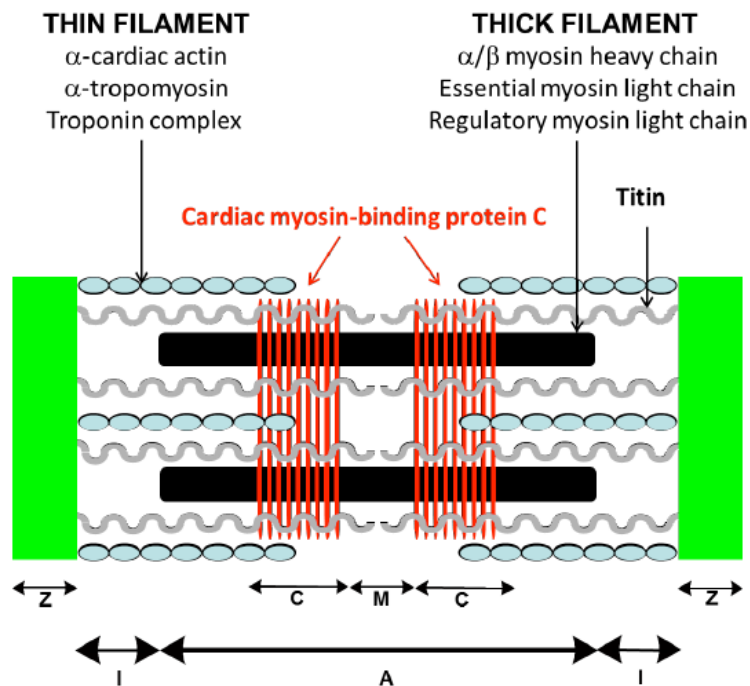


Figure 3: Organization of the cardiac sarcomere. Thin filaments are composed of  $\alpha$ -cardiac actin,  $\alpha$ -tropomyosin and the cardiac troponin complex. Thick filaments are located in the A-band and consist of myosin with  $\alpha/\beta$  myosin heavy chains, essential and regulatory myosin light chains. cMyBP-C is a thick filament-associated protein, aside titin, which itself is considered as the elastic component of the sarcomere (adapted from Schlossarek et al., 2011).

To enable proper interaction of actin and myosin additional proteins are needed. Thin filaments are further comprised of  $\alpha$ -tropomyosin and the cardiac troponin complex, including cardiac troponin T (cTnT), cardiac troponin I (cTnI) and cardiac troponin C

(cTnC), whereas cMyBP-C as a part of the thick filament. Next to the thin and thick filaments there is a third filament in the sarcomere: titin. Titin anchors the thick filament at the Z-disc, which is defined as the sarcomeric border. The distance from one Z-disc to the next represents the sarcomere length and is about 1.6  $\mu\text{m}$  in systole (i.e. contraction) and 2.4  $\mu\text{m}$  in diastole (i.e. relaxation; Sadayappan et al., 2014). Within this distance the sarcomere is organized in additional bands. Surrounding the Z-disc is the I-band followed by the A-band. The M-line and the C-zones are situated within the A-band. Actin filaments are mainly located in the I-band, extending to the A-band. Myosin is located throughout the A-band.

Interaction of actin and myosin generates cross-bridge formation and therefore cardiac contraction. The process of cross-bridge formation is controlled by two components: Adenosine triphosphate (ATP) and  $\text{Ca}^{2+}$  (Fig. 4).

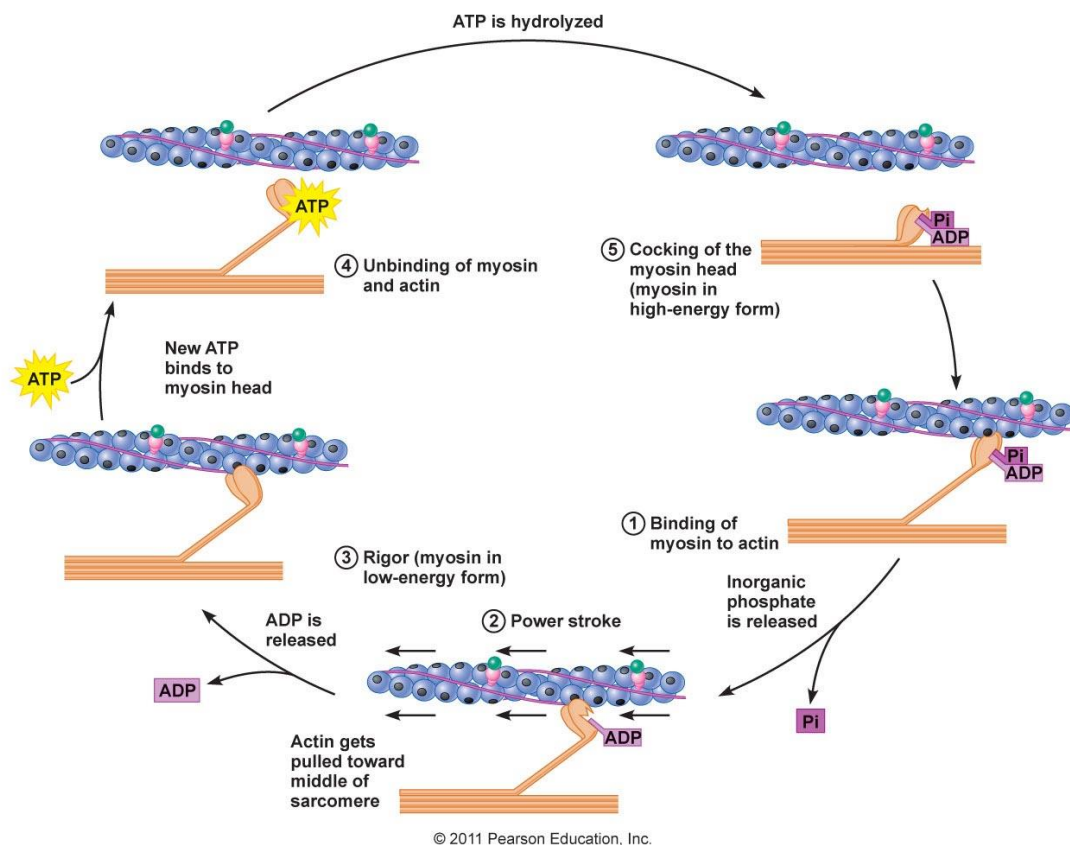


Figure 4: Mechanism of cross-bridge formation at the myofilament. Steps of contraction and relaxation are described in the figure (adapted from droualb.faculty.mjc.edu).

Each myosin is composed of two heads, which contain enzymes that are able to hydrolyze ATP, so called ATPases. Upon hydrolysis of ATP the myosin heads interact with their respective binding site on actin. Additionally, cross-bridge formation

is driven by intracellular  $\text{Ca}^{2+}$  levels in a process named excitation-contraction coupling (Fig. 5; for reviews, see Bers, 2002; Bers, 2008; Eschenhagen, 2010).

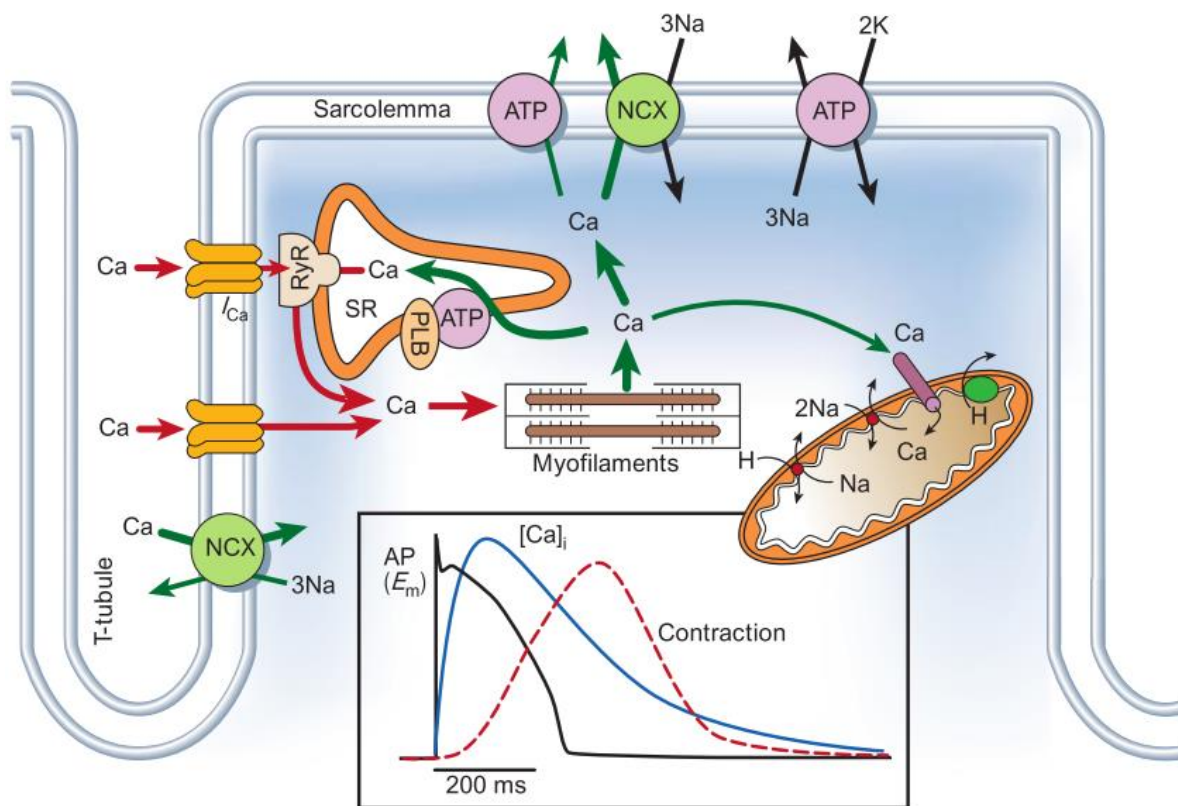


Figure 5:  $\text{Ca}^{2+}$  transport in ventricular myocytes. Red arrows depict influx of  $\text{Ca}^{2+}$  initiating contraction, green arrows depict outflux and therefore decreasing  $\text{Ca}^{2+}$  concentrations that are involved in relaxation. Inset shows the time course of a typical action-potential,  $\text{Ca}^{2+}$  transient and contraction process in a rabbit ventricular cardiomyocyte. Abbreviations used: SR, sarcoplasmic reticulum; RyR, ryanodine receptor; PLB, phospholamban; ATP, ATPase; NCX, sodium-calcium exchanger;  $E_m$ , membrane potential of the sarcolemma (adapted from Bers, 2002).

Central role in this process is the regulated in- and outflux of  $\text{Ca}^{2+}$ , triggered by action potentials (APs). Upon depolarization of the cell membrane L-type  $\text{Ca}^{2+}$  channels are being activated. This results in intracellular  $\text{Ca}^{2+}$  influx, which in turn activates the ryanodine receptors (RRs). RRs are located in the membrane of the sarcoplasmic reticulum (SR), which is the main compartment for intracellular  $\text{Ca}^{2+}$  storage. Activated RRs release  $\text{Ca}^{2+}$  from the SR leading to a further increase of intracellular  $\text{Ca}^{2+}$ .  $\text{Ca}^{2+}$  molecules bind to cTnC, which in turn increases affinity to cTnI, allowing movement of troponin and tropomyosin into the cleft of actin. This makes room for myosin to induce ATP-driven cross-bridge cycling with actin. Decreasing intracellular  $\text{Ca}^{2+}$  levels ends cross-bridge formation, as troponin and tropomyosin move back to their initial position and therefore block interaction of myosin and actin.  $\text{Ca}^{2+}$  level decrease is mediated by three factors: 1) inactivation of L-type  $\text{Ca}^{2+}$  channels and

RRs; II)  $\text{Ca}^{2+}$  transport back into the SR, mediated by the  $\text{Ca}^{2+}$ -ATPase (SERCA); III)  $\text{Ca}^{2+}$  outflux via the sodium  $\text{Ca}^{2+}$  exchanger (NCX). The interaction of cross-bridge cycling can be modulated by accessory proteins of thin and thick filaments. For example cMyBP-C function determines speed and force of cardiac contraction and assists in full relaxation of the sarcomere during diastole (Pohlmann et al., 2007). If this function is altered, it can have detrimental effects on normal heart function leading to the development of HCM.

### 1.1.2 Cardiac myosin-binding protein C

After the initial discovery of the skeletal isoforms as contaminant of myosin preparation in 1973, cMyBP-C was discovered by Murakami et al. (1976) in cardiac myosin preparations and characterized in 1983 by Yamamoto et al. (Offer et al., 1973; Murakami et al., 1976; Yamamoto et al., 1983). Characterization of the corresponding gene *MYBPC3* was reported over a decade later by locating it on human chromosome 11p11.2 in 1995 and by determining the sequence in 1997 (Gautel et al., 1995; Carrier et al., 1997). The *MYBPC3* gene consists of more than 21,000 bp, which contain 35 exons, of which 34 are coding for cMyBP-C that has a molecular weight of 150 kDa (Fig. 6). It is a multidomain protein appearing in doublets of transverse stripes approximately 43 nm apart from each other, which are located in the C-zone of the A-band (Fig. 3; Luther et al., 2008). cMyBP-C consists of eight immunoglobulin-like and three fibronectin-like domains, thus providing 11 modules building the molecule (Fig. 6). When compared to the slow and fast skeletal isoforms, cMyBP-C distinctly differs in three structural features: the N-terminal immunoglobulin-like C0 domain, the M-motif containing multiple phosphorylation sites and a 28 amino acid insertion within the C5 domain (Fig. 6; for review Carrier et al., 2015). The N-terminal region binds to actin and myosin, whereas the C-terminal region (C8-C10) serves an anchor to the thick filament (Gilbert et al., 1999; Gruen et al., 1999; Kulikovskaya et al., 2003). cMyBP-C fulfills a functional role in regulation of cross-bridge cycling between myosin and actin, myofilament  $\text{Ca}^{2+}$  sensitivity and relaxation of the sarcomere (Winegrad, 1999). Phosphorylation sites are responsible for controlling the regulatory actions of cMyBP-C (Fig. 6; Barefield et al., 2010). Over 17 putative phosphorylation sites have been identified of which the four main sites are located in the M-motif and are targets for a variety of kinases such as protein

kinase C, protein kinase A, protein kinase D and Ca<sup>2+</sup>/calmodulin-dependent protein kinase II (Kooij et al., 2013; Barefield et al., 2010). Phosphorylation of cMyBP-C increases cross-bridge cycling rate and enhances force development and relaxation, while dephosphorylation has the opposite effect (Stelzer et al., 2006; Moss et al., 2015; Sadayappan et al., 2009).

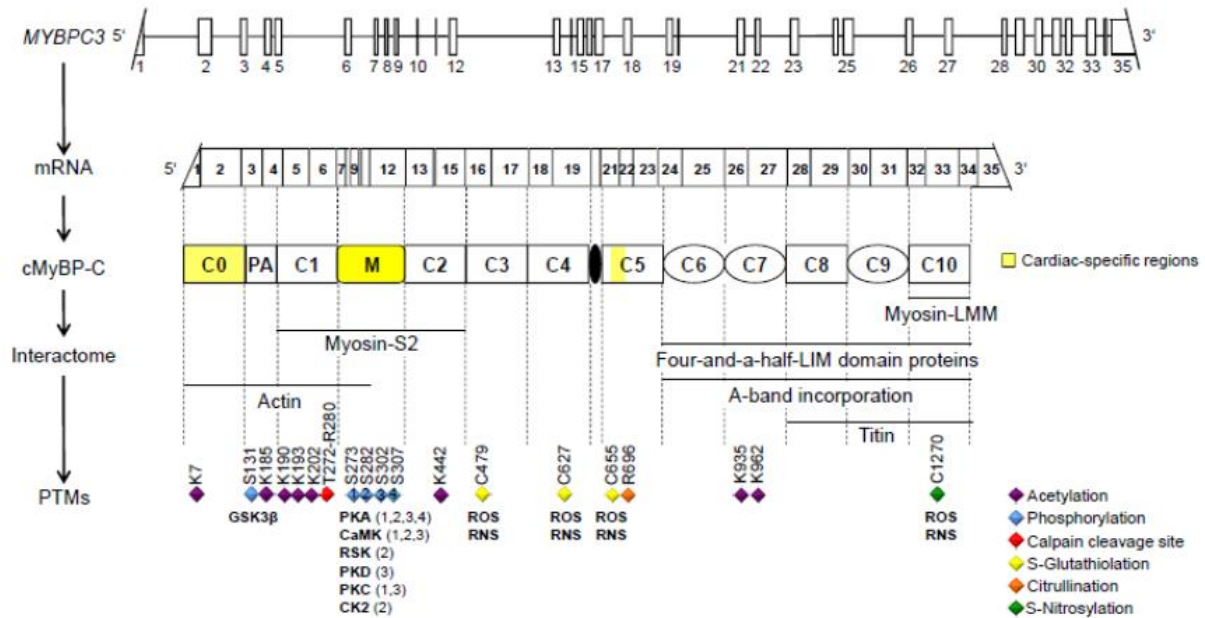


Figure 6: Representation of *MYBPC3* gene, mRNA and protein structure, its interaction partners (interactome) and sites of posttranslational modifications (PTMs). *MYBPC3* encompasses 21,000 bp and is composed of 35 exons, which is transcribed into a 3824-bp transcript. cMyBP-C is a multi-modular protein composed of 8 immunoglobulin-like (C0, C1, C2, C3, C4, C5, C8, C10) and 3 fibronectin-type III (C6, C7, C9) domains. The cardiac isoform differs from the slow-skeletal and the fast-skeletal isoforms by cardiac-specific regions (C0, M, 28-amino acid insertion in C5) that are highlighted in yellow. Between C0 and C1 exists a proline-alanine rich domain (Pro-Ala; PA). cMyBP-C is subject to a variety of PTMs, which are depicted by diamonds in different colors. Involved protein kinases are shown below the diamonds. Abbreviations used: CaMK, Ca<sup>2+</sup>/calmodulin dependent protein kinase; CK2, casein kinase 2; GSK3β, glycogen-synthase kinase isoform 3β; M, MyBP-C motif; PKA, cAMP-dependent protein kinase; PKD, protein kinase D; PKC, protein kinase C; RNS, reactive nitrogen species; ROS, reactive oxygen species; RSK, p90 ribosomal S6 kinase. Numbering of amino acids refers to the mouse sequence (adapted from Carrier et al., 2015).

It has been shown that cMyBP-C is necessary for normal cardiac function and thus cardioprotective (Sadayappan et al., 2005; Sadayappan et al., 2006). Therefore it is not surprising that *MYBPC3* mutations have detrimental effects on cardiomyocytes (CMs), leading to HCM. In 1995, mutations in the *MYBPC3* gene were associated with HCM for the first time (Bonne et al., 1995; Watkins et al., 1995). Since then over 350 distinct mutations in the *MYBPC3* gene have been linked to HCM (for review Behrens-Gawlik et al., 2014). Furthermore, *MYBPC3* gene mutations have also been associated with dilated cardiomyopathy (DCM) and left ventricular non-compaction (Hoedemaekers et al., 2010; Probst et al., 2011). As a matter of fact, mutations in the

*MYBPC3* gene are reported to be the most frequently mutated genes in cardiomyopathies and heart failure (Dhandapany et al., 2009; Haas et al., 2015). For most of the *MYBPC3* mutations the consequences at mRNA and protein levels are not known. It is predicted that more than 70% of all *MYBPC3* gene alterations are due to frameshift or nonsense mutations (Richard et al., 2006; Carrier et al., 2010; Marian, 2010). Frameshift mutations are point mutations, insertions or deletions, leading to a premature termination codon (PTC) in the transcript, therefore to a truncated cMyBP-C. Nonsense mutations are point mutations that directly result in a PTC. Interestingly, truncated forms of cMyBP-C have never been detected in myocardial samples of HCM patients (Marston et al., 2009; van Dijk et al., 2009). Probably due to control mechanisms in the cell, such as the nonsense-mediated mRNA decay, the ubiquitin-proteasome system and the autophagy-lysosomal pathway (Vignier et al., 2009; Schlossarek et al., 2011). Nevertheless, heterozygous patients with a truncating mutation in the *MYBPC3* gene exhibit 70 to 80% of the full-length cMyBP-C compared to healthy individuals, so-called haploinsufficiency (Marston et al., 2009; van Dijk et al., 2009; Marston et al., 2012). However, the reduced amount of cMyBP-C could cause an imbalance in the stoichiometry of the sarcomere components. This would lead to altered function and structure of the contractile apparatus, resulting in contractile deficits and higher myofilament  $Ca^{2+}$  sensitivity (Harris, 2002; Cazorla et al., 2006; van Dijk et al., 2009). Excessive myofilament activation is stated to result in basal cardiomyocyte hypercontractility and elevated energy consumption (Watkins et al., 2011). These conditions at the molecular level are probably the cause for the anatomical features observed in HCM, such as cardiac hypertrophy, myocardial disarray and interstitial fibrosis (Ashrafian et al., 2011).

### **1.1.3 $\alpha$ -Actinin 2**

$\alpha$ -Actinin 2 and its corresponding isoforms were mainly discovered and characterized in 1970's and 1980's, starting from the first description of  $\alpha$ -Actinin's in 1965 by Ebashi et al. (for review Blanchard et al., 1989; Ebashi et al., 1965).  $\alpha$ -Actinin 2 mainly anchors and crosslinks actin thin filaments to the Z-disk and interacts with titin (Fig. 2; Fig. 7; for review Sjöblom et al., 2008; Gautel et al., 2016). It is part of the spectrin superfamily, which consists of dystrophin, spectrin and their according



homologous and isoforms. Proteins of this family play crucial roles in assembling the actin cytoskeleton, crosslinking actin filaments, assembling large protein complexes for structural integrity, mechanosensation and cell signaling (for review Djinovic-Carugo et al., 2002; Broderick et al., 2005). The  $\alpha$ -Actinin family consists of 4 isoforms:  $\alpha$ -Actinin 1 and 4, which are expressed in non-muscle tissues and mainly associated with cytokinesis, cell adhesion and cell migration, and  $\alpha$ -Actinin 2 and 3, which are expressed in muscle tissues,  $\alpha$ -Actinin 2 being exclusively expressed in cardiac and slow, oxidative muscles and  $\alpha$ -Actinin 3 in fast, glycolytic muscle (for review Mills et al., 2001; Murphy et al., 2015).

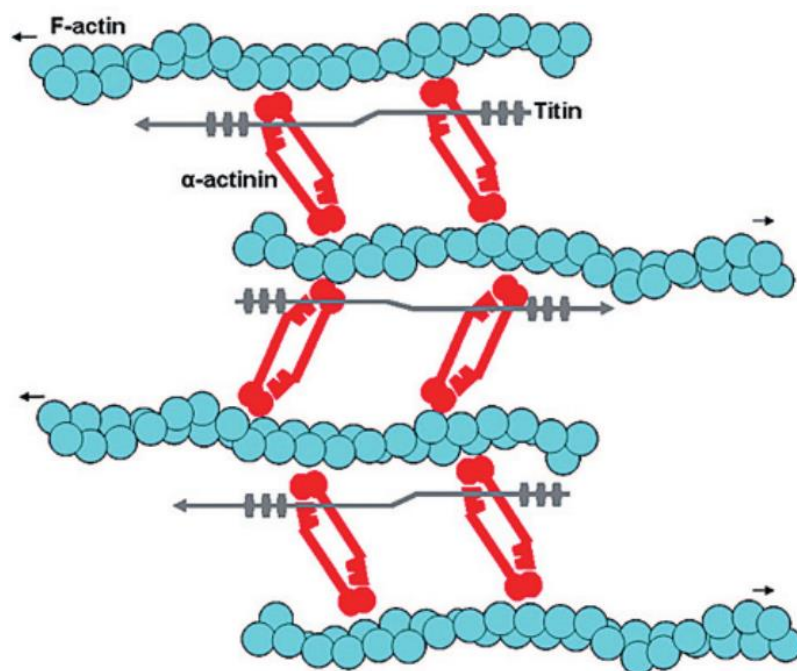


Figure 7: Schematic overview of  $\alpha$ -Actinin 2 interactions in striated muscle. Representation of sarcomeric Z-disk, where  $\alpha$ -Actinin 2 (red) cross-links anti-parallel actin thin filaments (blue) and also interacts with titin (adapted from Sjöblom et al., 2008).

Phylogenetic analysis of the  $\alpha$ -Actinin family revealed that  $\alpha$ -Actinin 2 was the first of the four  $\alpha$ -Actinins formed by gene duplication, giving rise to all other isoforms by gene divergence (Dixson et al., 2002).  $\alpha$ -Actinin 2 is the major component of the Z-disk (Fig. 3), even though it accounts for less than 20% of its mass (Robson et al., 1970). It is a 94-103 kDa protein composed of 894 amino acids and encoded by the *ACTN2* gene (for review Blanchard et al., 1989). This gene is located on the human chromosome 1q42-q43 and consists of more than 70,000 bp, structured in 23 exons (Beggs et al., 1992).  $\alpha$ -Actinin 2 is a rod-shaped monomer, approximately 35 nm in length and 3-4 nm wide, forming homodimers in an anti-parallel fashion (Fig. 8).

Additionally, it has been reported that  $\alpha$ -Actinin 2 is able to form heterodimers with  $\alpha$ -Actinin 3 in vitro and in vivo (Chan et al., 1998). It consists of three functional domains, the N-terminal globular actin-binding domain (ABD), the central rod domain, and a C-terminal calmodulin-like domain (CAMD), constituted by two pairs of EF hands (EF1-2 and EF3-4; Fig. 8; for review Sjöblom et al., 2008).

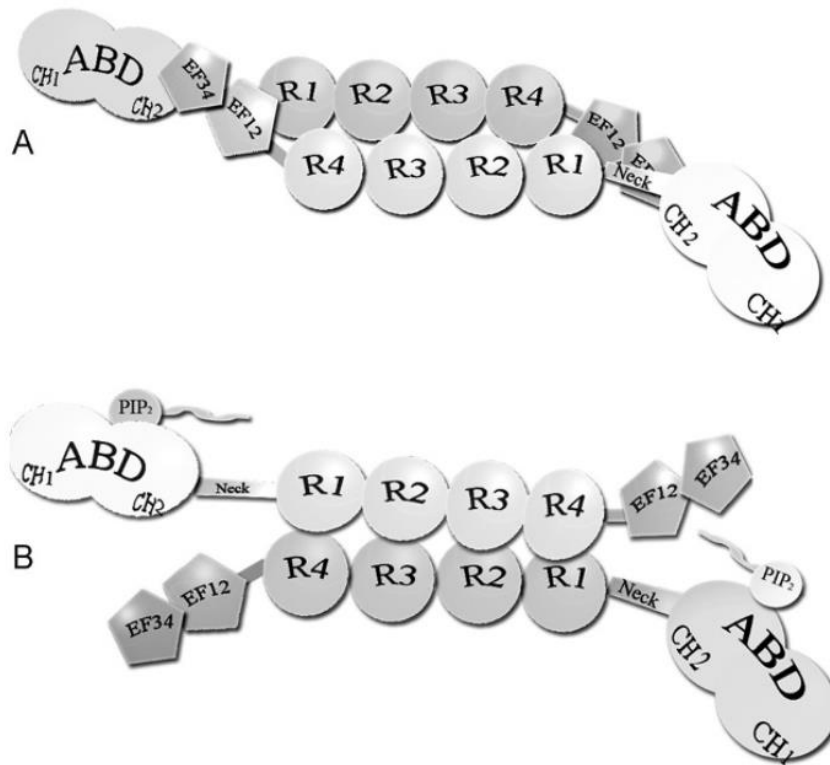


Figure 8: Scheme presenting  $\alpha$ -Actinin 2 homodimers. (A) Inactive form with the calmodulin (CaM)-like domain bound to the neck between actin-binding domain (ABD) and rod domain. (B) Addition of phosphatidylinositol 4,5-bisphosphate (PIP<sub>2</sub>) to muscle isoforms releases the CaM-like domain to interact with titin (adapted from Sjöblom et al., 2008).

The N-terminal ABD is the most conserved domain within the protein family and has been used to determine the phylogenetic history of the protein (Dixon et al., 2002). The ABD consists of two calponin homology domains (CH) that are divided in type 1 and type 2. Recently the crystal structure of  $\alpha$ -Actinin 2 homodimers was resolved with a resolution of 3.5 Å, contributing further insights into structure and function of  $\alpha$ -Actinin 2 (Ribeiro et al., 2014). Nevertheless, until today it is not fully understood how the ABD interacts with actin filaments. It is known that  $\alpha$ -Actinin 2 homodimers can undergo conformational change upon binding of phosphatidylinositol 4,5-bisphosphate (PIP<sub>2</sub>) to facilitate binding with titin (Young et al., 2000). In detail, PIP<sub>2</sub> binds with its polar group to the residues R163, R169, R192 in the CH2 domain, resulting in a release of EF3-4 from the neck and therefore enabling its interaction

with titin (Fig. 8; Franzot et al., 2005; Ribeiro et al., 2014). The neck is an  $\alpha$ -helical linker that connects the ABD to the central rod domain. The central rod domain consists of four spectrin-like repeats (SR) that assure rigidity of the homodimer and serve as an important interaction site for multiple structural and signaling proteins (for review Djinovic-Carugo et al., 2002). Besides the ABD and the rod domain, the CAMD also fulfills important functions in structural stabilization and signaling in the  $\alpha$ -Actinin 2 homodimer. For structural stabilization EF1-2 groups of each monomer bind to the SR4, by intercalating with the connecting loop of EF1 and EF2, between the  $\alpha$  helices 2 and 3 of the SR4 (Ribeiro et al., 2014). The EF3-4 group is interacting with the Z-repeats in the N-terminal region of titin and therefore set correct alignment of  $\alpha$ -Actinin 2 homodimers at the Z-disc (Young & Gautel, 2000). However, this interaction is just facilitated in the open structure of  $\alpha$ -Actinin 2 homodimers, when PIP2 is bound in the CH2 domain. In its closed conformation EF3-4 is connected to the hydrophobic  $\text{Ca}^{2+}$ /calmodulin-binding motif, termed 1-4-5-8, including hydrophobic residues A266, I269, C270 and L273 (Bayley et al., 1996). In contrast to the  $\alpha$ -Actinin 2 and 3, the CAMD of the non-muscle isoforms are  $\text{Ca}^{2+}$  sensitive (Burrige et al., 1981).

Considering this crucial role of  $\alpha$ -Actinin 2 in the Z-disc of the cardiac sarcomere, it is not surprising that *ACTN2* mutations are associated with different cardiomyopathies, including three reports on HCM (for review Murphy et al., 2015; Theis et al., 2006; Chiu et al., 2010; Haywood et al., 2016). So far solely missense mutations have been found in HCM patients. This leads to the hypothesis that mutated transcripts are translated into proteins that might alter functional characteristics of the protein, acting as so-called “poison peptides”. How exactly those mutated proteins affect function and why clinical presentations of patients carrying *ACTN2* mutations is so divers, is not fully understood yet and will have to be further elucidated in the future (Bagnall et al., 2014).

#### **1.1.4 Treatment of HCM**

So far there is no curative treatment against HCM, which reverses or prevents hypertrophy and dysfunction of the heart (for review Tardiff et al., 2015). Available drug-based therapies aim to relieve HCM-associated symptoms and decelerate disease progression. Examples for drugs used in this context are  $\beta$ -adrenoceptor

antagonists ( $\beta$ -blockers), which lower workload in the heart and increase time of diastolic filling (Marian, 2009). Furthermore,  $\text{Ca}^{2+}$  channel blockers are used in order to reduce heart rate and therefore lengthen LV filling time. Surgical interventions, such as septal myectomy, septal alcohol ablation and heart transplantation are last options to attenuate the severity of HCM symptoms (Maron, 2002; Ball et al., 2011; Shirani et al., 1993). None of these treatments targets the genetic cause of the disease. In the past years molecular-based interventions were studied, which could apply to HCM. Five prominent examples for those molecular-based therapies are exon-skipping, spliceosome-mediated RNA *trans*-splicing (*trans*-splicing), RNA interference (RNAi), gene replacement (GR) therapy and CRISPR/Cas9 genome editing. All interventions were used in the context of HCM and tested in different disease models (Gedicke-Hornung et al., 2013; Mearini et al., 2013; Jiang et al., 2013; Mearini et al., 2014; Ma et al., 2017; Prondzynski et al., 2017).

#### 1.1.4.1 Gene therapy approaches

Gene therapy approaches are able to directly target the cause of the disease and are therefore promising treatment options in the future. One limitation is sufficient delivery of molecular-based therapeutics into the patient's body without causing adverse effects. Two types of delivery systems are available: Non-viral and viral vectors. However, non-viral vectors are not the major focus of this thesis and therefore the following will focus on viral vectors (for review Chira et al., 2015). Viruses are appealing tools for transfer of molecular-based therapeutics as they exhibit high transduction efficiencies in a wide range of human cells. In fact, of the so far reported 1800 clinical gene therapy trials until 2012, approximately 70% of the vectors were represented by viral-based delivery systems (Ginn et al., 2013). Nevertheless, viruses are dangerous as their existence is determined by finding a host cell for replication, whereby they often introduce genomic information into the host's DNA. Therefore they are not only responsible for causing influenza, but also for the human immune deficiency syndrome (HIV), which is until today not curable. Additionally, they are also reported to contribute to human cancers, such as cervical cancer that is associated with the human papilloma virus (HPV; Dürst et al., 1983). This aspect of viruses was first observed in the context of gene therapy 18 years ago. Four days after receiving a trans-gene packaged in a recombinant adenovirus (Ad) the

participant of a gene therapy trial died of multi-organ failure, most likely caused by a severe immune response to the virus (Raper et al., 2003). Since then tremendous effort was invested in vector design and safety assessment. Nowadays, four main classes of viral based vectors are used for gene transfer: Ad, adeno-associated viruses (AAV), retroviruses and lentiviruses. In the cardiac field the most prominent vectors are Ads and AAVs as their efficiency and long-lasting gene expression has been shown in two studies using large-animal models (Kaye et al., 2007; Pleger et al., 2011). Especially the successful completion of a SERCA2a gene therapy Phase II trial demonstrates safety and feasibility of adeno-associated virus (AAV) serotype 1 mediated gene transfer in humans (Jessup et al., 2011). Unfortunately, this study failed in showing beneficial outcomes for gene therapy patients (Greenberg et al., 2016). Recently, our group and others have demonstrated that AAV serotype 9, combined with a cardiomyocyte-specific promoter is able to specifically target the heart after systemic administration in mice (Mearini et al., 2014; Werfel et al., 2014). Therefore, development of safe and efficient viral-based delivery vectors will be substantial for cardiac gene therapy in the future.

Gene therapy approaches that target the mRNA or RNA of the endogenous mutant allele are *trans*-splicing, exon skipping, and RNAi. The application and mechanisms of *trans*-splicing will be discussed in more detail in chapter 3.1. In short, it is defined as a splicing reaction between two independently transcribed RNA molecules, a target endogenous mutant pre-mRNA and a therapeutic pre-*trans*-splicing molecule, resulting in a full-length repaired mRNA (for review Wally et al., 2012). In frame exon skipping is an alternative approach for targeting mRNAs. Therefore antisense oligonucleotides (AONs) are designed, masking exonic splicing enhancer motifs, thus preventing binding of regulatory splicing proteins that mediate exon inclusion into the mature mRNA. This results in functional proteins with small internal deletions (Hammond et al., 2011). Finally, RNAi can be used for allele-specific silencing and therefore expression of mutant mRNAs can be suppressed (Jiang et al., 2013).

Replacing mutant proteins by overexpression of exogenous wild-type (WT) proteins is the basic idea of GR therapy. This concept is particularly interesting for HCM and *MYBPC3* mutations, since the sarcomere is a tightly regulated system with a preserved stoichiometry of all components, usually resulting in low level or absence of mutant proteins causing haploinsufficiency. Therefore additional expression of any

sarcomeric protein is expected to replace the endogenous protein level in the sarcomere and prevent haploinsufficiency (Mearini et al., 2014; Prondzynski et al., 2017). This concept of GR and its application will be further discussed in chapter 3.1.

In summary, all molecular interventions proved to be functional in vitro and in vivo. Further testing of those treatments in clinical trials will show, if the same result can also be expected in patients with HCM. One limitation is still safe, sufficient and targeted viral-based delivery of the molecular-based therapeutic to the heart. To circumvent viral-based delivery new molecular tools are available that can be directly applied to the human germ-line. Just recently a groundbreaking study by Ma et al. was published, describing the correction of a heterozygous *MYBPC3* mutation in human preimplantation embryos using CRISPR/Cas9 technology (Ma et al., 2017). The emergence of CRISPR/Cas9 revolutionized genome editing accuracy and efficiency by recognizing specific genomic sequences and inducing double strand breaks (DSB; Cong et al., 2013; Hsu et al., 2014; Kim et al., 2014; Mali et al., 2013). DSB can be resolved by endogenous DNA repair mechanisms such as non-homologous end-joining (NHEJ) and homology-directed repair (HDR). NHEJ is not applicable for gene correction applications since it introduces additional mutations in the form of insertions/deletions (indels). HDR, on the other hand, repairs the DSB site using the non-mutant homologous chromosome or a supplied exogenous DNA repair template, leading to the correction of the mutant allele (Wu et al., 2013; Lin et al., 2014). CRISPR/Cas9 technology proved to be a versatile tool in the past and has the potential to revolutionize human germline therapy in the future.

## 1.2 Human induced pluripotent stem cells

First successful experiments reported on two-dimensional (2D) in vitro cultures were conducted by Ross G. Harrison in 1907 more than 100 years ago (Harrison, 1907). Harrison demonstrated that explanting a fragment of nerve cord from a frog tadpole and placing it in a drop of frog lymph would promote in vitro growth. In 1922 Albert H. Ebeling published a series of reports including the description of a 10-year-old fibroblast culture and the co-cultivation of epithelial cells and fibroblasts in 2D (Fig.9; Ebeling, 1922; Ebeling et al., 1922).

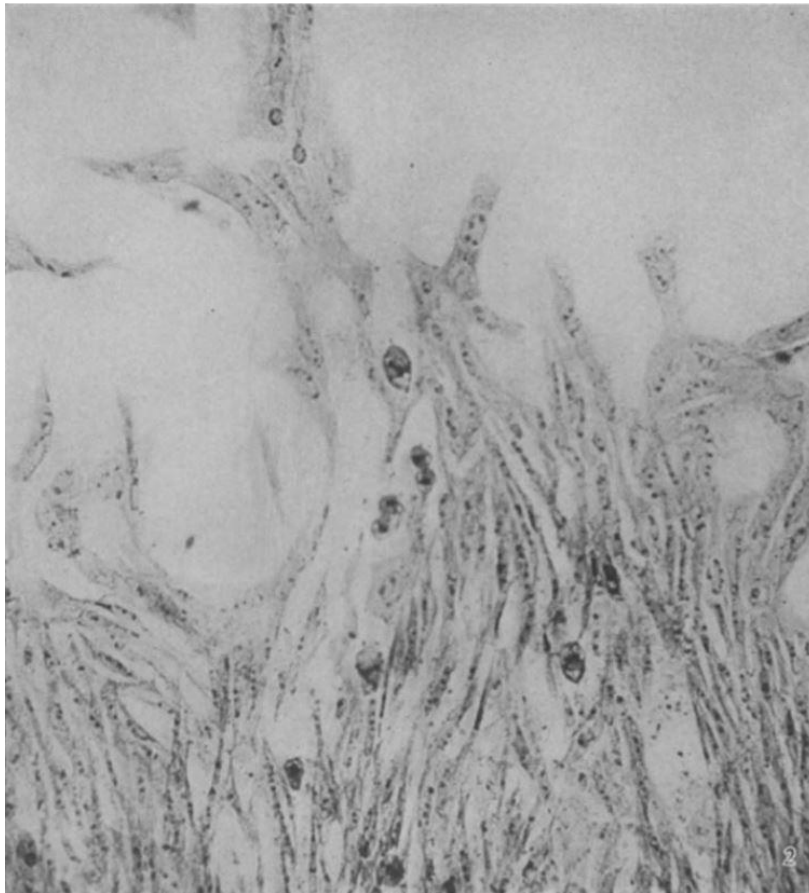


Figure 9: 10 year old fibroblast culture 24870-1 passaged for 1858 times. This culture was described by Ebeling as very active. The cells were stained with methylene blue after 48 hours growth and images were acquired at 300 x magnification (adapted from Ebeling, 1922).

Those studies showed that cell culture was stable over longer period of times and could maintain unlimited proliferation of fibroblasts accompanied by increasing cell mass. This was highly controversial at that time, because it was not known if 2D cultured cells use the substances contained in the medium for growth (Lewis & Lewis, 1912). In the following decade's tissue and cell cultures have been used for diverse studies that contributed to our understanding of cell biology and cell

organization. In order to unify the efforts of scientist working with cell cultures and to standardize the quality of cell cultures available, the American Tissue Culture Association was founded in 1947. The need of standardization and regular verification of cell lines in use is still required today, as reproducibility of biological experiments has been failing dramatically in the past years (Capes-Davis et al., 2010; Freedman et al., 2015; Yu et al., 2015). When embryonic stem cells (ESCs) emerged in the 1980's, their differentiation potential was shown in vitro and in vivo by injecting ESCs into mice resulting in teratocarcinomas (Evans et al., 1981; Martin, 1981). Those studies marked the beginning of stem cell research. In 1998 the H9 cell line was cultivated in vitro, which was the first ESC line derived from a human blastocyst (Fig. 10; Thomson et al., 1998).

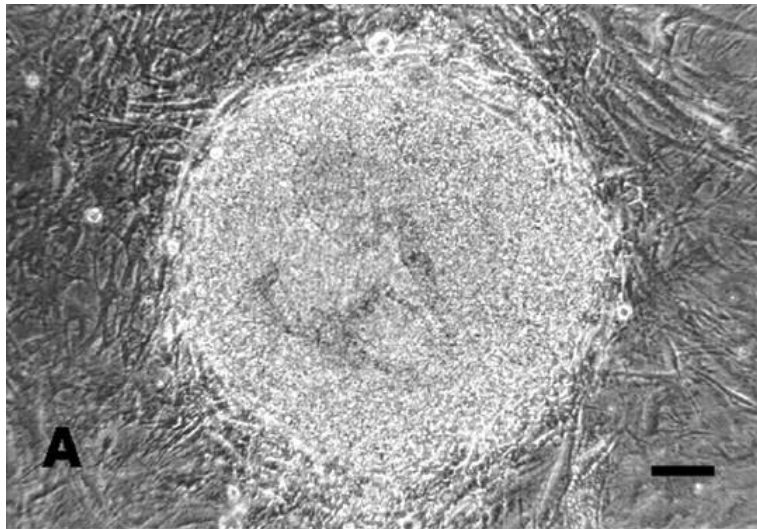


Figure 10: Derivation of the H9 cell line. Inner cell mass–derived cells attached to mouse embryonic fibroblast feeder layer after 8 days of culture, 24 hours before first dissociation. Scale bar, 100  $\mu\text{m}$  (adapted from Thomson et al., 1998).

This finding promised to revolutionize medicine, especially regenerative medicine. However, a major hurdle remained when working with human ESCs: International restrictions of receiving and experimenting with those cells. This fact makes them just available for a small community of scientists, who either live in countries with eased restrictions or are in possession of special permits. Despite this fact, mouse and human ESCs were used to establish standard protocols for culture conditions in the absence of animal-derived culture components and first tissue-specific differentiation protocols (Murry et al., 2008). ESCs were even tested in clinical trials for several diseases including macular degeneration, myopic macular degeneration, Stargardt's



macular dystrophy, spinal cord injury, type I diabetes mellitus and heart failure (Trounson et al., 2015).

In 2006, Yamanaka and his group published the discovery of induced pluripotent stem cells (iPSCs), by using a technique that converts adult mouse fibroblasts into pluripotent cells (Takahashi et al., 2006). Just one year later this protocol was adjusted to human fibroblasts (Takahashi et al., 2007). The tremendous impact of this discovery was honored with the Nobel Prize in Physiology or Medicine in 2012, just six years after the initial finding. Successful reprogramming of fibroblasts was accomplished by systematic testing of 24 candidate genes in cells from a mouse strain that carried an antibiotic resistance gene under the control of an embryonic gene promoter. Consequently, only those cells survived that adopted embryonic like gene expression and therefore expressed the antibiotic resistance gene. Those experiments revealed four main transcription factors: Oct3/4, Sox2, c-Myc and Klf4. Upon transduction with these genes, human dermal fibroblasts appeared like human embryonic stem cell-like colonies after 30 days of culture (Fig. 11).

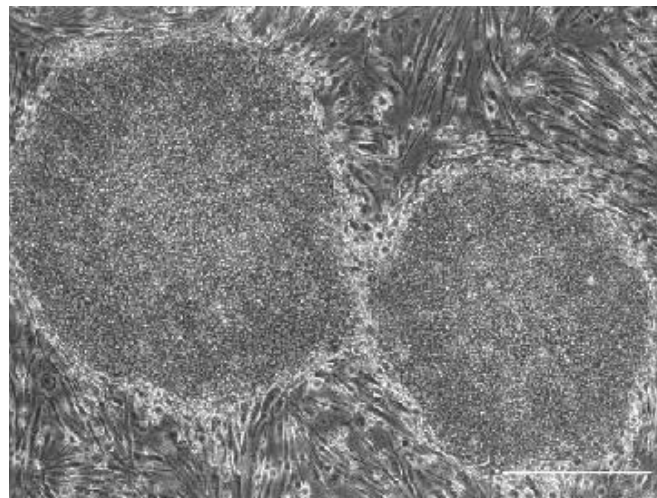


Figure 11: Phase contrast images of human iPSC cells derived from fibroblast-like synoviocyte (HFLS, clone 243H1; scale bar = 200  $\mu$ m; adapted from Takahashi et al., 2007).

These observations were also confirmed on molecular level by reverse transcriptase polymerase chain reaction (RT-PCR), immunofluorescence analysis and protein quantification of the described pluripotency markers. Furthermore, those cells were successfully differentiated to neuronal and cardiac cells using protocols established by other groups working with ESCs (Kawasaki et al., 2000; Laflamme et al., 2007). The iPSC technology makes disease modeling accessible for a larger community of scientists, studying all kinds of genetic diseases affecting a variety of different cells.

Human iPSCs (hiPSCs) provide an alternative to the use of ethically questioned human ESCs and are expected to speed up progression of personalized medicine (Robinton et al., 2012).

### **1.2.1 Disease modeling**

The idea of disease modeling originated from the first description of human ESCs and their potential to differentiate into any somatic cell type (Thomson et al., 1998). This event inspired clinicians and scientist alike to use those cells for clinical treatments, such as autologous cell transplantation for regenerative medicine, or for modeling of genetic diseases, to gain further insights into disease mechanisms on cellular level. However, before disease modeling could be conducted there was a need to establish differentiation protocols for generation of desired cell types. Three general approaches were established for the use of human ESCs as a starting point for differentiation. The first approach promotes aggregation of cells to enable formation of embryoid bodies (EBs; Doetschman et al., 1985). The second possibility is to co-culture ESCs directly on stromal cells during differentiation (Nakano et al., 1994). The third option is to differentiate ESCs as monolayer on extracellular matrix proteins (ECM; Nishikawa et al., 1998). Current iPSC differentiation protocols are based on EB formation or monolayer cultures on ECM proteins, inducing directed germ layer differentiation into Endo-, Meso- and Ectoderm (Breckwoldt et al., 2017; Palpant et al., 2016). Once cells are differentiated into a specific germ layer, they can be programmed to become a specific cell type like a hepatocyte, a cardiomyocyte (CMs) or a neuron (Hamazaki et al., 2001; Hescheler et al., 1997; Okabe et al., 1996). Establishment of valid differentiation protocols marked the beginning of disease modeling, as we know it today. However, the first study using human ESCs was reported in 2007 (Eiges et al., 2007). It was a considerably amount of time for the first disease modeling study to be published, since culture and differentiation protocols were available already for more than ten years. Reasons for this might be international restrictions using those cells, the scarcity of ESCs with inherited diseases and insufficient gene editing techniques. With the emergence of hiPSCs in 2007 disease modeling studies were easier to conduct, as human embryos were not needed anymore (Takahashi et al., 2007). Instead skin fibroblasts of patients carrying inherited diseases could be used as the basis for disease modeling studies. Just two

years later, first studies were published on disease modeling of spinal muscular atrophy and familial dysautonomia using patient-derived iPSCs (Ebert et al., 2009; G. Lee et al., 2009). Both studies were successful in observing disease-related phenotypes in patient-derived iPSCs when compared to healthy controls. Those studies illustrated that the promise of iPSC technology, gaining new insights into human pathogenesis and treatment, could be fulfilled. Since then, numerous studies have been published on different inherited diseases, including modeling of cardiac diseases.

#### 1.2.1.1 Modeling of cardiac diseases using iPSC technology

When modeling cardiac diseases, the desired cell types are ventricular-, atrial-, pacemaker- and nodal-like CMs. Before differentiation protocols for those subtype-specific differentiations were developed, first none subtype-specific protocols were published in 2011, which mainly relied on previously established protocols using human ESCs (BurrIDGE et al., 2012; Kattman et al., 2011; Laflamme et al., 2007). Main components of those protocols are: I) bone morphogenic proteins (BMPs), which are part of the transforming growth factor- $\beta$  (TGF- $\beta$ ) family; II) wingless/INT (WNTs) proteins; III) fibroblast growth factors (FGFs). Their sequential presence mainly conducts cardiac development. The topic of CM differentiation will be discussed in more detail in chapter 3.2 differentiation of CMs and generation of human engineered heart tissue (EHT; Breckwoldt et al., 2017). Nevertheless, there has been progress in production of subtype-specific CMs. To verify subtype-specific differentiation most protocols relied on genetically modified hiPSCs, which carry a fluorescent reporter under a subtype-specific promoter. This has been first reported for ventricular-like CMs in 2013 (Bizy et al., 2013). To circumvent genetically modifying iPSCs for subtype-specific differentiation it has been shown that pacemaker- and atrial-like CMs can be generated by controlling the retinoic acid and/or the FGF, BMP and Wnt signaling pathways (Birket et al., 2015; Devalla et al., 2015). Additionally, timed supplementation of the chemical compound 1-ethyl-2-benzimidazolinone was reported to promote the differentiation to nodal- and atrial-like CMs (Jara-Avaca et al., 2017). Time will tell if studying those subtype-specific CMs will also result in the observation of subtype-specific disease mechanisms. However,

most established protocols for cardiac differentiation generate ventricular-like CMs (Mummery et al., 2012).

With progress in CMs generation an increasing amount of studies modeling inherited cardiac diseases have been also published (Fig. 12; Brandão et al., 2017).

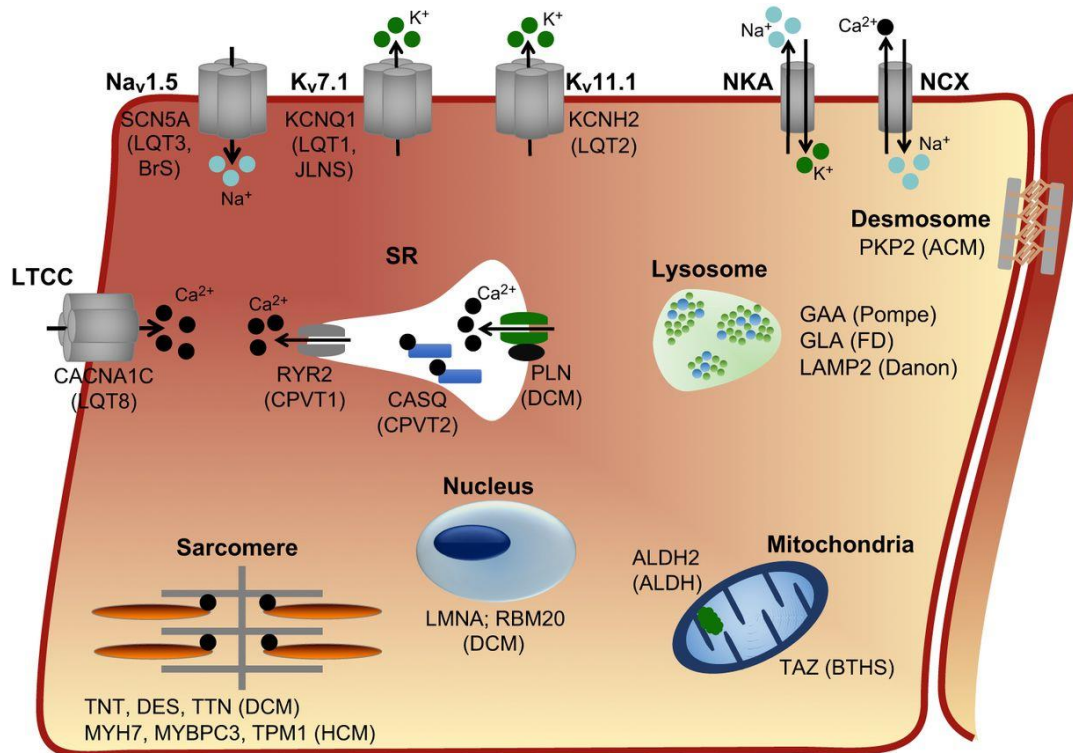


Figure 12: Overview of inherited cardiac diseases that have been studied with hiPSC-CMs. ACM, arrhythmogenic cardiomyopathy; ALDH, aldehyde dehydrogenase; BrS, Brugada syndrome; BTHS, Barth syndrome; LTCC, L-type Ca<sup>2+</sup> channel; CPVT, catecholaminergic polymorphic ventricular tachycardia; DCM, dilated cardiomyopathy; FD, Fabry disease; HCM, hypertrophic cardiomyopathy; JLNS, Jervell and Lange-Nielsen syndrome; LQTS, long QT syndrome; Kv7.1, voltage-gated, slow rectifier potassium channel; Kv11.1, voltage-gated, fast rectifier potassium channel; Nav1.5, voltage-gated cardiac sodium channel; NCX, sodium/Ca<sup>2+</sup> exchanger; NKA, sodium/potassium exchanger; SR, sarcoplasmic reticulum (adapted from Brandão et al., 2017)

Human iPSC-derived CMs (hiPSC-CMs) proved to be a versatile tool for contractile, morphological, optical and electrophysiological analysis. Electrophysiology is most commonly investigated when studying hiPSC-CMs using single-cell patch-clamping, automated patch-clamp, multielectrode arrays or sharp electrodes, which were mainly applied to 3D models of hiPSC-CMs (Moretti et al., 2010; Obergrussberger et al., 2016; Asakura et al., 2015; Lemoine et al., 2017). Electrophysiological recordings can distinguish between different subtypes of hiPSC-CMs and were for example investigated in the context of long QT syndrome (LQTS; Moretti et al., 2010; Lahti et al., 2012). LQTS is an inherited heart disease and patients have a prolonged QT interval in ECG recordings, which is reflected by a prolonged action potential duration

in hiPSC-CMs. Optical measurements of hiPSC-CMs are based on fluorescent voltage- or  $\text{Ca}^{2+}$ -sensitive dyes, which can be used to measure electrical components and  $\text{Ca}^{2+}$  dynamics at the same time (Lee et al., 2012). High-resolution microscopy enables not just real-time measurements of  $\text{Ca}^{2+}$  dynamics in the living cell, but can also be used to assess morphological parameters, starting from cell size down to organization and structure of organelles (Denning et al., 2016). Cell sizes of hiPSC-CMs are of interest, since patients diagnosed for HCM develop a higher heart-to-body-mass ratio, which might be reflected by increased cell size in vitro (Prondzynski et al., 2017). However, the topic of HCM and modeling this disease with hiPSC-CM will be presented in chapter 1.2.1.2 and in chapter 3.1. Apart from imaging organelles, it is also possible to measure metabolic activity, for example of mitochondria. Function of mitochondria can be measured by glycolysis and oxidative phosphorylation and plays a crucial role when modeling diseases like Barth syndrome (Denning et al., 2016; G. Wang et al., 2014). The parameter of contractility is most favorable measured in 3D constructs of hiPSC-CMs, due to high cell to cell variability and immaturity of 2D cultured hiPSC-CMs when compared to 3D models (Uzun et al., 2016). One of the most prominent 3D models in the field are EHTs (Stöhr et al., 2013; Stöhr et al., 2014; Breckwoldt et al., 2017). EHTs can be measured with an automated video-based analysis system, which provides a high-content readout of contractile function. Measurements can be done repeatedly under sterile, steady-state conditions without the need for manual handling. 3D models of hiPSC-CMs are important for modeling cardiac diseases, as it is reported that some disease-specific phenotypes, for example for DCM, can just be observed when studied in 3D models (Hinson et al., 2015).

#### 1.2.1.2 Modeling of HCM using iPSC technology

Modeling of HCM using hiPSC-CMs is able to recapitulate hallmarks of the disease observed in humans for instance altered gene expression, increased cell size, myofibrillar disarray, abnormal  $\text{Ca}^{2+}$  handling, altered electrophysiology and altered contractile force (Lan et al., 2013; Tanaka et al., 2014; Han et al., 2014; Dambrot et al., 2014; Birket et al., 2015; Ojala et al., 2016; Pioner et al., 2016; Prondzynski et al., 2017). HCM is caused by mutations in sarcomeric genes, with the highest prevalence in *MYH7* and *MYBPC3* genes, encoding  $\beta$ -MHC and cMyBP-C, respectively (Frey et

al., 2011). This is reflected by the studies that have been published so far, since they are only investigating patient-derived hiPSC-CMs with mutations in those two genes. However, *MYH7* is not the major focus of this thesis and therefore the following will focus on studies investigating *MYBPC3* mutations (for review refer to Brandão et al., 2017). In the first report published by Tanaka et al. (2014) hiPSC-CMs retrieved from three healthy donors and three HCM patients were compared. For one HCM patient sequencing of the *MYBPC3* gene revealed a frameshift mutation (Gly999-Gln1004del). hiPSC were differentiated to CMs using an EB formation protocol and cultured further in suspension. EBs were dissociated after 30, 60 and 90 days of culture and replated in 2D cultures for additional 7 days for subsequent analysis of cell size. Additionally, 60-day-old EBs were used to measure myofibrillar disarray using electron microscopy. The authors found that under baseline conditions the differences in those parameters were rather low, yet significant between diseased and healthy hiPSC-CMs. Seven days of endothelin-1 treatment induced a stronger phenotype in the patient-specific hiPSC-CMs and therefore unmasked the HCM phenotype. The authors assumed that this effect was due to the activation of the endothelin-1/endothelin A receptor axis, which affects endothelin-1 signaling and CM hypertrophy (Sugden, 2003). This study showed for the first time that modeling of *MYBPC3* mutations can be achieved using hiPSC-CMs and bring new insights of pathophysiology in HCM on cellular level. In the same year, the study of Dambrot et al. (2014) investigated the effects of serum supplementation in rat CMs, in hESC-derived CMs and in hiPSC-CMs from one healthy individual and three HCM patients with mutations in the *MYBPC3* gene (c.2373dupG). hiPSC-CMs were differentiated in 2D monolayers and after six days used for experimental analysis. By a series of different culture conditions and sequential supplementation and omission of serum for three of seven days, the authors found that HCM hiPSC-CMs exhibited a larger cell size without serum supplementation than control hiPSC-CMs. However, serum supplementation of HCM hiPSC-CMs induced no further effect on cell size in contrast to control hiPSC-CMs that showed up to 3-fold higher cell areas. This study shows that culture conditions can have an impact on the experimental outcome, independent of the fact if hiPSC-CMs are derived from healthy or diseased individuals. The authors suggested consistency improvement by carrying out the experiments under serum-free or low serum conditions. One year later Birket et al.

(2015) reported successful contractile force measurements of single hiPSC-CMs by supplementation of triiodothyronine (T3), insulin-like growth factor 1 (IGF-1), and dexamethasone to the culture medium. The same patient-derived hiPSC-CMs were used for their investigation as reported in Dambrot et al. (2014). The authors observed that T3 increased the resting membrane potential, whereas IGF-1 and dexamethasone stimulated cell energetics and force generation. These findings allowed measuring contractile forces of two control and three HCM hiPSC-CMs. Contractile force was assessed in single cells by plating them on soft micropatterned polyacrylamide gels containing fluorescent micro-beads. Bead displacement was imaged and converted to a value of traction stress (Ribeiro et al., 2015). HCM hiPSC-CMs showed lower force than control hiPSC-CMs. This study assessed contractile forces for the first time in *MYBPC3* mutant hiPSC-CMs and further improved culture of hiPSC-CMs under serum free conditions. One year later another group of researchers reported disease modeling using patient-derived hiPSC-CMs with an inherited *MYBPC3* mutation (Gln1061X; Ojala et al., 2016). The authors performed gene expression analysis,  $Ca^{2+}$  measurements, patch-clamp recordings and cell size analysis to distinguish the phenotype of the HCM hiPSC-CMs. hiPSC-CMs were differentiated in EB format and analyzed after one, three and six weeks in culture. Cell size was higher, gene expression profiles differed,  $Ca^{2+}$  transients were abnormal and electrophysiological recordings revealed more arrhythmogenic events in HCM hiPSC-CMs than in control hiPSC-CMs.

The four studies presented here showed that HCM phenotypes can be reproduced with different *MYBPC3* mutations in hiPSC-CMs to gain new insights into pathophysiology of HCM on cellular level. However, there are still limitations considering standardization of differentiation protocols, culture conditions, immaturity and therewith culture duration of analyzed hiPSC-CMs. Besides, none of the mentioned studies applied treatment options to reverse the disease related phenotypes. Those issues have to be addressed in the future to guarantee fast and safe development of hiPSC-CMs into valuable tools for disease modeling, drug safety assessment and regenerative medicine.

### 1.3 Aim of this thesis

Being aware of the fact that current treatment of HCM is empirical and focuses just on improving symptoms of the disease by pharmacological and/or surgical interventions, the aim of this study was to evaluate hiPSC-CMs as a tool to model HCM and for assessment of *trans*-splicing, GR and CRISPR/Cas9 genome editing as molecular-based interventions.

For this purpose three different iPSC lines were provided: one control cell line derived from a healthy individual and two cell lines derived from HCM patients identified with novel mutations in the *MYBPC3* (c.1358dupC; p.Val454CysFsX21) or the *ACTN2* (c.740C>T; p.Thr247Met) gene at the heterozygous state. These cell lines were the basic subjects of investigation in this thesis focusing on three aims:

- (1) Evaluation of *MYBPC3 trans*-splicing and gene replacement as therapeutic options in hiPSC-derived cardiomyocytes.
- (2) Differentiation of cardiomyocytes and generation of human engineered heart tissue.
- (3) Modeling of a novel *ACTN2* mutation (c.740C>T; p.Thr247Met) in hiPSC-derived cardiomyocytes using an isogenic control cell line.

(1) For evaluation of *MYBPC3 trans*-splicing and GR as therapeutic options, the patient-specific HCM cell line with a *MYBPC3* mutation (c.1358dupC; p.Val454CysFsX21) was used. Specific aims were to characterize molecular and morphological phenotypes of the HCM cell line in comparison to a healthy unrelated control hiPSC line. Furthermore, testing of *MYBPC3 trans*-splicing and GR in the HCM cell line should result in changes on molecular and morphological level, similar to what was observed in the healthy control cell line.

(2) For the development of a protocol focused on differentiation of cardiomyocytes and generation of human engineered heart tissue several hiPSC lines were used, including the healthy unrelated control and both patient-specific HCM cell lines with



mutations in the *MYBPC3* and the *ACTN2* gene. Specific aims of this point were to generate a cost-effective, EB-based, high-output differentiation protocol generating high purity of CM, which can be further assessed for their functional characteristics in a 3D model of EHTs.

(3) For evaluation of a novel *ACTN2* mutation (c.740C>T; p.Thr247Met) the patient-specific hiPSC line was used. Specific aims were to generate an isogenic control cell line with CRISPR/Cas9 genome editing and to characterize morphological phenotypes and functional characteristics of both hiPSC-CMs in 2D and in 3D.

## **2. Material and methods**

All materials and methods are stated in the publications presented in chapter 3.1 and 3.2, if not mentioned explicitly.

### **2.1 Material**

#### **2.1.1 Generation and analysis of a patient-specific hiPSC carrying a novel *ACTN2* mutation**

The HCM patient was recruited in the outpatient clinic at the University Heart Center Hamburg and provided written informed consent for the use of fibroblasts. The reprogramming was performed as described in chapter 3.1 (Prondzynski et al., 2017). DNA sequencing with a 19-gene cardiac panel identified a unique *ACTN2* c.740C>T transition (p.Thr247Met) in exon 8, part of the ABD. Patient-specific hiPSCs were subjected to the described cardiac differentiation protocol in chapter 3.2 (Breckwoldt et al., 2017) and analyzed in 2D-format and EHTs after 30 days in culture. Estimation of differentiation efficiency by flow cytometry analysis resulted in 80-90% hiPSC-CMs content within different batches (data not shown).

### **2.2 Methods**

#### **2.2.1 Generation of an isogenic control cell line with CRISPR/Cas9 technology**

For generation of an isogenic control cell line, patient-specific hiPSCs carrying a novel *ACTN2* mutation were used, hereafter named HCM cell line. CRISPR/Cas9 technology was used to repair the patient-specific mutation according to Ran et al.

(Ran et al., 2013). In short, Cas9 nickase approach was used for induction of a DSB in the desired locus. Single guide RNAs (sgRNAs) were designed using a publically available design tool (crispr.mit.edu) and cloned into the pSpCas9n(BB)-2A-GFP plasmid (Addgene). HDR was supported by supplying an exogenous repair template encoding the WT sequence of *ACTN2* from position g.54,148-54,270 (NG\_009081.1; Accession number NCBI). Repair templates were produced by IDT® as single-stranded oligo donors (ssODNs). Silent mutations were introduced at genomic positions 54,200 and 54,245 within the protospacer adjacent motif (PAM) sequence for prevention of repeated cutting events and verification of successful genome editing. HCM hiPSCs were transfected with the Amaxa Nucleofector™ (Lonza) using the P3 Primary Cell 4D-Nucleofector® X Kit and the pulse code CA 137. Each transfection approach consists of 800,000 HCM hiPSCs, 40 µM of ssODN, 1000 ng of each plasmid pSpCas9n(BB)-2A-GFP (Addgene) containing sgRNA A and B. One hour before transfection, HCM hiPSCs were treated with 10 µM Rock inhibitor Y-27632 (Biorbyt). For transfection HCM hiPSCs were washed twice with PBS and singularized with accutase (Gibco®; 5 min, 37 °C at 5% CO<sub>2</sub>). Enzymatic dissociation was stopped by adding the same volume of conditioned medium (COM) containing bFGF (30 ng/ml; Peprotech) and 10 µM Y. After counting, 800,000 cells were spun down for 3 min at 150 g and subsequently resuspended in the transfection mix and transferred into electroporation cuvettes (Lonza). After transfection, electroporation cuvettes were incubated for 5 minutes at 37 °C in 5% CO<sub>2</sub>. 500 µL pre-warmed COM, supplemented with FGF (30 ng/ml) and 10 µM Y was added to the transfection mix that subsequently was plated onto Matrigel-coated (1:60; Corning®) 12-Well plates. Transfected HCM hiPSCs were maintained for 48 hours and prepared for fluorescent activated cell sorting (FACS) by accutase dissociation as described above. FACS was performed using the FACS Aria™ III (BD; FACS Core facility UKE Hamburg) collecting GFP positive cells. GFP-positive cells were centrifuged for 3 minutes at 150 g and 2500 cells were plated into one well of a Matrigel-coated 6-well plate. Cells were maintained by daily medium change until colonies were visible. Picking was carried out using a 200-µl pipette, whereby each clone was transferred into one well of a Matrigel-coated 48-well plate. Clones were maintained until sufficient cell material was generated for cryopreservation and genomic analysis by PCR. If genomic analysis revealed successfully repaired HCM hiPSC clones, these

clones were subcloned by plating 1000 cells into one well of a Matrigel-coated 6-well plate. Subcloned repaired HCM hiPSC clones were again picked and cultured, until characterization could be repeated as described above. Furthermore, these clones were analyzed for off-targets by PCR. Subcloning was introduced to minimize chances of mixed clonal populations. Additionally, PCR fragments of these cells containing the modified *ACTN2* locus were subcloned using the CloneJET PCR Cloning Kit (ThermoFisher Scientific) for discrimination of allele-specific genotypes. Finally, all used cell lines were regularly genotyped by PCR for the affected *ACTN2* locus.

### **2.2.2 Genotyping and off-target analysis using polymerase chain reaction**

To amplify specific DNA fragments, PCR was conducted according to Mullis (Mullis et al., 1987). The applied PCR program was adapted to the used polymerase and annealing temperatures of the primers (listed in the data sheet supplied with the primers). The elongation time was adjusted to the length of the expected DNA fragment and the synthesis rate was estimated to be 1 kb/min, unless noted otherwise by the manufacturer. Genomic DNA template was used in an amount of 20 ng to 40 ng in a final volume of 20  $\mu$ l and 50 ng to 100 ng in a final volume of 50  $\mu$ l. All used primers are listed in the appendix (7.1.8).

For genotyping of putative CRISPR/Cas9 modified HCM hiPSCs clones, touchdown PCR (60 °C – 55 °C) was performed using PrimeStar® HS DNA Polymerase in a 50- $\mu$ l PCR approach, for 35 cycles according to the instructions of the manufacturers protocol (Table 1). For off-target analysis of successfully repaired HCM hiPSCs clones, touchdown PCR (60 °C – 55 °C) was performed using AmpliTaq® Gold DNA polymerase in a total volume of 20  $\mu$ l for 35 cycles according to the instructions of the manufacturers protocol (Table 2).

Table 1: Standard PCR program for PrimeStar® HS DNA Polymerase.

PCR step	Temperature (°C)	Time	
Denaturation	98	10 sec	11 cycles
Annealing	Touchdown* (-0.5 °C/per cycle)	30 sec	
Elongation	72	1kb/min	
Denaturation	98	10 sec	24 cycles
Annealing	55	30 sec	
Elongation	72	1kb/min	
Final Extension	72	7 min	
Cooling	4	∞	

\*60 °C - 55 °C

Table 2: Standard PCR program for AmpliTaq® Gold DNA Polymerase.

PCR step	Temperature (°C)	Time	
Initial Denaturation	94	5 min	11 cycles
Denaturation	94	30 sec	
Annealing	Touchdown* (-0.5 °C/per cycle)	30 sec	
Elongation	72	1kb/min	
Denaturation	94	30 sec	24 cycles
Annealing	55	30 sec	
Elongation	72	1kb/min	
Final Extension	72	7 min	
Cooling	4	∞	

\*60 °C - 55 °C

### 2.2.3 Sequencing of DNA

Sequencing analysis was performed by Eurofins MWG Operon according to the instructions of their sample submission guidelines.

### 2.2.4 Analysis of contractile force in EHTs

Contractile force was analyzed as previously described (Mannhardt et al., 2016). In short, 30-day old ( $\pm 5$  days) EHTs were incubated in modified Tyrode's solution at least two hours before starting an experiment (120 mM NaCl, 5.4 mM KCl, 1 mM MgCl<sub>2</sub>, 1.8 mM CaCl<sub>2</sub>, 0.4 mM NaH<sub>2</sub>PO<sub>4</sub>, 22.6 mM NaHCO<sub>3</sub>, 5 mM glucose, 0.05 mM Na<sub>2</sub>EDTA, and 25 mM HEPES) and incubated at 37°C in 7% CO<sub>2</sub> and 40% O<sub>2</sub>. The 24-well plate carrying the EHTs was placed inside a transparent chamber to maintain homeostatic temperature (37 °C) and CO<sub>2</sub> (5%). Automated video-optical recordings of silicon post deflection were enabled by a video camera placed above the chamber.

Tracking of EHT movement and determination of contractile force was analyzed based on the known mechanical properties of the silicon using a customized software (CMTV GmbH). EHTs were electrically paced for experimental analysis (1 V, 2 Hz, impulse duration 4 ms). The contraction peaks were analysed in terms of force, and contraction ( $T_1$ ) and relaxation time ( $T_2$ ) at 80% of peak height.

## 3. Results

### 3.1 Evaluation of *MYBPC3* trans-splicing and gene replacement as therapeutic options in human iPSC-derived cardiomyocytes.

In this chapter the report “Evaluation of *MYBPC3* trans-Splicing and Gene Replacement as Therapeutic Options in Human iPSC-Derived Cardiomyocytes” will be presented, which was published in June 2017 in the journal of *Molecular Therapy: Nucleic Acids*. In this report I was involved in conceptualization, methodology, investigation, formal analysis and visualization of all experiments, as in project administration, writing of the original manuscript and response to reviewers. My contributions in this project resulted in a first-authorship.

Title: Evaluation of *MYBPC3* trans-Splicing and Gene Replacement as Therapeutic Options in Human iPSC-Derived Cardiomyocytes

Authors: Maksymilian Prondzynski, Elisabeth Krämer, Sandra D. Laufer, Aya Shibamiya, Ole Pless, Frederik Flenner, Oliver J. Müller, Julia Münch, Charles Redwood, Arne Hansen, Monica Patten, Thomas Eschenhagen, Giulia Mearini and Lucie Carrier

Journal: *Molecular Therapy: Nucleic Acids*, Volume 7, June 2017, pages 475-486

DOI: 10.1016/j.omtn.2017.05.008

Results: In this study hiPSC-CMs were evaluated from an HCM patient carrying a novel *MYBPC3* mutation (c.1358dupC; p.Val454CysFsX21) and from a healthy donor. HCM hiPSC-CMs exhibited 50% lower *MYBPC3* mRNA and cMyBP-C protein levels than control, no truncated cMyBP-C, larger cell size, and altered gene expression, thus reproducing human HCM features (Fig. 1). 5' and 3' trans-splicing was evaluated in control hiPSC-CMs seven days after transduction with an AAV. Both trans-splicing approaches resulted in an efficiency of 1% compared to total amount of *MYBPC3* transcripts (Fig. 2, 3). GR therapy, using the full-length *MYBPC3* cDNA, resulted in 2.5-fold higher *MYBPC3* mRNA levels in HCM and control hiPSC-CMs (Fig. 4). Therefore cMyBP-C levels in HCM hiPSC-CMs were 81% of the control level, hypertrophy was suppressed, and gene expression was partially restored to control level in HCM hiPSC-CMs (Fig 4, 5).

# Evaluation of *MYBPC3* *trans*-Splicing and Gene Replacement as Therapeutic Options in Human iPSC-Derived Cardiomyocytes

Maksymilian Prondzynski,<sup>1,2</sup> Elisabeth Krämer,<sup>1,2</sup> Sandra D. Laufer,<sup>2,3</sup> Aya Shibamiya,<sup>2,3</sup> Ole Pless,<sup>4</sup> Frederik Flenner,<sup>1,2</sup> Oliver J. Müller,<sup>5,6</sup> Julia Münch,<sup>2,7</sup> Charles Redwood,<sup>8</sup> Arne Hansen,<sup>1,2</sup> Monica Patten,<sup>2,7</sup> Thomas Eschenhagen,<sup>1,2</sup> Giulia Mearini,<sup>1,2</sup> and Lucie Carrier<sup>1,2</sup>

<sup>1</sup>Department of Experimental Pharmacology and Toxicology, Cardiovascular Research Center, University Medical Center Hamburg-Eppendorf, 20246 Hamburg, Germany; <sup>2</sup>DZHK (German Centre for Cardiovascular Research), partner site Hamburg/Kiel/Lübeck, 20246 Hamburg, Germany; <sup>3</sup>Hamburg Zentrum für Experimentelle Therapieforschung (HEXT) Stem Cell Facility, University Medical Center Hamburg-Eppendorf, 20246 Hamburg, Germany; <sup>4</sup>Fraunhofer IME Screening-Port, 22525 Hamburg, Germany; <sup>5</sup>Department of Cardiology, Internal Medicine III, University Hospital Heidelberg, 69120 Heidelberg, Germany; <sup>6</sup>DZHK (German Centre for Cardiovascular Research), partner site Heidelberg/Mannheim, 69120 Heidelberg, Germany; <sup>7</sup>University Heart Center Hamburg, 20246 Hamburg, Germany; <sup>8</sup>Radcliffe Department of Medicine, University of Oxford, Oxford OX1 3PA, UK

**Gene therapy is a promising option for severe forms of genetic diseases. We previously provided evidence for the feasibility of *trans*-splicing, exon skipping, and gene replacement in a mouse model of hypertrophic cardiomyopathy (HCM) carrying a mutation in *MYBPC3*, encoding cardiac myosin-binding protein C (cMyBP-C). Here we used human induced pluripotent stem cell-derived cardiomyocytes (hiPSC-CMs) from an HCM patient carrying a heterozygous c.1358-1359insC *MYBPC3* mutation and from a healthy donor. HCM hiPSC-CMs exhibited ~50% lower *MYBPC3* mRNA and cMyBP-C protein levels than control, no truncated cMyBP-C, larger cell size, and altered gene expression, thus reproducing human HCM features. We evaluated RNA *trans*-splicing and gene replacement after transducing hiPSC-CMs with adeno-associated virus. *trans*-splicing with 5' or 3' pre-*trans*-splicing molecules represented ~1% of total *MYBPC3* transcripts in healthy hiPSC-CMs. In contrast, gene replacement with the full-length *MYBPC3* cDNA resulted in ~2.5-fold higher *MYBPC3* mRNA levels in HCM and control hiPSC-CMs. This restored the cMyBP-C level to 81% of the control level, suppressed hypertrophy, and partially restored gene expression to control level in HCM cells. This study provides evidence for (1) the feasibility of *trans*-splicing, although with low efficiency, and (2) efficient gene replacement in hiPSC-CMs with a *MYBPC3* mutation.**

## INTRODUCTION

In the last decade, several strategies have been developed to correct or remove gene mutations at the DNA or RNA level, including gene replacement by cDNA overexpression, CRISPR/Cas9 gene editing, exon skipping, spliceosome-mediated RNA *trans*-splicing (*trans*-splicing), and RNAi (as reviewed elsewhere<sup>1-3</sup>). Hypertrophic cardiomyopathy (HCM) is a myocardial disease with a revised estimated prevalence of 1:200 in the general population.<sup>4</sup> It is mainly character-

ized by hypertrophy of the left ventricle, increased interstitial fibrosis, and diastolic dysfunction.<sup>5</sup> Current therapies, including  $\beta$ -blockers and Ca<sup>2+</sup>-channel blockers, aim at the relief of symptoms, but they are not curative.<sup>6</sup> HCM is caused by mutations in genes encoding sarcomeric proteins. Among them, *MYBPC3*, encoding cardiac myosin-binding protein C (cMyBP-C), is the most frequently mutated gene.<sup>5,7</sup> To date more than 350 HCM-causing *MYBPC3* mutations have been reported in the literature.<sup>7</sup> The majority of *MYBPC3* mutations are truncating, leading to C-terminal-truncated cMyBP-C proteins, which were never detected in the myocardial tissue of HCM patients.<sup>8</sup>

cMyBP-C is a multidomain protein that plays a role in the regulation of cardiac function and in sarcomeric organization.<sup>9-11</sup> A growing body of evidence indicates that double heterozygous, compound heterozygous, and homozygous mutations in sarcomeric genes are associated with severe forms of cardiomyopathies.<sup>12-14</sup> Specifically, individuals carrying bi-allelic truncating *MYBPC3* mutations presented already at birth with various forms of cardiomyopathies (hypertrophic, dilated, and/or left ventricular non-compaction), which quickly developed into systolic heart failure and death within the first year.<sup>15-17</sup> For these infants, there is no curative therapy other than heart transplant. Recently, proof-of-concept studies reported the feasibility of exon skipping, *trans*-splicing, RNAi, or gene replacement

Received 22 November 2016; accepted 11 May 2017;  
<http://dx.doi.org/10.1016/j.omtn.2017.05.008>.

**Correspondence:** Lucie Carrier, Department of Experimental Pharmacology and Toxicology, University Medical Center Hamburg-Eppendorf, Martinistraße 52, 20246 Hamburg, Germany.

E-mail: l.carrier@uke.de

**Correspondence:** Giulia Mearini, Department of Experimental Pharmacology and Toxicology, University Medical Center Hamburg-Eppendorf, Martinistraße 52, 20246 Hamburg, Germany.

E-mail: g.mearini@uke.de



as gene therapy options in HCM mouse models.<sup>18–21</sup> To move this concept toward clinical application, advantage could be taken from the use of human induced pluripotent stem cell-derived cardiomyocytes (hiPSC-CMs). These cells have already been used for disease modeling of long-QT syndrome,<sup>22,23</sup> dilated cardiomyopathy,<sup>24–26</sup> and HCM,<sup>27–29</sup> and they could be used as a platform for testing different gene therapy options. In the present study, we evaluated the feasibility and efficiency of *MYBPC3* trans-splicing and gene replacement strategies in hiPSC-CMs obtained from a healthy donor and an HCM patient harboring a heterozygous truncating mutation in the *MYBPC3* gene.

*trans*-splicing involves two separate mRNAs, the target endogenous mutant pre-mRNA and an exogenous wild-type (WT) pre-*trans*-splicing molecule (PTM; as reviewed elsewhere<sup>30,31</sup>). After gene transfer of the PTMs, a splice event in *trans* can occur between the two molecules, resulting in a chimeric repaired mRNA, which is then translated into a corrected protein (Figure S1A). Beside the WT coding sequence, PTMs carry strong splice sequences and a binding domain for specific recognition of the target. Depending on the position of the mutation in the pre-mRNA, *trans*-splicing can occur in 5' or 3' mode, and PTMs will contain a splice donor or acceptor site, respectively. In the gene replacement approach, a correct copy of the defective gene, i.e., full-length WT cDNA, is provided to the cell in order to replace the non-functional and/or missing protein (Figure S1B; as reviewed elsewhere<sup>32,33</sup>). In the present work, PTMs carrying each half of the *MYBPC3* coding sequence and full-length WT *MYBPC3* cDNA were packaged into the adenovirus-associated virus serotype 9-SRLSPPS (hereafter AAV),<sup>34</sup> and analyses were done 7 days after AAV transduction.

## RESULTS

### HCM hiPSC-CMs Show Hypertrophy and cMyBP-C Haploinsufficiency

At the time of septal myectomy, the patient had an interventricular septal thickness of 26 mm, ejection fraction of >60%, and a left ventricular outflow gradient of 85 mmHg. Genetic testing of genomic DNA with a panel of 19 HCM genes revealed an insertion of a C in exon 16 of the *MYBPC3* gene (c.1358\_1359insC; Figure S2) on one allele of the HCM patient. This variant was not found in the Exome Association Consortium (ExAC) Browser, which harmonized sequencing data from more than 60,000 unrelated individuals (<http://exac.broadinstitute.org/>), supporting its causal effect. The mutation induced a frameshift and a premature termination codon (PTC) in exon 16. At the protein level, an amino acid substitution at position 454 was followed by 21 new amino acids (p.Val454CysfsX21) and truncation in the C3 domain of cMyBP-C.

Dermal fibroblasts from the HCM patient and from a healthy donor (control) were reprogrammed into hiPSCs, followed by differentiation into CMs (see the Materials and Methods). Both HCM and control hiPSC-CMs were seeded in a confluent monolayer and cultured for 7 days. hiPSC-CMs of both cell lines exhibited spontaneous beating (data not shown). After fixation, immunofluorescence analysis with an-

tibodies directed against cMyBP-C and  $\alpha$ -actinin showed a cross-striated pattern, indicating proper formation of sarcomeres (Figure 1A). Cell size, as determined by automated analysis of large numbers of cells (see the legend of Figure 1B), was significantly higher in HCM than in control hiPSC-CMs ( $3,656 \pm 201 \mu\text{m}^2$  versus  $2,213 \pm 145 \mu\text{m}^2$ ; Figure 1B). Total *MYBPC3* mRNA level was 50% lower in HCM than in control cells (Figure 1C). Mutant *MYBPC3* mRNA was not detected by Sanger sequencing or with a specific Taqman probe (data not shown). The amount of cMyBP-C protein normalized to  $\alpha$ -actinin tended to be lower ( $p = 0.064$ ) in HCM than in control hiPSC-CMs (Figures 1D and 1E). No truncated protein ( $\sim 52$  kDa) was detected in HCM cells (data not shown). The disease phenotype of HCM hiPSC-CMs was further evaluated by gene expression profile of 49 proteins involved in the regulation of cardiac hypertrophy and contraction with the nanoString nCounter Elements technology (Figure S3; Table S1). Most of the proteins associated with hypertrophy, cardiomyopathy, and/or PI3K-Akt signaling exhibited higher mRNA levels in HCM than in control CMs (green bars), whereas many proteins involved in excitation-contraction coupling or adrenergic signaling had lower mRNA levels in HCM than in control CMs (red bars).

### 5' *trans*-Splicing Is Feasible in hiPSC-CMs

We designed a 5' PTM that would be able, in principle, to repair all *MYBPC3* mutations contained in the first half of the gene. It carried the WT *MYBPC3* cDNA sequence from exon 1 to exon 21 under the control of a CM-specific promoter (*TNNT2*, human cardiac troponin T; Figure 2A). The 5' PTM included a binding domain for base pairing with a complementary sequence (120 nt) in intron 21 of the *MYBPC3* gene, a canonical 5' splice site sequence followed by a downstream intronic sequence enhancer element, which has been shown to markedly increase *trans*-splicing efficiency (Figure S4A).<sup>35</sup> To allow specific detection of *MYBPC3* *trans*-spliced mRNA and cMyBP-C protein, we included a FLAG-tag sequence at the N terminus of the coding sequence (Figure 2A). To prevent translation of the PTM, we removed the polyA signal as described previously.<sup>19</sup> For gene transfer in hiPSC-CMs, 5' PTMs were packaged into AAV. Beforehand, we tested the transduction efficiency of different MOIs of AAV-*TNNT2*-GFP in control hiPSC-CMs. The MOI of 10,000 proved to transduce >80% of hiPSC-CMs after 7 days of transduction (Figure S5).

Control hiPSC-CMs were then transduced with AAV-5' PTM or AAV-Mock (empty virus; both at an MOI of 10,000) and cultured for 7 days in 2D. Using PCR primers that amplify only *trans*-spliced *MYBPC3* transcript (Figure 2B), we obtained a specific fragment only in AAV-5' PTM-transduced hiPSC-CMs, but not in non-transduced or mock-transduced hiPSC-CMs (Figure 2C). After agarose gel extraction, sequencing of the 2,180-bp *trans*-spliced *MYBPC3* fragment validated the presence of the FLAG-tag (Figure S6A). To evaluate the effect of *trans*-splicing on *cis*-splicing, total *MYBPC3* mRNA (= *trans*-spliced + endogenous) was amplified with primers in exon 1 and exon 23 (Figure 2B). A specific amplicon was obtained in all samples without a major intensity difference among them (Figure 2C). To estimate the efficiency of 5' *trans*-splicing, cDNA from AAV-5'



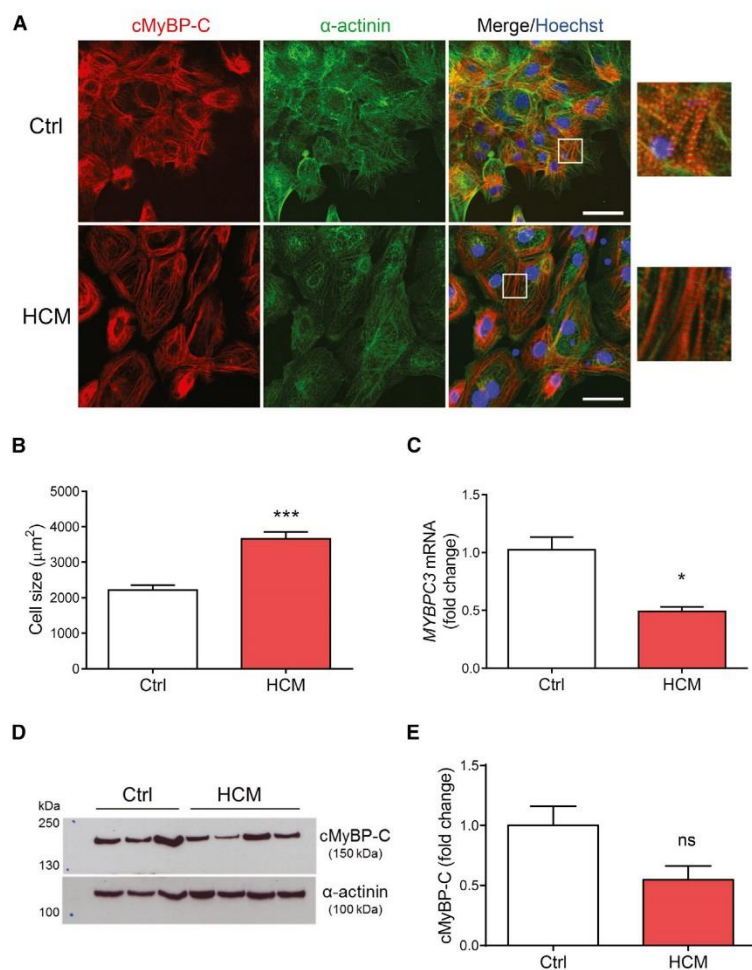


**Figure 1. Phenotypic Characterization of HCM hiPSC-Derived Cardiomyocytes**

Patient-specific (HCM) and control (Ctrl) hiPSC-derived cardiomyocytes (hiPSC-CMs) were seeded in a confluent monolayer, cultured for 7 days, and prepared for subsequent analysis. (A) Representative immunofluorescence images of HCM and control hiPSC-CMs. Both cell lines were stained with antibodies directed against cMyBP-C (red),  $\alpha$ -actinin (green), and with Hoechst33342 for nuclear staining (blue; scale bars, 50  $\mu$ m). Higher magnification images of a few sarcomeres are shown on the right panels. (B) Quantification of CM cell size. Control and HCM hiPSC-CMs were seeded in 96-well plates at a density of 10,000 cells/well, cultured for 7 days, and stained with an antibody against  $\alpha$ -actinin. Cell size was measured in 27–51 fields/well in both groups. Control hiPSC-CMs were evaluated from 33 wells of three independent experiments and HCM hiPSC-CMs from 21 wells of two independent experiments, for a total of 28,336 and 12,874 CMs, respectively. Images were taken with the Opera High-Content Screening System (PerkinElmer), and the analyses were performed with the Columbus Image Data Management and Analysis System. (C) Evaluation of *MYBPC3* mRNA levels determined by qRT-PCR with SYBR Green in control and HCM hiPSC-derived CMs ( $n = 3$ –5, with  $n =$  number of wells from one transduction experiment). (D) Western blot of control and HCM hiPSC-CMs stained with antibodies directed against cMyBP-C.  $\alpha$ -actinin was used as the loading control. (E) Quantification of cMyBP-C protein levels in control and HCM hiPSC-CMs normalized to  $\alpha$ -actinin and related to control ( $n = 3$ –4, with  $n =$  number of wells from two independent transduction experiments). Values are expressed as mean  $\pm$  SEM (\* $p < 0.05$  and \*\*\* $p < 0.001$ , unpaired Student's  $t$  test). cMyBP-C, cardiac myosin-binding protein C; CMs, cardiomyocytes; Ctrl, control.

PTM-transduced hiPSC-CMs was used to amplify either *trans*-spliced or total *MYBPC3* mRNA by PCR (25 cycles). PCR fragments were column-purified and further analyzed by qPCR using a common primer pair for amplification of the same fragment in all *MYBPC3* transcripts. The percentage of *trans*-spliced *MYBPC3* mRNA was calculated using a standard dilution ( $2 \times 10^9 - 2 \times 10^1$  copy number) of a plasmid encoding the full-length WT *MYBPC3* cDNA. Samples and standards were amplified with the same primer pair, enabling us to specifically calculate a 5' *trans*-splicing efficiency of 0.96% (Figure 2D). FLAG immunoprecipitation experiments to detect *trans*-spliced cMyBP-C protein were not successful (data not shown), probably due to low *trans*-splicing efficiency.

### 3' *trans*-Splicing Is Feasible in hiPSC-CMs

We designed a 3' PTM, that would principally be able to repair all *MYBPC3* mutations contained in the second half of the gene. It car-

minus to discriminate the *trans*-spliced *MYBPC3* mRNA and cMyBP-C protein from endogenous ones. To prevent any translation of the 3' PTM, no ATG sequence was introduced. To allow 3' *trans*-splicing, we also inserted in the 3' PTM a binding domain (same sequence as in 5' PTM) targeting intron 21 followed by a linker sequence, a branch point, a polypyrimidine tract, and a 3' splice site (Figure S4B). After packaging in AAV, control hiPSC-CMs were transduced with AAV-3' PTM or AAV-Mock (MOI 10,000), and they were cultured for 7 days in 2D prior to collection. Primer pairs for detection of *trans*-spliced or total *MYBPC3* mRNA are shown in Figure 4B. A specific 1,874-bp amplicon was obtained in the AAV-3' PTM-transduced sample with primers designed to recognize *trans*-spliced *MYBPC3* mRNA. Sequencing of this amplicon validated the presence of the FLAG sequence (Figures 3B and 3C; Figure S6B). A fragment of similar size was detected in the non-transduced sample, but sequencing did not reveal the FLAG sequence (data not shown).

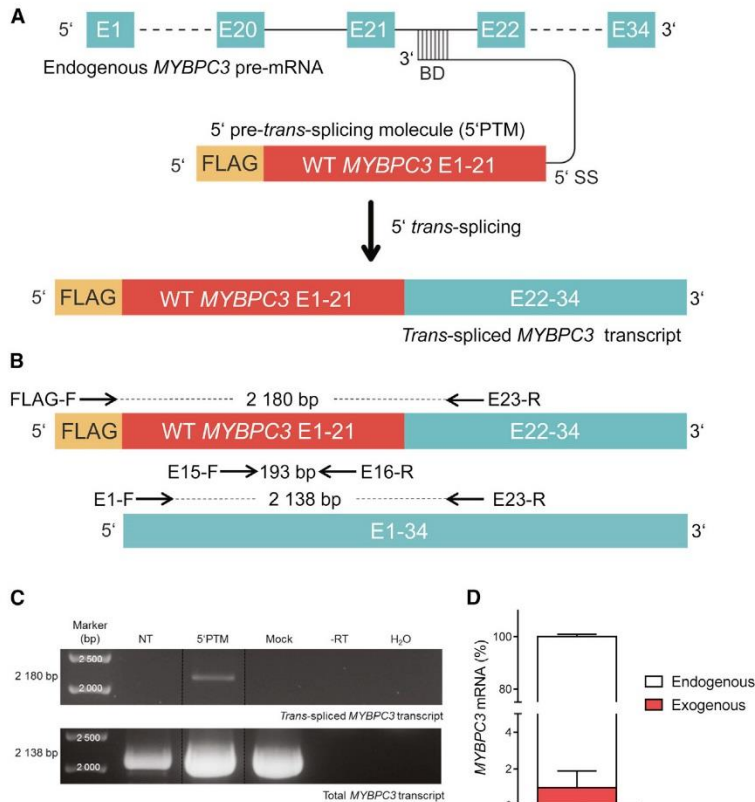


**Figure 2. 5' trans-splicing in Control hiPSC-Derived Cardiomyocytes**

(A) Schematic representation of 5' trans-splicing. 5' pre-trans-splicing molecules (5' PTMs) carry a 5' FLAG-tagged wild-type (WT) *MYBPC3* cDNA sequence from from exon 1 to exon 21, conserved 5' splice donor site (5' SS) sequences, and a binding domain (BD) targeting intron 21. Upon successful binding of 5' PTM to the endogenous *MYBPC3* pre-mRNA, 5' trans-splicing can occur and results in a trans-spliced *MYBPC3* mRNA. (B) Schematic illustration of primer pairs used to amplify either only trans-spliced or trans-spliced and/or endogenous (total) *MYBPC3* mRNAs. The primer pair FLAG-F/E23-R was used to generate a 2,180-bp fragment corresponding to the trans-spliced *MYBPC3* mRNA. trans-spliced and/or endogenous *MYBPC3* mRNA was amplified either using the primer pair E1-F/E23-R (2,138-bp fragment) or the primer pair E15-F/E16-R (193-bp fragment). (C) hiPSC-derived cardiomyocytes (hiPSC-CMs) were transduced with AAV-5' PTM or AAV-Mock (*TNNT2* promoter without insert) at an MOI of 10,000 and cultured in 2D for 7 days prior to harvesting. Representative agarose gel of RT-PCR, using specific primer pairs for trans-spliced and total *MYBPC3* mRNA, is shown ( $n = 5$ , from three independent transductions). (D) Determination of the percentage of trans-spliced *MYBPC3* mRNA by qRT-PCR. In a first round of PCR, either trans-spliced (FLAG-F/E23-R primers) or total (E1-F/E23-R primers) *MYBPC3* mRNAs were amplified from cDNA of AAV-5' PTM-transduced hiPSC-CMs. PCR fragments were column-purified and used in qPCR, together with a standard dilution of a plasmid encoding full-length wild-type *MYBPC3* cDNA, using a common primer pair (E15-F/E16-R primers). Data are expressed as mean  $\pm$  SEM with  $n = 3$  (three wells of one transduction experiment). AAV, adeno-associated virus; bp, base pair; CMs, cardiomyocytes; E, exon; F, forward; hiPSC, human induced pluripotent stem cell; NT, non-transduced; MOI, multiplicity of infection; R, reverse; RT, reverse transcriptase; WT, wild-type.

Similarly, PCR fragments also appeared in the AAV-3' PTM-transduced but without reverse transcriptase sample, indicating nonspecific binding of the primers to the endogenous mRNA. RT-PCR with a primer pair that amplified total *MYBPC3* mRNA showed a signal of similar intensity in non-transduced and in AAV-transduced samples (Figure 3C). As was done for 5' trans-splicing, the efficiency of 3' trans-splicing was determined by qRT-PCR with a standard dilution ( $2 \times 10^9 - 2 \times 10^1$  copy number) of the same plasmid carrying the full-length WT *MYBPC3* cDNA. The concentration of trans-spliced *MYBPC3* mRNA reached 1% of the total (Figure 3D). Similar to 5' trans-splicing, the trans-spliced cMyBP-C protein was not detected after FLAG immunoprecipitation (data not shown).

#### Gene Replacement in HCM hiPSC-CMs Partially Corrects cMyBP-C Haploinsufficiency and Reduces Cell Hypertrophy

To evaluate a gene replacement therapy option, the FLAG-tagged WT *MYBPC3* cDNA under the control of the *TNNT2* promoter was packaged in AAV (AAV-FLAG-*MYBPC3*). After transduction (MOI 10,000) of control and HCM hiPSC-CMs, cells were cultured for

7 days in 2D prior to harvesting. RT-PCR with specific primers for exogenous *MYBPC3* transcript revealed a specific fragment in both control and HCM transduced hiPSC-CMs (Figures 4A and 4B). A signal of lower intensity was also obtained in AAV-transduced samples, which were not retrotranscribed, corresponding to the transgene. The transcription of the entire FLAG-*MYBPC3* cDNA sequence was also validated (data not shown). Total *MYBPC3* transcript was amplified using a common primer pair in all samples, transduced or not (Figures 4A and 4B). To quantify the overall level of *MYBPC3* mRNA after transduction, a qRT-PCR was performed with a primer pair recognizing both exogenous and endogenous *MYBPC3* transcripts (Figures 4A and 4C). About 2.5-fold overexpression of *MYBPC3* was obtained in both control and HCM transduced hiPSC-CMs over the non-transduced cells (Figure 4C). To evaluate the efficiency of gene replacement, RT-PCR with specific primers to amplify either exogenous or total *MYBPC3* transcripts was performed in control and HCM transduced samples. PCR fragments were column-purified and used further for qPCR with a common primer pair, together with a standard dilution curve of a plasmid carrying

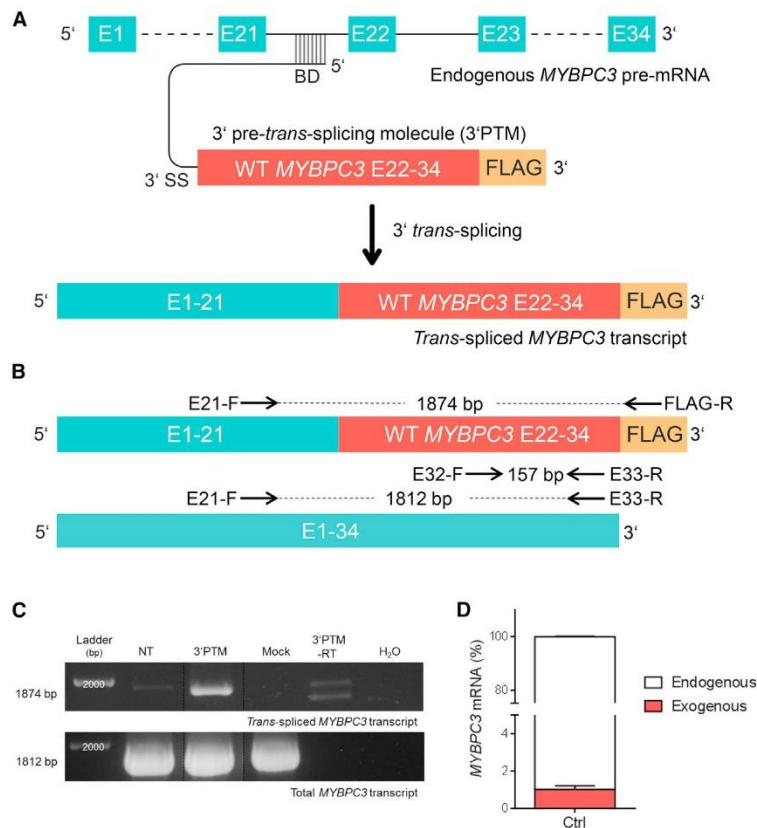


**Figure 3. 3' *trans*-Splicing in Control hiPSC-Derived Cardiomyocytes**

(A) Schematic illustration of 3' *trans*-splicing. 3' pre-trans-splicing molecules (3' PTMs) contain a BD complementary to *MYBPC3* intron 21, conserved 3' splice donor site sequences (3'SS), and a 3'-FLAG-tagged wild-type (WT) *MYBPC3* cDNA sequence from exon 22 to exon 34. Upon successful binding of the 3' PTM to the endogenous *MYBPC3* pre-mRNA, 3' *trans*-splicing can occur and results in *trans*-spliced *MYBPC3* mRNA. (B) Schematic representation of primer pairs used to amplify either only *trans*-spliced *MYBPC3* mRNA or *trans*-spliced and/or endogenous (total) *MYBPC3* mRNA. The primer pair E21-F/FLAG-R amplifies a 1,874-bp fragment specific of *trans*-spliced *MYBPC3* mRNA. The primer pairs E21-F/E33-R and E32-F/E33-R amplify in both *trans*-spliced and endogenous *MYBPC3* mRNA a 1,812-bp and a 157-bp fragment, respectively. (C) Control hiPSC-CMs were transduced with AAV-3' PTM or AAV-Mock (MOI 10,000) for 1 week prior to harvesting. Representative agarose gel of RT-PCR, using specific primer pairs for *trans*-spliced and total *MYBPC3* mRNA, is shown ( $n = 9$  from four independent transductions). (D) Determination of the percentage of *trans*-spliced *MYBPC3* mRNA by qRT-PCR was performed as described in Figure 2D, with the common primer pair E32-F/E33-R. Data are expressed as mean  $\pm$  SEM with  $n = 5$  (five wells of one transduction experiment). bp, base pair; CMs, cardiomyocytes; E, exon; F, forward; hiPSC, human induced pluripotent stem cell; NT, non-transduced; MOI, multiplicity of infection; R, reverse; RT, reverse transcriptase; WT, wild-type.

the full-length wild-type *MYBPC3* cDNA sequence ( $2 \times 10^9 - 2 \times 10^1$  copy number). In control and HCM hiPSC-CMs, exogenous *MYBPC3* transcript level reached 70% and 57% of total, respectively (Figure 4D). The level of cMyBP-C protein was determined by western blot analysis in protein samples, normalized to  $\alpha$ -actinin content and related to non-transduced control hiPSC-CM sample (Figures 4E and 4F). The total cMyBP-C protein level did not differ between transduced and non-transduced control hiPSC-CMs. In contrast, cMyBP-C protein level was 2.5-fold higher ( $p < 0.05$ , Student's *t* test) in transduced than in non-transduced HCM hiPSC-CMs, reaching 81% of the cMyBP-C level of the non-transduced control sample (Figures 4E and 4F).

Sarcomere organization after transduction of control and HCM hiPSC-CMs with AAV-FLAG-*MYBPC3* was evaluated by immunofluorescence analysis with anti-FLAG and anti- $\alpha$ -actinin antibodies. FLAG-cMyBP-C protein was properly organized in doublets at the A-band of the sarcomere, well alternating with  $\alpha$ -actinin located at the Z-disk (Figure 5A). Finally, we evaluated the impact of *MYBPC3* gene transfer on cell size. Cell size was significantly higher in non-transduced HCM than in control hiPSC-CMs (Figure 5B). *MYBPC3*

gene transfer did not affect cell size in control hiPSC-CMs ( $2,715 \pm 168 \mu\text{m}^2$  versus  $2,665 \pm 120 \mu\text{m}^2$  in non-transduced control). In contrast, cell size was significantly lower in *MYBPC3*-transduced than in non-transduced HCM hiPSC-CMs ( $3,205 \pm 139 \mu\text{m}^2$  versus  $4,409 \pm 217 \mu\text{m}^2$ ), and it did not differ from non-transduced control hiPSC-CMs (Figure 5B). *MYBPC3* gene replacement lowered mRNA levels of several proteins involved in cardiomyopathy and PI3K-Akt signaling, and it increased mRNA levels of calcium-handling proteins in HCM hiPSC-CMs (Figure 6).

## DISCUSSION

In this study, we report the principal feasibility of two gene therapy options for HCM in hiPSC-CMs from a healthy donor and an HCM patient carrying a *MYBPC3* truncating mutation. While our data suggest that *trans*-splicing efficiency is too low to be a therapeutic option to treat severe forms of HCM, the *MYBPC3* gene replacement strategy looks promising, particularly for its ability to circumvent haploinsufficiency of cMyBP-C (restoration of a correct amount of protein) and to reduce CM hypertrophy. Numerous studies have used hiPSC-CMs as a tool for disease modeling of different cardiac diseases, including HCM with *MYBPC3* mutations.<sup>22–29,36–39</sup>

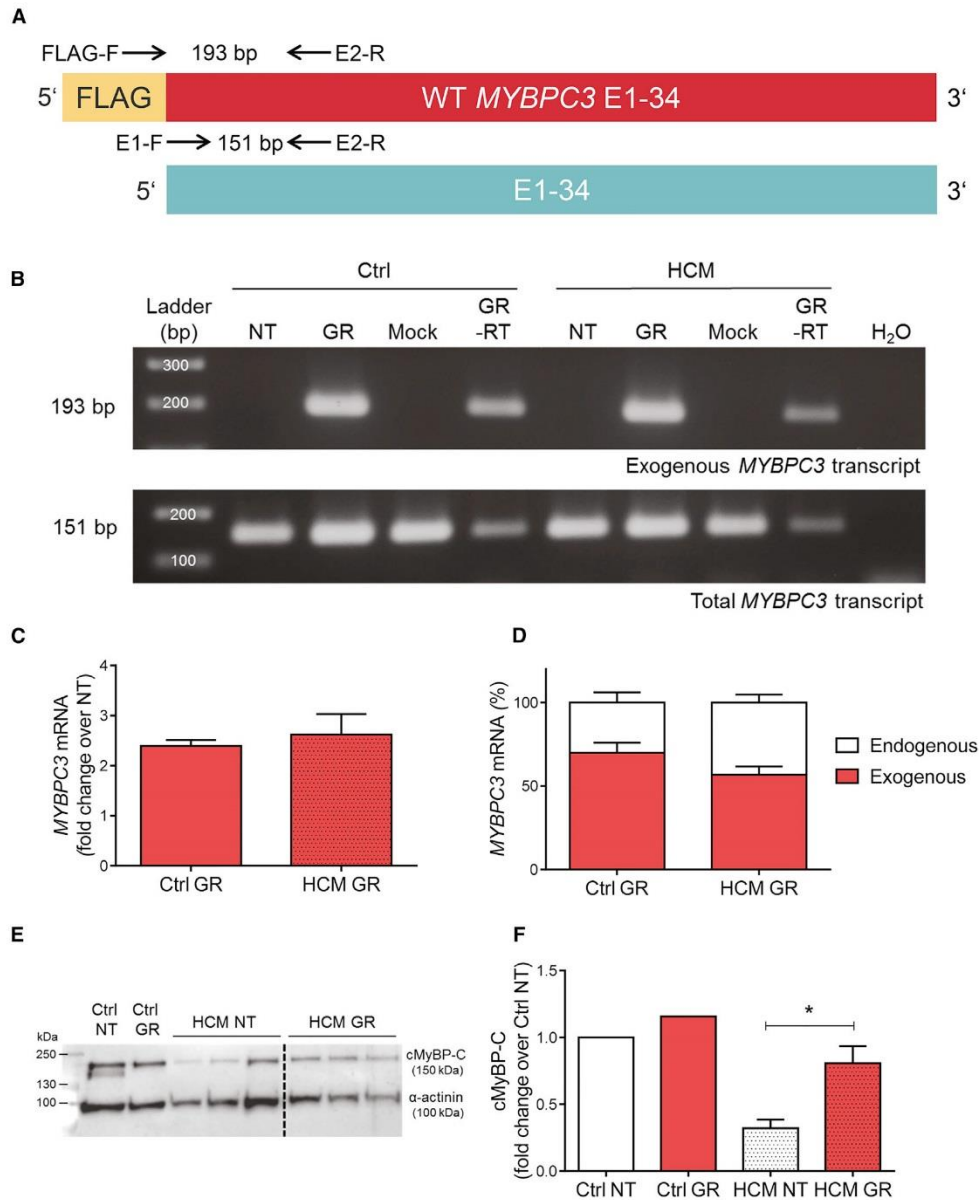


**Figure 4. Proof-of-Concept of MYBPC3 Gene Replacement in Human iPSC-Derived Cardiomyocytes**

(A) Schematic illustration of full-length wild-type (WT) exogenous and total MYBPC3 cDNA/mRNA sequence (exons 1–34). Location of primer pairs and size of amplicons are shown. The primer pair FLAG-F/E2-R amplifies exclusively the exogenous MYBPC3 sequence (amplicon size: 193 bp). The primer pair E1-F/E2-R is suitable for amplification of both exogenous and endogenous (total) MYBPC3 sequence (amplicon size: 151 bp). (B) Control and HCM hiPSC-CMs were transduced with AAV-FLAG-MYBPC3 (GR) or AAV-Mock (Mock) at an MOI of 10,000 and cultured in 2D for 7 days before harvesting. Representative RT-PCR using primers shown in (A) for specific amplification is shown ( $n = 3$ , one well each from three independent transductions). (C) Evaluation of MYBPC3 transcript levels in GR-transduced control and HCM hiPSC-CMs by qRT-PCR with a common primer pair ( $n = 3$ – $5$ , with  $n$  = number of wells of one transduction experiment). (D) Determination of the percentage of exogenous MYBPC3 mRNA by qRT-PCR. In a first round of RT-PCR, either exogenous (FLAG-F/E2-R primers) or total (E1-F/E2-R primers) MYBPC3 transcripts were amplified in control and HCM GR samples. After column purification of PCR fragments, a qPCR with a common primer pair (E1-F/E2-R) was performed together with a standard dilution of a plasmid encoding full-length (legend continued on next page)

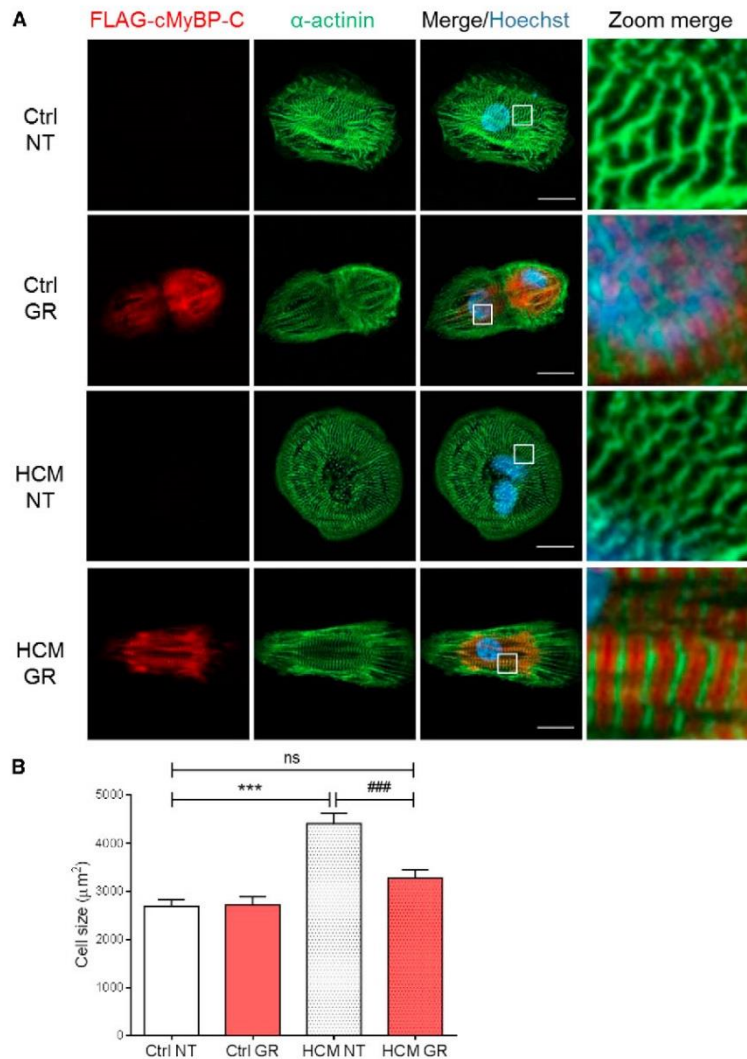


**Figure 5. Phenotypic Characterization of Control and HCM hiPSC-Derived Cardiomyocytes after MYBPC3 Gene Transfer**

(A) Representative images of non-transduced (NT) and transduced (GR) control (Ctrl) and HCM hiPSC-CMs after immunofluorescence staining with anti-FLAG and anti- $\alpha$ -actinin antibodies. Images were taken with a Zeiss LSM 800 microscope (scale bars, 20  $\mu$ m). Higher magnification images of a few sarcomeres are shown on the right panel. (B) Quantification of CM cell size. NT and GR control and HCM hiPSC-CMs were seeded in 96-well plates at a density of 10,000 cells/well, cultured for 1 week, and stained with antibodies against FLAG-tag and  $\alpha$ -actinin. Low-resolution images of >100 cells in each group from six wells of one experiment each (Ctrl NT n = 108; Ctrl GR n = 110; HCM NT n = 114; HCM GR n = 133) were taken with the Zeiss LSM 800 microscope and analyzed with Fiji software (ImageJ). Data are expressed as mean  $\pm$  SEM (\*\*\*p < 0.001, two-way ANOVA plus Bonferroni post-test; ###p < 0.001, unpaired Student's t test).

a >110-fold higher odds ratio to cause HCM.<sup>40</sup> Second, this specific mutation was not found in the population of about 60,000 unrelated individuals of the ExAC Browser (<http://exac.broadinstitute.org/>). HCM hiPSC-CMs revealed larger cell size, higher mRNA levels of proteins associated with hypertrophy, such as four and a half LIM domains 1 (*FHL1*), S100 calcium-binding protein A4 (*S100A4*), and connective tissue growth factor (*CTGF*), and lower mRNA levels of proteins involved in calcium handling, such as *PLN*, *SERCA2A* (*ATP2A2*), ryanodine receptor (*RYR2*), and inhibitor 1 (*PPP1R1A*) than control CMs, all hallmarks of HCM. This is in agreement with previous findings using HCM hiPSC-CMs or human embryonic stem cell (hESC) carrying *MYBPC3* mutations.<sup>28,29,37,41</sup> While Dambrot et al.<sup>37</sup> described that the supplementation of serum in culture medium masks the hypertrophic phenotype in 2D culture of hiPSC-CMs, in the present study

the enlarged cell size was evident already in the presence of serum, as also reported by Ojala et al.<sup>28</sup>

However, so far only one study used the gene replacement strategy to correct a phospholamban (*PLN*) mutation associated with dilated cardiomyopathy in vitro.<sup>39</sup>

In addition to hypertrophy, the HCM CMs used in the present work presented another hallmark of the *MYBPC3*-causing HCM, namely haploinsufficiency (for review, see Marston et al.<sup>42</sup>). Indeed, the amounts of *MYBPC3* mRNA and cMyBP-C protein were ~50% of

the enlarged cell size was evident already in the presence of serum, as also reported by Ojala et al.<sup>28</sup>

In addition to hypertrophy, the HCM CMs used in the present work presented another hallmark of the *MYBPC3*-causing HCM, namely haploinsufficiency (for review, see Marston et al.<sup>42</sup>). Indeed, the amounts of *MYBPC3* mRNA and cMyBP-C protein were ~50% of

WT *MYBPC3* cDNA (n = 3, three wells of one transduction experiment). (E) Western blot performed on pooled protein samples (n = 6, from three independent transduction experiments) of non-transduced (NT) or transduced (GR) control and single protein samples (n = 3, three wells of one transduction experiment) of HCM hiPSC-CMs with anti-cMyBP-C and anti- $\alpha$ -actinin antibodies. (F) Quantification of cMyBP-C level normalized to  $\alpha$ -actinin and related to control NT pooled sample. Data are expressed as mean  $\pm$  SEM (\*p < 0.05, unpaired Student's t test). E, exon; F, forward; NT, non-transduced; MOI, multiplicity of infection; R, reverse; WT, wild-type.

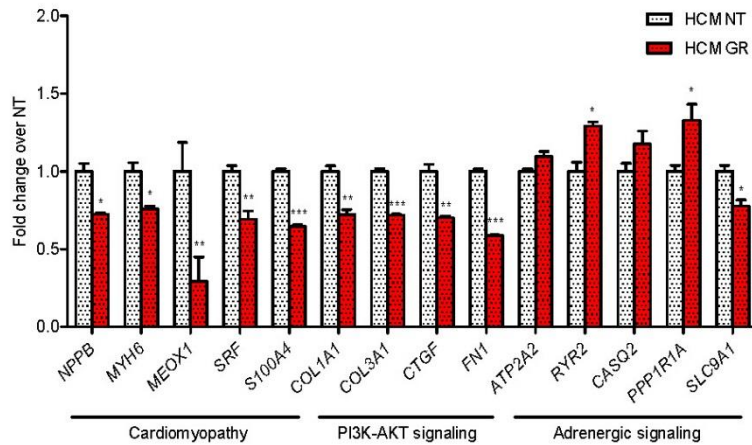


**Figure 6. Gene Expression Analysis of HCM hiPSC-Derived Cardiomyocytes in the Absence of or after *MYBPC3* Gene Transfer**

The mRNA levels of transduced (GR) and non-transduced (NT) HCM hiPSC-CMs were determined with the nanoString nCounter Elements technology, and related to NT CMs. Data are expressed as mean  $\pm$  SEM (\* $p < 0.05$ , \*\* $p < 0.01$ , and \*\*\* $p < 0.001$ , unpaired Student's *t* test;  $n = 3$ , with  $n =$  number of wells from one transduction experiment).

the control hiPSC-CMs. Furthermore, the mutant nonsense mRNA was not detected, suggesting that it is degraded by the nonsense-mediated mRNA decay (NMD), as previously shown in *Mybpc3*-targeted knockin HCM mice.<sup>43</sup> The location of the PTC at >50–55 nt upstream of the most 3' exon-exon junction perfectly matches the NMD rules,<sup>44</sup> therefore supporting its NMD-mediated degradation. The expected 52-kDa truncated cMyBP-C protein was also not detected by western blot, in agreement with previous observations in human myocardial samples with truncating *MYBPC3* mutations.<sup>8,45</sup> Thus, the combination of a unique truncating *MYBPC3* mutation, cMyBP-C haploinsufficiency, and CM hypertrophy makes this hiPSC cell line a good test bed for the application of different treatment options for HCM.

In the last years, mRNA *trans*-splicing has been evaluated both in vitro and in vivo as an alternative option for currently incurable genetic diseases, such as Duchenne muscular dystrophy and spinal muscular atrophy (as reviewed elsewhere<sup>30,31</sup>). In the case of HCM-associated *MYBPC3* mutations, the *trans*-splicing approach was appealing because by generating only two PTMs covering the first and the second half of the *MYBPC3* mRNA, one could principally repair all the mutations and, therefore, treat 40%–60% of all HCM patients.<sup>6,7</sup> In addition, and in contrast to exon skipping mediated by antisense oligonucleotides (AONs), *trans*-splicing is expected to result in a repaired full-length and functional cMyBP-C protein. Furthermore, FDA or EMA authorization for marketing of two PTMs as new medicinal products would be easier and quicker than for several AONs.

In the present study, we showed the feasibility of both 5' and 3' *trans*-splicing in control hiPSC-CMs. However, we did not test these approaches in HCM hiPSC-CMs, since the efficiency of the process was low and we were unable to detect repaired cMyBP-C protein. This supports our previous data obtained in vivo in *Mybpc3*-targeted knockin mice, in which the low amount of repaired cMyBP-C protein produced by 5' *trans*-splicing was not sufficient to prevent the development of the cardiac disease phenotype.<sup>19</sup> Efficient *trans*-splicing

depends on different factors, such as efficient delivery of PTMs to desired cell type and especially PTM design.<sup>30</sup> Increasing the number of viral particles used for transduction could be difficult, since at a certain point AAV turned to be toxic for the cells (data not shown). On

the other hand, PTM design could be improved, particularly for the binding domain. To have approximately the same packaging size for the 5' PTM and 3' PTM, we chose to target intron 21 in the *MYBPC3* gene. The binding domain covered 120 nt (of 246) and was located roughly in the middle. However, we included highly conserved splice donor and acceptor sites in the 5' PTM and 3' PTM, respectively, which could be even stronger than the corresponding sequences in *MYBPC3* intron 21. We are aware that additional systematic testing of different lengths and complementary regions might have led to higher binding affinities for the endogenous pre-mRNA and, therefore, to higher *trans*-splicing efficiencies. Further optimization should be done in the future. Nevertheless, this is the first proof of concept of *trans*-splicing in hiPSC-CMs.

Gene replacement by cDNA overexpression is another very attractive treatment option for sarcomeric cardiomyopathies. Indeed, we recently demonstrated that AAV-mediated delivery of full-length WT *Mybpc3* cDNA in homozygous *Mybpc3*-targeted knockin mice not only prevented the development of cardiac hypertrophy and dysfunction, by increasing the amount of cMyBP-C protein, but also suppressed the expression of the endogenous mutant alleles.<sup>21</sup> Exogenous expression of a sarcomeric protein is expected to replace in part or completely the endogenous counterpart, since the sarcomere is a tightly regulated system with a preserved stoichiometry of all structural components.<sup>46</sup> This is the case in this study for the control cell line since *MYBPC3* gene transfer resulted in a 2.4-fold higher level of *MYBPC3* mRNA without change in the level of full-length cMyBP-C protein. Similarly, *MYBPC3* gene transfer resulted in a 2.6-fold higher amount of *MYBPC3* mRNA in HCM cells. Importantly and because the basal level was lower than in control cell lines, the cMyBP-C amount after gene transfer in HCM CMs reached 81% of the control cell line. In this condition, we expected at least a partial correction of the disease phenotype, since we previously showed that restoration of 80% of the cMyBP-C level by *MYBPC3* gene transfer partially restores the disease phenotype of engineered heart tissue derived from *Mybpc3*-deficient mice.<sup>47</sup> Indeed, the partial restoration

of cMyBP-C haploinsufficiency was sufficient to suppress hypertrophy in HCM CMs. Exogenous FLAG-cMyBP-C proteins were properly incorporated into the sarcomere in both cell lines. *MYBPC3* gene replacement had a positive effect on mRNA levels of proteins associated with hypertrophy or calcium handling. For instance, serum response factor (*SRF*) and *S100A4*, which are known to be higher in cardiomyopathies,<sup>48,49</sup> were significantly reduced after 7 days of *MYBPC3* therapy. In addition, levels of mRNAs encoding proteins belonging to the PI3K-Akt Kyoto Encyclopedia of Genes and Genome (KEGG) pathway, such as *CTGF*, collagens (*COL1A1* and *COL3A1*), and fibronectin (*FNI*), were significantly reduced. The mechanism by which the latter are regulated by gene therapy is not certain, but it could be related to paracrine factors mediating the crosstalk between CMs and fibroblasts (as reviewed elsewhere<sup>50,51</sup>). Finally, gene therapy increased mRNA levels of calcium-handling proteins, suggesting improvement of the cardiac contraction. We are aware that a weakness of the findings reported here concerns the comparison of the diseased line to an unrelated control and not to a corrected isogenic hiPSC line. However, in line with our findings, adenoviral-mediated *MYBPC3* gene delivery for 7 days restored the amount of cMyBP-C protein toward WT level and prevented hypertrophy in CMs derived from hESCs.<sup>41</sup>

In conclusion, our findings support gene replacement by overexpression of *MYBPC3* cDNA as a promising therapeutic option, particularly for infants with bi-allelic truncating *MYBPC3* mutations.<sup>15–17</sup> This causal therapy could prolong and improve quality of life of these affected infants for whom no other therapy exists except heart transplantation. The evaluation of the efficacy of therapeutic options in a human cellular model, such as hiPSC-CMs, represents an intermediate step toward clinical application for these infants. Further studies with large animal models of severe forms of cardiomyopathy are still required to test AAV doses and delivery before going to first-in-patient.

## MATERIALS AND METHODS

### Vector Design

The 5' PTM was obtained by fusion PCR of *MYBPC3* exon 1–21 coding sequence (PCR1) and the binding domain in intron 21 (PCR2) with partially overlapping primers. The list of primers is given in Table S2. The amplicon of PCR1 was obtained with a forward primer (F5-1) containing the *NheI* restriction site, the FLAG sequence, and the first 16 coding nt of *MYBPC3* exon 1. The reverse primer (R5-1) for PCR1 contained the BamHI restriction site, the downstream intronic splicing enhancer (DISE) element sequence, followed by the 5' canonical splice donor site and the last 15 nt of *MYBPC3* exon 21. The *MYBPC3* coding sequence was amplified from the pSPORT-CMV-*MYBPC3*, clone BC151211.1 (Thermo Scientific). The amplicon of PCR2 was obtained with a forward primer (F5-2) containing a few nucleotides of the DISE, a BamHI restriction site, and 18 nt of intron 21. The reverse primer (R5-2) comprised an *NotI* restriction site and 18 nt of intron 21. Amplicons obtained in PCR1 and PCR2 were then used as templates for a third (fusion) PCR with primers F5-1 and R5-2. The 3' PTM was obtained by fusion PCR of three different PCRs. PCR1 was performed to amplify the

binding domain in intron 21 using a forward primer (F3-1) containing an *NheI* restriction site followed by 18 nt of *MYBPC3* intron 21 and a reverse primer (R3-1) comprising 14 nt of the linker sequence, a BamHI restriction site, and 18 nt of *MYBPC3* intron 21. PCR2 was performed to amplify the 3' splicing sequences with forward primer F3-2 (same sequence as R3-1) and reverse primer (R3-2) carrying 10 nt of *MYBPC3* exon 22, 3' canonical splice acceptor site sequence, and the polypyrimidine tract. PCR3 was performed to amplify the *MYBPC3* coding sequence from exon 22 to exon 34 with a forward primer F3-3 (same sequence as R3-2) and a reverse primer R3-3 carrying an *NotI* restriction site, the stop codon TGA, the FLAG sequence, and 12 nt of exon 34. PCR1 and PCR2 were then used as templates in PCR4 with primers F3-1 and R3-2 and finally PCR4 and PCR3 were fused in PCR5 with primers F3-1 and R3-3.

### Production and Titration of AAV Particles

For production of AAV vectors, HEK293T cells were triple transfected with modified *rep2/cap9*-plasmid p5E18-VD-2/9-SLRSPPS,<sup>34</sup> plasmid pDGΔVP containing adenovirus helper functions, and one of the ITR-containing plasmids (scAAV-TNNT2-EGFP,<sup>52</sup> pGG2-TNNT2-FLAG-*MYBPC3*, pGG2-TNNT2-5' PTM, or pGG2-TNNT2-3' PTM, with FLAG-*MYBPC3*, 5' PTM, and 3' PTM inserted by *NheI* and *NotI*). Transfection, harvesting, and purification were performed as described previously.<sup>34</sup> In brief, cells were transfected with PEI (Polysciences), harvested after 48–72 hr cells by Trypsin-EDTA, and lysed in cell lysis buffer (50 mM Tris-Cl [pH 8.5], 150 mM NaCl, and 5 mM MgCl<sub>2</sub>). Cell lysates were sonicated with a Sonorex TK device for 1 min at 48 W (Bandelin) and treated with 100 U Benzoxase (Sigma-Aldrich) per milliliter of lysate for 30 min at 37°C. AAV particles were then purified by iodixanol density gradient ultracentrifugation, desalted (ZebaSpin desalting columns, recommended for processing compounds >7,000 Da [7 MWCO]; Thermo Fisher Scientific) from 40% iodixanol to 1× PBS, followed by concentration using Vivaspin6 columns (10 MWCO, Sartorius).

### Generation of Patient-Specific hiPSC Line

The HCM patient was recruited in the outpatient clinic at the University Heart Center Hamburg and provided written informed consent for the use of fibroblasts. A skin biopsy was taken, washed in PBS, minced, and placed in a six-well plate in fibroblast medium (DMEM with 10% fetal bovine serum [FBS, PAA], 2 mM L-glutamine, and 0.5% penicillin and streptomycin; all Life Technologies). Dermal fibroblasts growing out of the explants were collected for passaging or cryopreservation and used for subsequent reprogramming at passage 5. The reprogramming was performed according to previously published protocols with retroviruses encoding the human transcription factors OCT3/4, SOX2, KLF4, and L-MYC.<sup>53–55</sup>

### CM Differentiation, AAV Transduction, and Culture

CM differentiation from hiPSCs was performed following a three-step protocol with generation of embryoid bodies (EBs) in spinner flasks as described.<sup>56,57</sup> After dissociation with collagenase 2, beating CMs were transduced in suspension for 1 hr at 37°C with AAV at an MOI of 10,000. Transduced and non-transduced CMs were plated on

Geltrex-coated (1:100, Gibco) 12-well or 96-well plates at a density of 440,000 cells/well or 10,000 cells/well, respectively. CMs were maintained in culture as a monolayer in DMEM (10% heat inactivated fetal calf serum [FCS, Gibco], 0.1% insulin [Sigma-Aldrich], and 0.5% penicillin/streptomycin [Gibco]) for 7 days at 37°C and 10% CO<sub>2</sub> prior to further analyses.

#### Immunofluorescence Staining of hiPSC-CMs

Human iPSC-CMs were cultured for 7 days in 96-well plates (µclear, Greiner), then rinsed once with pre-warmed 1× PBS and fixed with Histofix (Carl Roth) for 20 min at 4°C. After washing two times in cold 1× PBS, hiPSC-CMs were incubated with primary antibodies directed against the M-motif of cMyBP-C (1:200, custom made), FLAG (1:800, Sigma), and α-actinin (1:800, Sigma); diluted in permeabilization buffer (1× PBS [Gibco], milk powder 3% [w/v, Carl Roth], and Triton X-100 0.1% [Carl Roth]); and incubated overnight at 4°C under gentle agitation. After washing two times in cold 1× PBS, hiPSC-CMs were incubated with secondary antibodies anti-mouse Alexa Fluor 488 (1:800, Life Technologies) and anti-rabbit Alexa Fluor 546 (1:800, Life Technologies), diluted in permeabilization buffer, and incubated for 1–2 hr at room temperature under gentle agitation and protected from light. In a final step, Hoechst 33342 (1:2,500, Thermo Fisher Scientific) diluted in 1× PBS was added to the wells and incubated for an additional 20 min. After washing two times in 1× PBS, hiPSC-CMs were ready for subsequent analysis in the Opera High-Content Screening System (PerkinElmer) or by confocal microscopy using a Zeiss LSM 800 microscope with Airyscan technology.

#### Measurement of CM Size

For quantification of hiPSC-CMs and for cell size analysis, the Opera High-Content Screening System and the Zeiss LSM 800 with Airyscan technology system were used. For Opera analysis, stained hiPSC-CMs in 96-well plates were loaded into the microscope, and, depending on how many wells were included in the analysis, 500–2,500 images were taken in 10× magnification. Those images were transferred in the Columbus Image Data Management and Analysis System (PerkinElmer). Columbus delivers pre-tested scripts, which were modified according to the characteristics of the used hiPSC-CMs. In this process, single building blocks were defined and accustomed to the hiPSC-CMs. Using the customized script, bulk analyses of the experiments were done and cell parameters of interest were obtained. For confocal microscopy, hiPSC-CMs were stained in 96-well plates and >100 images per sample were recorded, prepared according to the Opera analysis. Cell sizes from confocal images were measured by using Fiji software (ImageJ). Quality criteria for hiPSC-CM inclusion were set for single cells with well-formed sarcomeres.

#### RNA Isolation and Expression Analysis

Total RNA was extracted from hiPSC-CMs using TRIzol Reagent (Life Technologies), following the manufacturer's protocol. The conversion of cDNA was performed with SuperScript III First-Strand Synthesis System (Invitrogen), according to the manufacturer's in-

structions. For reverse transcription, oligo(dT) primers supplied in the kit and 200 ng extracted RNA were used. Touchdown RT-PCR to detect different *MYBPC3* transcripts in 5' or 3' *trans*-splicing experiments (63°C–58°C and 67°C–62°C, respectively) was performed using Phusion Hot Start II High-Fidelity DNA Polymerase (Thermo Fisher Scientific) in a total volume of 20 µL for 35 cycles, according to the instructions of the manufacturer's protocol. The qRT-PCR was performed in triplicates with SYBR-Green (Fermentas) according to the manufacturer's instructions. Glyceraldehyde 3-phosphate dehydrogenase (*GAPDH*) was used as the housekeeping gene. The target sequences were amplified during 40 cycles in an AbiPrism7000HT cyclor (Applied Biosystems). For expression analysis with the nanoString nCounter Elements technology, a total amount of 50 ng RNA was hybridized with a customized nanoString Gene Expression CodeSet (Table S1) and analyzed using the nCounter Sprint Profiler. The mRNA levels were normalized to five housekeeping genes (*ABCF1*, *CLTC*, *GAPDH*, *PGKI*, and *TUBB*) and expressed as fold change in HCM over control CMs.

#### Western Blot

Western blot analysis was performed on total crude protein lysates from cultured hiPSC-CMs in the different conditions. Same amount of proteins (20 µg/lane) of single samples or pooled samples (n = 5–6) were separated on a 10% SDS-polyacrylamide (29:1) mini-gels (Bio-Rad) and transferred by wet-electroblotting to nitrocellulose membranes. Membranes were stained with the primary antibodies directed against the M-motif of cMyBP-C (polyclonal, 1:10,000, custom made) and α-actinin (monoclonal, 1:10,000, Sigma). Peroxidase-conjugated secondary antibodies against mouse (1:20,000, Dianova) or against rabbit (1:20,000, Sigma) were used. Proteins were visualized using Amersham ECL Prime Western Blotting Detection Reagent (GE Healthcare), and the signals were detected on Amersham Hyperfilm MP (GE Healthcare). Signals were quantified with GeneTools image analyzing software (Syngene).

#### Statistical Analysis

Data are presented as mean ± SEM. Statistical analyses were performed by Student's t test and two-way ANOVA with Bonferroni post-test using the GraphPad Prism 6.0 software. A value of p < 0.05 was considered significant.

#### SUPPLEMENTAL INFORMATION

Supplemental Information includes six figures and two tables and can be found with this article online at <http://dx.doi.org/10.1016/j.omtn.2017.05.008>.

#### AUTHOR CONTRIBUTIONS

Conceptualization, M. Prondzynski, G.M., and L.C.; Methodology, M. Prondzynski, G.M., and L.C.; Investigation, M. Prondzynski, E.K., and G.M.; Formal Analysis, M. Prondzynski, G.M., and L.C.; Visualization, M. Prondzynski; Resources, S.D.L., A.S., A.H., F.F., O.P., O.J.M., J.M., C.R., M. Patten, T.E., and L.C.; Writing – Original Draft, M. Prondzynski and G.M.; Writing – Review & Editing, M. Prondzynski, T.E., G.M., and L.C.; Project Administration,



M. Prondzynski, G.M., and L.C.; Supervision, G.M. and L.C.; Funding Acquisition, T.E., G.M., and L.C.

### CONFLICTS OF INTEREST

L.C., T.E., O.J.M., and G.M. are co-authors of a provisional European patent application EP13164212, filed April 17, 2013, Gene-therapy vectors for treating cardiomyopathy, followed by an international patent US20160108430, application US 14/785,188, publication date April 21, 2016 (filing date April 17, 2014). The remaining authors declare no conflicts of interest.

### ACKNOWLEDGMENTS

We are thankful to Alessandra Moretti (Department of Cardiology, Klinikum rechts der Isar, Technische Universität München) for providing the control hiPSC cell line. We would like to thank the cardiac differentiation team, especially Ingra Mannhardt-Vollert, Tessa Werner, and Bärbel Ulmer for precious help (UKE-Pharmacology) and Andreas Jungmann for support with AAV productions (Internal Medicine III, University Hospital Heidelberg). We also want to thank Oliver Keminer for his help and technical assistance with the Opera High-Content Screening System and the Columbus Image Data Management and Analysis System (Fraunhofer IME Screening-Port). Finally, we would like to thank Suellen Lopes Oliveira for graphic design (<http://www.suelopes.com>) and visualization. This work was supported by the DZHK (German Centre for Cardiovascular Research, the German Ministry of Research Education (BMBF), and by the Seventh Framework Program of the European Union (Health-F2-2009–241577; Big-Heart project).

### REFERENCES

- Hammond, S.M., and Wood, M.J. (2011). Genetic therapies for RNA mis-splicing diseases. *Trends Genet.* 27, 196–205.
- Doudna, J.A., and Charpentier, E. (2014). Genome editing. The new frontier of genome engineering with CRISPR-Cas9. *Science* 346, 1258096.
- Wang, D., and Gao, G. (2014). State-of-the-art human gene therapy: part I. Gene delivery technologies. *Discov. Med.* 18, 67–77.
- Semsarian, C., Ingles, J., Maron, M.S., and Maron, B.J. (2015). New perspectives on the prevalence of hypertrophic cardiomyopathy. *J. Am. Coll. Cardiol.* 65, 1249–1254.
- Elliott, P.M., Anastasakis, A., Borger, M.A., Borggrefe, M., Cecchi, F., Charron, P., Hagege, A.A., Lafont, A., Limongelli, G., Mahrholdt, H., et al.; Authors/Task Force members (2014). 2014 ESC Guidelines on diagnosis and management of hypertrophic cardiomyopathy: the Task Force for the Diagnosis and Management of Hypertrophic Cardiomyopathy of the European Society of Cardiology (ESC). *Eur. Heart J.* 35, 2733–2779.
- Behrens-Gawlik, V., Mearini, G., Gedicke-Hornung, C., Richard, P., and Carrier, L. (2014). MYBPC3 in hypertrophic cardiomyopathy: from mutation identification to RNA-based correction. *Pflugers Arch.* 466, 215–223.
- Carrier, L., Mearini, G., Stathopoulou, K., and Cuello, F. (2015). Cardiac myosin-binding protein C (MYBPC3) in cardiac pathophysiology. *Gene* 573, 188–197.
- Marston, S., Copeland, O., Jacques, A., Livesey, K., Tsang, V., McKenna, W.J., Jalilzadeh, S., Carballo, S., Redwood, C., and Watkins, H. (2009). Evidence from human myectomy samples that MYBPC3 mutations cause hypertrophic cardiomyopathy through haploinsufficiency. *Circ. Res.* 105, 219–222.
- Craig, R., Lee, K.H., Mun, J.Y., Torre, I., and Luther, P.K. (2014). Structure, sarcomeric organization, and thin filament binding of cardiac myosin-binding protein-C. *Pflugers Arch.* 466, 425–431.

- Sequeira, V., Witjas-Paalberends, E.R., Kuster, D.W., and van der Velden, J. (2014). Cardiac myosin-binding protein C: hypertrophic cardiomyopathy mutations and structure-function relationships. *Pflugers Arch.* 466, 201–206.
- Moss, R.L., Fitzsimons, D.P., and Ralphe, J.C. (2015). Cardiac MyBP-C regulates the rate and force of contraction in mammalian myocardium. *Circ. Res.* 116, 183–192.
- Marziliano, N., Merlini, P.A., Vignati, G., Orsini, F., Motta, V., Bandiera, L., Intrieri, M., and Veronese, S. (2012). A case of compound mutations in the MYBPC3 gene associated with biventricular hypertrophy and neonatal death. *Neonatology* 102, 254–258.
- Ho, C.Y., Lever, H.M., DeSanctis, R., Farver, C.F., Seidman, J.G., and Seidman, C.E. (2000). Homozygous mutation in cardiac troponin T: implications for hypertrophic cardiomyopathy. *Circulation* 102, 1950–1955.
- Maron, B.J., Maron, M.S., and Semsarian, C. (2012). Double or compound sarcomere mutations in hypertrophic cardiomyopathy: a potential link to sudden death in the absence of conventional risk factors. *Heart Rhythm* 9, 57–63.
- Wessels, M.W., Herkert, J.C., Frohn-Mulder, I.M., Dalinghaus, M., van den Wijngaard, A., de Krijger, R.R., Michels, M., de Coo, I.F., Hoedemaekers, Y.M., and Dooijes, D. (2015). Compound heterozygous or homozygous truncating MYBPC3 mutations cause lethal cardiomyopathy with features of noncompaction and septal defects. *Eur. J. Hum. Genet.* 23, 922–928.
- Lekanne Deprez, R.H., Muurling-Vlietman, J.J., Hruđa, J., Baars, M.J., Wijnaendts, L.C., Stolte-Dijkstra, I., Alders, M., and van Hagen, J.M. (2006). Two cases of severe neonatal hypertrophic cardiomyopathy caused by compound heterozygous mutations in the MYBPC3 gene. *J. Med. Genet.* 43, 829–832.
- Xin, B., Puffenberger, E., Tumbush, J., Bockoven, J.R., and Wang, H. (2007). Homozygosity for a novel splice site mutation in the cardiac myosin-binding protein C gene causes severe neonatal hypertrophic cardiomyopathy. *Am. J. Med. Genet. A.* 143A, 2662–2667.
- Gedicke-Hornung, C., Behrens-Gawlik, V., Reischmann, S., Geertz, B., Stimpel, D., Weinberger, F., Schlossarek, S., Précigout, G., Braren, I., Eschenhagen, T., et al. (2013). Rescue of cardiomyopathy through U7snRNA-mediated exon skipping in Mybpc3-targeted knock-in mice. *EMBO Mol. Med.* 5, 1128–1145.
- Mearini, G., Stimpel, D., Krämer, E., Geertz, B., Braren, I., Gedicke-Hornung, C., Précigout, G., Müller, O.J., Katus, H.A., Eschenhagen, T., et al. (2013). Repair of Mybpc3 mRNA by 5'-trans-splicing in a Mouse Model of Hypertrophic Cardiomyopathy. *Mol. Ther. Nucleic Acids* 2, e102.
- Jiang, J., Wakimoto, H., Seidman, J.G., and Seidman, C.E. (2013). Allele-specific silencing of mutant Myh6 transcripts in mice suppresses hypertrophic cardiomyopathy. *Science* 342, 111–114.
- Mearini, G., Stimpel, D., Geertz, B., Weinberger, F., Krämer, E., Schlossarek, S., Mourot-Filiatre, J., Stoehr, A., Dutsch, A., Wijnker, P.J., et al. (2014). Mybpc3 gene therapy for neonatal cardiomyopathy enables long-term disease prevention in mice. *Nat. Commun.* 5, 5515.
- Moretti, A., Bellin, M., Welling, A., Jung, C.B., Lam, J.T., Bott-Flügel, L., Dorn, T., Goedel, A., Höhnke, C., Hofmann, F., et al. (2010). Patient-specific induced pluripotent stem-cell models for long-QT syndrome. *N. Engl. J. Med.* 363, 1397–1409.
- Lahti, A.L., Kujala, V.J., Chapman, H., Koivisto, A.P., Pekkanen-Mattila, M., Kerkelä, E., Hyttinen, J., Kontula, K., Swan, H., Conklin, B.R., et al. (2012). Model for long QT syndrome type 2 using human iPSC cells demonstrates arrhythmogenic characteristics in cell culture. *Dis. Model. Mech.* 5, 220–230.
- Hinson, J.T., Chopra, A., Nafissi, N., Polachek, W.J., Benson, C.C., Swist, S., Gorham, J., Yang, L., Schafer, S., Sheng, C.C., et al. (2015). HEART DISEASE. Titin mutations in iPSC cells define sarcomere insufficiency as a cause of dilated cardiomyopathy. *Science* 349, 982–986.
- Sun, N., Yazawa, M., Liu, J., Han, L., Sanchez-Freire, V., Abilez, O.J., Navarrete, E.G., Hu, S., Wang, L., Lee, A., et al. (2012). Patient-specific induced pluripotent stem cells as a model for familial dilated cardiomyopathy. *Sci. Transl. Med.* 4, 130ra47.
- Granlich, M., Pane, L.S., Zhou, Q., Chen, Z., Murgia, M., Schötteri, S., Goedel, A., Metzger, K., Brade, T., Parrotta, E., et al. (2015). Antisense-mediated exon skipping: a therapeutic strategy for titin-based dilated cardiomyopathy. *EMBO Mol. Med.* 7, 562–576.
- Lan, F., Lee, A.S., Liang, P., Sanchez-Freire, V., Nguyen, P.K., Wang, L., Han, L., Yen, M., Wang, Y., Sun, N., et al. (2013). Abnormal calcium handling properties underlie

- familial hypertrophic cardiomyopathy pathology in patient-specific induced pluripotent stem cells. *Cell Stem Cell* 12, 101–113.
28. Ojala, M., Prajapati, C., Pölonen, R.P., Rajala, K., Pekkanen-Matila, M., Rasku, J., Larsson, K., and Aalto-Setälä, K. (2016). Mutation-Specific Phenotypes in hiPSC-Derived Cardiomyocytes Carrying Either Myosin-Binding Protein C Or  $\alpha$ -Tropomyosin Mutation for Hypertrophic Cardiomyopathy. *Stem Cells Int.* 2016, 1684792.
  29. Tanaka, A., Yuasa, S., Mearini, G., Egashira, T., Seki, T., Kodaira, M., Kusumoto, D., Kuroda, Y., Okata, S., Suzuki, T., et al. (2014). Endothelin-1 induces myofibrillar disarray and contractile vector variability in hypertrophic cardiomyopathy-induced pluripotent stem cell-derived cardiomyocytes. *J. Am. Heart Assoc.* 3, e001263.
  30. Berger, A., Maire, S., Gaillard, M.C., Sahel, J.A., Hantraye, P., and Bemelmans, A.P. (2016). mRNA trans-splicing in gene therapy for genetic diseases. *Wiley Interdiscip. Rev. RNA* 7, 487–498.
  31. Wally, V., Muraier, E.M., and Bauer, J.W. (2012). Spliceosome-mediated trans-splicing: the therapeutic cut and paste. *J. Invest. Dermatol.* 132, 1959–1966.
  32. Wang, D., and Gao, G. (2014). State-of-the-art human gene therapy: part II. Gene therapy strategies and clinical applications. *Discov. Med.* 18, 151–161.
  33. Collins, M., and Thrasher, A. (2015). Gene therapy: progress and predictions. *Proc. Biol. Sci.* 282, 20143003.
  34. Varadi, K., Michelfelder, S., Korff, T., Hecker, M., Trepel, M., Katus, H.A., Kleinschmidt, J.A., and Müller, O.J. (2012). Novel random peptide libraries displayed on AAV serotype 9 for selection of endothelial cell-directed gene transfer vectors. *Gene Ther.* 19, 800–809.
  35. Lorain, S., Peccate, C., Le Hir, M., and Garcia, L. (2010). Exon exchange approach to repair Duchenne dystrophin transcripts. *PLoS ONE* 5, e10894.
  36. Ma, D., Wei, H., Lu, J., Ho, S., Zhang, G., Sun, X., Oh, Y., Tan, S.H., Ng, M.L., Shim, W., et al. (2013). Generation of patient-specific induced pluripotent stem cell-derived cardiomyocytes as a cellular model of arrhythmogenic right ventricular cardiomyopathy. *Eur. Heart J.* 34, 1122–1133.
  37. Dambrot, C., Braam, S.R., Tertoolen, L.G., Birket, M., Atsma, D.E., and Mummery, C.L. (2014). Serum supplemented culture medium masks hypertrophic phenotypes in human pluripotent stem cell derived cardiomyocytes. *J. Cell. Mol. Med.* 18, 1509–1518.
  38. Wang, G., McCain, M.L., Yang, L., He, A., Pasqualini, F.S., Agarwal, A., Yuan, H., Jiang, D., Zhang, D., Zangi, L., et al. (2014). Modeling the mitochondrial cardiomyopathy of Barth syndrome with induced pluripotent stem cell and heart-on-chip technologies. *Nat. Med.* 20, 616–623.
  39. Karakikes, I., Stilitano, F., Nonnenmacher, M., Tzimas, C., Sanoudou, D., Termglinchan, V., Kong, C.W., Rushing, S., Hansen, J., Ceholski, D., et al. (2015). Correction of human phospholamban R14del mutation associated with cardiomyopathy using targeted nucleases and combination therapy. *Nat. Commun.* 6, 6955.
  40. Walsh, R., Thomson, K.L., Ware, J.S., Funke, B.H., Woodley, J., McGuire, K.J., Mazzarotto, F., Blair, E., Sellar, A., Taylor, J.C., et al. (2017). Reassessment of Mendelian gene pathogenicity using 7,855 cardiomyopathy cases and 60,706 reference samples. *Genet. Med.* 19, 192–203.
  41. Monteiro da Rocha, A., Guerrero-Serna, G., Helms, A., Luzod, C., Mironov, S., Russell, M., Jalife, J., Day, S.M., Smith, G.D., and Herron, T.J. (2016). Deficient cMyBP-C protein expression during cardiomyocyte differentiation underlies human hypertrophic cardiomyopathy cellular phenotypes in disease specific human ES cell derived cardiomyocytes. *J. Mol. Cell. Cardiol.* 99, 197–206.
  42. Marston, S., Copeland, O., Gehmlich, K., Schlossarek, S., and Carrier, L. (2012). How do MYBPC3 mutations cause hypertrophic cardiomyopathy? *J. Muscle Res. Cell Motil.* 33, 75–80.
  43. Vignier, N., Schlossarek, S., Fraysse, B., Mearini, G., Krämer, E., Pointu, H., Mougenot, N., Guiard, J., Reimer, R., Höhenberg, H., et al. (2009). Nonsense-mediated mRNA decay and ubiquitin-proteasome system regulate cardiac myosin-binding protein C mutant levels in cardiomyopathic mice. *Circ. Res.* 105, 239–248.
  44. Nagy, E., and Maquat, L.E. (1998). A rule for termination-codon position within intron-containing genes: when nonsense affects RNA abundance. *Trends Biochem. Sci.* 23, 198–199.
  45. van Dijk, S.J., Dooijes, D., dos Remedios, C., Michels, M., Lamers, J.M., Winegrad, S., Schlossarek, S., Carrier, L., ten Cate, F.J., Stienen, G.J., and van der Velden, J. (2009). Cardiac myosin-binding protein C mutations and hypertrophic cardiomyopathy: haploinsufficiency, deranged phosphorylation, and cardiomyocyte dysfunction. *Circulation* 119, 1473–1483.
  46. Tardiff, J.C., Carrier, L., Bers, D.M., Poggesi, C., Ferrantini, C., Coppini, R., Maier, L.S., Ashrafian, H., Huke, S., and van der Velden, J. (2015). Targets for therapy in sarcomeric cardiomyopathies. *Cardiovasc. Res.* 105, 457–470.
  47. Wijnter, P.J., Friedrich, F.W., Dutsch, A., Reischmann, S., Eder, A., Mannhardt, I., Mearini, G., Eschenhagen, T., van der Velden, J., and Carrier, L. (2016). Comparison of the effects of a truncating and a missense MYBPC3 mutation on contractile parameters of engineered heart tissue. *J. Mol. Cell. Cardiol.* 97, 82–92.
  48. Doroudgar, S., Quijada, P., Konstandin, M., Ilves, K., Broughton, K., Khalafalla, F.G., Casillas, A., Nguyen, K., Gude, N., Toko, H., et al. (2016). S100A4 protects the myocardium against ischemic stress. *J. Mol. Cell. Cardiol.* 100, 54–63.
  49. Zhang, X., Azhar, G., Chai, J., Sheridan, P., Nagano, K., Brown, T., Yang, J., Khrapko, K., Borras, A.M., Lawitts, J., et al. (2001). Cardiomyopathy in transgenic mice with cardiac-specific overexpression of serum response factor. *Am. J. Physiol. Heart Circ. Physiol.* 280, H1782–H1792.
  50. Mooren, F.C., Vierendeck, J., Krüger, K., and Thum, T. (2014). Circulating microRNAs as potential biomarkers of aerobic exercise capacity. *Am. J. Physiol. Heart Circ. Physiol.* 306, H557–H563.
  51. Takeda, N., and Manabe, I. (2011). Cellular Interplay between Cardiomyocytes and Nonmyocytes in Cardiac Remodeling. *Int. J. Inflamm.* 2011, 535241.
  52. Werfel, S., Jungmann, A., Lehmann, L., Ksienzyk, J., Bekeredjian, R., Kaya, Z., Leuchs, B., Nordheim, A., Backs, J., Engelhardt, S., et al. (2014). Rapid and highly efficient inducible cardiac gene knockout in adult mice using AAV-mediated expression of Cre recombinase. *Cardiovasc. Res.* 104, 15–23.
  53. Takahashi, K., Okita, K., Nakagawa, M., and Yamanaka, S. (2007). Induction of pluripotent stem cells from fibroblast cultures. *Nat. Protoc.* 2, 3081–3089.
  54. Takahashi, K., Tanabe, K., Ohnuki, M., Narita, M., Ichisaka, T., Tomoda, K., and Yamanaka, S. (2007). Induction of pluripotent stem cells from adult human fibroblasts by defined factors. *Cell* 131, 861–872.
  55. Ohnuki, M., Takahashi, K., and Yamanaka, S. (2009). Generation and characterization of human induced pluripotent stem cells. *Curr. Protoc. Stem Cell Biol. Chapter 4, Unit 4A.2.*
  56. Mannhardt, I., Breckwoldt, K., Letuffe-Brenière, D., Schaaf, S., Schulz, H., Neuber, C., Benzin, A., Werner, T., Eder, A., Schulze, T., et al. (2016). Human Engineered Heart Tissue: Analysis of Contractile Force. *Stem Cell Reports* 7, 29–42.
  57. Breckwoldt, K., Letuffe-Brenière, D., Mannhardt, I., Schulze, T., Ulmer, B., Werner, T., Benzin, A., Klampe, B., Reinsch, M.C., Lauffer, S., et al. (2017). Differentiation of cardiomyocytes and generation of human engineered heart tissue. *Nat. Protoc.* 12, 1177–1197.

OMTN, Volume 7

## Supplemental Information

### **Evaluation of *MYBPC3* *trans*-Splicing and Gene Replacement as Therapeutic Options in Human iPSC-Derived Cardiomyocytes**

**Maksymilian Prondzynski, Elisabeth Krämer, Sandra D. Laufer, Aya Shibamiya, Ole Pless, Frederik Flenner, Oliver J. Müller, Julia Münch, Charles Redwood, Arne Hansen, Monica Patten, Thomas Eschenhagen, Giulia Mearini, and Lucie Carrier**

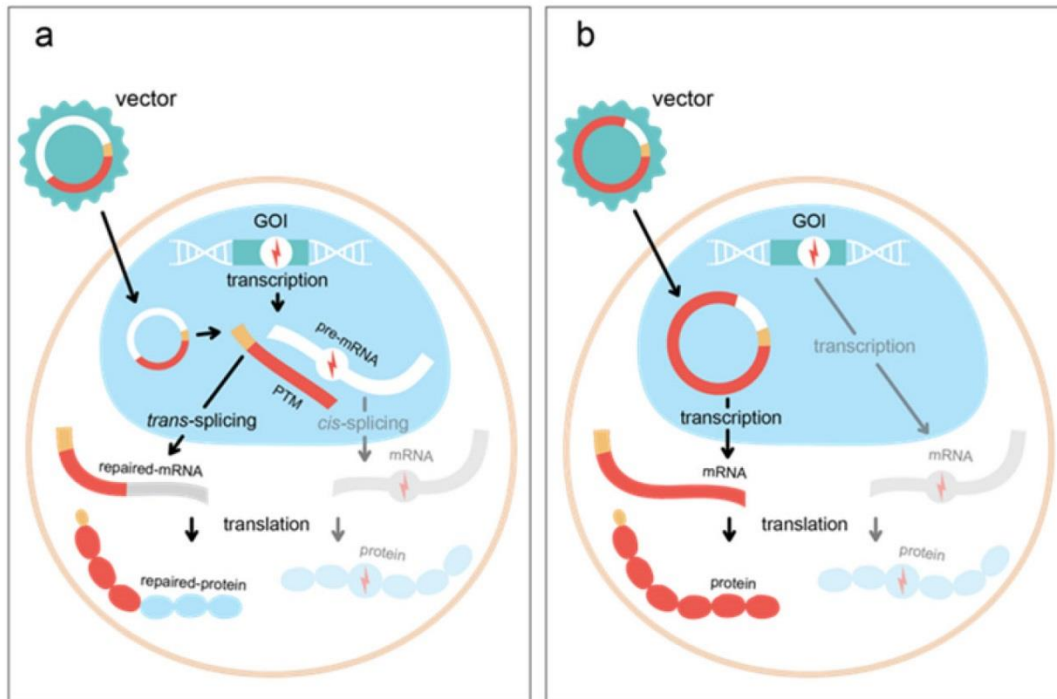


**Figure S1: Schematic representation of two gene therapy approaches. (a)** RNA *trans*-splicing. After virus-mediated delivery, pre-*trans*-splicing molecules (PTMs) are transcribed in the nucleus. PTMs target the pre-mRNA of the gene of interest (GOI) and produce via *trans*-splicing a repaired, chimeric mRNA, without mutation. Translation of the repaired mRNA leads to a corrected fully functional protein. This process is competing with *cis*-splicing, the classical splicing mechanism, by which endogenous mRNA and proteins are produced. **(b)** Gene replacement. The mutation in the GOI results in low level or the absence of corresponding protein. After virus-mediated delivery, a full-length wild-type cDNA of GOI is transcribed in the nucleus. The resulting mRNA is translated into functional protein that replaces the missing mutant endogenous protein. GOI: gene of interest; yellow tag: i.e. FLAG to discriminate exogenous molecules; red bolt: gene mutation.

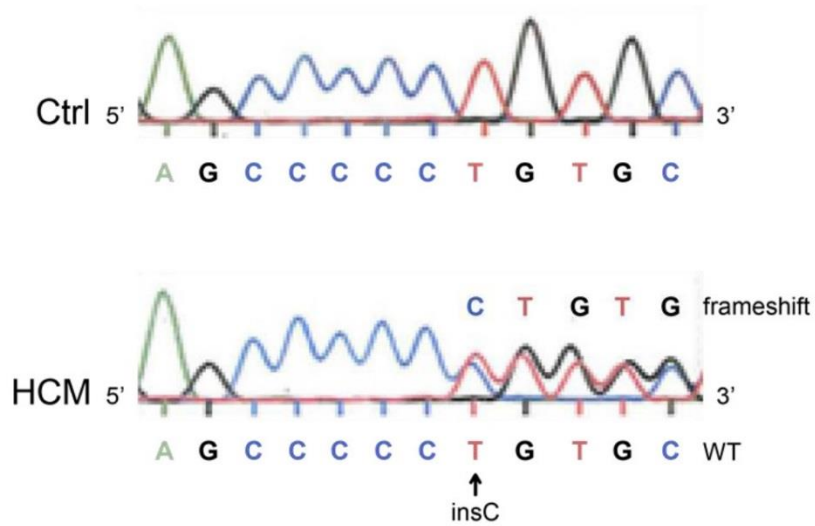


**Figure S2: Validation of the *MYBPC3* mutation at the genomic level.** PCR was performed on genomic DNA from blood cells from the HCM patient using intronic primers around *MYBPC3* exon 16 and compared to a human control sequence. Sanger sequencing confirmed the presence of an insertion of a C (c.1358\_1359insC) at the heterozygous state in the HCM patient. Wild-type and frameshift sequences are also shown.

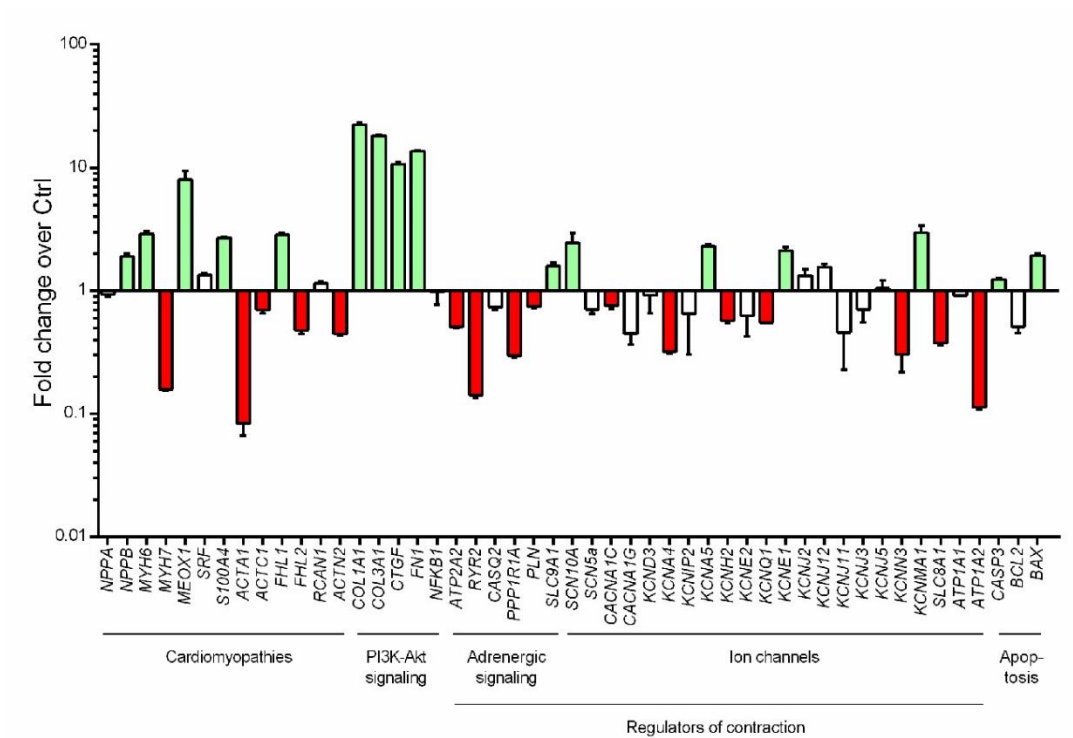


**Figure S3: Gene expression analysis of Ctrl and HCM hiPSC-derived cardiomyocytes.** Evaluation of mRNA levels determined by nCounter NanoString technology in Ctrl and HCM hiPSC-derived CM (n=3-6, with n=number of wells from one transduction experiment). Green bars are significantly upregulated and red bars are significantly downregulated. Data are expressed as mean  $\pm$  SEM.  $P < 0.05$ , unpaired Students *t*-test.



**Figure S4: Schematic illustration of PTMs. (a)** The 5'PTM plasmid carries the 5'-FLAG-tagged wild-type (WT) *MYBPC3* coding sequence of exons 1 to 21 under the control of the human cardiac troponin T promoter (*TNNT2*). The 5'PTM also included a chimeric intron, containing sequences from the human  $\beta$ -globin and immunoglobulin (IgG) genes, conserved splice donor site (5'SS) followed by an intronic region (DISE) from the rat fibroblast growth factor receptor 2 gene and 120 nucleotides for binding to *MYBPC3* intron 21 (5' BD I-21). **(b)** The 3'PTM plasmid carries wild-type (WT) *MYBPC3* coding sequence of exons 22 to 34 under the control of the human cardiac troponin T promoter (*TNNT2*). The sequence is FLAG-tagged at the 3' end before the stop codon (TGA). The 3'PTM includes the same intron as in (a) and the binding domain targets the same sequence in *MYBPC3* intron 21 as 5'PTM. In addition, conserved 3' splicing sequences such as branch point (BP) and polypyrimidine tract (PTT) are present. ATG, start codon; BP, branch point; DISE, downstream intronic splicing enhancer element;  $P_{TNNT2}$ , cardiac troponin T promoter; PPT, polypyrimidine tract; TGA, stop codon; 5'SS, 5'-splice site; 3'SS, 3'-splice site.

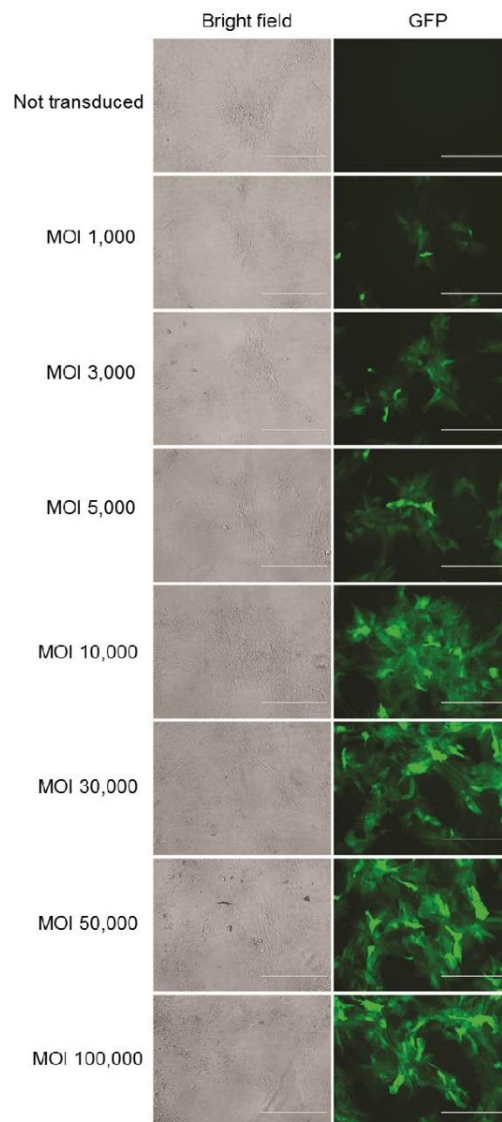


**Figure S5: Efficiency of AAV-TNNT2-GFP-mediated transduction in control hiPSC-derived cardiomyocytes.** hiPSC-CMs were transduced with MOIs of 1,000 up to 100,000 and cultured in 2D for seven days. GFP expression was evaluated by epifluorescence microscopy. Corresponding bright field images are also shown. Scale bars, 400  $\mu$ m. GFP, green fluorescent protein; MOI, multiplicity of infection.



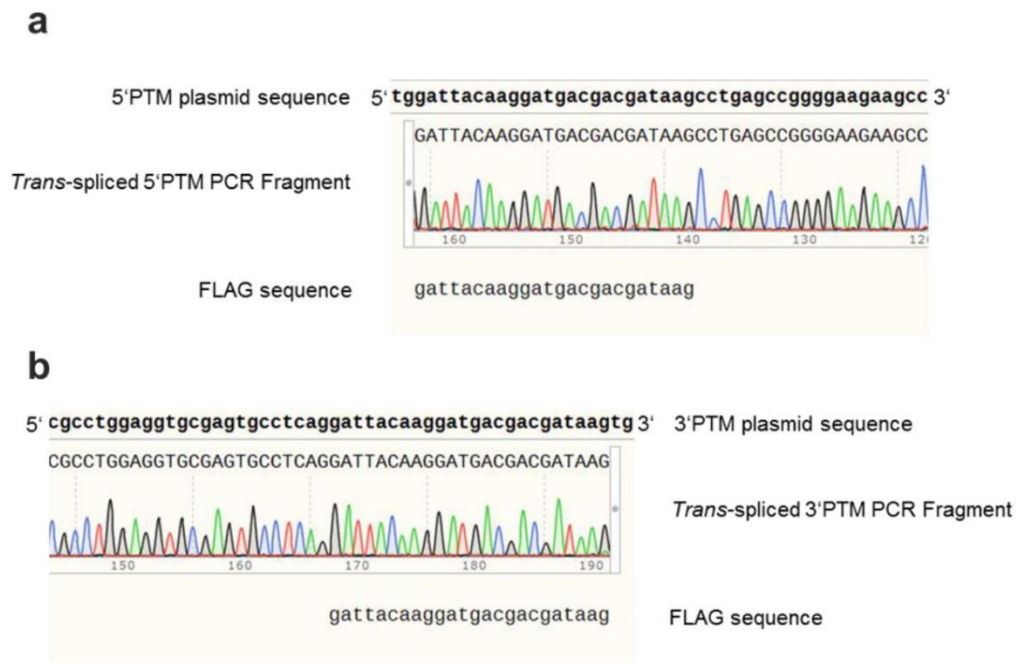


**Figure S6: Validation of *trans*-spliced *MYBPC3* mRNA after 5'- and 3'-mode of *trans*-splicing.** (a) Sequencing of the gel-extracted 2,180-bp fragment amplified by RT-PCR with primers FLAG-F/E23-R in the AAV-5'PTM-transduced hiPSC-CMs sample validated the presence of the FLAG sequence after alignment with the 5'PTM plasmid. (b) Sequencing of the gel-extracted 1,874-bp fragment amplified by RT-PCR with primers E21-F/FLAG-R in AAV-3'PTM-transduced hiPSC-CMs sample validated the presence of the FLAG sequence after alignment with the 3'PTM. Alignment was performed with SnapGene® software. E, exon; RT-PCR, reverse transcriptase PCR.

**Supplemental Table S1.** Acronyms and names of genes evaluated with the nanoString nCounter® Elements technology.

Acronym	Name	Accession number (NCBI)
ABCF1	ATP binding cassette subfamily F member 1	NM_001090.2
ACTA1	Actin, alpha, skeletal muscle	NM_001100.3
ACTC1	Actin, alpha, cardiac muscle 1	NM_005159.4
ACTN2	Alpha-Actinin 2	NM_001103.2
ATP1A1	Na/K-ATPase $\alpha$ 1 subunit	NM_000702.3
ATP1A2	Na/K-ATPase $\alpha$ 2 subunit	NM_001681.3
ATP2A2	ATPase sarcoplasmic/endoplasmic reticulum Ca <sup>2+</sup> transporting 2	NM_001681.3
BAX	BCL2 associated X, apoptosis regulator	NM_138761.3
BCL2	BCL2, apoptosis regulator	NM_000657.2
CACNA1C	Calcium voltage-gated channel subunit alpha1 C (L-Type Ca <sup>2+</sup> channel)	NM_199460.2
CACNA1G	Calcium voltage-gated channel subunit alpha1 G (T type Ca <sup>2+</sup> channel)	NM_198397.1
CASP3	Caspase 3	NM_032991.2
CASQ2	Calsequestrin-2	NM_001232.3
CLTC	Clathrin heavy chain	NM_004859.2
COL1A1	Collagen type I alpha 1	NM_000088.3
COL3A1	Collagen type III alpha 1	NM_000090.3
CTGF	Connective tissue growth factor	NM_001901.2
FHL1	Four-and-a-half-LIM-domains 1	NM_001449.4
FHL2	Four-and-a-half-LIM-domains 2	NM_001039492.2
FN1	Fibronectin 1	NM_212482.1
GAPDH	Glyceraldehyde-3-phosphate dehydrogenase	NM_002046.3
KCNA4	Potassium voltage-gated channel subfamily A member 4 (Ito,s K+ channel)	NM_002233.3
KCNA5	Potassium voltage-gated channel subfamily A member 5 (IKUR)	NM_002234.2
KCND3	Potassium voltage-gated channel subfamily D member 3 (Ito, f beta subunit, Kv4.3)	NM_004980.4
KCNE1	Potassium voltage-gated channel subfamily E regulatory subunit 1 (MinK, Iks)	NM_001127670.1
KCNE2	Potassium voltage-gated channel subfamily E regulatory subunit 2 (MIRP2, Ikr)	NM_172201.1
KCNH2	Potassium voltage-gated channel subfamily H member 2 (Ikr K+ channel)	NM_172057.2
KCNIP2	Potassium voltage-gated channel interacting protein 2 (KChIP2 beta subunit, Ito)	NM_014591.4
KCNJ11	Potassium voltage-gated channel subfamily J member 11 (Kir 6.2, IkATP)	NM_000525.3
KCNJ12	Potassium voltage-gated channel subfamily J member 12 (Ik1 channel subunit 2)	NM_021012.4
KCNJ2	Potassium voltage-gated channel subfamily J member 2 (Ik1 channel)	NM_000891.2
KCNJ3	Potassium voltage-gated channel subfamily J member 3 (IKACH)	NM_001260508.1
KCNJ5	Potassium voltage-gated channel subfamily J member 5 (IKACH)	NM_000890.3
KCNMA1	Potassium calcium-activated channel subfamily M alpha 1 (BK Channel)	NM_001014797.2
KCNN3	Potassium calcium-activated channel subfamily N member 3 (SK3)	NM_002249.4
KCNQ1	Potassium voltage-gated channel subfamily Q member 1 (Iks K+ channel)	NM_181798.1
MEOX1	Mesenchyme homeobox 1	NM_001040002.1
MYH6	Myosin heavy chain 6	NM_002471.3
MYH7	Myosin heavy chain 7	NM_000257.2
NFKB1	Nuclear factor kappa B subunit 1	NM_003998.2
NPPA	Natriuretic peptide A	NM_006172.2
NPPB	Natriuretic peptide B	NM_002521.2
PGK1	Phosphoglycerate kinase 1	NM_000291.2
PLN	Phospholamban	NM_002667.3
PPP1R1A	Protein phosphatase 1, regulatory (inhibitor) subunit 1A (I-1)	NM_006741.3
RCAN1	Regulator of calcineurin 1	NM_004414.5
RYR2	Ryanodine receptor 2	NM_001035.2
S100A4	S100 calcium binding protein A4 (=FSP1)	NM_002961.2
SCN10A	Sodium voltage-gated channel alpha subunit 10 (Na+ channel, Nav1.8)	NM_006514.2
SCN5A	Sodium voltage-gated channel alpha subunit 5 (Na+ channel, Nav1.5)	NM_198056.2
SLC8A1	Solute carrier family 8 member A1 (Sodium-Calcium Exchanger, NCX)	NM_021097.1
SLC9A1	Solute carrier family 9 member A1 (Na+/H+ exchanger)	NM_003047.4
SRF	Serum response factor	NM_003131.3
TUBB	Tubulin beta class 1	NM_178014.3

**Supplemental Table S2.** Sequences of PCR primers

Primer	Sequence (5' to 3')
E1-F	GCCAGTCTCAGCTTTTAGCAA
E2-R	CAGGCCGTA CT TGTGCTG
I15-F	CTGGGACCTGAGGATGTGGG
I16-R	GGTGGGTGGGTGGCAAGTG
E15-F	CCAAGCGTACCCTGACCA
E16-R	CCCTCCTCCGATACTTACACA
E21-F	CCATTGTGGTTGTAGCTGGA
E23-R	CACACAGCAGCTTCTTGTC A
E33-F	CCCAAGATTTCCCTGGTTCAAA
E33-R	CCTCGCCCTGTAAGTTGGT
FLAG-F	GGATTACAAGGATGACGACGA
FLAG-R	CTTATCGTCGTCATCCTTGTAATC
GAPDH-F	ATGTTTCGTCATGGGTGTGAA
GAPDH-R	TGAGTCCTTCCACGATACCA
F3-1	TTCGACGCTAGCACCCACACTGCCACCTT
R3-1	TGTTCCGCGGGGATCCTGTGTGGAACCAAG
F3-2	GTTCCACACAGGATCCCCGCGGAACATTATTATAAC
R3-2	CCTTATCCCCTGTTTCCGGAAA
F3-3	TTCCGGAAAACAGGGGAATAAGGC
R3-3	TTCGACGCGGCCGCTCACTTATCGTCGTCATCCTTGTAATCCTGAGGCACTCG
F5-1	TTCGACGCTAGCATGGATTACAAGGATGACGACGATAAGCCTGAGCCGGGAAGA
R5-1	AGTGTGGGTGGATCCAGGCCAACCCATGGAAAGAAAAGCTGTACTACCTGCCTGATAGCCTTCTG
F5-2	GGGTGGCCTGGATCCACCCACACTGCCACCTT
R5-2	TTCGACGCGGCCGCTGTGTGGAACCAAG

### **3.2 Differentiation of cardiomyocytes and generation of human engineered heart tissue**

In this chapter the report on “differentiation of cardiomyocytes and generation of human engineered heart tissue” will be presented, which was published in May 2017 in the journal *Nature Protocols*. In this report I was involved in the development and validation of the protocol by applying it to the investigated hiPSC lines in this thesis and performing regular FACS analysis of all generated hiPSC-CMs in our department. My contributions in this project resulted in a co-authorship.

Title: Differentiation of cardiomyocytes and generation of human engineered heart tissue


Authors: Kaja Breckwoldt, David Letuffe-Brenière, Ingra Mannhardt, Thomas Schulze, Bärbel Ulmer, Tessa Werner, Anika Benzin, Birgit Klampe, Marina C Reinsch, Sandra Laufer, Aya Shibamiya, Maksymilian Prondzynski, Giulia Mearini, Dennis Schade, Sigrid Fuchs, Christiane Neuber, Elisabeth Krämer, Umber Saleem, Mirja L Schulze, Marita L Rodriguez, Thomas Eschenhagen and Arne Hansen

Journal: *Nature Protocols*, Volume 12, Number 6, May 2017, pages 1177-1197

DOI: 10.1038/nprot.2017.033

Results: In this study various lines of hiPSCs were used to develop a differentiation protocol for CMs, which can be used for the generation of human EHTs. This protocol describes expansion of hiPSCs, standardized generation of defined EBs, growth factor and small-molecule-based cardiac differentiation and standardized generation of EHTs. hiPSC-CMs were generated with purities over 90% (Fig. 1), which occurred within 14 days in a three-step protocol (Fig. 3). For further use of hiPSC-CMs in the EHT format, EBs were enzymatically dissociated to undergo 3D assembly (Fig. 4). This produced fibrin-based EHTs that generate force under auxotonic stretch conditions. Ten to fifteen days after casting, the EHTs can be used for contractility measurements and further experimental testing (Fig. 7).

# Differentiation of cardiomyocytes and generation of human engineered heart tissue

Kaja Breckwoldt<sup>1</sup> , David Letuffe-Brenière<sup>1</sup>, Ingra Mannhardt<sup>1</sup>, Thomas Schulze<sup>1</sup>, Bärbel Ulmer<sup>1</sup>, Tessa Werner<sup>1</sup>, Anika Benzin<sup>1</sup>, Birgit Klampe<sup>1</sup>, Marina C Reinsch<sup>1</sup>, Sandra Laufer<sup>2</sup>, Aya Shibamiya<sup>2</sup>, Maksymilian Prondzynski<sup>1</sup>, Giulia Mearini<sup>1</sup>, Dennis Schade<sup>3</sup>, Sigrid Fuchs<sup>4</sup>, Christiane Neuber<sup>1</sup>, Elisabeth Krämer<sup>1</sup>, Umber Saleem<sup>1</sup>, Mirja L Schulze<sup>1</sup>, Marita L Rodriguez<sup>1</sup>, Thomas Eschenhagen<sup>1</sup> & Arne Hansen<sup>1</sup>

<sup>1</sup>Department of Experimental Pharmacology and Toxicology, Cardiovascular Research Center, University Medical Center Hamburg-Eppendorf, and DZHK (German Center for Cardiovascular Research), Partner Site Hamburg/Kiel/Lübeck, Hamburg, Germany. <sup>2</sup>HEXT-Stem Cell Facility, University Medical Center Hamburg-Eppendorf, Hamburg, Germany. <sup>3</sup>Faculty of Chemistry and Chemical Biology, TU Dortmund University, Dortmund, Germany. <sup>4</sup>Department of Human Genetics, University Medical Center Hamburg-Eppendorf, Hamburg, Germany. Correspondence should be addressed to A.H. (ar.hansen@uke.de).

Published online 11 May 2017; doi:10.1038/nprot.2017.033

Since the advent of the generation of human induced pluripotent stem cells (hiPSCs), numerous protocols have been developed to differentiate hiPSCs into cardiomyocytes and then subsequently assess their ability to recapitulate the properties of adult human cardiomyocytes. However, hiPSC-derived cardiomyocytes (hiPSC-CMs) are often assessed in single-cell assays. A shortcoming of these assays is the limited ability to characterize the physiological parameters of cardiomyocytes, such as contractile force, due to random orientations. This protocol describes the differentiation of cardiomyocytes from hiPSCs, which occurs within 14 d. After casting, cardiomyocytes undergo 3D assembly. This produces fibrin-based engineered heart tissues (EHTs)—in a strip format—that generate force under auxotonic stretch conditions. 10–15 d after casting, the EHTs can be used for contractility measurements. This protocol describes parallel expansion of hiPSCs; standardized generation of defined embryoid bodies, growth factor and small-molecule-based cardiac differentiation; and standardized generation of EHTs. To carry out the protocol, experience in advanced cell culture techniques is required.

## INTRODUCTION

Human-pluripotent-stem-cell-derived cardiomyocytes are extraordinarily powerful tools within the field of cardiovascular research. Cardiomyocytes differentiated from hiPSCs via various protocols have been used to address questions related to cardiac toxicity and disease modeling<sup>1,2</sup>. The majority of these protocols are based on single-cell models. An important limitation of single-cell assays is their poor representation of the *in vivo* cardiovascular environment. Single cardiomyocytes lack important characteristics such as cellular networks, a 3D extracellular matrix and a defined auxotonic load. Furthermore, sarcomeric organization of myofilaments, a hallmark of mature functional cardiomyocytes, is primitively developed in single cardiomyocytes<sup>3</sup>. Evaluation of contractile force in single cells is therefore poorly established.

Engineered 3D heart tissues can improve these limitations. Several protocols for generating cardiac constructs from single cells have been established during the past two decades. These protocols mix single cells from neonatal animal hearts, or pluripotent-stem-cell-derived cardiomyocytes from mice or humans, with extracellular matrices such as fibrinogen, collagen or Matrigel. Depending on the specific protocol, different modes of tissue stretching (isometric/static and auxotonic) and contractile force analysis (force transducer, video-optical monitoring) are used. Progress in the field can be expected from improved protocols to differentiate cardiomyocytes with high efficiency at large scale and reasonable cost with suitable formats for generating EHTs at high levels of standardization. This protocol describes a step-by-step procedure for expanding undifferentiated hiPSCs, differentiating them into cardiomyocytes and generating fibrin-based EHTs in a 24-well plate format<sup>4–6</sup>. It includes detailed information regarding scalability and the optimal ratio of input cells to cell culture medium.

The scalability and efficiency of this differentiation protocol and the easy, reliable method of generating EHTs provide the opportunity to study physiological and pharmacological properties of human heart tissue *in vitro*. Using the protocol described here, it has been shown that EHTs with hiPSC-CMs have a high similarity to native human heart tissue, indicating that human EHTs are useful for predictive safety pharmacology and toxicology testing, as well as disease modeling<sup>7</sup>. Concerning the electrophysiological properties of hiPSC-CMs, it has been shown that they express L-type Ca<sup>2+</sup> current at the same density as human adult CMs and that the EHT culture format favors their maturation<sup>8</sup>. Furthermore, human EHTs formed large grafts after transplantation onto injured guinea pig hearts. They improved left ventricular and electrophysiological function and were able to electrically couple to host myocardium<sup>9</sup>.

## Development of the protocol

Among the cell culture protocols currently in use for the expansion of undifferentiated hiPSCs, the largest differences are in the level of standardization and price<sup>10–14</sup>. We decided to optimize our protocol based on a cost-effective medium composition, in which pluripotency is driven by a combination of three growth factors (basic fibroblast growth factor (bFGF), transforming growth factor- $\beta$  (TGF $\beta$ ), activin A and the small-molecule bone morphogenetic protein (BMP) inhibitor dorsomorphin)<sup>14</sup>. bFGF, which is very important for maintaining hiPSC pluripotency<sup>15–19</sup>, is both temperature and protease sensitive. To circumvent these problems, we replaced standard bFGF with an engineered bFGF variant with increased thermostability and higher resistance to proteases, while retaining the same biological properties as naturally occurring bFGF<sup>20</sup>.

Several protocols for cardiac differentiation are available<sup>21–25</sup>, but the inter- and intra-laboratory variability is high<sup>26</sup> (reviewed

## PROTOCOL

in Moretti *et al.*<sup>27</sup>). We have optimized a previously published protocol based on embryoid body (EB) formation, as suspension-culture-based protocols are better suited to large-scale production. This is because, in contrast to 2D cultures, the number of cultivated cells is not limited to the growth surface, and the volume of culture medium can be adjusted accordingly. An important shortcoming of EB-based protocols is the difficulty involved in consistently producing homogeneous EBs. Spontaneous EB formation is difficult and sensitive to the confluency of the undifferentiated cells, and the EBs are often heterogeneous in size. EB formation by forced aggregation, on the other hand, does not, in our experience, depend on cell confluency, and it produces EBs of a defined size. However, microcavity plates are expensive, and scaling up this technique is difficult and very laborious. Conversely, spinner-flask-based protocols for EB formation require only dissociation of hiPSCs into single cells and subsequent culture of hiPSCs in stirred spinner flasks with glass bulb impellers. Such protocols have also been described for expansion of hiPSCs in suspension<sup>28,29</sup>. This method is, in our experience, very reliable and it provides EBs that are homogeneous in size, independent of cell line and confluency of the hiPSC culture. Furthermore, spinner-flask-based protocols have a high potential for scalability.

Mesoderm induction is achieved by the parallel addition of bFGF, BMP-4 and activin A in an RPMI-based medium composition. The small-molecule WNT-signaling activator CHIR99021 has also been shown to be an effective inducer of mesodermal progenitors<sup>30–33</sup>. As compared with protein growth factors, small molecules tend to be more consistent in quality and more cost-effective. Pilot experiments indicate that our protocol is compatible with CHIR99021 for mesoderm induction, leading to efficient cardiomyocyte differentiation from various stem cell lines. We chose to optimize our protocol for mesoderm induction with BMP4, activin A and bFGF, as this combination was previously shown to faithfully recapitulate mammalian embryonic development<sup>23</sup>. Given the complexity of embryonic cardiac development and the lack of an understanding of how to promote cardiomyocyte maturation, we hypothesized that a protocol that closely replicates the steps involved in mammalian mesoderm/cardiac specification represents the best possible starting point. Further cardiac specification is conducted with potent small-molecule WNT antagonists and subsequently with insulin<sup>30,34</sup>. Using this protocol, the onset of spontaneous beating is observed between

days 8 and 10 (**Supplementary Videos 1–3**). WNT antagonists are omitted after day 11. hiPSC-CMs are dissociated into single cells and subjected to further analysis and EHT generation.

Several different techniques for the generation of EHTs are currently available<sup>5,35–39</sup>. They differ in the size of the construct, the mode of tissue anchoring, the choice of extracellular matrix and the techniques used to analyze the tissue. The fibrin-based, strip-format EHTs described in this protocol can be repeatedly generated with minimal manual handling in a 24-well format<sup>4,5</sup>.

**Advantages and limitations of the method.** This protocol allows for the standardized production of hiPSC-CMs at both a scale and cost that are suitable for the generation of EHTs. In a successful differentiation run,  $60 \times 10^6$  hiPSCs (four T80 flasks) on average give rise to  $48 \times 10^6$  hiPSC-cardiomyocytes (70–97% Troponin T-positive; **Tables 1 and 2**, **Fig. 1** and **Supplementary Fig. 1**), which are enough cells to prepare two 24-well plates of EHTs (**Table 1**). The estimated cost associated with preparing one plate of EHTs is 180 €, including costs incurred during hiPSC culture (for 4 d), cardiomyocyte differentiation, EHT generation and EHT cultivation (for 21 d).

The differentiation procedure described here is based on EB differentiation protocols, which were shown to recapitulate distinct stages of embryonic development and mesodermal germline commitment<sup>23</sup>. Compared with activating WNT signaling with the small-molecule CHIR99021, which has also been shown to be an effective inducer of mesodermal progenitors<sup>30–33</sup>, there are disadvantages, including the limited stability of proteins, variability in their biologic activity and higher costs. However, although protein growth factors are more expensive than small molecules, the media compositions used in our protocol are cheaper overall as compared with those used in many of the published protocols using mTeSR, Stem Pro-34 or other media. For WNT signal inhibition during cardiac differentiation, an IWR-1 (4-(1,3,3a,4,7,7a-hexahydro-1,3-dioxo-4,7-methano-2H-isoindol-2-yl)-N-8-quinolinyl-benzamide) analog (DS-I-7) was used. This analog has been found to have a higher selectivity than IWP, as well as a higher potency and stability as compared with those of IWR-1 (ref. 34).

Contractile force is a very important parameter of cardiomyocyte function. Depolarization of a cardiomyocyte by an action potential leads to the entry of calcium into the cell through L-type

**TABLE 1** | Format, timing and concentrations for cardiomyocyte differentiation of hiPSCs.

Step(s)	Culture format	Number of culture formats	Number of cells/EB volume	Volume of medium/format	Timing
8: hiPSC expansion	T80 cell culture flask	4	$60 \times 10^6$ ( $15 \times 10^6$ per T80)	20 ml of FTDA	4 d
23–40: EB formation	Spinner flask	1	$60 \times 10^6$ , suspension	200 ml of EB formation medium	1 d
41–55: Mesoderm induction	T175 cell culture flask	2	300- $\mu$ l EB volume, suspension	40 ml of mesoderm induction medium	3 d
56–66: Cardiac differentiation	T175 cell culture flask	1	200- $\mu$ l EB volume, suspension	46 ml of cardiac differentiation medium I/II/III	10 d
67–76: Dissociation	T175 cell culture flask	1	$48 \times 10^6$	20 ml of collagenase II solution	4 h

**TABLE 2** | Differentiation efficiency and efficacy of different control and disease-specific cell lines.

Cell line	Ctr. 1, <i>n</i> = 23	Ctr. 2, <i>n</i> = 6	Ctr. 3, <i>n</i> = 4	CPVT, <i>n</i> = 6	DCM-1, <i>n</i> = 3	DCM-2, <i>n</i> = 11	HCM, <i>n</i> = 5	DM1, <i>n</i> = 6	Average, <i>n</i> = 64
cTNT-positive cells (%)	87 ± 8	88 ± 5	86 ± 11	86 ± 4	89 ± 3	82 ± 11	86 ± 5	87 ± 7	85 ± 4
CMs per hiPSC	1.2 ± 0.8	0.3 ± 0.1	0.6 ± 0.5	1.5 ± 0.6	1.4 ± 0.6	0.6 ± 0.5	0.6 ± 0.2	0.5 ± 0.3	0.8 ± 0.5

Replicate numbers refer to the number of performed differentiations. CMs per hiPSC compare final numbers of CMs with the input of hiPSCs for embryoid body formation. Mean values ± s.d. are given. CPVT, catecholaminergic polymorphic ventricular tachycardia; cTNT, cardiac troponin T; Ctr., Control; DCM, dilated cardiomyopathy; DM, myotonic dystrophy; HCM, hypertrophic cardiomyopathy.

calcium channels and the subsequent release of calcium from the sarcoplasmic reticulum (SR) through ryanodine receptors. The free calcium binds to troponin-C at the regulatory complex of the actin filaments, which induces a conformational change of troponin-I. The resulting binding of actin to the myosin ATPase located on the myosin head results in ATP hydrolysis, which supplies energy for a conformational change to occur in the actin–myosin complex. The movement between the myosin heads and actin leads to shortening of the sarcomere length. At the end of the action potential, calcium is sequestered by the SR via an ATP-dependent calcium pump (SERCA, sarco-endoplasmic reticulum calcium-ATPase). In this way, the cytosolic calcium concentration and conformational changes are reversed, and the initial sarcomere length is restored. The majority of heart diseases have a direct (effect on sarcomeric proteins) or indirect (effect on ion channels) impact on cardiomyocyte force production. Therefore, the ability to measure and analyze force in a standardized and reproducible manner is highly beneficial. Furthermore, as the ultimate goal is the development of a surrogate for the human heart, human engineered tissues have inherent advantages over laboratory animal models because of their lack of species differences. This is partly balanced by engineering artifacts and a nonphysiological cellular composition. Analyzing cardiomyocyte contractile forces in single-cell assays is a very difficult task. Disorganized myofilaments in single cells make repeated and accurate force measurements difficult. Conversely, EHTs can be generated by standardized procedures, and are characterized by improved cellular alignment and sarcomeric organization of myofilaments. A key aspect of this technique is that the tissues are attached to flexible polydimethylsiloxane (PDMS) posts, which provide an auxotonic stretching environment. Auxotonic stretch is a combination of isometric and isotonic stretching, and is considered to be the physiological mode of stretching within the heart. This EHT protocol is complementary to other 3D<sup>35,36,39–44</sup> or muscular thin-film-based<sup>45</sup> technologies. Important characteristics are cell number per construct, depending on construct size ( $1 \times 10^6$  cells per EHT,  $1 \times 10^6$  cells per construct<sup>36,39,42,44</sup>, 500 cells per construct<sup>40</sup>,  $6 \times 10^3$  to  $10 \times 10^3$  cells per construct<sup>45</sup>,  $2.5 \times 10^5$  cells per construct<sup>35</sup> or  $2.5 \times 10^6$  cells per construct<sup>43</sup>), and the requirement of additional fibroblasts or stromal cells for remodeling<sup>36,40</sup>.

In the EHT format, contractile force can be studied by conventional force transducers, as well as video–optical recording. Measurements with conventional force transducers<sup>46–48</sup> offer the advantage of absolute force determination under isometric conditions. On the other hand, they require transfer to organ baths and are therefore generally performed as end-point measurements under nonsterile conditions. The procedures are less standardized because more manual handling is required, provide a low level of automation and do not allow for long-term analyses. We therefore prefer video–optical recordings of auxotonically contracting 24-well EHTs under steady-state conditions.

A number of *in vitro* tools, such as adeno-associated virus transduction<sup>49</sup>, electrophysiology<sup>8</sup>, calcium-transient measurements<sup>50</sup> and afterload modification<sup>7</sup>, can all be adapted to the human EHT format. Therefore, technologies for generating and analyzing EHTs will have a catalyzing impact on research areas such as disease modeling, regeneration of damaged heart tissue, predictive safety pharmacology/toxicology screening and basic research in cardiovascular medicine.

An important limitation of this technology, as compared with single-cell assays, is the high number of cells required ( $1.0 \times 10^6$

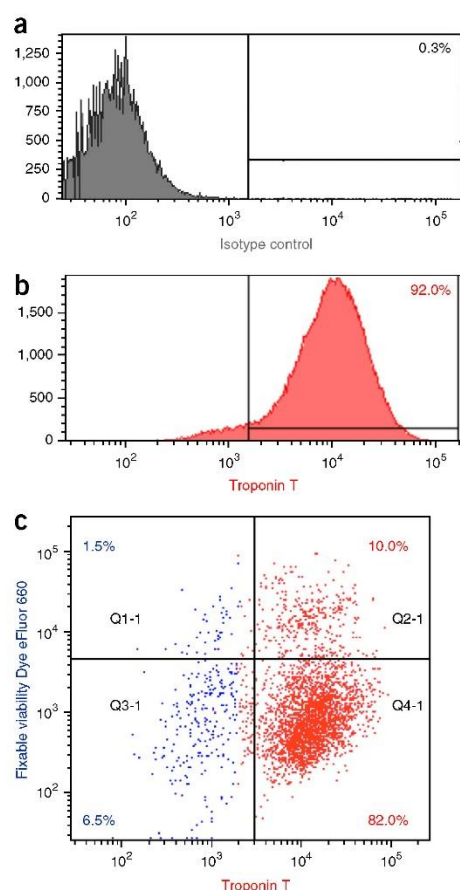


**Figure 1** | Quantitative analysis of cardiomyocytes differentiated from hiPSCs (day 17). (a) Isotype control. (b) Staining with an antibody directed against troponin T. (c) Staining of dead cells with Fixable Viability Dye eFluor 660 after thawing of cardiomyocytes, cryopreserved on day 17 of differentiation. Number of analyzed cells is  $5 \times 10^4$  (a),  $1 \times 10^5$  (b) and 5,000 (c). For details about antibodies and gating strategy, see **Supplementary Figure 1**.

## PROTOCOL

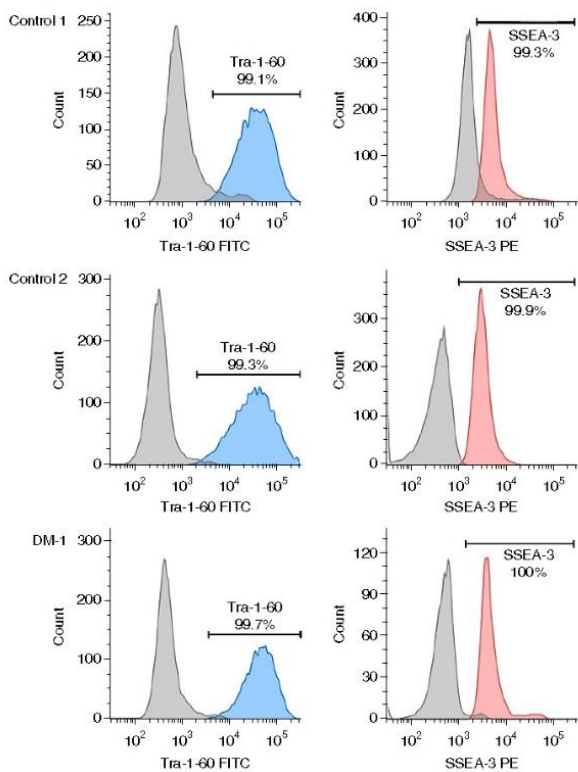


**Figure 2** | Expression of pluripotency markers by hiPSCs. Representative FACS analysis of two different control cell lines and a patient-derived myotonic dystrophy cell line (DM-1) after staining with antibodies directed against TRA-1-60 (blue) and SSEA-3 (pink) with respective isotype controls (gray). For details about antibodies, number of analyzed cells and gating strategy, see **Supplementary Figure 2**.

cells per EHT). In addition, although our protocol is cost-effective, the differentiation efficiency and efficacy show variability between different cell lines and differentiation runs (see also the 'Anticipated Results' section and **Table 2**). In addition, smaller EHTs with fewer cardiomyocytes per tissue, in a 96-well format, are desirable, as they would result in a higher experimental throughput. However, achieving this would require advanced manufacturing technologies, and such small tissues would be difficult to handle manually.

### Experimental design

In this protocol, cardiomyocyte differentiation begins with the expansion of undifferentiated pluripotent stem cells. We passage undifferentiated hiPSCs twice per week (usually on Monday and Thursday) and seed  $6.5 \times 10^4$  cells per  $\text{cm}^2$ , leading to a cell density of  $1.9 \times 10^5$  to  $2.5 \times 10^5$  cells per  $\text{cm}^2$  ( $15 \times 10^6$  to  $20 \times 10^6$  cells per T80 flask) after 3 d in culture. EB formation is initiated 1 week after expanding hiPSC culture from a six-well maintenance culture to a T80 flask format. Important measures for quality control are the microscopic verification of typical morphology for undifferentiated hiPSC colonies, passaging intervals, FACS analysis of the pluripotency markers TRA-1-60 and SSEA-3 (ref. 32) (**Fig. 2**, **Supplementary Fig. 2**), PCR screening for mycoplasma contamination<sup>51</sup> and karyotyping.

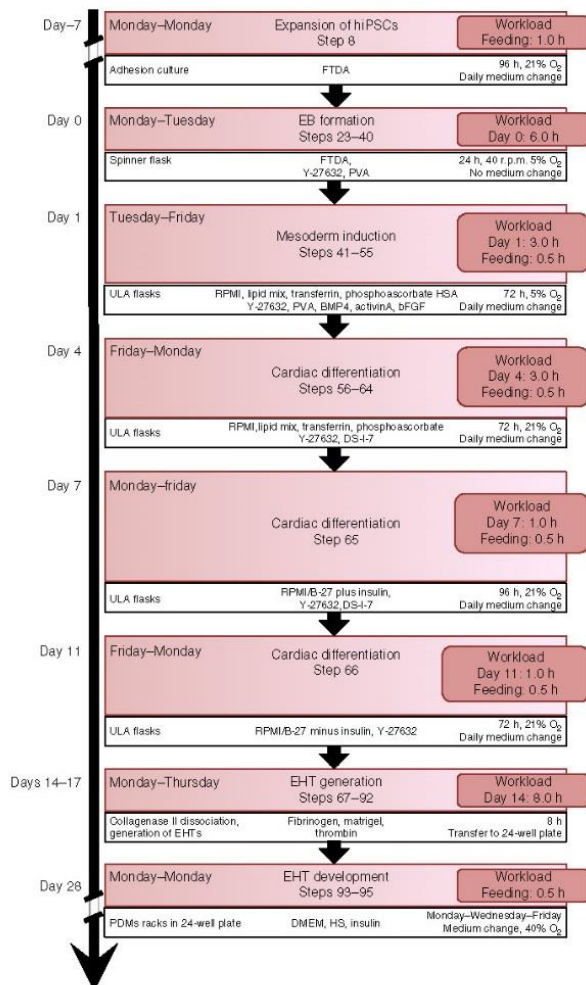


**Figure 3** | Schematic of the protocol for differentiation of cardiomyocytes from hiPSCs and EHT generation. BMP4, activin A and bFGF were used for mesoderm induction and DS-1-7 (IWR-1 analog) was used for WNT signal inhibition. FTDA, hiPSC medium with bFGF, TGF $\beta$ 1, dorsomorphin and activin A; HSA, human serum albumin; HS, horse serum; PVA, polyvinyl alcohol; ULA, ultra-low-attachment.

After overnight EB formation, hiPSCs are prepared for the cardiac differentiation process and EHT generation as described in **Figures 3** and **4**. Corresponding bright-field images at different stages of the cardiac differentiation protocol are shown in **Figure 5**.

Mesoderm induction is initiated on day 1. The EBs are collected and pooled, in order to get an estimate of the total wet volume of the combined EB yield (**Fig. 6**). The EBs are transferred to T175 cell culture flasks coated with Pluronic F-127 (ref. 52), as a cost-effective alternative to commercially available ultra-low-attachment flasks. On this day,  $30 \times 10^6$  undifferentiated input hiPSCs give rise to  $\sim 150 \mu\text{l}$  of EB wet volume. For mesoderm induction, this amount of EBs is cultivated in 40 ml of medium, of which 50% is exchanged on each of the two subsequent days (days 2 and 3). The volume of medium is proportionally adjusted to the measured wet volume of EBs (details are given in PROCEDURE Step 49).



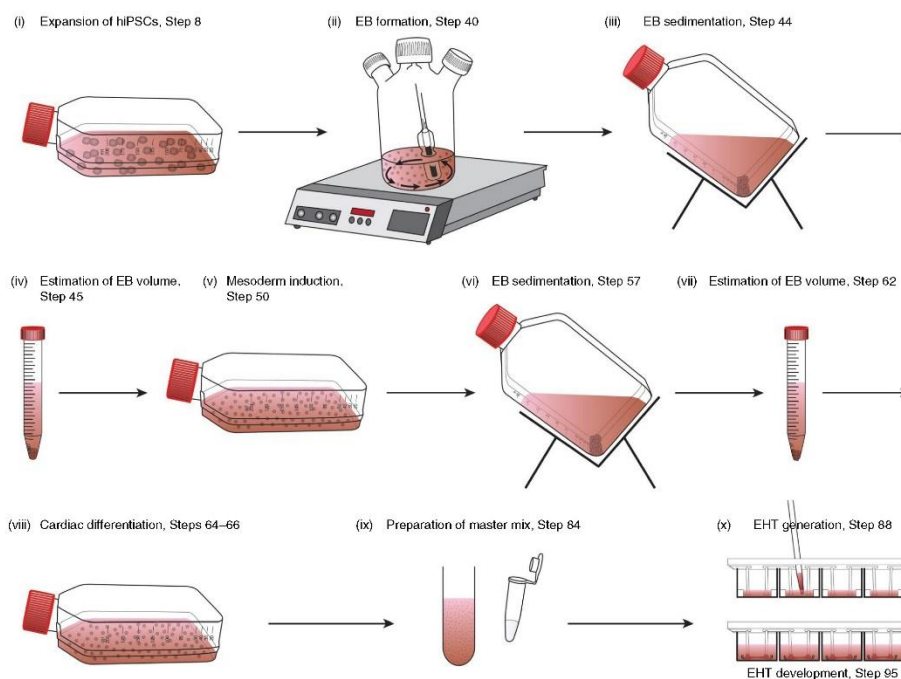


**Figure 4** | Graphical illustration of differentiation and EHT generation. (i) Undifferentiated colonies of hiPSCs are expanded in T80 flasks. (ii) EBs are formed in spinner flasks. (iii) EBs are sedimented on V-shaped sedimentation racks. (iv) EB volume is estimated in 15-ml Falcon tubes. (v) EBs are transferred to Pluronic-F-127-coated suspension flasks and mesoderm progenitors are induced. (vi) EBs are sedimented on V-shaped sedimentation racks. (vii) EB volume is estimated in 15-ml Falcon tubes. (viii) EBs are transferred to Pluronic-F-127-coated suspension flasks and cardiomyocytes are differentiated. (ix) Cardiomyocytes are dissociated and EHT master mix plus thrombin aliquot is prepared. (x) EHTs are cast and maintained under cell culture conditions.

For medium changes, the flasks are transferred to V-shaped sedimentation racks and placed in the incubator (for a maximum of 20 min) to enable EB sedimentation in the bottom corner of

the flask (**Fig. 6b**). Approximately half of the medium is then exchanged for new medium to reduce sedimentation time and the time in which EBs are condensed into a pellet, which could

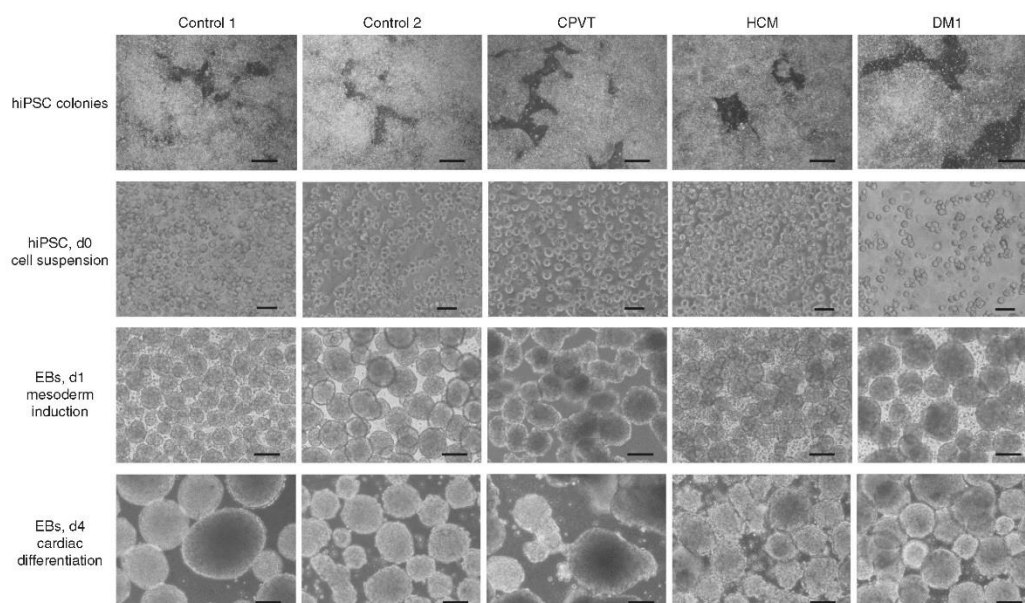


**Figure 5** | Bright-field images at different time points of cardiac differentiation with five different cell lines, showing the typical morphology. Scale bars, 1,000  $\mu\text{m}$  (first row); 100  $\mu\text{m}$  (second row); 250  $\mu\text{m}$  (third and fourth rows).

## PROTOCOL

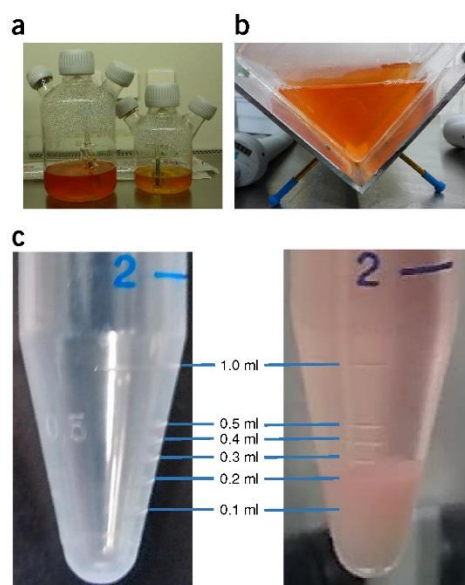


**Figure 6** | Estimation of EB volume after EB formation. (a) Spinner flasks with EBs in EB formation medium. (b) Sedimentation of transferred EBs in T175 flasks on a V-shaped sedimentation rack. (c) 15-ml tube with scale in the lower volume range (left) and example of EB volume (0.2 ml; right).

lead to disintegration of EBs because of cell death. In addition, by leaving more medium, potential (not yet fully defined) paracrine signaling effects are taken advantage of<sup>53</sup>. Only when initiating the next differentiation step is the medium is changed completely and the medium retention reduced to 10–20% to remove the previous medium composition. **Table 1** provides details on the suggested ratio for EB volume, cell culture medium and cell culture flask size. In our experience, BMP-4 (10 ng/ml), activin A (3 ng/ml) and bFGF (5 ng/ml) in the absence of insulin are able to effectively differentiate stem cells from various hiPSC lines into cardiac mesoderm progenitors. Insulin, a key regulator of cardiac differentiation, has previously been shown to inhibit cardiac mesoderm formation and promote cardiac differentiation of human pluripotent stem cells<sup>54–56</sup>.

Cardiac differentiation is initiated on day 4 (Friday) by sedimenting the EBs, removing most of the cell culture medium and pooling the EBs in a graduated 15-ml Falcon tube to estimate EB volume (**Fig. 6c**). Cardiac differentiation is performed with 80–150  $\mu$ l of EB volume per T75 flask or 200–250  $\mu$ l of EB volume per T175 flask. WNT signal inhibition and insulin are the two most important components of this differentiation step. WNT signal inhibition is started on day 4 and is omitted on day 11. Insulin is added on day 7. In comparative studies using FACS analysis, we found these timings for treatment to be the most efficient in inducing differentiation to cardiomyocytes. The first spontaneous beating is generally observed by days 8–10. **Supplementary Videos 1–3** show beating EBs. Between days 14 and 17, the cardiomyocytes can be dissociated from EBs into single cells and cast as EHTs. A sample of these dissociated cells was FACS-analyzed to determine its cardiomyocyte purity (**Fig. 1, Supplementary Fig. 1**). A more detailed FACS analysis of hiPSC-CMs directly after differentiation and after cultivation in EHT format can be found elsewhere<sup>7,9</sup>.

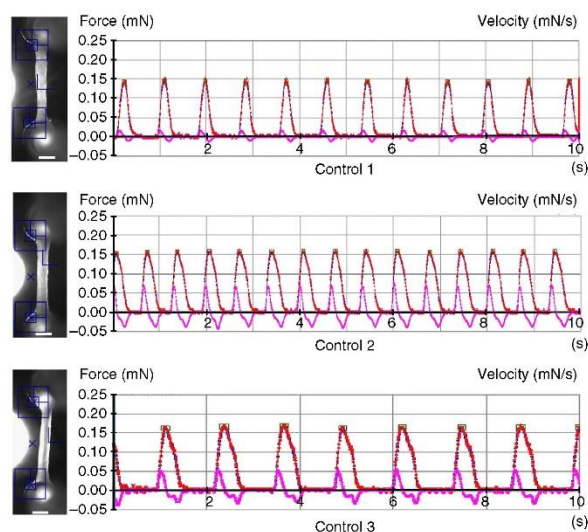


**Figure 7** | Pictures of EHTs from hiPSC-CMs of three different control cell lines taken during a contractility measurement (left) and representative force recording (right). The blue crosses define the top and bottom reference positions for each EHT (left). The red line indicates force, and the purple line indicates velocity (right). Measurements were done in medium (control 1 and control 2) or Tyrode's solution (1.8 mM  $\text{Ca}^{2+}$ , control 3). Scale bars, 1 mm.

The EHT generation procedure relies on the generation of agarose casting molds and formation of fibrin gels with single-cell suspension around flexible PDMS posts<sup>5</sup>. To produce EHTs, a mixture of isolated cardiomyocytes, medium, fibrinogen and thrombin is cast around two PDMS posts, within an agarose mold. Within 2 h, the mixture polymerizes and forms a fibrin block around the posts. **Supplementary Video 4** illustrates the process of EHT generation. Fibrin was chosen as the extracellular matrix for this protocol because it is readily available from different species, it is biodegradable, it has short gelation times and it readily adheres to PDMS. In the beginning of EHT construction, when the fibrin gel is formed, the flexible PDMS posts are oriented parallel to one another. Subsequent remodeling of the matrix by the resident cells leads to shortening of the muscle strip and, thus, bending of the flexible PDMS posts. This configuration of the PDMS posts is a key asset of this EHT system. The tension in the posts applies an auxotonic load to the tissues, and thereby facilitates the longitudinal alignment of the embedded cardiomyocytes. Static stretch, in contrast, is not a physiological environment and promotes a pathological form of hypertrophy in neonatal rat cardiomyocyte EHTs<sup>6</sup>. Approximately 10–15 days after the production of the tissues, EHTs begin to spontaneously beat. As the tissues beat, they further deflect the PDMS posts to which they are attached. This deflection can then be recorded video-optically and measured to assess the force-producing capability of the tissues (**Fig. 7; Supplementary Videos 5–8**). The analysis of EHTs by video-optical recording has proven very useful, as it is performed with high levels of standardization and reproducibility under sterile conditions<sup>5,7</sup>. This last point cannot be overemphasized, as it enables repeated and long-term analysis.

**MATERIALS**

**REAGENTS**

**General reagents**

- 10 × DMEM (Gibco, cat. no. 52100-021)
- 1-Thioglycerol (Sigma-Aldrich, cat. no. M6145)
- 2-propanol (Sigma-Aldrich, cat. no. 278475)
- Agarose (Invitrogen, cat. no. 15510-027)
- Aprotinin (Sigma-Aldrich, cat. no. A1153)
- Sterile water for injection (Baxter, cat. no. 001428)
- B27 plus insulin (Gibco, cat. no. 17504-044)
- BIOMYC-1 (PromoCell, cat. no. PK-CC03-036-1B)
- BIOMYC-2 (PromoCell, cat. no. PK-CC03-037-1B)
- *N*-benzyl-*p*-toluenesulfonamide (BTS; TCI, cat. no. B3082-25G)
- Cytoseal 60 mounting medium (Science Services, cat. no. 18006)
- DMEM (Biochrom, cat. no. F0415)
- DMEM/F-12 without glutamine (Gibco, cat. no. 21331-046)
- DMSO (Sigma-Aldrich, cat. no. D4540)
- EDTA (Roth, cat. no. 8043.2)
- FBS superior (Biochrom, cat. no. S0615)
- Fibrinogen (Sigma-Aldrich, cat. no. F8630)
- Fixable Viability Dye eFluor 660 (eBioscience, cat. no. 65-0864)
- Gelatin (Sigma-Aldrich, cat. no. G1890)
- Geltrex (Gibco, cat. no. A1413302)
- Giemsa stain (Sigma-Aldrich, cat. no. G9641)
- Glacial acetic acid (Roth, cat. no. 3738.1)
- HBSS minus Ca<sup>2+</sup>/Mg<sup>2+</sup> (Gibco, cat. no. 14175-053)
- HBSS plus CaCl<sub>2</sub>/MgCl<sub>2</sub> (Gibco, cat. no. 14025-092)
- HEPES (Roth, cat. no. 9105.4)
- Horse serum (Life Technologies, cat. no. 26050088)
- Human pluripotent stem cell lines: We have used C25 (control 1)<sup>57</sup>, and all other cell lines used were reprogrammed from skin fibroblasts<sup>58</sup> of healthy donors (controls 2 and 3) or from patients suffering from catecholaminergic polymorphic ventricular tachycardia (CPVT), hypertrophic cardiomyopathy (HCM), dilated cardiomyopathy (DCM; DCM-1 and DCM-2) and myotonic dystrophy (DM; DM1) **! CAUTION** The cell lines used in your research should be regularly checked to ensure that they are authentic and that they are not infected with mycoplasma.
- KaryoMax Colcemid in HBSS (10 µg/ml; Life Technologies, cat. no. 15210-040)
- KCl (75 mM; Sigma-Aldrich, cat. no. P9541)
- L-Glutamine (Gibco, cat. no. 25030-081)
- Lipid mix (Sigma-Aldrich, cat. no. L5146)
- Matrigel Basement Membrane Matrix (BD, cat. no. 354234)
- Methanol (J.T. Baker, cat. no. 8045)
- Mucosal (Sigma-Aldrich, cat. no. Z637181)
- Ham's F10 Nutrient Mix (Life Technologies, cat. no. 31550-015)
- PBS (Gibco, cat. no. 10010-049)
- Penicillin/streptomycin (Gibco, cat. no. 15140)
- Phosphoascorbate (2-Phospho-L-ascorbic acid trisodium salt; Sigma-Aldrich, cat. no. 49752)
- Pluronic F-127 (Sigma-Aldrich, cat. no. P2443)
- Polyvinyl alcohol (Sigma-Aldrich, cat. no. P8136)
- Potassium chloride (KCl; Merck, cat. no. 1.04936)
- RPMI 1640 (Gibco, cat. no. 21875)
- Saponin from Quillaja bark (Sigma-Aldrich, cat. no. S7900)
- Selenium (Sigma-Aldrich, cat. no. S5261)
- Sodium selenite (Sigma-Aldrich, cat. no. S5261)
- Thrombin (Biopur, cat. no. BP11-10-1104)
- Titrisol (Sigma-Aldrich, cat. no. 31103)
- Trypsin/EDTA (Gibco, cat. no. 25300)

**Proteins and small molecules**

- Activin-A, stock concentration, 50 µg/ml (R&D Systems, cat. no. 338-AC)
- Basic FGF, improved sequence, stock concentration, 100 µg/ml (Miltenyi Biotec, cat. no. 130-104-921)
- BMP-4, stock concentration, 50 µg/ml (R&D Systems, cat. no. 314-BP)
- Collagenase II (Worthington, cat. no. LS004176)
- DNase II, type V (from bovine spleen; Sigma, cat. no. D8764)
- DS-1-7(IWR-1 analog, 4-(*cis*-endo-1,3-dioxooctahydro-2*H*-4,7-methanoisindol-2-yl)-*N*-(quinolin-8-yl)-*trans*-cyclohexylcarboxamide), stock concentration, 100 mM in DMSO

- Dorsomorphin (Abcam, cat. no. ab120843)
- Human serum albumin (Biological Industries, cat. no. 05-720-1B)
- Insulin, stock concentration, 10 mg/ml (Sigma-Aldrich, cat. no. I9278)
- IWR-1, stock concentration, 20 mg/ml (Sigma-Aldrich, cat. no. I0161)
- TGFβ1 (Peprotech, cat. no. 100-21)
- Thrombin, stock concentration, 100 U/ml (Biopur, cat. no. BP11-10-1104)
- Transferrin (Sigma-Aldrich, cat. no. T8158)
- Y-27632, stock concentration, 10 mM (Biorbyt, cat. no. orb60104)

**Primary antibodies**

- Anti-α-actinin, clone EA-53, monoclonal, 1:800 (Sigma-Aldrich, cat. no. A7811)
- Anti-cardiac troponin T-FITC, clone REA400, 1:10 (Miltenyi Biotec, cat. no. 130-106-687)
- Anti-myosin light chain 2 (MLC-2V; Proteintech, cat. no. 10906-1-AP, 1:100)
- Anti-myosin light chain A, clone 56F5, monoclonal, 1:100 (MLC-2A, Synaptic Systems, cat. no. 311011)
- Anti-human TRA-1-60-FITC, clone TRA-1-60, 1: (BD Biosciences, cat. no. 5608765)
- Anti-SSEA-3-PE, clone MC-631, 1:5 (BD Biosciences, cat. no. 560879)
- Mouse IgG1 isotype control, clone MOPC-21, 1:250 (BD Biosciences, cat. no. 554121)
- FITC mouse IgM, κ isotype control, clone G155-228, 1:200 (BD Biosciences, cat. no. 553474)
- PE rat IgM, κ isotype control, clone R4-22, 1:80 (BD Biosciences, cat. no. 553943)
- REA Control (I)-FITC (IgG1 isotype control, clone REA400, 1:10; Miltenyi Biotec, cat. no. 130-104-611)

**Secondary antibodies**

- Anti-mouse Alexa Fluor 488 (Life Technologies, cat. no. A-11001, 1:800)
- Anti-mouse Alexa Fluor 546 (Life Technologies, cat. no. A-11060, 1:800)
- Anti-rabbit Alexa Fluor 488 (Life Technologies, cat. no. A-11034, 1:800)

**EQUIPMENT**

- 6-Well cell culture plates (Nunc, cat. no. 140675)
- 24-Well plates (Nunc, cat. no. 144530) **▲ CRITICAL** Use Nunc plates (cat. no. 144530) for EHT generation, as 24-well plates do not have standardized dimensions and plates from other suppliers might not be compatible with the PDMS racks or Teflon spacers.
- 250-ml 'rapid' Filtermax vacuum filtration unit (TPP, cat. no. 99250)
- 500-ml 'rapid' Filtermax vacuum filtration unit (TPP, cat. no. 99500)
- Cell scraper (Sarstedt, cat. no. 83.1830)
- Centrifuge tubes, 15 ml (Sarstedt, cat. no. 62.554.502 and Greiner, cat. no. 188280)
- Coplin jar (Sigma-Aldrich, cat. no. S6016-6EA)
- Coverslips (Sigma-Aldrich, cat. no. Z692271)
- CytoVision image analysis system (Leica Biosystems)
- Flow Cytometer (FACSCanto II; BD Bioscience)
- Flow cytometry tubes (Sarstedt, cat. no. 55.1579)
- EHT contractility analysis instrument (EHT Technologies, cat. no. A0001)
- PCR cyclor (e.g., Mastercycler Pro; Eppendorf, cat. no. 6321000515)
- PDMS racks (dimensions: length/width of rack, 79 × 18.5 mm; length of posts, 12 mm; diameter, 1 mm; plate diameter, 2 mm; distance (center-center), 8.5 mm; Young's modulus, 1.7 MPa; EHT Technologies, cat. no. C0001)
- Slides (76 × 26 × 1 mm; Marienfeld, cat. no. REF 1000200)
- Spinner flask (1,000 ml; Integra, cat. no. 182 101)
- Spinner flask (500 ml; Integra, cat. no. 182 051)
- Stirrer, Variomag/Cimarec Biosystem 4 Direct (Thermo Fisher Scientific, cat. no. 50088060)
- Stirrer, Variomag/Cimarec Biosystem Direct (Thermo Fisher Scientific, cat. no. 70101)
- T175 cell culture flask (Sarstedt, cat. no. 83.1812.002)
- T75 cell culture flask (Sarstedt, cat. no. 83.1813.002)
- T80 cell culture flask (Nunc, cat. no. 178905)
- T175 suspension cell culture flask (Sarstedt, cat. no. 83.3912.502)
- Teflon spacers (dimensions: length, 12 mm; width, 3 mm; height, 13.5 mm; EHT Technologies, cat. no. C0002)
- Video-optical force analysis system (EHT Technologies, cat. no. A0001)
- V-shaped sedimentation rack (custom-made; dimensions of the two side panels of the metal bracket: 30 cm × 10 cm; angle: 90°)

## PROTOCOL

### REAGENT SETUP

**10× DMEM** Dissolve 134 mg/ml DMEM powder in 5 ml of sterile water for injection. Sterilize the solution by passing it through a 0.2- $\mu$ m filter, and store the solution at 4 °C for up to 2 months. Store the DMEM powder at 4 °C for up to 36 months, and make sure that the box is properly closed, as DMEM is hygroscopic.

**Agarose** Dissolve 2% agarose (wt/vol) in 300 ml of PBS and autoclave the solution. Store it at 60 °C immediately in a heated cabinet for up to 2 months. **▲ CRITICAL** Do not use water to dissolve the agarose because this will substantially compromise EHT development. Keep agarose at room temperature (18–22 °C) only for up to 10 min; otherwise, it will solidify.

**Aprotinin** Dissolve 33 mg/ml aprotinin in sterile water for injection and make aliquots of 250  $\mu$ l. Store the aliquots at –20 °C for up to 1 year.

**BTS solution** Dissolve BTS in DMSO to a concentration of 30 mM and make aliquots of 250  $\mu$ l. Store the aliquots at –20 °C for up to 1 year.

**DNase solution** Dissolve 100 mg of DNase II, type V in 50 ml of PBS, and make aliquots of 2 ml. Store the aliquots at –20 °C for up to 1 year.

**EDTA solution** Dissolve EDTA in PBS to a concentration of 0.5 mM and sterilize the solution by passing it through a 0.2- $\mu$ m filter; then make aliquots of 50 ml. Store the aliquots at 4 °C for up to 6 months.

**Fibrinogen** Prewarm 0.9% (wt/vol) NaCl solution (37 °C). Grind the lumps of fibrinogen to a fine powder. Dissolve the fibrinogen at a concentration of 200 mg/ml in warm 0.9% (wt/vol) NaCl solution. Incubate the solution in a water bath (37 °C) until the fibrinogen is completely dissolved. Add aprotinin stock (33 mg/ml) to a final concentration of 100  $\mu$ g/ml. Make aliquots of 500  $\mu$ l and store them at –20 °C for up to 2 months, or at –80 °C for up to 1 year.

**Gelatin solution** Dissolve gelatin in water to make a 0.1% (wt/vol) solution and prepare 500-ml aliquots. Store the aliquots at 4 °C for up to 6 months.

**HEPES stock solution** Dissolve HEPES in PBS to a concentration of 1 M, and adjust the pH to 7.4 with potassium hydroxide. Sterilize the solution by passing it through a 0.2- $\mu$ m filter, and make 500-ml aliquots. Store the aliquots at 4 °C for up to 1 year.

**Sodium selenite** Dissolve 33 mg of sodium selenite (382  $\mu$ M) in 500 ml of PBS and prepare 500-ml aliquots. Store the aliquots at 4 °C for up to 1 year.

**Pluronic F-127 solution** Dissolve Pluronic F-127 in PBS to a concentration of 1% (wt/vol). Sterilize the solution by passing it through a 0.2- $\mu$ m filter, and make 500-ml aliquots. Store the aliquots at 4 °C for up to 1 year.

**Polyvinyl alcohol stock solution (50×)** Dissolve 20 g of polyvinyl alcohol in 100 ml of dH<sub>2</sub>O by adding the polyvinyl alcohol slowly and stirring at ~20 °C. After dispersal, the temperature should be increased to 80 °C, while stirring constantly, and then should be held until the polyvinyl alcohol is fully dissolved. Afterward, while stirring, the temperature should be decreased to below 35 °C. Make aliquots of 50 ml and store them at 4 °C for up to 1 year. After the addition of polyvinyl alcohol to the medium, filter-sterilize the medium using a 0.2- $\mu$ m filter.

**Thrombin** Dissolve thrombin at 100 U/ml in 60% (vol/vol) PBS and 40% (vol/vol) sterile water for injection. Mix the solution thoroughly. Make 450- $\mu$ l aliquots (stock) or 3- $\mu$ l aliquots for EHT generation, and store them at –20 °C for up to 1 year.

**Transferrin–selenium** Dissolve 100 mg of transferrin in 2 ml of sodium selenite and make aliquots of 55  $\mu$ l. Store them at –20 °C for up to 1 year.

**hiPSC medium with bFGF, TGF $\beta$ 1, dorsomorphin and activin A (FTDA)** hiPSC medium contains DMEM/F-12 without glutamine, L-Glutamine (2 mM), lipid mix (1/1,000), penicillin/streptomycin (0.5% (vol/vol)), transferrin–selenium stock solution (1/10,000; 5 mg/liter transferrin; 5  $\mu$ g/liter selenium), human serum albumin (0.1% (vol/vol)), insulin (5  $\mu$ g/ml), activin-A (2.5 ng/ml), basic FGF (30 ng/ml), dorsomorphin (50 nM) and TGF $\beta$ 1 (0.5 ng/ml). Filter-sterilize the medium by passing it through a 0.2- $\mu$ m filter, and store it at 4 °C for up to 1 week.

We recommend aliquotting cold FTDA for daily medium changes and only prewarming the aliquot. **▲ CRITICAL** We recommend using basic FGF with improved sequence, because of its increased thermostability and higher resistance to proteases. As the manufacturer does not further specify bFGF kinetics, we recommend considering use of the same precautions as those for normal bFGF, to ensure the highest bFGF stability. Basic FGF is added immediately before using the medium, as diminished concentrations of bFGF can lead to spontaneous differentiation of hiPSCs.

**2× Freezing medium for pluripotent stem cells** 2× Freezing medium contains FTDA (80% (vol/vol)), and DMSO (20% (vol/vol)). Store the medium at 4 °C for up to 2 months.

**EB formation medium** EB formation medium contains FTDA, polyvinyl alcohol (4 mg/ml) and Y-27632 (10  $\mu$ M). Filter-sterilize the medium by passing it through a 0.2- $\mu$ m filter, and store it at 4 °C for up to 1 week.

**Mesoderm induction medium** Mesoderm induction medium contains RPMI 1640, polyvinyl alcohol (4 mg/ml), HEPES (10 mM), penicillin/streptomycin (0.5% (vol/vol)), human serum albumin (0.05% (vol/vol)), phosphoascorbate (250  $\mu$ M), transferrin–selenium stock solution (1/10,000; 5 mg/l transferrin; 5  $\mu$ g/l selenium), lipid mix (1/1,000), Y-27632 (10  $\mu$ M), activin-A (3 ng/ml), BMP-4 (10 ng/ml), and basic FGF (5 ng/ml). Filter-sterilize the medium by passing it through a 0.2- $\mu$ m filter, and store it at 4 °C for up to 1 week without growth factors. We do not recommend storing the medium supplemented with BMP4, activin A and bFGF because growth factor activity may decline during storage.

**▲ CRITICAL** Cardiomyocyte differentiation is substantially hampered if insulin is present during mesoderm induction. We recommend using basic FGF with improved sequence because of its increased thermostability and higher resistance to proteases. As the manufacturer does not further specify bFGF kinetics, we recommend considering use of the same precautions as those for normal bFGF to ensure the highest bFGF stability. Basic FGF is added immediately before using the medium, as diminished concentrations of bFGF can lead to spontaneous differentiation of hiPSCs.

**Cardiac differentiation medium I** Cardiac differentiation medium I contains RPMI 1640, HEPES (10 mM), penicillin/streptomycin (0.5% (vol/vol)), human serum albumin (0.05% (vol/vol)), phosphoascorbate (250  $\mu$ M), transferrin–selenium stock solution (1/10,000; 5 mg/l transferrin; 5  $\mu$ g/l selenium), lipid mix (1/1,000), Y-27632 (1  $\mu$ M), and DS-I-7 (IWR-1 analog (100 nM)). Filter-sterilize the medium by passing it through a 0.2- $\mu$ m filter, and store it at 4 °C for up to 1 week.

**Cardiac differentiation medium II** Cardiac differentiation medium II contains RPMI 1640, B27 plus insulin (2% (vol/vol)), HEPES (10 mM), penicillin/streptomycin (0.5% (vol/vol)), 1-Thioglycerol (500  $\mu$ M), Y-27632 (1  $\mu$ M), and DS-I-7 (IWR-1 analog (100 nM)). Filter-sterilize the medium by passing it through a 0.2- $\mu$ m filter, and store it at 4 °C for up to 1 week.

**Cardiac differentiation medium III** Cardiac differentiation medium III contains RPMI 1640, B27 minus insulin (2% (vol/vol)), HEPES (10 mM), penicillin/streptomycin (0.5% (vol/vol)), 1-Thioglycerol (500  $\mu$ M), and Y-27632 (1  $\mu$ M). Filter-sterilize the medium by passing it through a 0.2- $\mu$ m filter, and store it at 4 °C for up to 1 week.

**Collagenase II solution** Collagenase II solution contains HBSS minus Ca<sup>2+</sup>/Mg<sup>2+</sup>, Collagenase II (200 units per ml), HEPES (10 mM), Y-27632 (10  $\mu$ M), and BTS (30  $\mu$ M). Filter-sterilize the solution by passing it through a 0.2- $\mu$ m filter, and store it at 4 °C for up to 1 week or at –20 °C for up to 1 year. Add Y-27632 and BTS directly before use.

**Dissociation medium** Dissociation medium contains DMEM and DNase (6  $\mu$ l/ml). We do not recommend storing this solution.

**Freezing medium for hiPSC-derived cardiomyocytes** Freezing medium contains heat inactivated FBS (90% (vol/vol)) and DMSO (10% (vol/vol)). We do not recommend storing this solution.

**2× DMEM** 2× DMEM contains 10× DMEM (20% (vol/vol)), heat inactivated horse serum (20% (vol/vol)), penicillin/streptomycin (2% (vol/vol)) and sterile water for injection (58% (vol/vol)). Filter-sterilize the solution by passing it through a 0.2- $\mu$ m filter, and store it at 4 °C for up to 2 months.

**▲ CRITICAL** Use heat-inactivated horse serum to prevent resolving of the EHT.

**EHT medium** EHT medium contains DMEM, heat-inactivated horse serum (10% (vol/vol)), penicillin/streptomycin (1% (vol/vol)), aprotinin (0.1% (wt/vol)); 33  $\mu$ g/ml, and insulin (0.1% (wt/vol); 10  $\mu$ g/ml). Filter-sterilize the medium by passing it through a 0.2- $\mu$ m filter, and store it at 4 °C for up to 1 week.

**▲ CRITICAL** Use heat-inactivated horse serum to prevent resolving of the EHT.

**Normal cardiomyocyte medium** Normal cardiomyocyte medium (NCM) contains DMEM, heat-inactivated FBS (10% (vol/vol)), glutamine (1% (vol/vol)), and penicillin/streptomycin (1% (vol/vol)). Store the medium at 4 °C for up to 2 weeks. **▲ CRITICAL** Use heat-inactivated FBS to prevent resolving of the EHT. For heat inactivation, incubate FBS for 1 h in a 60 °C water bath.

**Washing medium** Washing medium contains RPMI 1640, HEPES (10 mM), and penicillin/streptomycin (0.5% (vol/vol)). Store the medium at 4 °C for up to 2 months.

**FACS buffer for staining of intracellular antigens** This buffer contains 500 ml of PBS, FBS (5% (vol/vol); 25 ml), Saponin (0.5% (wt/vol); 2.5 g), and sodium azide (0.05% (wt/vol); 0.25 g). Store it at 4 °C for up to 2 months. **! CAUTION** Saponin is very hazardous in case of eye contact or inhalation, and must be weighed in a fume hood.

**FACS buffer for staining of extracellular antigens** This buffer contains 500 ml of PBS, FBS (5% (vol/vol); 25 ml), and sodium azide (0.05% (wt/vol); 0.25 g). Store the buffer at 4 °C for up to 2 months.

**F10 complete medium** F10 complete medium contains 10 ml of FBS and 100 ml of Ham's F10 Nutrient Mix. Store the medium at 4 °C for up to 1 week.

**Fixative solution for karyotyping** Add 10 ml of glacial acetic acid to 30 ml of methanol, and keep the solution at -20 °C until use.

We do not recommend storing this solution.

#### EQUIPMENT SETUP

**Geltrex coating of cell culture plates and flasks** Thaw Geltrex on ice and dilute it 1:100 in ice-cold DMEM. Coat the growth surface of the desired culture plates with 1 ml per 10 cm<sup>2</sup>. Incubate the plates at 37 °C for 30 min. Coated plates can be stored at 2–8 °C for up to 2 weeks.

**Pluronic F-127 coating of cell culture flasks** Add 1 ml of 1% (wt/vol) Pluronic F-127 solution to the suspension cell culture flasks per 10-cm<sup>2</sup> growth area.

Incubate the flasks at 37 °C overnight. Wash the flasks twice with 1.5 ml of PBS per 10-cm<sup>2</sup> culture surface. Remove the PBS and add 2 ml of mesoderm induction medium per 10 cm<sup>2</sup>. The cell culture flasks are now ready to use. Coated flasks can be stored at 37 °C for up to 2 weeks.

**▲ CRITICAL** Do not let the surfaces dry out. Longer coating times (for several days) are not detrimental.

**Cleaning protocol for spinner flasks** Clean the spinner flasks and the impellers with dH<sub>2</sub>O and a bottle brush.

Reassemble the spinner flasks and autoclave them. **▲ CRITICAL** Do not use soap/detergent to clean the spinner flasks, and ensure that the spinner flask lids are not fully closed during autoclaving.

**Preparation of Teflon spacers and PDMS racks** Clean the Teflon spacers and PDMS racks with dH<sub>2</sub>O. Boil the Teflon spacers and PDMS racks in dH<sub>2</sub>O twice. Autoclave the Teflon spacers and PDMS racks. **▲ CRITICAL** Do not use soap/detergent to clean the Teflon spacers and PDMS racks. Make sure to place the PDMS racks upside down in the autoclave containers, so that the flexible posts are not bent or distorted during the autoclaving process.

#### PROCEDURE

##### Thawing and expansion of undifferentiated pluripotent stem cells ● TIMING 30 min plus 4 d for expansion before EB formation, including continuous maintenance

- 1| Remove the frozen tube of hiPSCs from liquid nitrogen or -150 °C and thaw the cells at 37 °C.
- 2| Transfer the cells to a 15-ml tube.
- 3| Add 10 ml of FTDA, drop by drop for the first 2 ml.
- 4| Centrifuge the mixture at 200g for 5 min at room temperature.
- 5| Remove the supernatant and resuspend the hiPSCs in the desired volume of FTDA including 10 μM Y-27632.
- 6| Aspirate the liquid from the Geltrex-coated plate, and seed the hiPSCs into the Geltrex-coated wells.
- 7| Put the plate into the incubator and distribute the cells in the well by moving the plate in short side-to-side and back-and-forth motions. Incubator conditions should be set to 37 °C, 5% CO<sub>2</sub>, 21% O<sub>2</sub> and 90% humidity.
- 8| Feed the hiPSCs daily with 2 ml of warm FTDA per 10-cm<sup>2</sup> growth surface until they are 80% confluent. When feeding cells, leave 10–20% of the old medium in the well.

#### ? TROUBLESHOOTING

##### Passaging of undifferentiated hiPSCs ● TIMING 10 min

- 9| Wash the hiPSCs twice with warm (37 °C) PBS.
- 10| Incubate the hiPSCs with 0.5 mM EDTA for 4–5 min at room temperature (1 ml of EDTA per 10-cm<sup>2</sup> growth surface).
- 11| Remove the EDTA solution.

#### Box 1 | Freezing of undifferentiated hiPSCs ● TIMING 15 min

1. Mix 500 μl of freezing medium with 500 μl of the resuspended cells.
2. Add 10 μM Y-27632.
3. Transfer the hiPSCs to a freezing tube.
4. Freeze the tube at -80 °C overnight in a 2-propanol-filled freezing container.
5. Transfer the tubes to liquid nitrogen or -150 °C for long-term storage.

## PROTOCOL

### Box 2 | Mycoplasma screening and treatment ● TIMING 3.5 h or up to 2 weeks

#### Additional reagents

Taq DNA Polymerase Kit (Qiagen, cat. no. 201205) containing:  
10× buffer  
Q-Solution  
MgCl<sub>2</sub> (25 mM)  
Deoxynucleoside triphosphate (DNTP)  
Polymerase  
BIOMYC-1 (PromoCell, cat. no. PK-CC03-036-1B)  
BIOMYC-2 (PromoCell, cat. no. PK-CC03-037-1B)

1. Remove 250 µl of the cell culture medium after overnight incubation and transfer it to a sterile reaction tube.
2. Add 750 µl of sterile water and mix.
3. Incubate the diluted sample for 10 min in a thermoblock at 100 °C.
4. Centrifuge at 250g for 5 min at room temperature.
5. Prepare the PCR master mix by combining the following reagents.

Component	Per reaction
H <sub>2</sub> O	26.75 µl
10× buffer	5.00 µl
Q-Solution	10.00 µl
MgCl <sub>2</sub> (25 mM)	4.00 µl
Primer pool (10 pM) Myco-dw <sup>51</sup> : 5'-TGC ACC ATC TGT CAC TCT GTT AAC CTC-3'	1.00 µl
Primer pool (10 pM) Myco-up <sup>51</sup> : 5'-ACT CCT ACG GGA GGC AGC AGT A-3'	1.00 µl
DNTPs	1.00 µl
Polymerase	0.25 µl
Sum	48.00 µl

6. Take 2 µl of the sample supernatant and add it to 48 µl of the master mix solution. Use water (negative control) and a contaminated supernatant (positive sample) as references.
7. Immediately start the PCR Cyclor set to the following program:

Cyclor	time (t)	°C	Cycles
Initiation	15 min	95	} 40
Denaturation	30 s	94	
Annealing	30 s	56	
Extension	1 min	72	} 1
Final extension	10 min	72	

8. After completing the PCR, load the samples on a 1% (wt/vol) agarose gel and run the reaction for 25 min. If cells test positive for mycoplasma, please follow the next steps; if cells are not infected, please continue to follow the main procedure from Step 23.
9. For the treatment of mycoplasma infections, sequentially treat the contaminated cell culture with BIOMYC-1 for 4 d and then with BIOMYC-2 for 3 d, according to the manufacturer's instructions.
10. Repeat two to three treatment cycles to avoid antibiotic resistance.

**12|** Vigorously flush the surface of the wells with 3 ml of FTDA per 10-cm<sup>2</sup> growth surface to detach cell clusters. At this step, the cells can be frozen for storage; see **Box 1** for details.

**13|** Pool the detached cell clusters.

**14|** Remove the Geltrex solution from new six-well dishes/T80 flasks and immediately add the cell solution to the prepared culture flasks/plates at ratios of 1:2 to 1:6 (6.5 × 10<sup>4</sup> cells per cm<sup>2</sup>). Before preparing hiPSCs for cardiomyocyte differentiation, we recommend performing mycoplasma testing as described in **Box 2** and regularly performing karyotyping as described in **Box 3**.

#### ? TROUBLESHOOTING

**FACS analyses of hiPSCs for pluripotency markers: staining of extracellular antigens ● TIMING 90 min**

**15|** Harvest hiPSCs as described in Steps 9–13.

**16|** Resuspend the cells in 500 µl of FACS buffer and incubate for 15 min at 4 °C.

### Box 3 | Karyotyping of hiPSCs ● TIMING 2.5 h, plus analysis of arresting cells in metaphase

1. Use at least  $4 \times 10^6$  hiPSCs (20-cm<sup>2</sup> growth area) for karyotyping to ensure that you have a sufficient amount of metaphases for analysis.
2. Add 40  $\mu$ l of colcemid to each well and incubate for 5 h at 37 °C and 5% CO<sub>2</sub>.

#### Harvesting of hiPSCs

3. Wash the hiPSCs twice with PBS. Incubate the hiPSCs with 0.5 mM EDTA for 5 min at room temperature (1 ml of EDTA per 10-cm<sup>2</sup> growth surface). Remove the EDTA solution. Vigorously flush the growth surface with 2 ml of F10 complete medium per 10 cm<sup>2</sup> to detach the hiPSCs.
4. Triturate the cells four times with a 10-ml pipette.
5. Transfer the hiPSCs to a centrifuge tube.
6. Centrifuge at 250g for 10 min at room temperature.
7. Remove the supernatant, and while swirling the cell suspension on a vortex mixer keep the centrifuge tube in a slanted position and pour the 7 ml of warm 75 mM KCl solution dropwise gently along the inner wall of the tube onto the cell suspension.

▲ **CRITICAL STEP** This step is critical because the hiPSCs swell in the hypotonic solution and the chromosomes can spread out, which provides better results for chromosome analysis.

8. Invert the tube gently to mix, and incubate for 15 min at 37 °C.
9. With a glass Pasteur pipette, add 13 drops of fixative solution to the suspension, invert gently and centrifuge at 250g for 10 min at room temperature.
10. Remove up to 1 ml of the supernatant.
11. Resuspend the cell pellet on a vortex mixer and add 6 ml of ice-cold fixative, drop by drop, while swirling to prevent cell clumping.
12. Centrifuge at 250g for 10 min at room temperature, and repeat the fixative addition step two more times. At this point the fixative can be added more quickly to the suspension.
13. After the last fixative addition step, remove enough fixative so that the resuspended cell solution appears slightly cloudy.
14. The cell suspension is now ready for slide making or may be stored.

■ **PAUSE POINT** The cell suspension can be stored at -20 °C for several years. If cells were stored for more than 4 weeks, repeat steps 12 and 13.

#### Slide preparation

15. Wipe the slides with a tissue soaked in 70% (vol/vol) ethanol on both sides. Arrange the slides alternately straight across and diagonally in a 150-ml slide staining dish. Rinse the slides with the detergent solution Mucosal in hot water and cover. Let the slides sit overnight at room temperature. Remove the washing solution and rinse the slides with water for 15 min. Rinse two more times with purified water and fill the dish with sterile water for injection. The slides are now ready to use and should be kept in water at 4 °C until use.

■ **PAUSE POINT** The slides can be kept at 4 °C for 4 weeks.

#### Slide making

16. Preheat a laboratory oven to 80 °C and place a beaker inside with 50 ml of dH<sub>2</sub>O to increase humidity.
- ▲ **CRITICAL STEP** Optimal environmental conditions to ensure good slide quality are 45–50% humidity and a temperature of 20–22 °C.
17. Place the centrifuge tube with the hiPSC suspension on ice.
18. Cut off the end of a pipette tip from a 100- $\mu$ l pipette and use it to resuspend the cells by gently pipetting.
19. Take a slide from step 15 out of the Coplin jar and place 80–100  $\mu$ l of hiPSCs onto the wet slide from a height of ~20 cm.
20. Wipe off excess fluid from the back of the slide, label the slide and place it in the oven on top of the beaker until all the fixative has evaporated.
21. Check the cell density and metaphase spreading using a phase-contrast microscope.

#### ? TROUBLESHOOTING

22. Incubate the slides before staining in a laboratory oven at 95 °C for 15 min or keep them at room temperature for several days.

#### Trypsin G-banding

23. For Trypsin G-banding (GTG-banding), prepare three Coplin jars, one with 0.25% (vol/vol) trypsin in HBSS (jar 1), another with 1 $\times$  PBS (jar 2) and a final jar containing 10% (vol/vol) Giemsa Stain in Titrisol, pH 7.2 (jar 3).
24. Place the slide into jar 1 for 5 s. Then dab the slide onto a wiper to remove excess trypsin.
25. Dip the slide into jar 2 twice and dab the slide onto a wiper to remove excess fluid.
26. Place the slides into jar 3 for 6 min.
27. Rinse the slide with cold water.
28. Use a wiper to clean the backs of the slides, and then let the slides air-dry for a few minutes.

#### Analysis of chromosomes

29. Cover the slides with a coverslip and Cytoseal 60. For each cell line, analyze 15 metaphases under a light microscope at a 1,000 $\times$  magnification.

▲ **CRITICAL** For analysis of the chromosomes, a banding resolution of at least 400 b.p.h. (bands per haploid) is generally required, and the chromosomes should be well separated to permit their clear visualization.

#### ? TROUBLESHOOTING

30. Choose the best mitotic spreads for karyotypes. Long chromosomes, few overlaps and clear bands are important criteria for judging good spreads. At least four metaphases of each cell line should be karyotyped using an appropriate cytogenetic image analysis system.

#### ? TROUBLESHOOTING

## PROTOCOL

- 17| Centrifuge the cell suspension at 4 °C for 5 min at 200g, and discard the supernatant.
- 18| In one FACS tube, resuspend  $2 \times 10^5$  cells in 100  $\mu$ l of FACS buffer containing the directly labeled antibody (e.g., FITC-anti-human TRA-1-60 (1:5 dilution) or PE-anti-SSEA-3 (1:5 dilution)) and in another FACS tube resuspend  $2 \times 10^5$  cells in 100  $\mu$ l of FACS buffer with the respective isotype control (e.g., FITC mouse IgM,  $\kappa$  isotype (1:200 dilution) or PE rat IgM,  $\kappa$  isotype (1:80 dilution)).
- 19| Incubate the cells for 30 min at 4 °C.
- 20| Wash the cells with 2.5 ml of FACS buffer and centrifuge at 200g for 5 min at 4 °C; discard the supernatant and repeat the wash.
- 21| Resuspend the cells in 150  $\mu$ l of PBS.
- 22| Analyze the cells with a flow cytometer, adjusting the gates according to the isotype control (**Supplementary Fig. 2**). If the cells express pluripotency markers, continue with EB formation (Step 23).

### Embryoid body formation ● **TIMING 2 h per cell line and 10 flasks, plus 1 d for incubation**

- 23| Expand the hiPSCs from Step 22 in T80 flasks to 80% confluency.
- 24| Add 10  $\mu$ M Y-27632 to the T80 flasks containing 80% confluent hiPSCs in FTDA.
- 25| Incubate the hiPSCs for 1 h at 37 °C.
- 26| Remove the FTDA.
- 27| Wash the hiPSCs twice with 10 ml of PBS.
- 28| Incubate the hiPSCs with 0.5 mM EDTA for 5–10 min at room temperature (1 ml of EDTA per 10-cm<sup>2</sup> growth surface).  
▲ **CRITICAL STEP** Monitor the hiPSCs during EDTA incubation because detachment varies between cell lines. If the hiPSCs detach very easily, shortening of the incubation time might be necessary to avoid cell loss. At the same time, make sure that you obtain a single-cell suspension.
- 29| Remove the EDTA solution.
- 30| Add 1 ml of warm PBS per 10-cm<sup>2</sup> growth surface.
- 31| Tap the flasks on the bench to detach the hiPSCs.
- 32| Triturate the cells three times with a 10-ml pipette.
- 33| Transfer the hiPSCs to a 50-ml Falcon tube containing 10 ml of EB formation medium.
- 34| Rinse the cell culture flasks with 5 ml of Ca<sup>2+</sup>-containing RPMI medium and add it to the cell suspension from Step 33.
- 35| Centrifuge the hiPSCs at 250g for 5 min at room temperature.
- 36| Resuspend the hiPSCs in 10 ml of EB formation medium by triturating five times with a 10-ml pipette.
- 37| Count the hiPSCs.
- 38| Resuspend the hiPSCs in the EB formation medium at a concentration of  $30 \times 10^6$  cells per 100 ml.
- 39| Add the hiPSC suspension to the spinner flask.
- 40| Incubate the flask overnight at 37 °C, 5% CO<sub>2</sub>, 5% O<sub>2</sub>, 90% humidity, rotating at 40 r.p.m.



**Induction of mesodermal progenitor cells ● TIMING 1 h per spinner flask, plus 3 d for cultivation**

- 41| Transfer 50 ml of the EB suspension from the spinner flask to a Falcon tube.
- 42| Transfer the rest of the EB suspension to T175 flasks (a maximum of 200 ml per flask).
- 43| Place the T175 cell culture flasks on a prewarmed V-shaped sedimentation rack.
- 44| Put the rack back in the incubator, and let the EBs sediment in the lower corner of the flask for 5–20 min (maximum), depending on EB (~100–300 μm).  
**▲ CRITICAL STEP** Once sedimented, process the EBs as soon as possible.
- 45| Remove the supernatant from the 50-ml Falcon tube, add 5 ml of washing medium, transfer the EBs to a 15-ml Falcon tube with a marked scale to estimate the EB volume (**Fig. 6**), and calculate the total EB volume by extrapolating to the total volume of EB formation medium.  
**▲ CRITICAL STEP** EBs should not be left in the Falcon tube for more than 5 min after sedimentation.
- 46| Remove 90% of EB formation medium in the T175 flask from Step 44, and add the EBs from the Falcon tube. If there is more than one flask, you can pool all the EBs together.
- 47| Wash the EBs with prewarmed washing medium.
- 48| Remove at least 90% of the washing medium, and resuspend the EBs carefully in mesoderm induction medium.
- 49| Transfer the EBs to Pluronic-F-127-coated suspension cell culture flasks. If you are using a T75 cell culture flask, transfer 50–100 μl of EBs in 20 ml of mesoderm induction medium; if you are using a T175 cell culture flask transfer 150–250 μl of EBs in 40 ml of mesoderm induction medium.  
**▲ CRITICAL STEP** If you have more than one T175 flask per cell line, check the volume of medium in which the EBs are kept, divide it by the number of flasks you need and then remove the volume for one flask at a time to make sure that the EBs are distributed equally.
- 50| Incubate the flasks for 3 d at 37 °C, 5% CO<sub>2</sub>, 5% O<sub>2</sub> and 90% humidity. Change the medium daily.  
**? TROUBLESHOOTING**
- 51| For medium change, place the T175 cell culture flask on a V-shaped sedimentation rack.
- 52| Let the EBs sediment in the lower corner of the flask (~5 min).
- 53| Remove 50% of the medium (20 ml).
- 54| Add 20 ml of medium/200 μl of EB volume.
- 55| Place the flasks back into the incubator.

**Cardiac differentiation ● TIMING 1 h per cell line and 10 flasks, plus 10 d for cultivation**

- 56| Place the T175 cell culture flask on a V-shaped sedimentation rack.
- 57| Let the EBs sediment in the lower corner of the flask (5 min).  
**▲ CRITICAL STEP** Once sedimented, process the EBs as soon as possible.
- 58| Remove 90% of mesoderm induction medium and add 20 ml of washing medium. Let the EBs sediment.
- 59| Remove 90% of washing medium and add 5 ml of cardiac differentiation medium I.
- 60| Transfer the EBs to a 15-ml Falcon tube.
- 61| Let the EBs sediment.

## PROTOCOL

**62|** Estimate the EB volume with the aid of the scale on the 15-ml Falcon tube (**Fig. 6**).

**▲ CRITICAL STEP** Use 15-ml tubes with a marked scale to facilitate estimation of EB volume (**Fig. 6**). Once sedimented, process the EBs as soon as possible. EBs should not be left in sediment in the Falcon tube for >5 min.

**63|** Transfer the EBs to Pluronic-F-127-coated cell culture flasks. If you are using a T75 flask, transfer 80–150  $\mu$ l of EBs in 20 ml of medium; if you are using a T175 flask, transfer 200–250  $\mu$ l of EBs in 46 ml of medium.

**64|** Incubate the cells for 3 d. Leave the cells for 1 d and on days 2 and 3 change the medium (50% medium exchange). Incubate the cells at 37 °C, 5% CO<sub>2</sub>, 21% O<sub>2</sub> and 90% humidity.

**▲ CRITICAL STEP** When changing the medium, ensure that the EBs are not left in sediment and are processed as soon as possible.

**? TROUBLESHOOTING**

**65|** Switch to cardiac differentiation medium II, and incubate the cells for an additional 4 d with daily medium changes (50% medium exchange). Incubate the cells at 37 °C, 5% CO<sub>2</sub>, 21% O<sub>2</sub> and 90% humidity.

**▲ CRITICAL STEP** When changing the medium, ensure that the EBs are not left in sediment and are processed as soon as possible.

**? TROUBLESHOOTING**

**66|** Switch to cardiac differentiation medium III and incubate the cells for an additional 3 d with daily medium changes (50% medium exchange). Incubate the cells at 37 °C, 5% CO<sub>2</sub>, 21% O<sub>2</sub> and 90% humidity.

**▲ CRITICAL STEP** When changing the medium, ensure that the EBs are not left in sediment and are processed as soon as possible.

**? TROUBLESHOOTING**

### Generation of human EHT ● **TIMING 1 d, plus 2–3 weeks for maintenance**

**67|** For dissociation of hiPSC-CMs, remove cardiac differentiation medium III.

**68|** Wash the hiPSC-CMs carefully with HBSS twice.

**69|** Add 1 ml of collagenase II solution per 10-cm<sup>2</sup> growth surface.

**70|** Incubate the mixture for 3–4 h at 37 °C, 5% CO<sub>2</sub>, 21% O<sub>2</sub> and 90% humidity. During this time, monitor the progress of cell dissociation microscopically.

**71|** In the meantime, prewarm DMEM to 37 °C, prepare dissociation medium and have sterile Teflon spacers, sterile PDMS racks, fibrinogen stock, thrombin aliquots, 24-well plates, liquid sterile agarose (keep in the heated cabinet at 60 °C), 2× DMEM, EHT medium and a cell counting instrument ready to use for the generation of EHTs.

**72|** Transfer the dissociated hiPSC-CMs to a 50-ml Falcon tube.

**73|** Flush the cell culture flask with dissociation medium and place the medium in the same Falcon tube.

**74|** Centrifuge the hiPSC-CMs for 10 min at 100g at room temperature.

**▲ CRITICAL STEP** Cardiomyocytes are sensitive to centrifugation at high speed. Do not centrifuge faster than 100g.

**75|** Discard the supernatant and resuspend the hiPSC-CMs in 20 ml of DMEM, or in 40 ml of medium (for a larger pellet to aid cell counting).

**76|** Count the cells with an automated cell counter.

**▲ CRITICAL STEP** Cell counting, especially with a Neubauer chamber, is difficult to standardize. We suggest using an automated procedure for cell counting.

**? TROUBLESHOOTING**

**77|** Centrifuge the hiPSC-CMs at 100g for 10 min at room temperature. After this step, continue to the next step to prepare the fibrinogen containing the master mix solution and the casting molds for EHT generation. Alternatively, follow **Box 4** for cryopreservation and thawing of cardiomyocytes or **Box 5** for FACS analyses of dissociated hiPSC-cardiomyocytes.

**▲ CRITICAL STEP** Cardiomyocytes are sensitive to centrifugation at high speed. Do not centrifuge faster than 100g.

**Box 4 | Freezing and thawing of cardiomyocytes ● TIMING 30 min, plus 4 h for dissociation of cardiomyocytes**

▲ **CRITICAL** Volumes are given for one cryovial. When thawing two or three vials of the same cells, pool the cell suspension before adding the rinse and final volumes of medium. Adjust the media volumes accordingly.

1. Dissociate the cardiomyocytes as described in the 'Generation of human EHT' section (Steps 67–76).
2. Resuspend the cardiomyocyte pellet in cold freezing medium for hiPSC-CMs. Use 1 ml of freezing medium per cryovial. Freeze at least 2 million hiPSC-CMs per vial.
3. Distribute the cells into cryovials. Avoid making bubbles or touching the cryovial cap.
4. Place the cryovials into a cryobox.
5. Place the cryobox at –80 °C for 12–24 h.
6. Transfer the cryovials to a –150 °C freezer or liquid nitrogen.

■ **PAUSE POINT** The cells can be stored at –150 °C for several years.

7. For thawing of cardiomyocytes, remove the cryovial from the storage tank (–150 °C).

8. Warm one vial at a time in your hand until the freezing medium is almost completely thawed.

▲ **CRITICAL STEP** Do not thaw more than three vials of cardiomyocytes at one time.

9. If necessary, cryovials can be placed on dry ice for up to 10 min before thawing.

10. Gently transfer the cryovial cell suspension to a sterile 50-ml Falcon tube using a 1-ml pipette.

11. Rinse the empty cryovial with 1 ml of room-temperature RPMI to recover any residual cells from the vial.

12. Transfer the 1 ml of RPMI from the cryovial dropwise over 90 s to the 50-ml Falcon tube containing the cell suspension.

▲ **CRITICAL STEP** Dropwise addition of medium to the cell suspension is critical in order to minimize osmotic shock.

13. Gently swirl the tube while adding the medium.

14. Slowly add 8 ml of room-temperature RPMI to the 50-ml Falcon tube. Add the first 1 ml dropwise over 30–60 s. Then add the remaining 7 ml over 30 s. Gently swirl the tube while adding the medium.

15. Gently mix the Falcon tube by inverting two to three times.

▲ **CRITICAL STEP** Avoid pipetting or vortexing.

16. Count the cells within the cell suspension.

? **TROUBLESHOOTING**

17. Centrifuge the cell suspension to pellet the cardiomyocytes at 100g for 5 min at room temperature before EHT generation (Steps 78–92).

**78|** Prepare the master mix based on the cell count. Calculate the number of EHTs that will be generated ( $1.0 \times 10^6$  per EHT) (see table below for guidance).

	Per EHT	Per 24-well plate
NCM medium	81.9 µl	1,965.6 µl
Fibrinogen stock	2.5 µl	60.0 µl
Matrigel Basement Membrane Matrix	10.0 µl	240.0 µl
2× DMEM	5.5 µl	132.0 µl
Y-27632	0.1 µl	2.4 µl
Dissociated cells	$1.0 \times 10^6$	$24 \times 10^6$
Total	100.0 µl	2,400.0 µl

**79|** Resuspend the corresponding volume of fibrinogen stock in cold NCM.

▲ **CRITICAL STEP** Fibrinogen must be room temperature for pipetting. Dissolve the fibrinogen thoroughly.

**80|** Add Y-27632 (final concentration 10 µM).

**81|** Add 2× DMEM.

**82|** Add Matrigel Basement Membrane Matrix.

## PROTOCOL

### Box 5 | FACS analyses of dissociated hiPSC–cardiomyocytes ● TIMING 3 h, plus 4 h for dissociation of cardiomyocytes

1. Dissociate the cardiomyocytes as described in the 'Generation of human EHT' section (Steps 67–76).
2. Prepare two FACS tubes, each with 200,000 freshly dissociated hiPSC-CMs.
3. Wash with 3 ml of PBS, centrifuge for 5 min at 200g at room temperature and discard the supernatant. Repeat this wash step.
4. Resuspend the cells in 500 µl of cold methanol (–20 °C) and fix the cells for 20 min on ice.
5. Wash twice with 500 µl of FACS buffer.
6. For further permeabilization, resuspend the fixed cells in 500 µl of FACS buffer and incubate for at least 45 min at 4 °C.
7. Staining of intracellular antigens: resuspend permeabilized cells from one FACS tube in 100 µl of FACS buffer containing the primary or directly labeled antibody (e.g., anti-cardiac Troponin T-FITC, 1:10 dilution) and the resuspend the cells from the other tube with the respective isotype control (e.g., REA Control (I)-FITC). Incubate for 30 min at 4 °C.
8. Wash twice with 2.5 ml of FACS buffer.
9. If you are using a secondary antibody, repeat steps 7 and 8 with the secondary antibody.
10. Resuspend the cells in 150 µl of PBS.
11. Analyze the cells with a flow cytometer, adjusting the gates according to the isotype control (Supplementary Fig. 2).

83| Pipette up and down thoroughly until the fibrinogen is dissolved.

84| Resuspend the cell pellet in the fibrinogen containing the master mix and keep it on ice.

▲ **CRITICAL STEP** Cardiomyocytes are sensitive to shear stress and repeated resuspension. Prepare the fibrinogen containing the master mix and resuspend the hiPSC-CMs directly in the master mix.

▲ **CRITICAL STEP** Avoid air bubble formation during pipetting.

▲ **CRITICAL STEP** Calculate 10% extra volume to compensate for loss during pipetting.

85| *Generation of casting molds.* Pipette 1.6 ml of liquid agarose into 8 wells of a 24-well plate. Place the Teflon spacers onto these wells directly after pipetting, as agarose solidifies very quickly. Repeat with the following wells. Let the agarose solidify at room temperature (10–15 min).

▲ **CRITICAL STEP** Prolonged solidification results in fine cracks in the surface of the agarose. This makes the casting molds leaky and decreases the efficiency of EHT generation.

86| Remove the Teflon spacers.

87| Position the PDMS racks on the 24-well plate such that each pair of PDMS posts is positioned within one agarose casting mold.

88| *Pipetting of EHTs.* Mix 100 µl of master mix with one thrombin aliquot (3 µl) briefly. Pipette the mixture quickly into an agarose casting mold with the PDMS racks placed on top. Repeat this step for each EHT separately.

▲ **CRITICAL STEP** Use a new filter pipette tip for pipetting each EHT. Resuspend the master mix carefully after 4–8 EHTs. Avoid air bubble formation during pipetting, by pressing the pipette only until the first pressure point.

89| Place the 24-well plate in the incubator at 37 °C, 7% CO<sub>2</sub>, 40% O<sub>2</sub> and 90% humidity for 120 min.

90| Supplement the fibrin gels in the casting molds with 200–300 µl of DMEM per well.

▲ **CRITICAL STEP** Adding the medium on top of the EHT before transfer will ease the removal from the casting molds and improve the efficiency of EHT generation.

91| Incubate the gels for an additional 10 min.

92| Prepare a 24-well plate with prewarmed EHT medium (1.5 ml per well), and transfer the PDMS racks with fibrin gels carefully from the casting mold plate to the new cell culture plate.

93| Incubate the EHTs at 37 °C, 40% O<sub>2</sub>, 7% CO<sub>2</sub> and 90% humidity for at least 2 weeks.

#### ? TROUBLESHOOTING

**94| EHT medium change.** Perform medium changes on Mondays, Wednesdays and Fridays. To do this, prepare a second 24-well plate with new EHT medium, and transfer the PDMS rack/EHTs carefully.

Make sure that the EHTs do not touch the edges of the wells while doing this.

**▲ CRITICAL STEP** Use two 24-well plates for the entire batch of EHTs and refill with new medium to transfer the EHTs back and forth between the two plates.

**95|** Monitor the EHTs during development by observing single-cell contraction and coherent contraction of small areas of cells microscopically and coherent contraction of entire EHTs by video–optical analysis in the following steps.

**? TROUBLESHOOTING**

**Video–optical analysis of contractile force ● TIMING 20 min for a baseline measurement of one 24-well plate—20 s per EHT**

**96|** 1 h before the experiment, turn on the hardware, heating, gas supply (O<sub>2</sub>, N<sub>2</sub> and CO<sub>2</sub>), axis system, LEDs and computer.

**97|** Make sure that the temperature, humidity and CO<sub>2</sub> in the internal incubator box have reached target values. We recommend using 37 °C, 90% humidity and 7% CO<sub>2</sub>.

**98|** Start the software.

**99|** Place the 24-well cell culture plate with the EHTs into the internal incubator box on top of the LED panel on the small metal pins.

**100|** Use the manual ‘EHT contractility analysis instrument’ to set up the experiment.

**101|** Define the parameters for contractility analysis. Standard parameters for human EHT are as follows: peak force, 4; filter level, 10; baseline level, 0.95; force threshold, 0.02–0.05 mN; minimum factor, 0.2; maximum peak dist., 60 s; contraction velocity/relaxation velocity (CV/RV) threshold factor, 0.2.

**102|** Define the top and bottom reference positions (blue crosses) for each EHT per well by optimizing the xyz coordinates.

**103|** Start the measurement. Details in regard to the analysis of data are provided in the manual of the EHT contractility analysis instrument.

**? TROUBLESHOOTING**

Critical steps throughout this protocol are emphasized for each differentiation step. Low differentiation efficiencies can be the result of diverse problems that must be excluded systematically. As mentioned above, the quality of hiPSC culture is the most important prerequisite for efficient differentiation. Undesired spontaneous differentiation of hiPSCs may occur in cultures that are either too sparsely or too densely populated. 80% confluency is the optimal cell density for starting a differentiation. In addition, the passage number may have an impact on hiPSC quality. Usually it takes some passages after thawing before the hiPSCs show their normal growth behavior. On the other hand, mutations may accumulate over time. We regularly perform karyotyping and dispose of cultures with a passage number >100. Therefore, it is important to maintain a large cell bank of hiPSCs with a low passage number. Media composition is also critical to maintaining the stem cells’ undifferentiated state. FTDA contains bFGF, TGFβ1 and activin A, which cooperatively support proliferation, whereas dorsomorphin inhibits spontaneous differentiation<sup>14</sup>. bFGF is not stable at 37 °C, which leads to large fluctuations in bFGF levels in the culture medium<sup>59</sup>. To improve the efficiency of this essential growth factor, we use bFGF which has an increased thermostability and higher resistance to proteases, and which retains the same biological properties as naturally occurring bFGF<sup>20</sup>. This growth factor variant is also advantageous for the induction of mesodermal progenitor cells. We observed that the absence of bFGF during mesoderm induction is detrimental to the differentiation efficiency.

Insulin, in contrast, inhibits differentiation of hiPSCs to mesodermal progenitor cells<sup>54</sup>. Therefore, it is added only during the progression of mesodermal cells toward cardiomyocytes (day 7 until day 11). During this stage, potent small-molecule inhibitors of canonical WNT signaling promote cardiac differentiation.

With regard to handling of the EBs, it is important to keep all processing steps as short as possible and to avoid long resting times in the sedimented state. In addition, EBs must be pipetted carefully at early steps and should not be centrifuged, because this will lead to disaggregation of the cell clusters.

Handling of cardiomyocytes must be performed carefully as well, as they are sensitive to shear stress and more susceptible to high-speed centrifugation than other cells. Therefore, dissociation of differentiated cardiomyocytes and generation of EHTs must be carried out in a conscientious manner. EHTs can also be generated from cryopreserved cardiomyocytes. Viability after thawing is usually 80–90% (**Fig. 1c**). With regard to EHT generation, it is important to prepare the master

## PROTOCOL

mix on ice, to avoid bubbles during pipetting and to use heat-inactivated serum to avoid dissolving of the fibrin matrix. Overall, EHT generation is a very robust process if differentiation efficiency is sufficient and cardiomyocyte viability is high. Further troubleshooting advice can be found in **Table 3**.

**TABLE 3** | Troubleshooting table.

Step	Problem	Possible reasons	Solution
8: Thawing of hiPSCs	Poor attachment of hiPSCs to Geltrex-coated plates	No ROCK inhibitor Y-27632 was included in FTDA medium	Add Y-27632 to the FTDA medium
8: Cultivation of hiPSCs	Spontaneous differentiation of hiPSCs	Cultures were too sparsely or too densely populated	Adjust passage ratio
		Growth factors with low activity	Always prepare fresh FTDA
14: Passaging of hiPSCs	hiPSCs are proliferating very slowly	After thawing, hiPSCs must be passaged several times before they show their normal growth behavior	Wait for some passages to occur
		Mycoplasma infection	Perform mycoplasma test
		Karyotype abnormalities	Perform karyotyping
14: Passaging of hiPSCs	Many dead cells	Imperfect coating	Passage hiPSCs to newly coated plates/flasks
		EDTA incubation lasted too long	Monitor the cells under a microscope and stop dissociation at the right time
Box 3, step 21: Karyotyping	Cell density was too high; (ii) Cell density was too low	An enzyme was used for dissociation	Enzyme-free dissociation is more gentle and increases the likelihood of cell survival
		Volume was not sufficient for the number of cells	Dilute the suspension with a few drops of ice-cold fixative
		The number of cells was too low for the volume used	Centrifuge at 250g for 10 min at 4 °C and resolve the pellet in a smaller volume of fixative
Box 3, step 30: Karyotyping	Chromosomes do not show satisfactory spreading	Humidity and/or temperature was unfavorable for spreading	Try to adjust the humidity to 45–50% and keep the slide at 20 °C–30 °C while placing the drops on the slide
		Staining does not give a clear distinction between pale staining and dark staining of different chromosomal regions	Adjust trypsin treatment time Optimize Giemsa staining
50 and 64–66: Differentiation of cardiomyocytes	EBs are dissolving	Trypsin was incubation too long/short	Adjust trypsin treatment time
		Giemsa staining was not sufficient	Optimize Giemsa staining
66: Differentiation of cardiomyocytes	No spontaneously contracting cells on day 14	EBs were kept sedimented too long	Keep transfer steps as short as possible—e.g., 50% medium exchange within a differentiation step
		EBs were processed carelessly	Pipette EBs carefully and do not centrifuge
66: Differentiation of cardiomyocytes	No spontaneously contracting cells on day 14	Poor-quality hiPSC culture	See solutions concerning problems during cultivation of hiPSCs
		Low bFGF activity during EB formation and/or mesoderm induction	Use stable bFGF and add it directly before use of medium
76: Dissociation of cardiomyocytes	Many dead cardiomyocytes	Incubation in collagenase solution lasted too long	Monitor dissociation microscopically
		Cardiomyocytes were processed carelessly	Pipette cardiomyocytes carefully and do not centrifuge faster than 100g
93: Generation of human EHT	EHTs are dissolving	Active serum was used for one of the components or the medium	Only use heat-inactivated serum
		Reduced activity/degradation of aprotinin	Replace aprotinin

(continued)

TABLE 3 | Troubleshooting table (continued).

Step	Problem	Possible reasons	Solution
95: Generation of human EHT	EHTs are not contracting on day 15	Differentiation efficiency was too low	Only use differentiated cell populations with $\geq 60\%$ troponin-T-positive cells
Box 4, step 16: Thawing of cardiomyocytes	Many dead cardiomyocytes after thawing	Freezing medium was unsuitable Freezing process damaged cardiomyocytes Thawing process damaged cardiomyocytes	Use 90% (vol/vol) FBS plus 10% DMSO (vol/vol) for freezing cardiomyocytes Always use cryoboxes, freeze at $-80\text{ }^{\circ}\text{C}$ and store at $-150\text{ }^{\circ}\text{C}$ Thaw cardiomyocytes as quickly as possible, but add medium slowly to minimize osmotic shock

● TIMING

- Steps 1–7, thawing of hiPSCs: 30 min
- Step 8, daily maintenance of hiPSCs: 4 d
- Steps 9–14, passaging of hiPSCs: 10 min
- Steps 15–22, FACS analysis of hiPSCs: 90 min
- Steps 23–66, differentiation of cardiomyocytes: 14 d
- Steps 23–40, EB formation: 2 h per cell line and 10 flasks, plus 24-h for incubation
- Steps 41–49, induction of mesodermal progenitor cells: 1 h per spinner flask
- Steps 50–55, induction of mesodermal progenitor cells: 3 d
- Steps 56–63, cardiac differentiation: 1 h per cell line and 10 flasks
- Steps 64–66, cardiac differentiation: 10 d
- Steps 67–92, generation of human EHT: 1 d
- Steps 93–95, maintenance of human EHT: 14 d
- Steps 96–103, video–optical analysis of contractile force: 20 min for baseline measurement
- Box 1, freezing of undifferentiated hiPSCs: 15 min
- Box 2, mycoplasma screening and treatment: 3.5 h or up to 2 weeks
- Box 3, karyotyping of hiPSCs: 2.5 h, plus analysis of arresting cells in metaphase
- Box 4, freezing and thawing of cardiomyocytes: 30 min, plus 4 h for dissociation of cardiomyocytes
- Box 5, FACS analyses of dissociated hiPSC-cardiomyocytes: 3 h, plus 4 h for dissociation of cardiomyocytes

ANTICIPATED RESULTS

This protocol describes how to perform efficient differentiation of cardiomyocytes and subsequent EHT generation from hiPSC lines. Suspension culture facilitates upscaling because, in contrast to 2D cultures, the number of cultivated cells is not limited to the growth surface, and this allows differentiation of high cell numbers. Differentiation efficiencies and efficacies for several control and disease-specific cell lines are given in Table 2. High-quality hiPSC culture, free of differentiated cells, is critical to successful cardiac differentiation. One T80 cell culture flask of hiPSCs grown to 80% confluency contains  $\sim 15 \times 10^6$  hiPSCs. A few hours after growth of the hiPSC suspension in the spinner flasks, EB formation can be observed.  $60 \times 10^6$  hiPSCs give rise to an average EB volume of 300  $\mu\text{l}$  (Table 1). During induction of mesodermal progenitor cells, there is a decline in EB volume because of apoptotic cells (Table 1). However, we have observed that this has no adverse effects on the outcome of the differentiation. The first spontaneously contracting EBs can generally be observed between days 8 and 10, depending on the cell line and quality of the starting hiPSC culture. Supplementary Videos 1–3 show hiPSC-CMs in EB format. The time point of first beating activity is a good indicator of the differentiation efficiency, with earlier onset (day 8) in cell populations with higher cardiomyocyte content. A successful differentiation experiment results in  $18\text{--}174 \times 10^6$  cardiomyocytes (70–97% Troponin T-positive; Fig. 1 and Supplementary Fig. 1) from  $60 \times 10^6$  hiPSCs, depending on cell line and quality of undifferentiated hiPSCs (Table 2). Directly after differentiation, hiPSC-CMs express MLC2a (refs. 7,9). Bright-field images at different time points of cardiac differentiation are shown in Figure 5.

For the successful development of EHTs, the differentiation efficiency should be at least 60%, as we observed a correlation between cardiomyocyte purity and force development. With an increasing number of noncardiomyocytes such as fibroblasts in the input cell population, EHTs shrink rapidly after casting and do not start contracting. For some disease-specific cell lines with mutations leading to weaker contraction of the cardiomyocytes, a higher differentiation efficiency than that needed for healthy cardiomyocytes can be necessary for sufficient EHT performance. In contrast to cardiomyocyte purity, the differentiation method does not influence EHT performance. We recently used commercial hiPSC-CMs (CDI iCell; Axiogenesis Cor.4U)

## PROTOCOL

**TABLE 4** | Details of contraction parameters.

Cell line	Frequency (b.p.m.)	Force (mN)	T1 contraction time (s)	T2 relaxation time (s)
Control 1, $n = 75/77$	$61 \pm 17$	$0.152 \pm 0.052$	$0.120 \pm 0.017$	$0.163 \pm 0.026$
Control 2, $n = 46/3$	$92 \pm 31$	$0.138 \pm 0.019$	$0.174 \pm 0.083$	$0.215 \pm 0.049$
Control 3, $n = 23/3$	$61 \pm 15$	$0.115 \pm 0.044$	$0.151 \pm 0.024$	$0.238 \pm 0.085$

Replicate number is the number of EHTs/number of batches. Intra-batch variability is negligible. Values are given as  $\pm$  s.d. Age: control 1: 20–25 days; control 2: 15–20 days; control 3: 20–30 days. Measurements were done in culture medium (control 1 and 2) or Tyrode's solution (1.8 mM  $\text{Ca}^{2+}$ , Ctr. 3). Data for control 1 were taken from Mannhardt *et al.*<sup>7</sup>. T1 is time of 20% to peak force; T2 is time of peak force to 80% relaxation ( $\approx$ 20% above baseline).

for comparison with our in-house cell line and observed no differences in contractile function of the EHTs<sup>7</sup>. Normally, 2–5 d after EHT generation, single-cell contractions can be observed. Between 5 and 10 d, small clusters of hiPSC-CMs begin contracting, and coherent contraction of the entire EHT generally occurs between days 10 and 15. We usually perform experiments and video-optical analysis between days 14 and 28, although EHTs show a high robustness in long-term culture (up to day 100; **Supplementary Video 8**). Details of contraction parameters are given in **Table 4**. On average, 95% of cast EHTs can be analyzed. Sometimes single EHTs detach from the post while the PDMS rack is being transferred from the casting molds to the culture plate or cannot be analyzed because of enclosed air bubbles. **Supplementary Videos 5–8** show EHTs from control cell lines. After casting, EHTs are progressively remodeled, and after 3 weeks in culture they have a diameter of  $223.4 \pm 10.4 \mu\text{m}$  ( $n = 10$ ), a length of  $6.09 \pm 0.23 \text{ mm}$  ( $n = 10$ ) and an estimated volume of  $0.24 \pm 0.03 \text{ mm}^3$  ( $n = 10$ ). Over time of EHT cultivation, an increase in cell length, longitudinal orientation and network formation, paralleled by a reduction of extracellular space, can be observed histologically<sup>60</sup>. Myosin light-chain expression changes during cultivation from MLC2a to MLC2v (refs. 7,9), indicating maturation. hiPSC-CMs possess L-type  $\text{Ca}^{2+}$  currents ( $I_{\text{Ca,L}}$ ) as high as those in human adult cardiomyocytes, but in contrast to adult cardiomyocytes T-type  $\text{Ca}^{2+}$  currents ( $I_{\text{Ca,T}}$ ) coexist. Furthermore, serotonin does not increase  $I_{\text{Ca,L}}$  values in hiPSC-CMs, indicating an immature ventricular phenotype<sup>8</sup>.

Note: Any Supplementary Information and Source Data files are available in the online version of the paper.

**ACKNOWLEDGMENTS** We thank A. Moretti and K.-L. Laugwitz (University of Munich, Germany) for provision of the C25-hiPSC clone. This study was supported by the Deutsche Forschungsgemeinschaft (grants DFG Es 88/12-1 and DFG HA 3423/5-1), the British National Centre for the Replacement, Refinement, and Reduction of Animals in Research (NC3Rs CRACK-IT grant 35911-259146), the European Research Council (ERC-AG IndivHeart), the EU (FP7 Biodesign), the German Centre for Cardiovascular Research (DZHK), the German Ministry of Education and Research (BMBF), British Heart Foundation grant RM/13/30157, the German Heart Foundation, the Freie und Hansestadt Hamburg and Era-Net E-RARE (grant 01GM1305).

**AUTHOR CONTRIBUTIONS** K.B. designed and performed the experiments, analyzed the data and wrote the paper. T.S., I.M., B.U., M.C.R., T.W., A.B., D.L.-B., B.K., M.P., G.M., S.L., A.S., D.S., S.F., C.N., E.K., U.S., M.L.S. and M.L.R. contributed to the development or validation of this protocol. A.H. supervised the project. A.H. and T.E. wrote and approved the final paper.

**COMPETING FINANCIAL INTERESTS** The authors declare competing financial interests: details are available in the online version of the paper.

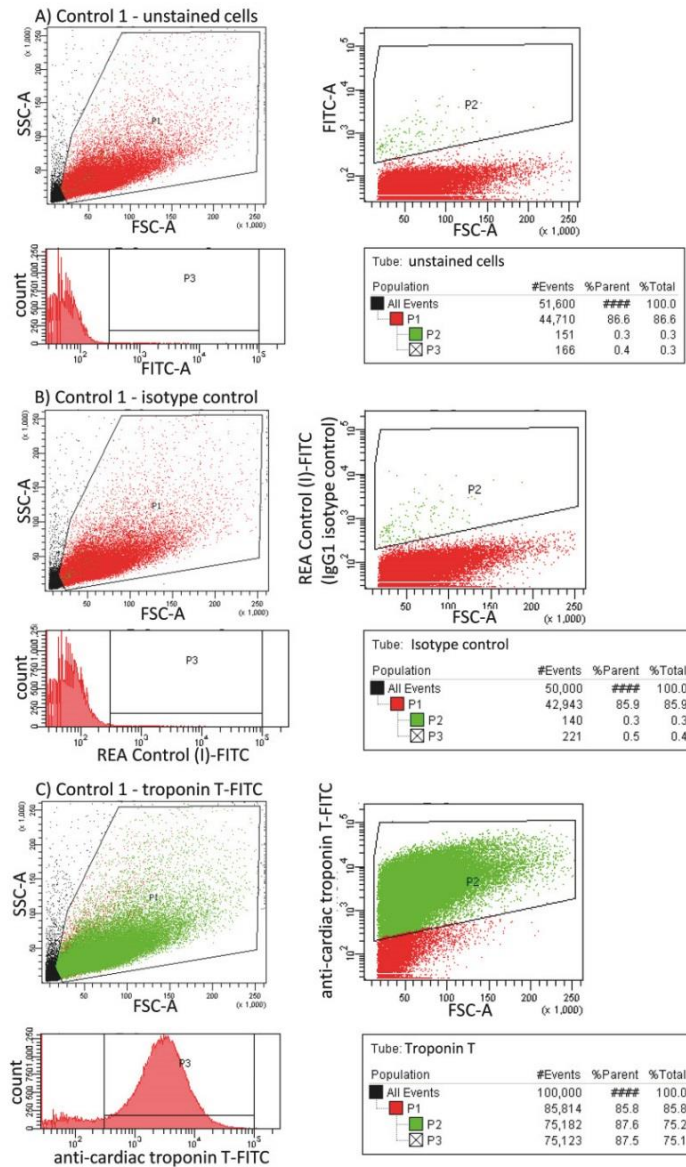
Reprints and permissions information is available online at <http://www.nature.com/reprints/index.html>. Publisher's note: Springer Nature remains neutral with regard to jurisdictional claims in published maps and institutional affiliations.

- Burridge, P.W., Keller, G., Gold, J.D. & Wu, J.C. Production of *de novo* cardiomyocytes: human pluripotent stem cell differentiation and direct reprogramming. *Cell Stem Cell* **10**, 16–28 (2012).
- Mercola, M., Colas, A. & Willems, E. Induced pluripotent stem cells in cardiovascular drug discovery. *Circ. Res.* **112**, 534–548 (2013).
- Knollmann, B.C. Induced pluripotent stem cell-derived cardiomyocytes: boutique science or valuable arrhythmia model? *Circ. Res.* **112**, 969–976 (2013).
- Hansen, A. *et al.* Development of a drug screening platform based on engineered heart tissue. *Circ. Res.* **107**, 35–44 (2010).

- Schaaf, S. *et al.* Human engineered heart tissue as a versatile tool in basic research and preclinical toxicology. *PLoS One* **6**, e26397 (2011).
- Hirt, M.H. *et al.* Increased afterload induces pathological cardiac hypertrophy: a new *in vitro* model. *Basic Res. Cardiol.* **107**, 307 (2012).
- Mannhardt, I. *et al.* Human engineered heart tissue: analysis of contractile force. *Stem Cell Rep.* **7**, 29–42 (2016).
- Uzun, A.U. *et al.*  $\text{Ca}^{2+}$ -currents in human induced pluripotent stem cell-derived cardiomyocytes effects of two different culture conditions. *Front. Pharmacol.* **7**, 300 (2016).
- Weinberger, F. *et al.* Cardiac repair in guinea pigs with human engineered heart tissue from induced pluripotent stem cells. *Sci. Transl. Med.* **8**, 363ra148 (2016).
- Thomson, J.A. *et al.* Embryonic stem cell lines derived from human blastocysts. *Science* **282**, 1145–1147 (1998).
- Ludwig, T.E. *et al.* Derivation of human embryonic stem cells in defined conditions. *Nat. Biotechnol.* **24**, 185–187 (2006).
- Chen, G. *et al.* Chemically defined conditions for human iPSC derivation and culture. *Nat. Methods* **8**, 424–429 (2011).
- Xu, C. *et al.* Feeder-free growth of undifferentiated human embryonic stem cells. *Nat. Biotechnol.* **19**, 971–974 (2001).
- Frank, S., Zhang, M., Scholer, H.R. & Greber, B. Small molecule-assisted, line-independent maintenance of human pluripotent stem cells in defined conditions. *PLoS One* **7**, e41958 (2012).
- Lanner, F. & Rossant, J. The role of FGF/Erk signaling in pluripotent cells. *Development* **137**, 3351–3360 (2010).
- Vallier, L., Alexander, M. & Pedersen, R.A. Activin/Nodal and FGF pathways cooperate to maintain pluripotency of human embryonic stem cells. *J. Cell Sci.* **118**, 4495–4509 (2005).
- Eiselleova, L. *et al.* A complex role for FGF-2 in self-renewal, survival, and adhesion of human embryonic stem cells. *Stem Cells* **27**, 1847–1857 (2009).
- Ding, V.M. *et al.* FGF-2 modulates Wnt signaling in undifferentiated hESC and iPSC cells through activated PI3-K/GSK3beta signaling. *J. Cell Physiol.* **225**, 417–428 (2010).
- Zoumaro-Djayoon, A.D. *et al.* Investigating the role of FGF-2 in stem cell maintenance by global phosphoproteomics profiling. *Proteomics* **11**, 3962–3971 (2011).



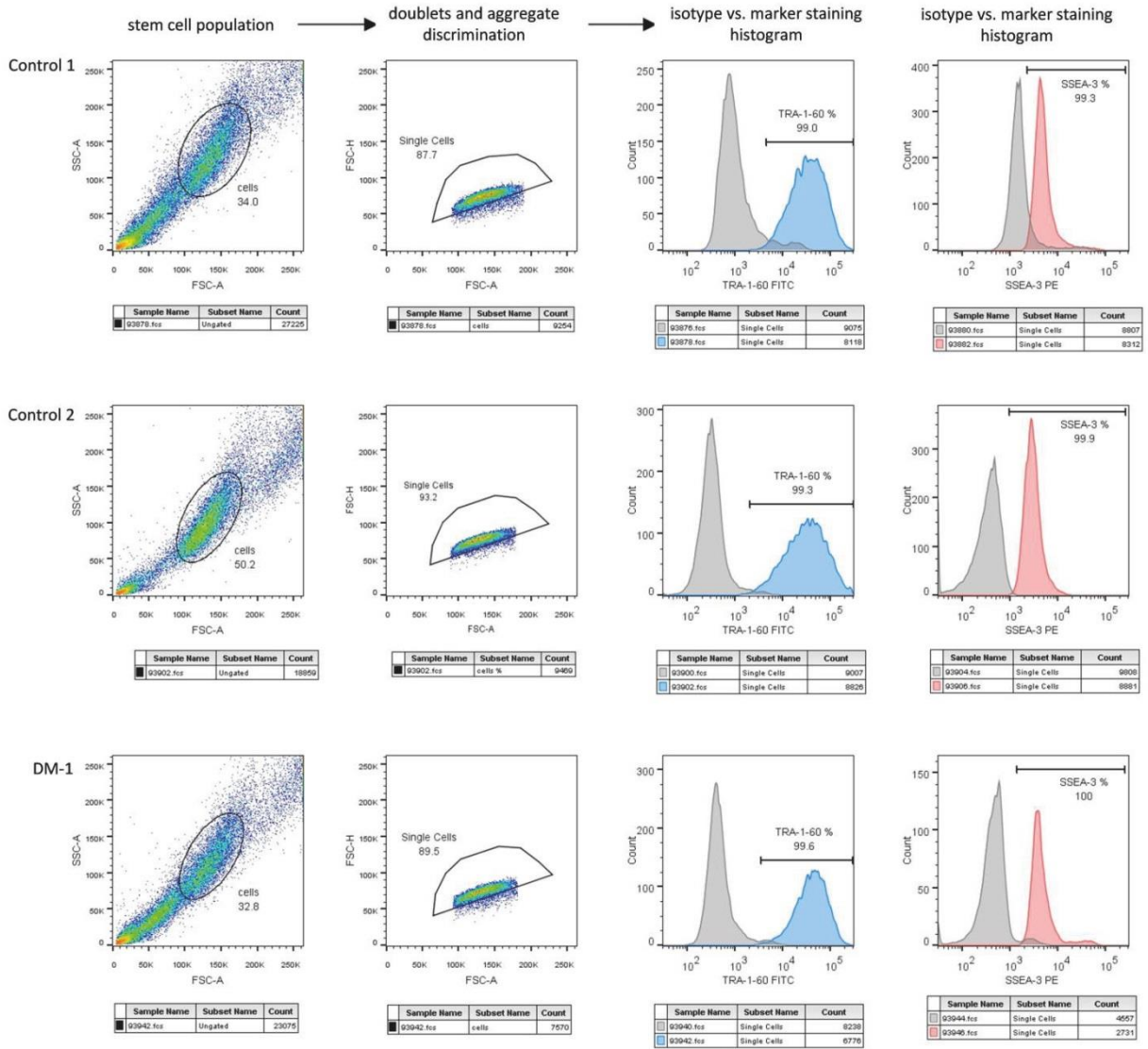
20. Miltenyi Biotec. Human FGF-2 IS. <http://www.miltenyibiotec.com/en/products-and-services/macscell-culture-and-stimulation/cytokines-and-growth-factors/premium-and-research-grade/human-fgf-2-is.aspx>.
21. Burridge, P.W. *et al.* A universal system for highly efficient cardiac differentiation of human induced pluripotent stem cells that eliminates interline variability. *PLoS One* **6**, e18293 (2011).
22. Burridge, P.W. *et al.* Chemically defined generation of human cardiomyocytes. *Nat. Methods* **11**, 855–860 (2014).
23. Yang, L. *et al.* Human cardiovascular progenitor cells develop from a KDR+ embryonic-stem-cell-derived population. *Nature* **453**, 524–528 (2008).
24. Laflamme, M.A. *et al.* Cardiomyocytes derived from human embryonic stem cells in pro-survival factors enhance function of infarcted rat hearts. *Nat. Biotechnol.* **25**, 1015–1024 (2007).
25. Mummery, C. *et al.* Differentiation of human embryonic stem cells to cardiomyocytes: role of coculture with visceral endoderm-like cells. *Circulation* **107**, 2733–2740 (2003).
26. Kattman, S.J. *et al.* Stage-specific optimization of activin/nodal and BMP signaling promotes cardiac differentiation of mouse and human pluripotent stem cell lines. *Cell Stem Cell* **8**, 228–240 (2011).
27. Moretti, A., Laugwitz, K.L., Dorn, T., Sinnecker, D. & Mummery, C. Pluripotent stem cell models of human heart disease. *Cold Spring Harb. Perspect. Med.* **3** <http://dx.doi.org/10.1101/cshperspect.a014027> (2013).
28. Zweigerdt, R., Olmer, R., Singh, H., Haverich, A. & Martin, U. Scalable expansion of human pluripotent stem cells in suspension culture. *Nat. Protoc.* **6**, 689–700 (2011).
29. Olmer, R. *et al.* Suspension culture of human pluripotent stem cells in controlled, stirred bioreactors. *Tissue Eng. Part C Methods* **18**, 772–784 (2012).
30. Lian, X. *et al.* Directed cardiomyocyte differentiation from human pluripotent stem cells by modulating Wnt/ $\beta$ -catenin signaling under fully defined conditions. *Nat. Protoc.* **8**, 162–175 (2013).
31. Kempf, H. *et al.* Controlling expansion and cardiomyogenic differentiation of human pluripotent stem cells in scalable suspension culture. *Stem Cell Rep.* **3**, 1132–1146 (2014).
32. Kempf, H., Kropp, C., Olmer, R., Martin, U. & Zweigerdt, R. Cardiac differentiation of human pluripotent stem cells in scalable suspension culture. *Nat. Protoc.* **10**, 1345–1361 (2015).
33. Chen, V.C. *et al.* Development of a scalable suspension culture for cardiac differentiation from human pluripotent stem cells. *Stem Cell Res.* **15**, 365–375 (2015).
34. Lanier, M. *et al.* Wnt inhibition correlates with human embryonic stem cell cardiomyogenesis: a structure-activity relationship study based on inhibitors for the Wnt response. *J. Med. Chem.* **55**, 697–708 (2012).
35. Tulloch, N.L. *et al.* Growth of engineered human myocardium with mechanical loading and vascular coculture. *Circ. Res.* **109**, 47–59 (2011).
36. Kensah, G. *et al.* Murine and human pluripotent stem cell-derived cardiac bodies form contractile myocardial tissue *in vitro*. *Eur. Heart J.* **34**, 1134–1146 (2013).
37. Nunes, S.S. *et al.* Biowire: a platform for maturation of human pluripotent stem cell-derived cardiomyocytes. *Nat. Methods* **10**, 781–787 (2013).
38. Thavandiran, N. *et al.* Design and formulation of functional pluripotent stem cell-derived cardiac microtissues. *Proc. Natl. Acad. Sci. USA* **110**, E4698–4707 (2013).
39. Turnbull, I.C. *et al.* Advancing functional engineered cardiac tissues toward a preclinical model of human myocardium. *FASEB J.* **28**, 644–654 (2014).
40. Hinson, J.T. *et al.* HEART DISEASE. Titin mutations in iPS cells define sarcomere insufficiency as a cause of dilated cardiomyopathy. *Science* **349**, 982–986 (2015).
41. Kuppusamy, K.T. *et al.* Let-7 family of microRNA is required for maturation and adult-like metabolism in stem cell-derived cardiomyocytes. *Proc. Natl. Acad. Sci. USA* **112**, E2785–2794 (2015).
42. Stillitano, F. *et al.* Genomic correction of familial cardiomyopathy in human engineered cardiac tissues. *Eur. Heart J.* **37**, 3282–3284 (2016).
43. Riegler, J. *et al.* Human engineered heart muscles engraft and survive long term in a rodent myocardial infarction model. *Circ. Res.* **117**, 720–730 (2015).
44. Zhang, D. *et al.* Tissue-engineered cardiac patch for advanced functional maturation of human ESC-derived cardiomyocytes. *Biomaterials* **34**, 5813–5820 (2013).
45. Wang, G. *et al.* Modeling the mitochondrial cardiomyopathy of Barth syndrome with induced pluripotent stem cell and heart-on-chip technologies. *Nat. Med.* **20**, 616–623 (2014).
46. Eschenhagen, T. *et al.* Three-dimensional reconstitution of embryonic cardiomyocytes in a collagen matrix: a new heart muscle model system. *FASEB J.* **11**, 683–694 (1997).
47. Zimmermann, W.H. *et al.* Three-dimensional engineered heart tissue from neonatal rat cardiac myocytes. *Biotechnol. Bioeng.* **68**, 106–114 (2000).
48. Zimmermann, W.H. *et al.* Tissue engineering of a differentiated cardiac muscle construct. *Circ. Res.* **90**, 223–230 (2002).
49. Neuber, C. *et al.* Paradoxical effects on force generation after efficient  $\beta$ 1-adrenoceptor knockdown in reconstituted heart tissue. *J. Pharmacol. Exp. Ther.* **349**, 39–46 (2014).
50. Stohr, A. *et al.* Contractile abnormalities and altered drug response in engineered heart tissue from Mybp3-targeted knock-in mice. *J. Mol. Cell. Cardiol.* **63**, 189–198 (2013).
51. Dussurget, O. & Roulland-Dussoix, D. Rapid, sensitive PCR-based detection of mycoplasmas in simulated samples of animal sera. *Appl. Environ. Microbiol.* **60**, 953–959 (1994).
52. Ungrin, M.D., Joshi, C., Nica, A., Bauwens, C. & Zandstra, P.W. Reproducible, ultra high-throughput formation of multicellular organization from single cell suspension-derived human embryonic stem cell aggregates. *PLoS One* **3**, e1565 (2008).
53. Kempf, H. *et al.* Bulk cell density and Wnt/TGF $\beta$  signalling regulate mesendodermal patterning of human pluripotent stem cells. *Nat. Commun.* **7**, 13602 (2016).
54. Lian, X., Zhang, J., Zhu, K., Kamp, T.J. & Palecek, S.P. Insulin inhibits cardiac mesoderm, not mesoderm, formation during cardiac differentiation of human pluripotent stem cells and modulation of canonical Wnt signaling can rescue this inhibition. *Stem Cells* **31**, 447–457 (2013).
55. Tran, T.H. *et al.* Wnt3a-induced mesoderm formation and cardiomyogenesis in human embryonic stem cells. *Stem Cells* **27**, 1869–1878 (2009).
56. Freund, C. *et al.* Insulin redirects differentiation from cardiogenic mesoderm and endoderm to neuroectoderm in differentiating human embryonic stem cells. *Stem Cells* **26**, 724–733 (2008).
57. Moretti, A. *et al.* Patient-specific induced pluripotent stem-cell models for long-QT syndrome. *N. Engl. J. Med.* **363**, 1397–1409 (2010).
58. Takahashi, K. *et al.* Induction of pluripotent stem cells from adult human fibroblasts by defined factors. *Cell* **131**, 861–872 (2007).
59. Eschenhagen, T., Eder, A., Vollert, I. & Hansen, A. Physiological aspects of cardiac tissue engineering. *Am. J. Physiol. Heart Circ. Physiol.* **303**, H133–H143 (2012).
60. Lotz, S. *et al.* Sustained levels of FGF2 maintain undifferentiated stem cell cultures with biweekly feeding. *PLoS One* **8**, e56289 (2013).



**Supplementary Figure 1**

Gating strategy used for FACS analysis of hiPSC-cardiomyocytes.

Given are details for forward and side scatter gates of the starting cell population and the gating to isolate cardiac troponin T-FITC-positive cells with the help of unstained cells (A) and cells stained with REA Control (I)-FITC isotype control (B). Absolute numbers of the cells analyzed and percentages of the relevant cell populations are provided. Cells were sorted with a BD FACSCanto II Flow Cytometer and analyzed with the BD FACSDiva Software.



Supplementary Figure 2

Gating strategy used for FACS analysis of hiPSCs.

Given are details for forward and side scatter gates of the starting cell population, the gating to discriminate doublets and aggregates and the gating to isolate TRA-1-60/SSEA-positive cells with the help of cells stained with isotype controls. Absolute numbers of the cells analyzed and percentages of the relevant cell populations are provided. Cells were sorted with a BD FACSCanto II Flow Cytometer and analyzed with the FlowJo Software.

### **3.3 Modeling of a novel *ACTN2* mutation (c.740C>T; p.Thr247Met) in hiPSC-CMs using an isogenic control cell line**

In this chapter results on the functional analysis of hiPSC-CMs carrying a novel *ACTN2* mutation and its CRISPR/Cas9 repaired isogenic control will be presented. This evaluation is part of a manuscript in preparation with the preliminary title “patient-specific iPSC-derived cardiomyocytes reveal a disease-causing role for a novel *ACTN2* mutation in hypertrophic cardiomyopathy”. In this manuscript, I am involved in conceptualization, methodology, investigation, formal analysis, visualization, project administration and writing of the original draft. My contributions in this project will most likely result in a first-authorship.

#### **3.3.1 Novel *ACTN2* mutation causes HCM**

The novel *ACTN2* mutation (c.740C>T; p.Thr247Met) investigated in this thesis has never been reported before. It was described in a female patient, who was diagnosed with HCM and presented a prolonged QT interval. DNA sequencing with a 19-gene cardiac panel identified the *ACTN2* c.740C>T transition in exon 8, which is located in the CH2 domain of the ABD. Additionally, this mutation was found to co-segregate within two family members and has not been described in the Exome Association Consortium Browser (ExAC; <http://exac.broadinstitute.org>), supporting its causal effect.

#### **3.3.2 Generation of an isogenic control cell line using CRISPR/Cas9**

In order to evaluate cell characteristics of the HCM cell line carrying a novel *ACTN2* mutation, the first goal of this investigation was to generate an isogenic control cell line in which the underlying mutation is reversed to the WT. For induction of genomic DSBs at the desired location, sgRNAs A 5'-GCAAGAGACGTACGTCATGA-3' and B 5'-CTACCACGCTTTTGC GGGCG-3' were cloned into the pSpCas9n(BB)-2A-GFP plasmid. Transfection of 800,000 HCM iPSCs resulted in 11351 GFP-positive cells analyzed by FACS 48 hours after transfection. GFP-positive cells were plated and cultured until colonies were visible. Handpicking of 140 clones and analysis by sequencing revealed two successfully repaired clones from which one was further subcloned, hereafter named HCM #26. Subcloning of HCM #26 resulted in the

subclone  $rep$ HCM, which has been genotyped positively for the *ACTN2* WT sequence (Fig. 13).



Figure 13: Representative Sanger sequencing results of the affected *ACTN2* locus in the HCM and  $rep$ HCM cell line. Depicted are the mutation on position g.54,208 (c.740C>T), the repair template from g.54,148-54,270 (-strand), the according silent mutations encoded on the repair template on position g.54,200 (G>C; -strand) and g.54,245 (C>G; -strand), and sgRNAs A and B. (A; B) Shown are representative Sanger sequences of HCM iPSCs (A) and HCM iPSC-derived CMs (B). (C; D) Shown are representative Sanger sequences of  $rep$ HCM iPSCs (C) and  $rep$ HCM iPSC-derived CMs (D). sil. Mut., silent mutation; rep. temp., repair template.

Sequencing also revealed that instead of the nucleotide C, the nucleotide T was introduced as a silent mutation on genomic position g.54,200 at the heterozygous state, resulting in the nucleotide A on the + strand (5' to 3'). The second silent mutation was correctly introduced on position g.54,245 and therefore the nucleotide C was detected on the + strand. Unexpectedly, this silent mutation was introduced at the homozygous state. Additionally, investigation of 13 potential off-targets in exons and introns by Sanger sequencing resulted in the absence of detection of altered sequences (Table 3).

Table 3: Shown are NCBI accession numbers and genomic loci of analyzed off-targets resulting from the usage of sgRNA A and B.

NCBI accession number		off-target position
NG_029480	Exon	g.81,841-81,860
NM_016642	Exon	c.1037-1056
NG_013304	Exon	g.14,262-14,281
NG_029938	Exon	g.149,593-149,612
NM_000827	Exon	c.2942-2961
NG_009061	Exon	g.24,969-24,988
NM_025268	Exon	c.898-917
NC_018924	Intron	g.109,195,197-109,195,219
NC_018930	Intron	g.39,202,757-39,202,779
NC_018931	Intron	g.60,206,273-60,206,295
NC_018919	Intron	g.81,458,539-81,458,561
NC_018916	Intron	g.16,615,937-16,615,959
NC_018929	Intron	g.73,770,186-73,770,208

The human iPSC clone  $_{rep}HCM$ , derived from the HCM cell line, was defined as the isogenic control cell line for this study.

### 3.3.3 HCM hiPSC-CMs exhibit hypertrophy in 2D

For evaluation of cell sizes in the HCM and the  $_{rep}HCM$  cell line, CMs were cultured for 30 days, prepared for immunofluorescence analysis, imaged by confocal microscopy (LSM800 Airyscan Zeiss) and analyzed with Fiji (ImageJ) as described previously (Prondzynski et al., 2017). Single CMs with developed sarcomeric structures were included into the analysis (Fig. 14), whereby aggregates of CMs were excluded.

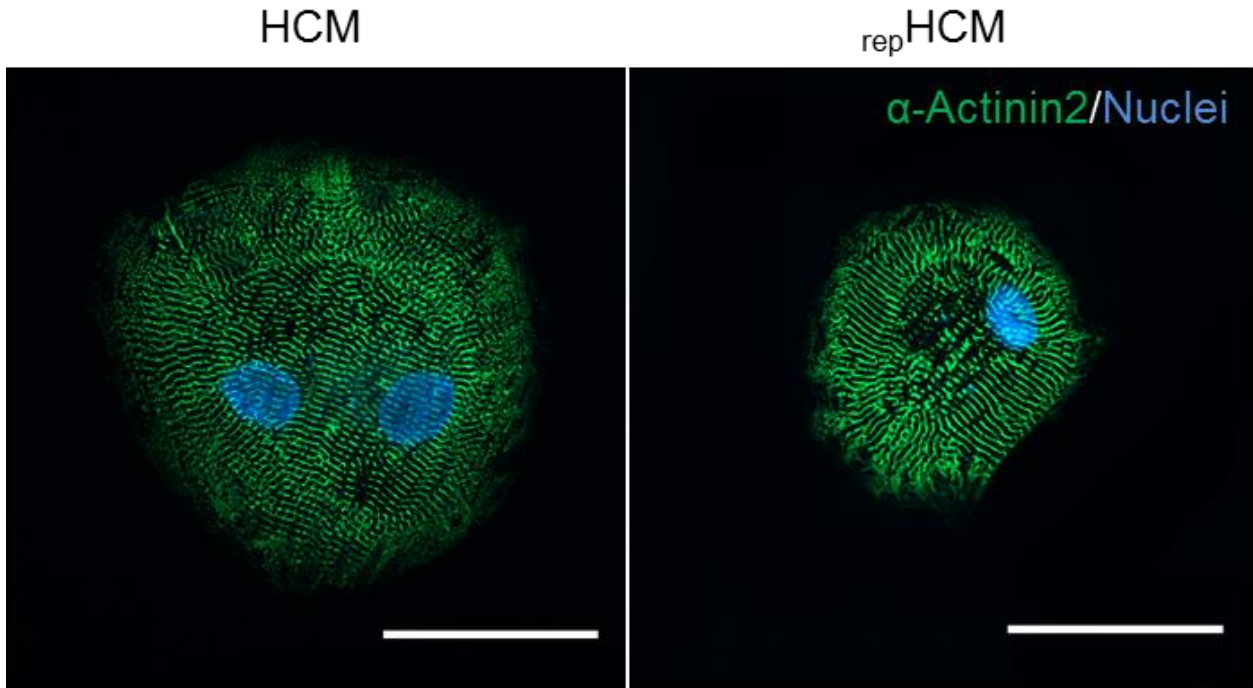


Figure 14: Representative immunofluorescence images of HCM and  $rep$ HCM CMs. Both cell lines were stained with an antibody directed against  $\alpha$ -Actinin 2 (green) and with Hoechst 33342 for nuclear staining (blue; scale bars, 50  $\mu$ m).

Cell sizes in HCM were significantly higher than in the isogenic control cell line  $rep$ HCM ( $4,512 \pm 224 \mu\text{m}^2$  versus  $2,482 \pm 138 \mu\text{m}^2$ ; Figure 15).

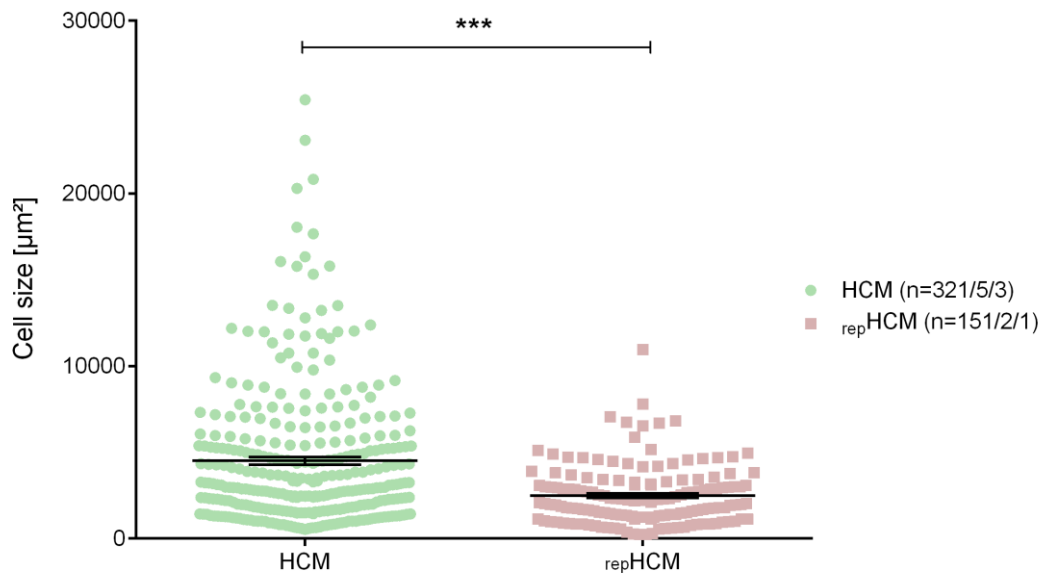


Figure 15: Quantification of CM cell size. HCM and  $rep$ HCM were seeded in 96-well plates at a density of 10,000 cells per well, cultured for 30 days, and stained with antibodies against  $\alpha$ -Actinin 2. Low-resolution images of CMs ( $n$  = number of analyzed cells/ number of analyzed wells/ number of differentiation batches) were taken with the Zeiss LSM 800 microscope and analyzed with Fiji software (ImageJ). Data are expressed as mean  $\pm$  SEM (\*\*\*)  $p < 0.0001$ , unpaired Student's  $t$ -test).

These measurements suggest that HCM cell line develop CM hypertrophy when compared to the isogenic control cell line.

### **3.3.4 HCM EHTs exhibit hypercontractility and prolonged relaxation time**

To obtain functional data of the HCM and the  $_{rep}$ HCM cell line, CMs were casted in EHT format and analyzed under paced conditions (1 Hz, 2 Volts) in 1.8 mM  $Ca^{2+}$ -Tyrode solution for force (mN), contraction time ( $T_{1(80\%)}$ ) and relaxation time ( $T_{2(80\%)}$ ; Breckwoldt et al., 2017). HCM EHTs (30  $\pm$  5 day-old) showed a higher force development (0.178  $\pm$  0.008 mN versus 0.130  $\pm$  0.005 mN; Fig. 16 A) and a longer relaxation time (0.252  $\pm$  0.004 sec versus 0.207  $\pm$  0.003 sec; Fig. 16 C) than  $_{rep}$ HCM EHTs. Contraction time did not differ between HCM and  $_{rep}$ HCM EHTs (0.158  $\pm$  0.002 sec versus 0.157  $\pm$  0.005 sec; Fig. 16 B). Taken together, these results suggest that hypercontractility and prolonged relaxation time measured in HCM EHTs are caused by the *ACTN2* mutation, as those phenotypes were not present in the CRISPR/Cas9 repaired isogenic control cell line. Additionally, the isogenic control cell line exhibits similar cell areas and functional characteristics of EHTs as the unrelated control cell line, which has also been investigated in this thesis (data not shown).



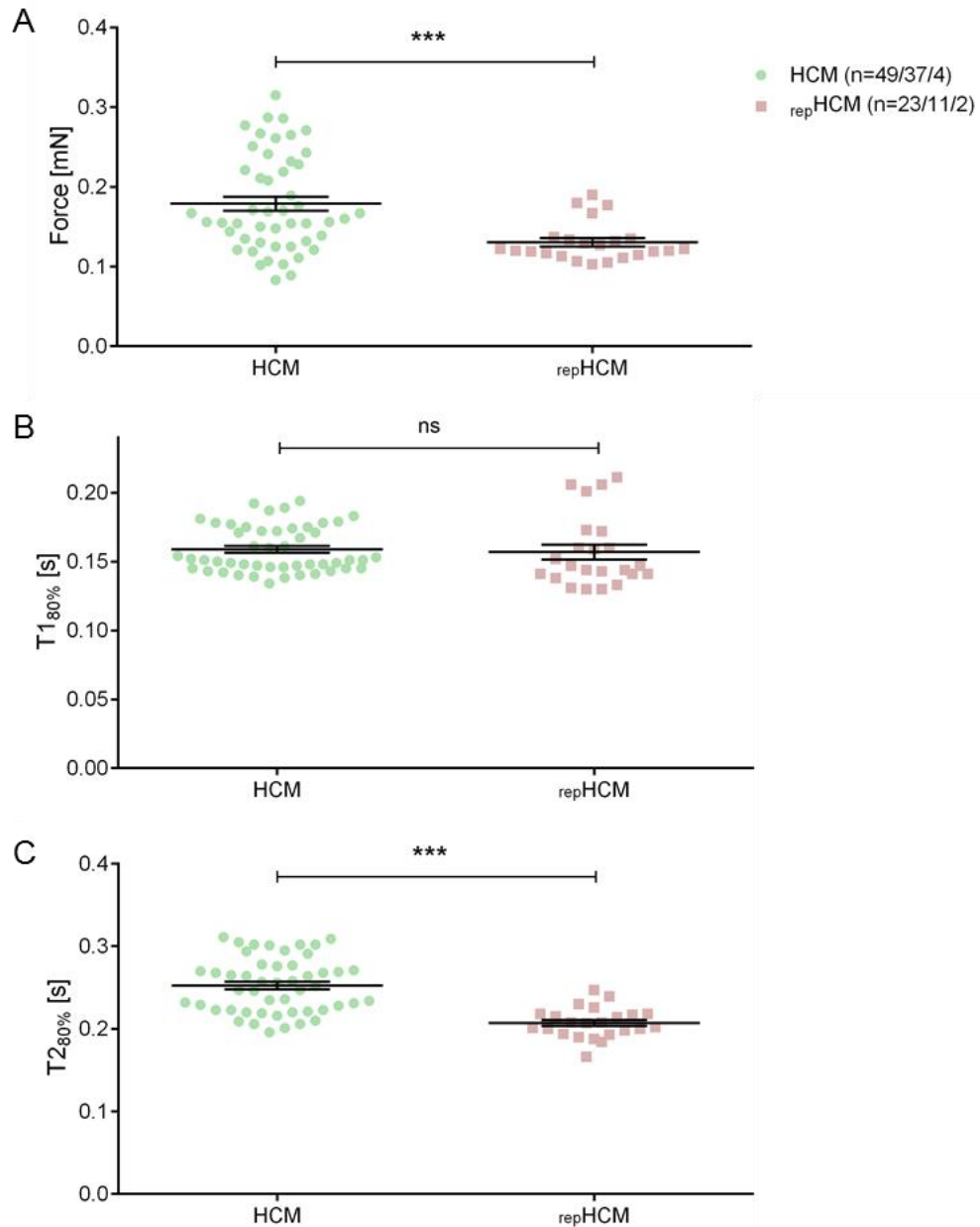


Figure 16: Functional parameters of  $30 \pm 5$  day-old HCM EHTs and isogenic control  $_{\text{rep}}\text{HCM}$  EHTs. EHTs were paced at 1 Hz in 1.8 mM  $\text{Ca}^{2+}$  in Tyrode solution at 37 °C. (A) Force, (B) contraction time ( $T_{1(80\%)}$ ) and (C) relaxation time ( $T_{2(80\%)}$ ) were evaluated (n= number of pooled EHT measurements/ number of measured EHTs/ number of differentiation batches). Values are expressed as mean  $\pm$  SEM. \*\*\*p < 0.001, unpaired Students *t*-test.

## 4. Discussion

Although the first description of HCM dates back to the late 50s, it was 30 years later that the first mutation in *MYH7* gene, encoding the sarcomere component  $\beta$ -MHC was found to be associated with the disease (Geisterfer-Lowrance et al., 1990). Additionally, molecular links between genetics and clinical outcome are still elusive and no curative treatment is available up to date. Recent technological advances in the form of hiPSCs revolutionized the study of human diseases (Takahashi et al., 2007). The ability of hiPSCs to differentiate into any kind of cell creates a valuable human disease model, offering a potentially unlimited source for material of human origin, devoid of ethical concerns and governmental restrictions. Combining the study of HCM and the technique of hiPSCs makes it possible to differentiate CMs of individuals with disease-relevant mutations, thereby offering a brilliant chance for gaining new insights into pathophysiology and investigation of new therapeutics that target the genetic causes of HCM.

The goal of this work was to evaluate hiPSC-CMs as a tool to model HCM and to assess molecular-based interventions, such as *trans*-splicing, GR and CRISPR/Cas9 genome editing. Therefore three aims were defined and the main findings were

- (1) for the first aim successful characterization of a patient-derived hiPSC line carrying a novel *MYBPC3* mutation in comparison to an unrelated healthy control line and application of *trans*-splicing and GR as new molecular-based interventions.
- (2) for the second aim successful development of a differentiation protocol for CMs, which is EB-based, cost-effective and generates high purity of hiPSC-CMs. This protocol was successfully applied to all investigated cell lines in this thesis. Furthermore, this protocol allowed efficient generation of EHTs using the patient-derived hiPSC-CMs carrying a novel *ACTN2* mutation and its isogenic control cell line.
- (3) for the third aim successful generation of an isogenic control cell line using CRISPR/Cas9 genome editing, as the description of morphological and

functional parameters of a patient-derived hiPSC line carrying a novel *ACTN2* mutation and its isogenic control cell line <sub>rep</sub>HCM

The three aims of this thesis and their corresponding results were all defined and achieved in the past three years in the Department of Experimental Pharmacology and Toxicology and in collaborations with other scientists. Protocols on differentiation of CMs, molecular, morphological and functional characterization in 2D- and 3D-formats, and evaluation of gene therapy approaches were developed in that time frame. Therefore, all three defined aims in this thesis are strongly interdependent and led to standardized procedures for disease modeling of human inherited cardiomyopathies with hiPSC-CMs.

#### **4.1 hiPSC-CMs as a suitable tool for modeling of HCM**

Before the emergence of hiPSC-CMs alternatives were and are still used to study and model inherited cardiomyopathies. One of the most desired samples to acquire is human heart tissue. Due to the fact that 5% of HCM patients undergo surgical septal myectomy, a unique opportunity is created to study the intrinsic CM pathology (Spirito et al., 1997). In contrast to other heart tissue samples that can be used for in vitro experiments, such as from patients with terminal heart failure (HF) or pressure-overloaded hearts, usually pathological triggers lie outside the cardiac myocytes in the form of stenosis in coronary arteries, increased resistance in peripheral vasculature or failing heart valves (Ponikowski et al., 2016). Nevertheless, important findings were made with human heart tissue studying the trabeculae carneae, freshly isolated CMs, skinned cells and with the usage of actin-myosin sliding assays as well as biochemical and gene expression analysis (for review Eschenhagen et al., 2015). Highlights of this research in respect to HCM were findings of in vivo energetic alterations in HCM patients, especially with mutations in the *MYH7* and *MYPBC3* genes, which could be reproduced with human in vitro muscle strips (Ingwall et al., 2004; Crilley et al., 2003; Teerlink et al., 2011). Additionally, experiments with skinned human preparations from HCM patients showed increased myofilament  $\text{Ca}^{2+}$  sensitivity, faster cross-bridge cycling and reduced maximal force generation, as higher energy consumption and tension cost (Sequeira et al., 2013; Witjas-Paalberends et al., 2013; Witjas-Paalberends, Ferrara, et al., 2014; Witjas-Paalberends, Güclü, et al., 2014). However, there are also limitations in usage and

interpretation of data that is obtained from human tissue samples. HCM myectomy samples develop a high degree of fibrosis, which can hinder cell isolation and therefore lead to artefacts in functional experiments or misinterpretation of data obtained in biochemical or gene expression analysis, since it's usually compared to a non-failing control tissue sample (Lamke et al., 2003). Ultimately, human samples are rare, just available in irregular intervals and can be used for a limited amount of time, making them experimentally challenging. Investigators also need to be in close proximity to a cardiovascular clinic or collaborate with cardiologists and cardiac surgeons to obtain these samples.

To circumvent these limitations and to study underlying disease mechanisms animal models are used, such as primates, pigs, dogs, rabbits, rats and mice (for review Zaragoza et al., 2011). However, when working with animal models it is important to consider, which animal recreates human disease the best and is affordable in respect to infrastructure, specialized personnel and ethical guidelines. One of the most extensive studied animals are mice. Mouse models have proven to be the gold standard in understanding of underlying disease mechanisms in human inherited diseases. Mice share over 90% of their genome with humans and 98% of experimentally defined binding sites for skeletal-muscle-specific transcription factors (Chinwalla et al., 2002; Wasserman et al., 2000). Additionally, they exhibit striking similarity in human physiology and anatomy. Compared to large-animal models, costs in maintaining mice are much lower and ethical concerns are not addressed, when using mice instead of primates. However, mice are not human and when investigating cardiac diseases major electrophysiological differences remain (Nerbonne, 2004). Nevertheless, there are have been several mouse models created for HCM research, mimicking disease-relevant mutations expressed in the patient (Geisterfer-lowrance et al., 1996; Yang et al., 1998; Lim et al., 2001; Vignier et al., 2009). Those models have been extensively used to investigate pathology and pathomechanisms on cellular and physiological level in HCM, giving us direct insights that are translatable to humans. Especially investigation of mouse models with *Mybpc3* mutations showed haploinsufficiency, cardiac hypertrophy, higher myofilament  $Ca^{2+}$  sensitivity, faster cross-bridge cycling and diastolic dysfunction, major hallmarks of HCM (for review Marston et al., 2012). Nevertheless, mice are not human.

Closest model to humans on cellular level has been for a long time hESCs. Unfortunately, scarcity of hESCs with inherited diseases and insufficient gene editing techniques just resulted in few studies published in the context of cardiovascular disease and HCM (Cao et al., 2008; Burrige et al., 2012; Lan et al., 2013; Monteiro da Rocha et al., 2016). Observations in these studies were that common limitations are apparent in hESC-derived CMs, such as developmental immaturity in the form of similar gene expression profiles to fetal CMs, as well as lower levels of  $\beta$ -myosin than in adult CMs. Nevertheless, transient haploinsufficiency, hypertrophy, sarcomeric disarray, impaired  $\text{Ca}^{2+}$  impulse propagation, abnormal  $\text{Ca}^{2+}$  handling and arrhythmias were reported.

One goal of this thesis was to evaluate hiPSC-CMs as a suitable tool for HCM disease modeling. Investigated hiPSC-CMs from patients with novel *MYBPC3* (c.1358dupC; p.Val454CysFsX21) and *ACTN2* (c.740C>T; p.Thr247Met) mutations exhibited both hallmarks of HCM, and are therefore in line with previous findings in different models of the disease. The *MYBPC3* mutant cell line exhibited haploinsufficiency, characterized by 50% lower *MYBPC3* mRNA and cMyBP-C protein levels than unrelated healthy control, as already reported previously in HCM hiPSC-CMs (Chapter 3.1, Fig.1; Birket et al., 2015). Additionally, mutant nonsense mRNA was not detected, suggesting that it is degraded by the nonsense-mediated mRNA decay, as already reported in a *Mybcp3*-targeted knock-in mouse model of HCM (Vignier et al., 2009). The PTC is located >50-55 nucleotides upstream of the most 3' exon-exon junction, therefore matching NMD rules (Nagy et al., 1998). The truncated cMyBP-C protein was also not detected by Western blot. This is in line with previous investigations of human tissue samples with truncating *MYBPC3* mutations (Marston et al., 2009; van Dijk et al., 2009). Nonetheless, it has also been reported the absence of haploinsufficiency in an analysis of human tissue samples from HCM patients with truncating *MYBPC3* mutations (Helms et al., 2014). Furthermore, transient haploinsufficiency was reported in hESC-CMs with a disease relevant truncating *MYBPC3* mutation (Monteiro da Rocha et al., 2016). Haploinsufficiency was detected in 17-day-old HCM hESC-CMs, but not in 30-day-old HCM hESC-CMs. Therefore, 7-day-old *MYBPC3* mutant hiPSC-CMs investigated here might have just exhibited a transient haploinsufficiency. If this is the case has to be elucidated in the future. However, Birket et al observed haploinsufficiency in 25-day-old HCM hiPSC-

CMs carrying a truncating *MYBPC3* mutation. For now the role of haploinsufficiency being either responsible for initiation or progression of HCM remains controversial (Marston et al., 2012; Strande, 2015). In the *ACTN2* mutant cell line it is not known if haploinsufficiency is causative for HCM, since protein levels have not been investigated yet. In contrast to the *MYBPC3* mutant line, the *ACTN2* line carries a missense mutation. This leads to the hypothesis that mutated transcripts are translated into proteins that might alter functional characteristics of the protein, acting as so-called “poison peptides”. How exactly those mutated proteins affect function will be addressed in future experiments.

Besides haploinsufficiency, alterations in gene expression profiles were also detected in the *MYBPC3* mutant cell line. The mRNA levels of proteins associated with hypertrophy, such as four and a half LIM domains 1 (*FHL1*), S100 Ca<sup>2+</sup> binding protein A4 (*S100A4*) and connective tissue growth factor (*CTGF*) were higher and mRNA levels of proteins involved in Ca<sup>2+</sup> handling, such as phospholamban (*PLN*), SERCA2a (*ATP2A2*), ryanodine receptor (*RYR2*) and inhibitor 1 (*PPP1R1A*) were lower than in the healthy unrelated control (Chapter 3.1, Fig. 6). This is in agreement with previous findings using HCM hiPSC-CMs and hESC-CMs carrying *MYBPC3* mutations (Dambrot et al., 2014; Ojala et al., 2016; Tanaka et al., 2014; Uesugi et al., 2014).

Hypertrophy was apparent in both investigated HCM cell lines. Cell size was 1.6-fold higher after seven days in culture in *MYBPC3* mutant cell line than in a healthy unrelated control cell line (Chapter 3.1, Fig. 1, 5). Cell size was investigated in this study by two independent methods: confocal microscopy and with a high-content screening microscope. Both methods were able to complement each other by giving similar results in independent experiments. 30-day-old *ACTN2* mutant cell line exhibited a 1.8-fold higher cell area by confocal microscopy than isogenic control cell line (Chapter 3.3, Fig. 15), whereby there was no significant difference between the isogenic and the unrelated healthy control (data not shown). Most studies observing hypertrophy in 2D cultured hiPSC-CMs and hESC-CMs detect similar cell sizes for control cell lines ranging from 1000 to 2000  $\mu\text{m}^2$  and for *MYBPC3* mutant cell lines ranging from 3000 to 4000  $\mu\text{m}^2$ , which is in line with the findings reported in this thesis (Dambrot et al., 2014; Uesugi et al., 2014; Birket et al., 2015; Monteiro da Rocha et al., 2016). Nevertheless, Dambrot et al. described that serum

supplementation of 5% to 20% in culture medium can mask hypertrophic phenotypes in 2D culture of hiPSC-CMs. This could not be observed in the present study, in which 10% of serum was supplemented to the culture medium, as in several other reports where up to 20% of serum was used and hypertrophy was still detected (Tanaka et al., 2014; Monteiro da Rocha et al., 2016; Ojala et al., 2016). In a follow up study by Birket et al. using the same cell lines as in the study of Dambrot et al., culture conditions were improved by supplementation of T3, IGF-1 and dexamethasone to the culture medium. Supplementation of these factors led to no significant differences in cell sizes between 25-day-old control and HCM hiPSC-CMs, whereby the HCM lines adjusted to the size of the controls (Birket et al., 2015). As media compositions can have an impact on hypertrophy it has also been shown that culture density is important. In a study by Uesugi et al. commercially available iCell Cardiomyocytes (CDI) were used to investigate the impact of high density and low density culturing for 7 days in 96-well plates. High density conditions were defined as 2800 to 4800 cells/mm<sup>2</sup> and low density as 500 to 1200 cells/mm<sup>2</sup>. The authors showed that hiPSC-CMs cultured in low density developed hallmarks of HCM, such as hypertrophy, altered gene expression profiles and altered electrophysiology. In contrast to this study, all hiPSC-CMs investigated in this thesis have been cultured in a density of 300 cells/mm<sup>2</sup> and hypertrophic phenotypes were clearly distinguishable between mutant and control cell lines. Important to note is that in the study of Uesugi et al. commercial medium was used for hiPSC-CMs culture supplemented with serum. However, in-house experiments showed that a culture density of 500 to 1200 cells/mm<sup>2</sup> results in confluent monolayers, which in our experimental set-up is not preferable, since hiPSC-CMs are measured as single cells. In general, reported n-numbers are very low when assessing cell sizes in hiPSC-CMs, what can be a limitation in some studies (Uesugi et al., 2014; Dambrot et al., 2014; Birket et al., 2015; Monteiro da Rocha et al., 2016; Ojala et al., 2016). Whether hypertrophy is a valid marker of HCM in hiPSC-CMs remains unclear and future studies have to elucidate the mechanisms that lead to this development and define hypertrophy in 2D.

Investigation of hiPSC-CMs in 3D is an attractive tool for evaluation of functional characteristics, such as contractile force amplitude and kinetics as well as electrophysiological parameters. Part of this thesis was to adapt previous protocols

for the generation of EHTs to hiPSC-CMs (Hansen et al., 2010; Schaaf et al., 2011). This model has been successfully applied to hiPSC-CMs in the past and EHTs generated with the *ACTN2* mutant cell line and its isogenic control, grants first evidence that this model can also be used in the context of disease modeling (Uzun et al., 2016; Mannhardt et al., 2016; Lemoine et al., 2017; Mannhardt et al., 2017). In comparison to their isogenic control, mutant *ACTN2* EHTs exhibited significantly higher and longer contraction force and relaxation time, respectively (Chapter 3.3, Fig. 15). This might be interpreted as hypercontractility and diastolic dysfunction, since EHTs consisting of hiPSC-CMs of an unrelated healthy control exhibited similar functional parameters as the isogenic control (data not shown). EHTs were in a similar range of force generation as reported previously, but relaxation time was almost two fold higher in both cell lines under paced conditions (Mannhardt et al., 2016; Mannhardt et al., 2017). This could be due to reported batch to batch variabilities or different genetic backgrounds in the hiPSC-CMs (Mannhardt et al., 2017). Therefore it remains unclear if observed phenotypes of mutant *ACTN2* EHTs are due to the underlying genetic mutation or natural variability, since disease modeling with EHTs has not been reported before with hiPSC-CMs. Previous studies used a knock-in model of mice with a *MYBPC3* mutation for analysis in EHT formats and reported higher contractile forces and a low number of EHTs with tetanic contractions, extreme prolongations in relaxation time, similar to findings in the *ACTN2* mutant EHTs (Stöhr et al., 2013). Further investigation of EHTs using *MYBPC3* KO mice was reported in 2016 by Wijnker et al. (Wijnker et al., 2016). In this study EHTs were generated from *Mybpc3*-targeted KO and WT mouse cardiac cells. KO EHTs displayed higher maximal forces when compared to WT EHTs, similar to *ACTN2* mutant EHTs. Additionally, AAV-mediated overexpression of a *MYBPC3* missense mutation revealed correct incorporation of missense cMyBP-C in the sarcomere. Suggesting that these missense proteins act as “poison peptides”, similar to what is expected in the *ACTN2* mutant line. Since investigated species are different, results are not completely transferable to hiPSC-CMs, but similar findings might lead to the same underlying disease mechanisms. Nevertheless, differences in EHTs were observed in comparison to an isogenic control, which is at present the best control available (Brandão et al., 2017). Other 3D models of DCM have been reported in the past (Tulloch et al., 2011; Kensah et al., 2013; Kuppusamy et al.,



2015; Riegler et al., 2015; Turnbull et al., 2014; Zhang et al., 2013; Tiburcy et al., 2017; Hinson et al., 2015; Stillitano et al., 2016). The only report on contraction measurements in hiPSC-CMs with a truncating *MYBPC3* mutation was by Birket et al. in 2D cultured single cells (Birket et al., 2015). This was accomplished by plating hiPSC-CMs on soft micropatterned polyacrylamide gels containing fluorescent microbeads. Micro-bead displacement was imaged and converted to a value of traction stress (Ribeiro et al., 2015). Ultimately, HCM hiPSC-CMs showed lower contractile force when compared to unrelated healthy controls. This is in stark contrast to the findings in EHTs. Reasons for this could be the fundamental difference of measuring one cell to a 3D construct of cells, which has been shown to develop a more mature phenotype (Uzun et al., 2016; Lemoine et al., 2017). Therefore it might be true that single HCM hiPSC-CMs reach lower contractile forces, since intrinsic pathomechanisms, such as haploinsufficiency caused by truncating mutations, cannot be compensated by functional 3D composites of hiPSC-CMs. This discrepancy has to be further investigated in the future.

Besides the possibility of using 3D constructs for modeling of inherited cardiomyopathies it is also important to note that these models are at the forefront of regenerative medicine, as their potential in improving cardiac function has been proven for several times now, also with EHTs (for review Shadrin et al., 2016; Weinberger et al., 2016). The most recent publication highlights a newly developed cardiopatch, which is a highly functional human cardiac tissue with clinically relevant dimensions of 4 x 4 cm (Shadrin et al., 2017). Additionally, cardiopatches robustly engraft, undergo vascularization by host vessels, maintain electrical function, and do not increase the incidence of arrhythmias. General limitations of these 3D models are efficient delivery of nutrients and oxygen to the cells, since vascularization is not apparent in engineered human heart tissues. Therefore 3D constructs of hiPSC-CMs can also be generated by alternative scaffolds, such as decellularized plants (Gershlak et al., 2017). This study describes how vascular structures of the plant can be utilized as prevascularized scaffolds for tissue engineering applications. Plant scaffolds were recellularized with human endothelial and mesenchymal cells as well as hiPSC-CMs and showed contractile function and  $Ca^{2+}$  handling properties over 21 days in culture. These studies provide the foundation for future use of hiPSC-CM tissues in regenerative medicine.

Taken together, hiPSC-CMs have shown to reproduce disease related-phenotypes of HCM in 2D and 3D and are therefore a good testbed for the investigation of underlying disease mechanisms.

#### **4.1.2 hiPSC-CMs as a suitable tool for evaluation of treatment options in HCM**

Another goal of this thesis was to evaluate hiPSC-CMs as a tool to assess molecular-based interventions, such as *trans*-splicing, GR and CRISPR/Cas9 genome editing in hiPSC-CMs.

*Trans*-splicing has been evaluated in the past as a new treatment option for inherited diseases, such as Duchenne muscular dystrophy, spinal muscular atrophy and HCM (for review Berger et al., 2016; Wally et al., 2012; Mearini et al., 2013). *Trans*-splicing is an attractive approach in the case of HCM-associated *MYBPC3* mutations, since by generating only two *pre-trans*-splicing molecules (PTMs) it is principally possible to repair all mutations and therefore treat 40-60% of all HCM patients, covering the first and the second half of the *MYBPC3* mRNA (Behrens-Gawlik et al., 2014; Carrier et al., 2015). In this thesis feasibility of 5' and 3' *trans*-splicing was tested in healthy control hiPSC-CMs (Chapter 3.1, Fig. 2, 3). However, *trans*-splicing efficiencies were very low and repaired cMyBP-C protein was not detected. Therefore *trans*-splicing was not tested in the *MYBPC3* mutant line. Since this study is the first to test *trans*-splicing in hiPSC-CMs, other reports on *trans*-splicing efficiencies are not available. However, a study in CCL-136 cells on dystrophia myotonica type 1 reported *trans*-splicing efficiencies of 1 to 7.4%, showing that higher *trans*-splicing efficiencies can be reached in cellular models (Chen et al., 2009). Other previous data obtained in our department showed that AAV-mediated *trans*-splicing efficiencies of up to 66% *in vitro* and 0.14% *in vivo* in *Mybpc3*-targeted knock-in mice (Mearini et al., 2013). Nevertheless, low amount of repaired cMyBP-C protein produced by 5' *trans*-splicing was not sufficient to prevent the development of the cardiac disease phenotype. One possibility of increasing *trans*-splicing efficiencies is by optimizing PTM design, especially for the binding domain (BD). The BD was located roughly in the middle and covered 120 nucleotides of the endogenous *MYBPC3* mRNA targeting intron 21, resulting in approximately the same packaging size for both PTMs. To increase *trans*-splicing efficiencies, systematic testing of different lengths and complementary regions might lead to higher binding affinities for the endogenous *pre*-mRNA.

However, highly conserved splice donor and acceptor sites were included in both PTMs that could be even stronger than the corresponding sequences in the *MYBPC3* intron 21. Another way of higher *trans*-splicing efficiencies is by evaluating different delivery vectors for PTMs. In this thesis AAV vectors were used, which allow specific delivery to hiPSC-CMs but also showed to be toxic in higher transduction doses than used. Additionally, other delivery vectors could be tested, whereby potential toxicity effects, especially when working towards clinical applications, should be considered. Nevertheless, this is the first proof-of-concept of *trans*-splicing in hiPSC-CMs.

GR is another very attractive treatment option for human inherited diseases already tested in several clinical trials worldwide. In the cardiovascular field one of the most promising clinical trials might have been the phase 2b CUPID 2 trial (Greenberg et al., 2016). Idea of this trial was to improve clinical outcome of heart failure patients by AAV1-mediated SERCA2a gene transfer. CUPID 2 followed the successful completion of phase I trials, which reported a beneficial outcome for study participants (Jessup et al., 2011; Zsebo et al., 2014). Those clinical studies were inspired by previous reports showing that deficiencies in SERCA2a activity in the failing heart can be corrected by gene transfer in experimental models (Byrne et al., 2008; del Monte et al., 2001; Kawase et al., 2008; Sakata et al., 2007). Unfortunately, no benefits have been observed in gene therapy recipients of the CUPID 2 trial. Reasons could lie in inadequate delivery and uptake of the vector, or the fact that SERCA2a is not an adequate target for gene therapy in patients with heart failure (HF). Therefore, gene therapy in HCM patients might be more straight forward, because underlying sarcomeric mutations are known and overexpression of sarcomeric proteins is expected to replace in part or completely the endogenous counterpart, since the sarcomere is a tightly regulated system with a preserved stoichiometry (Tardiff et al., 2015). Preserved stoichiometry of the sarcomere could be observed in the control hiPSC-CMs, where *MYBPC3* gene transfer resulted in 2.4-fold higher level of *MYBPC3* mRNA without change in the level of full-length cMyBP-C protein (Chapter 3.1, Fig. 4) Similarly in *MYBPC3* mutant hiPSC-CMs, gene transfer resulted in 2.6-fold higher amount of *MYBPC3* mRNA and restored cMyBP-C protein amounts to 81% of the healthy control (Chapter 3.1, Fig. 4). Additionally, partial restoration of cMyBP-C haploinsufficiency was sufficient to suppress hypertrophy in the *MYBPC3* mutant line and had no effect on cell sizes measured in

the healthy control (Chapter 3.1, Fig. 5). Exogenous FLAG-cMyBP-C proteins were properly incorporated into the sarcomere in both cell lines (Chapter 3.1, Fig. 5). Furthermore, gene expression profiles changed beneficially after *MYBPC3* gene replacement, reflected in mRNA levels of proteins associated with hypertrophy and  $\text{Ca}^{2+}$  handling. For example, mRNA levels of serum response factor (*SRF*) and *S100A4*, which are known to be higher in cardiomyopathies (Zhang et al., 2001; Doroudgar et al., 2016), were significantly reduced after 7 days of GR therapy (Chapter 3.1, Fig. 6). Additionally, levels of mRNAs encoding proteins belonging to the PI3K-Akt Kyoto Encyclopedia of Genes and Genome (KEGG) pathway, such as *CTGF*, collagens (*COL1A1*, *COL3A1*) and fibronectin (*FN1*) were significantly reduced. Finally, gene therapy increased mRNA levels of  $\text{Ca}^{2+}$  handling proteins, suggesting improvement of the cardiac contraction (Chapter 3.1, Fig. 6). Similar observations were reported in vivo using GR in *Mybpc3*-targeted knock-in mice (Mearini et al., 2014). GR treatment prevented the development of cardiac hypertrophy and dysfunction by increasing the amount of cMyBP-C protein and suppressed the expression of the endogenous mutant alleles. Furthermore, GR has been tested in hiPSC-CMs modeling catecholaminergic polymorphic ventricular tachycardia (CPVT) using an AAV9 vector for delivery of the human calsequestrin (*CASQ2*) gene (Lodola et al., 2016). Viral gene transfer decreased the percentage of delayed afterdepolarizations (DADs), reestablished  $\text{Ca}^{2+}$  transient amplitudes and lead to normalization of density and duration of  $\text{Ca}^{2+}$  sparks. Beneficial outcomes using GR treatment were also reported in hESC-CMs carrying a truncating *MYBPC3* mutation (Monteiro da Rocha et al., 2016). Viral gene transfer of full-length *MYBPC3* via AV prevented hypertrophy, sarcomeric disarray and improved  $\text{Ca}^{2+}$  impulse propagation in HCM hESC-CMs. In line with the data reported in this thesis, the authors showed correct incorporation of the M2-Flag-cMyBP-C proteins into the A-band of the sarcomere and suppressed hypertrophy in hESC-CMs after 7 days of treatment. Additionally, Western blot analyses suggests that the HCM hESC-CMs produced more exogenous cMyBP-C than control hESC-CMs, which fits to preserved stoichiometry of the sarcomere as described before. Unfortunately, gene expression profiles before and after GR were not analyzed in this study. Taken together, studies and data presented in thesis support GR as a promising therapeutic option, which could be particularly important for infants with bi-allelic truncating *MYBPC3* mutations

(Lekanne Deprez et al., 2006; Xin et al., 2007; Wessels et al., 2015). GR could prolong and improve quality of life of affected infants for whom no other therapy exists except heart transplantation. Evaluation of GR in HCM hiPSC-CMs has been reported in this thesis for the first time and therefore represents an intermediate step towards clinical application. Nevertheless, studies with large animal models are still required to test AAV doses and delivery before going to first-in patient.

CRISPR/Cas9 transformed the field of genome editing by storm. Before its emergence mostly technologies such as zinc finger nuclease (ZNFs) and transcription activator-like effector nucleases (TALENs) were used, which proved to be very costly and labor intensive (for review Hockemeyer et al., 2016). CRISPR/Cas9 on the other hand is a very cheap and fast method to generate desired genomic modifications in many of the scientifically used disease models (for review Sander et al., 2014). Originally the CRISPR/Cas9 system was found to be an adaptive immune response in bacteria and its first description was 30 years ago (for review Hsu et al., 2014; Marraffini, 2015). In 2012 Jinek et al. demonstrated that CRISPR type-2 system proteins, called Cas9, can also function as designer nucleases by associating with an engineered sgRNA that is complementary to a genetic locus of interest (Jinek et al., 2012). In less than 5 years CRISPR/Cas9 was exploited as a “high-throughput” genome editing tool in hiPSCs to generate or repair mutations causing human inherited diseases (for review Hockemeyer et al., 2016). One of the major contributions of this tool is to create isogenic control cell lines, as they can be used to directly assess the role of a mutation to cellular pathology without worrying about genome variability in an unrelated control. In this thesis the first ever reported isogenic control cell line for a disease-associated *ACTN2* mutation was created (Chapter 3.3, Fig. 13). Therefore *ACTN2* mutant hiPSCs were subjected to CRISPR/Cas9 editing following a protocol that was published in 2013, using a modified ssODN as a repair template (Ran et al., 2013). HDR efficiencies of 1.4% were reached with this approach and resulted in the generation of the <sub>rep</sub>HCM clone. Due to the fact that the Cas9 nickase enzyme (Cas9n) was used in this experiment, it is not surprising that editing efficiencies are rather low, as it is reported that Cas9n approaches are about 10% less efficient when compared to the WT Cas9 (Ran et al., 2013). However, higher editing efficiencies have been reached either by delivery of the Cas9 in viral vectors, by promoting HDR pathways in the cell or by using different

Cas9 enzymes (for review Hockemeyer et al., 2016; Chu et al., 2015; Burstein et al., 2017). Nonetheless, Cas9ns have been chosen for this experimental approach, since there is an ongoing debate about off-target effects, especially when developing it towards therapeutic purposes (for review Martin et al., 2016). As Cas9ns induce single strand breaks (SSBs) both Cas9ns have to nick in close proximity to each other for generation of DSBs, with no harm of causing off-target effects by creating a SSBs. Analysis of 13 intronic and exonic sites of the genome with off-target potential revealed no altered sequences in the  $_{rep}$ HCM clone (Chapter 3.3, Table 3). However, since the  $_{rep}$ HCM clone has not been subjected to whole genome sequencing the answer to the question whether off-targets have been introduced remains unclear. Another important issue is clonal stability of successfully edited clones, as manual hand picking can hold the danger of expanding a clonal mix of cells and therefore generate a chimeric population. Further expansion, differentiation and analysis of these clones can lead to falsified results, since it has been observed in previous experiments in our department that passaging of hiPSCs more than eight times results in one dominating clone (Letuffe-Brenière et al., unpublished). Therefore, in this thesis successfully edited hiPSC clones were again subcloned and regularly monitored for the affected genomic locus by Sanger sequencing. So far, there is only one report on the generation of isogenic controls using CRISPR/Cas9 in the context of HCM. Just recently Wang et al. reported the introduction of a disease-relevant HCM mutation (cTnT (*TNNT2*)-I79N) into a healthy hiPSC line by CRISPR/Cas9 editing (Wang et al., 2017). However, due to the publishing format it is not disclosed how exactly isogenic controls were generated. Nevertheless, this recent study gives new insights about underlying disease mechanism for *TNNT2* mutations in HCM as the authors conclude that action potential (AP) triangulation and AP instability, induced by an NCX-mediated mechanism, leads to an increased risk for arrhythmias. Furthermore, CRISPR/Cas9 has also been exploited in the cardiac field for the generation of new mouse models. Several studies have shown that CMs can be edited in the postnatal murine heart using viral-based vectors for delivery of CRISPR/Cas9 components (Carroll et al., 2016; Guo et al., 2017; Xie et al., 2016; Johansen et al., 2017). In the latest study of Johansen et al. transgenic mice were created with cardiac-restricted expression of Cas9 enzymes, using a floxed Cas9 cassette with a green fluorescent protein (GFP) reporter knocked into the Rosa26

locus. This was complemented with an  $\alpha$ -myosin heavy chain-Cre ( $\alpha$ MHC-Cre) transgene. Other reported mouse models have chosen a similar approach for cardiac-restricted Cas9 expression (Carroll et al., 2016; Guo et al., 2017). Overall Cas9 overexpression in CMs did not alter baseline cardiac function. Delivery of sgRNAs was mediated by AAV9, which displays cardiac tropism and postnatal pups were injected with a single dose of the virus. This study showed that CRISPR/Cas9 editing by delivering a single sgRNA is target-dependent, as just the *Myh6* gene disruption resulted in a cardiac phenotype. For disruption of the *Sav1* gene a dual sgRNA approach was used, which significantly increased editing efficiency. Generally, editing efficiencies and a mosaic pattern of gene disruption are still limitations when using CRISPR/Cas9 in vivo. Nevertheless, CRISPR/Cas9 editing was already applied to rescue disease-related phenotypes in mice with muscular dystrophy and PRKAG2 cardiac syndrome by targeted exon skipping and allele-specific silencing, respectively (Long et al., 2016; Xie et al., 2016). Taken together, since its initial description as a genome editing tool in 2012, CRISPR/Cas9 has already profoundly contributed to the field of hiPSC research by generation of relevant disease models and unraveling of cellular disease mechanisms. Nevertheless, it's important to note that CRISPR/Cas9 is also at the forefront of human germline therapy as several studies have shown efficient and successful editing of human embryos (Kang et al., 2016; Liang et al., 2015; Ma et al., 2017; Tang et al., 2017). Especially the study by Ma et al. is intriguing as the correction of a heterozygous *MYBPC3* mutation in human preimplantation embryos by CRISPR/Cas9 directly affects this thesis. The authors report that correction of germline mutations was achieved by activating an endogenous, germline-specific DNA repair response, which led to the finding that DSBs at the mutant paternal allele were predominantly repaired using the homologous wild-type maternal gene instead of a synthetic DNA template. Additionally, HDR efficiency was reported to vary between 13 and 27% amongst targeted clones, no off-targets events were found and no mosaicism was reported. However, these findings remain controversial as inter-homologue recombination was never reported before and has to be further validated in the future. Nevertheless, these studies show that treatment of human germline mutations can be accomplished by using CRISPR/Cas9.

All molecular-based interventions tested in this thesis have proven to work when applied to hiPSC-CMs. Therefore this model represents a good testbed for the investigation of new treatment options and an intermediate step towards clinical application.

#### **4.1.3 Limitations of hiPSC-CMs for disease modeling**

When working with hiPSCs it is important to consider possible limitations of the model such as unstable genome integrity, diverse differentiation protocols, immaturity and variability between hiPSC lines (for review Puri et al., 2012; Eschenhagen et al., 2015; Brandão et al., 2017).

One of the most pressing and probably least controlled limitations is instable genome integrity of hiPSCs. During expansion and prolonged passage of hiPSCs abnormal karyotypes and single nucleotide polymorphism (SNPs) are acquired constantly (Kilpinen et al., 2017; Mayshar et al., 2010; Taapken et al., 2011). Hot-spots of karyotype aberration are trisomies in the chromosomes 1, 8, 9 and 12, whereby duplications of chromosome 12 result in significant enrichment for cell cycle-related genes. SNPs are acquired in a more random fashion but seem to be linked to hot-spots of chromosomal aberrations (Mayshar et al., 2010). In general, hiPSCs are derived from somatic cells. Therefore, these cells are not meant for passing on hereditary information and are not subjected to evolutionary selective forces that act on mutations in germline cells. In comparison to hESCs, hiPSCs carry permanent genetic changes that are acquired during somatic cell development or during the reprogramming process and it is possible that none of these stages have developed mechanisms to protect the genome. Unfortunately, techniques for controlling genome integrity such as G-banding, copy number determination and whole exome/genome sequencing are still very expensive and cannot be used routinely for some hiPSC lines. Also in this thesis hiPSC lines were not subjected to whole genome sequencing, but G-banding resulted in the conformation of euploid karyotypes for all used cell lines except for the  $_{rep}$ HCM, which has not been tested yet. Another important aspect of genome integrity has been termed “epigenetic memory” (Bar-Nur et al., 2011; Ghosh et al., 2010; K. Kim et al., 2010; Marchetto et al., 2009; Polo et al., 2010). This effect is caused by incomplete removal of somatic cell-specific DNA methylation at regions in proximity to CpG islands (Doi et al., 2009; Kim et al., 2010).



It has been reported that with prolonged passaging of iPSCs and treatment with molecular inhibitors of DNA methyltransferase activity residual DNA methylation patterns are lost (Kim et al., 2010; Polo et al., 2010). These studies suggest that origin of hiPSCs could directly influence observations, which are made in disease modeling experiments. This is a limitation that could also affect this thesis, as hiPSCs were generated from human dermal skin fibroblast and cell-specific DNA methylation patterns have not been investigated. However, new technologies have to be developed to monitor constant changes in the genome in a low-cost and high throughput fashion, thereby guaranteeing stable genome integrity of investigated hiPSC lines.

Next to hiPSCs culture protocols, protocols for targeted differentiation of these cells have also to be validated and improved for generation of more defined hiPSC-CMs. Until now most CM-specific differentiation protocols generate ventricular-like CMs, including the protocol presented in this thesis (Mummery et al., 2012; Breckwoldt et al., 2017). Modeling of HCM with hiPSC-CMs has been therefore rather straightforward, since cell-autonomous ventricular aspects are modeled best with these cells. Nevertheless, for example mutations in *ACTN2* have never been investigated before in hiPSC-CMs, therefore it is not known if further testing of the same cell line in subtype-specific hiPSC-CMs would give further insights into underlying disease mechanisms. This also applies to the *MYBPC3* mutant cell line investigated in this thesis as the heart consists of additional cells beside CMs, such as fibroblasts, smooth muscle and endothelial cells, which might have an impact on disease development and progression. Therefore it is also important that heterotypic cell models are generated, which could help to unravel cell-to-cell communication and its impact on HCM. For instance, 7 days after GR treatment in the *MYBPC3* hiPSC-CMs mRNA levels of *CTGF*, collagens (*COL1A1* and *COL3A1*) and *FN1* were significantly reduced (Chapter 3.1, Fig. 6). This could be related to paracrine factors mediating the crosstalk between CMs and fibroblasts (for review Mooren et al., 2014; Takeda et al., 2011). First attempts have been made in this direction by protocols generating epicardium, epicardium-derived smooth muscle cells (EPI-SMCs) and cardiac fibroblasts from hiPSCs (Iyer et al., 2015; Witty et al., 2014). Additionally, heterotypic 3D models are reported consisting out of 75% hiPSC-CMs and 25% stromal cells, giving first insights into patients with cardio-facio-cutaneous syndrome

(CFCS), which is also associated with HCM (Cashman et al., 2016). It remains unclear, if observed HCM phenotypes in this 3D model are related to the heterotypic culture model, but further improvement of these models might contribute to the description of so far unknown disease mechanisms.

Immaturity of hiPSC-CMs is another important aspect when these cells are used for disease modeling (for review Eschenhagen et al., 2015; Brandão et al., 2017). Generally observed immature phenotypes in hiPSC-CMs are spontaneous contraction, depolarized resting membrane potential and altered  $\text{Ca}^{2+}$  handling properties (Lundy et al., 2013; Ma et al., 2011). Additionally, conduction velocities in hiPSC-CMs are substantially slower than in adult CMs (Lee et al., 2012). This is complemented by fetal gene expression profiles, morphological characteristics typical for fetal CMs and their predominant energy production by glycolysis, instead of fatty-acid oxidation (Synnergren et al., 2012; van den Berg et al., 2015; Veerman et al., 2015 Kim et al., 2013). Similar phenotypes were also observed in this thesis and have to be taken into consideration when evaluating data generated with hiPSC-CMs. Therefore 3D models, such as EHTs, can serve as a “maturation platform”, since several reports have shown impact on maturation when hiPSC-CMs were cultured in EHTs instead of a 2D monolayer (Mannhardt et al., 2016; Uzun et al., 2016; Lemoine et al., 2017). Furthermore, it is possible to increase culture duration for hiPSC-CMs and consequently time of maturation, for instance by establishing an “EHT-housing”, complementary to “mouse-housing”. If maturation can be also achieved in 2D cultures by increased culture duration remains unclear since culture of hiPSC-CMs over 30, 60 and 90 days did not show any maturation of the phenotype (Tanaka et al., 2014). On the other hand it is possible to contribute to maturation of 2D-cultured hiPSC-CMs by the supplementation of T3, IGF-1 and dexamethasone to the culture medium (Birket et al., 2015).

Finally, for every scientific experiment a suitable control is needed. Disease modeling experiments with hiPSC-CMs usually compare a patient-specific cell line to an unrelated healthy control cell line. Therefore genetic differences could influence experimental outcomes of these experiments and lead to false conclusions. It is reported that even between different control hiPSC-CMs electrophysiological properties can be significantly different (for review Sala et al., 2016). One possibility to circumvent this limitation is to generate isogenic control cell lines with

CRISPR/Cas9. As it is reported by Wang et al. and in this thesis, isogenic controls can be generated and help to directly decipher underlying disease mechanisms (Wang et al., 2017). Nevertheless, off-target mutations and the possibility of mixed clonal populations have to be critically monitored. Besides inter-person variability, intra-person variability can also play a crucial role in hiPSC-CMs. It is reported that mitochondrial DNA (mtDNA) variants in hiPSCs show low levels of potentially pathogenic mutations in original fibroblasts, which are revealed through reprogramming and therefore generate mutant hiPSCs (Perales-Clemente et al., 2016). Especially hiPSC-CMs with non-related human disease mtDNA mutations showed impaired mitochondrial respiration. Therefore the authors proposed next generation sequencing of mtDNA as a new selection criterion to ensure hiPSC quality and to reduce intra-person variability. This has also to be taken into consideration for the investigated cell lines in this thesis.

Despite many challenges discussed in this thesis, hiPSCs and hiPSC-CMs have had a significant impact on cardiac disease modeling in recent years. While animal and heterologous cell-based model systems will likely not be replaced by hiPSCs, this model has proven to be a powerful platform leading to novel mechanistic insights for HCM and other inherited human diseases. Limitations of hiPSCs will be further addressed in the future by lowering sequencing costs and new technologies to guarantee fast and safe development of hiPSCs into valuable tools for disease modeling, drug safety assessment, regenerative and precision medicine.

#### **4.2 Implications for modeling *ACTN2* mutations associated with HCM**

In contrast to *MYBPC3*, the role of *ACTN2* mutations as being causative for HCM is controversial. This is mostly due to its low prevalence in HCM patients of 1% and to the fact that *ACTN2* mutations are also associated with various other forms of cardiomyopathies (Table 4; for review Murphy et al., 2015; Maron et al., 2013).

Table 4:  $\alpha$ -Actinin 2 mutations and associated disease or phenotypes (modified from Murphy et al. 2015).

Mutation	Domain	Disease/Phenotype	Reference
Gln9Arg	ABD	DCM	Mohapatra et al., 2003
Gly111Val	ABD, CH1	HCM	Theis et al., 2006; Haywood et al., 2016
Ala119Thr	ABD, CH1	HCM, DCM, IVF, LVNC, SUD	Bagnall et al., 2014; Chiu et al., 2010; Haywood et al., 2016
Met228Thr	ABD, CH2	HCM + Atrial Arrhythmias	Girolami et al., 2014
Thr247Met	ABD, CH2	HCM + mild LQT	Prondzynski et al., unpublished
Thr495Met	Rod, SR2	HCM	Chiu et al., 2010; Theis et al., 2006
Glu583Ala	Rod, SR3	HCM	Chiu et al., 2010
Glu628Gly	Rod, SR3	HCM	Chiu et al., 2010
*Arg759Thr	CaM, EF12	HCM	Theis et al., 2006

The \* indicates that these are equivalent Arg residues in a sequence alignment of  $\alpha$ -Actinin 1 and 2. Abbreviations used: IVF, Idiopathic ventricular fibrillation; LVNC, Left ventricular non-compaction; LQTS, Long-QT-syndrome; SUD, Sudden unexplained death; HCM, Hypertrophic cardiomyopathy; DCM, Dilated cardiomyopathy.

Additionally, for just a few of the reported *ACTN2* mutations associated with HCM, underlying disease mechanisms have been described or investigated experimentally (Chiu et al., 2010; Girolami et al., 2014; Haywood et al., 2016; Theis et al., 2006). In an attempt to answer these question Haywood et al. investigated the Gly111Val and Met228Thr mutations in in vitro purified ABDs by circular dichroism and X-ray crystallography. Analysis of secondary and tertiary structures revealed small but distinct differences that might be responsible for reduced F-actin binding affinity in both mutants (Haywood et al., 2016). Furthermore, the authors used a full-length mEos2 tagged protein for overexpression studies in adult rat CMs and found that Z-disk localization and dynamic behavior of both mutants is altered. In conclusion Haywood et al. found “small effects on structure, function and behavior, which may contribute to a mild phenotype for this disease”. This statement of the authors is in stark contrast to the clinical findings that were described for the Ala119Thr mutation as DCM, left ventricular non-compaction, idiopathic ventricular fibrillation and unexplained sudden death (Bagnall et al., 2014; Chiu et al., 2010). Therefore additional disease modifiers must exist or previous experiments were not able to reveal the real impact of this mutation. Another Gln9Arg mutation was found in a DCM patient and tested in overexpression studies using mouse myoblasts (C2C12; Mohapatra et al., 2003). Transfection of these cells with the Gln9Arg variant revealed disrupted interaction with muscle LIM proteins (MLPs) in co-immunoprecipitation experiments and inhibited  $\alpha$ -Actinin 2 function analyzed by immunofluorescent imaging, thus proposing that the underlying DCM mechanism is compromised cytoarchitecture or altered myocyte differentiation. The novel *ACTN2* mutation (c.740C>T; p.Thr247Met) investigated in this thesis has never been reported before.

So far, experimental analysis of HCM hiPSC-CMs revealed hypertrophy in 2D and higher contractile forces and relaxation times in 3D compared to the isogenic control (Chapter 3.3, Fig. 14, 15). These results strongly suggest that observed in vitro hallmarks of HCM are caused by the *ACTN2* mutation, as those phenotypes were not present in the CRISPR/Cas9 repaired isogenic control cell line. However, it is hard to predict molecular consequences of this mutation, as those phenotypes are commonly observed in hiPSC-CMs modeling HCM-associated mutations. In another study Girolami et al identified a novel *ACTN2* mutation in an Italian family associated with mid-apical LV hypertrophy and juvenile onset of atrial fibrillation (Girolami et al., 2014). The Met228Thr mutation is located in the CH2 domain of the ABD and is just 19 amino acids (AA) away from the investigated *ACTN2* mutation in this thesis. This might indicate that both mutations contribute to a similar pathology, since they are in the same functional domain and both patient cohorts exhibit an electrophysiological component besides LV hypertrophy. But none of the Italian family members was diagnosed with LV outflow obstruction. Nevertheless, altered electrophysiology of affected patients might be reflected by the prolonged relaxation time exhibited in the *ACTN2* mutant EHTs. Experimental evidence that  $\alpha$ -Actinin 2 interacts with various ion channels such as voltage-gated sodium channel subunit 5 ( $\text{Na}_v1.5$ ), potassium voltage-gated channel member 5 ( $\text{K}_v1.5$ ), L-type  $\text{Ca}^{2+}$  channels and small conductance  $\text{Ca}^{2+}$ -activated potassium channels (SK2) was obtained in previous studies showing that its role in CMs is not fully understood yet (Ziane et al., 2010; Maruoka et al., 2000; Sadeghi et al., 2002; Lu et al., 2009). Interaction partners for  $\alpha$ -Actinin 2 were found in yeast two-hybrid systems and experimentally verified in in vitro studies (Sadeghi et al., 2002). These reports come all to the conclusion that  $\alpha$ -Actinin 2 links cytoskeleton to membrane proteins such as ion channels. Furthermore, in vitro experiments using the Thr247Met variant revealed that it is more prone to aggregation and exhibits higher F-actin binding affinities (Mathias Gautel, personal communication). Weins et al. reported about a similar observation in a disease-associated  $\alpha$ -Actinin 4 variant Lys255Glu (Weins et al., 2007). The authors analyzed this mutant in different in vitro systems and described higher F-actin binding affinities, resulting in aggregate formation and therefore impaired physiological function. Responsible for this phenotype is a constant exposure of the actin-binding site 1, which is buried in the WT protein. Since this mutation is just eight AA away

from the Thr247Met variant and in close proximity to the Met228Thr variant, a common disease mechanism could be apparent in both isoforms. Constant activation of the actin-binding site 1 could result in aggregate formation and impaired function of  $\alpha$ -Actinin 2 in the CMs. Thus, resulting in hypertrophy, sarcomeric disarray, contractile dysfunction and altered electrophysiology since  $\alpha$ -Actinin 2 fulfills different functions in CMs as  $\alpha$ -Actinin 4 does in podocytes. However, most of these studies were performed in cancer cell lines or in ex vivo analyzed rat and mouse CMs, therefore these results have to be validated in hiPSC-CMs first. Further experiments with the Thr247Met variant focusing on the mechanisms discussed above will help to understand the diverse role of  $\alpha$ -Actinin 2 in HCM.

## **5. Conclusion**

Despite many challenges objected in this thesis, hiPSC-CMs have proven to be a powerful platform for evaluation of disease-related phenotypes in HCM and for applications of new molecular-based treatment options. Apart from this thesis, hiPSC-CMs have already substantially contributed to novel mechanistic insights into disease pathologies and were able to translate cellular pathologies onto the individual patient level. Additionally, new therapeutic compounds can be tested on hiPSC-CMs that might lead to individually tailored treatment options in the future. Limitations of hiPSCs will be further addressed in the future allowing hiPSCs to grow to their full potential in disease modeling, drug safety assessment, regenerative and individualized medicine also in the field of HCM.

## 6. Bibliographie

- Abbott, B. P., Abbott, R., Abbott, T. D., Abernathy, M. R., Acernese, F., Ackley, K., ... Zweizig, J. (2016). Observation of gravitational waves from a binary black hole merger. *Physical Review Letters*, *116*(6), 1–16. <http://doi.org/10.1103/PhysRevLett.116.061102>
- Asakura, K., Hayashi, S., Ojima, A., Taniguchi, T., Miyamoto, N., Nakamori, C., ... Sawada, K. (2015). Improvement of acquisition and analysis methods in multi-electrode array experiments with iPSC cell-derived cardiomyocytes. *Journal of Pharmacological and Toxicological Methods*, *75*, 17–26. <http://doi.org/10.1016/j.vascn.2015.04.002>
- Ashrafian, H., McKenna, W. J., & Watkins, H. (2011). Disease pathways and novel therapeutic targets in hypertrophic cardiomyopathy. *Circulation Research*, *109*(1), 86–96. <http://doi.org/10.1161/CIRCRESAHA.111.242974>
- Ashrafian, H., & Watkins, H. (2007). Reviews of Translational Medicine and Genomics in Cardiovascular Disease: New Disease Taxonomy and Therapeutic Implications. Cardiomyopathies: Therapeutics Based on Molecular Phenotype. *Journal of the American College of Cardiology*, *49*(12), 1251–1264. <http://doi.org/10.1016/j.jacc.2006.10.073>
- Atlas, C., Aad, G., Abajyan, T., Abbott, B., Abdallah, J., Abdel Khalek, S., ... Zwalinski, L. (2012). Observation of a new particle in the search for the Standard Model Higgs boson with the ATLAS detector at the LHC. *Physics Letters, Section B: Nuclear, Elementary Particle and High-Energy Physics*, *716*(1), 1–29. <http://doi.org/10.1016/j.physletb.2012.08.020>
- Bagnall, R. D., Molloy, L. K., Kalman, J. M., & Semsarian, C. (2014). Exome sequencing identifies a mutation in the ACTN2 gene in a family with idiopathic ventricular fibrillation, left ventricular noncompaction, and sudden death. *BMC Medical Genetics*, *15*(1), 99. <http://doi.org/10.1186/s12881-014-0099-0>
- Ball, W., Ivanov, J., Rakowski, H., Wigle, E. D., Linghorne, M., Ralph-Edwards, A., ... Woo, A. (2011). Long-term survival in patients with resting obstructive hypertrophic cardiomyopathy comparison of conservative versus invasive treatment. *Journal of the American College of Cardiology*, *58*(22), 2313–2321. <http://doi.org/10.1016/j.jacc.2011.08.040>
- Bar-Nur, O., Russ, H. A., Efrat, S., & Benvenisty, N. (2011). Epigenetic memory and preferential lineage-specific differentiation in induced pluripotent stem cells derived from human pancreatic islet beta cells. *Cell Stem Cell*, *9*(1), 17–23. <http://doi.org/10.1016/j.stem.2011.06.007>
- Barefield, D., & Sadayappan, S. (2010). Phosphorylation and function of cardiac myosin binding protein-C in health and disease. *Journal of Molecular and Cellular Cardiology*, *48*(5), 866–75. <http://doi.org/10.1016/j.yjmcc.2009.11.014>
- Bayley, P. M., Findlay, W. A., & Martin, S. R. (1996). Target recognition by calmodulin: dissecting the kinetics and affinity of interaction using short peptide sequences. *Protein Science: A Publication of the Protein Society*, *5*(7), 1215–1228. <http://doi.org/10.1002/pro.5560050701>
- Beggs, A. H., Byers, T. J., Knoll, J. H. M., Boyce, F. M., Bruns, G. A. P., & Kunkel, L. M. (1992). Cloning and characterization of two human skeletal muscle alpha-actinin genes located on chromosomes 1 and 11. *J. Biol. Chem.*, *267*(13), 9281–9288.
- Behrens-Gawlik, V., Mearini, G., Gedicke-Hornung, C., Richard, P., & Carrier, L. (2014). MYBPC3 in hypertrophic cardiomyopathy: From mutation identification to RNA-based correction. *Pflugers Archiv European Journal of Physiology*, *466*(2), 215–223. <http://doi.org/10.1007/s00424-013-1409-7>
- Berger, A., Maire, S., Gaillard, M. C., Sahel, J. A., Hantraye, P., & Bemelmans, A. P. (2016). mRNA trans-splicing in gene therapy for genetic diseases. *Wiley Interdisciplinary Reviews: RNA*, *7*(4), 487–498. <http://doi.org/10.1002/wrna.1347>
- Bers, D. M. (2002). Cardiac excitation–contraction coupling. *Nature*, *415*, 198–205. <http://doi.org/10.1038/415198a>
- Bers, D. M. (2008). Calcium Cycling and Signaling in Cardiac Myocytes. *Annual Review of Physiology*, *70*(1), 23–49. <http://doi.org/10.1146/annurev.physiol.70.113006.100455>
- Birket, M. J., Ribeiro, M. C., Kosmidis, G., Ward, D., Leitoguinho, A. R., van de Pol, V., ... Mummery, C. L. (2015). Contractile Defect Caused by Mutation in MYBPC3 Revealed under Conditions Optimized for Human PSC-Cardiomyocyte Function. *Cell Reports*, *13*(4), 733–745. <http://doi.org/10.1016/j.celrep.2015.09.025>
- Birket, M. J., Ribeiro, M. C., Verkerk, A. O., Ward, D., Leitoguinho, A. R., den Hartogh, S. C., ... Mummery, C. L. (2015). Expansion and patterning of cardiovascular progenitors derived from human pluripotent stem cells. *Nature Biotechnology*, *33*(9), 970–979. <http://doi.org/10.1038/nbt.3271>
- Bizy, A., Guerrero-Serna, G., Hu, B., Ponce-Balbuena, D., Willis, B. C., Zarzoso, M., ... Jalife, J. (2013). Myosin light chain 2-based selection of human iPSC-derived early ventricular cardiac myocytes. *Stem Cell Research*, *11*(3), 1335–1347. <http://doi.org/10.1016/j.scr.2013.09.003>
- Blanchard, A., Ohanian, V., & Critchley, D. (1989). The structure and function of alpha-actinin. *Journal of Muscle Research and Cell Motility*, *10*, 280–289. <http://doi.org/10.1002/yea>
- Bonne, G., Carrier, L., Bercovici, J., Cruaud, C., Richard, R., Hainque, B., ... Schwartz, K. (1995). Cardiac myosin binding protein-C gene splice acceptor site mutation is associated with familial hypertrophic cardiomyopathy. *Nature Genetics*, *11*, 438–440.
- Brandão, K. O., Tabel, V. A., Atsma, D. E., Mummery, C. L., & Davis, R. P. (2017). Human pluripotent stem cell models of cardiac disease: from mechanisms to therapies. *Disease Models & Mechanisms*, *10*(9), 1039–1059. <http://doi.org/10.1242/dmm.030320>
- Breckwoldt, K., Letuffe-Brenière, D., Mannhardt, I., Schulze, T., Ulmer, B., Werner, T., ... Hansen, A. (2017). Differentiation of cardiomyocytes and generation of human engineered heart tissue. *Nature Protocols*, *12*(6), 1177–1197. <http://doi.org/10.1038/nprot.2017.033>

- Broderick, M. J. F., & Winder, S. J. (2005). Spectrin, Alpha-Actinin, and Dystrophin. *ADVANCES IN PROTEIN CHEMISTRY*, 70(04), 203–246. [http://doi.org/10.1016/S0065-3233\(04\)70007-8](http://doi.org/10.1016/S0065-3233(04)70007-8)
- Burridge, K., & Feramisco, J. R. (1981). Non-muscle alpha-actinins are calcium-sensitive actin-binding proteins. *Nature*, 294, 565–567.
- Burridge, P. W., Keller, G., Gold, J. D., & Wu, J. C. (2012). Production of de novo cardiomyocytes: Human pluripotent stem cell differentiation and direct reprogramming. *Cell Stem Cell*, 10(1), 16–28. <http://doi.org/10.1016/j.stem.2011.12.013>
- Burstein, D., Harrington, L. B., Strutt, S. C., Probst, A. J., Anantharaman, K., Thomas, B. C., ... Banfield, J. F. (2017). New CRISPR–Cas systems from uncultivated microbes. *Nature*, 542(7640), 237–241. <http://doi.org/10.1038/nature21059>
- Byrne, M. J., Power, J. M., Prevolos, A., Mariani, J. A., Hajjar, R. J., & Kaye, D. M. (2008). Recirculating cardiac delivery of AAV2/1SERCA2a improves myocardial function in an experimental model of heart failure in large animals. *Gene Therapy*, 15(23), 1550–1557. <http://doi.org/10.1038/gt.2008.120>
- Cao, F., Wagner, R. A., Wilson, K. D., Xie, X., Fu, J.-D., Drukker, M., ... Wu, J. C. (2008). Transcriptional and Functional Profiling of Human Embryonic Stem Cell-Derived Cardiomyocytes. *PLoS ONE*, 3(10), 1–12. <http://doi.org/10.1371/journal.pone.0003474>
- Capes-Davis, A., Theodosopoulos, G., Atkin, I., Drexler, H. G., Kohara, A., MacLeod, R. A. F., ... Freshney, R. I. (2010). Check your cultures! A list of cross-contaminated or misidentified cell lines. *International Journal of Cancer*, 127(1), 1–8. <http://doi.org/10.1002/ijc.25242>
- Carrier, L., Bonne, G., Bahrend, E., Yu, B., Richard, P., Niel, F., ... Schwartz, K. (1997). Organization and Sequence of Human Cardiac Myosin Binding Protein C Gene (MYBPC3) and Identification of Mutations Predicted to Produce Truncated Proteins in Familial Hypertrophic Cardiomyopathy. *Circ. Res.*, 80(3), 427–434. <http://doi.org/10.1161/01.RES.80.3.427>
- Carrier, L., Mearini, G., Stathopoulou, K., & Cuello, F. (2015). Cardiac myosin-binding protein C (MYBPC3) in cardiac pathophysiology. *Gene*, 573(2), 188–197. <http://doi.org/10.1016/j.gene.2015.09.008>
- Carrier, L., Schlossarek, S., Willis, M. S., & Eschenhagen, T. (2010). The ubiquitin-proteasome system and nonsense-mediated mRNA decay in hypertrophic cardiomyopathy. *Cardiovascular Research*, 85(2), 330–338. <http://doi.org/10.1093/cvr/cvp247>
- Carroll, K. J., Makarewich, C. A., McAnally, J., Anderson, D. M., Zentilin, L., Liu, N., ... Olson, E. N. (2016). A mouse model for adult cardiac-specific gene deletion with CRISPR/Cas9. *Proceedings of the National Academy of Sciences*, 113(2), 338–343. <http://doi.org/10.1073/pnas.1523918113>
- Cashman, T. J., Josowitz, R., Johnson, B. V., Gelb, B. D., & Costa, K. D. (2016). Human engineered cardiac tissues created using induced pluripotent stem cells reveal functional characteristics of BRAF-mediated hypertrophic cardiomyopathy. *PLoS ONE*, 11(1), 1–17. <http://doi.org/10.1371/journal.pone.0146697>
- Cazorla, O., Szilagyi, S., Vignier, N., Salazar, G., Krämer, E., Vassort, G., ... Lacampagne, A. (2006). Length and protein kinase A modulations of myocytes in cardiac myosin binding protein C-deficient mice. *Cardiovascular Research*, 69(2), 370–380. <http://doi.org/10.1016/j.cardiores.2005.11.009>
- Chan, Y., Tong, H.-Q., Beggs, A. H., & Kunkel, L. M. (1998). Human skeletal muscle-specific alpha-actinin-2 and -3 isoforms form homodimers and heterodimers in vitro and in vivo. *Biochemical and Biophysical Research Communications*, 248(1), 134–139. <http://doi.org/10.1006/bbrc.1998.8920>
- Chen, H. Y., Kathirvel, P., Yee, W. C., & Lai, P. S. (2009). Correction of dystrophin myotonia type 1 pre-mRNA transcripts by artificial trans-splicing. *Gene Therapy*, 16, 211–217. <http://doi.org/10.1038/gt.2008.150>
- Chinwalla, A. T., Cook, L. L., Delehaunty, K. D., Fewell, G. D., Graves, T. A., & AI, E. (2002). Initial sequencing and comparative analysis of the mouse genome. *Nature*, 420, 520–562.
- Chira, S., Jackson, C. S., Oprea, I., Ozturk, F., Pepper, M. S., Diaconu, I., ... Berindan-Neagoe, I. (2015). Progresses towards safe and efficient gene therapy vectors. *Oncotarget*, 6(31), 30675–30703. <http://doi.org/10.18632/oncotarget.5169>
- Chiu, C., Bagnall, R. D., Ingles, J., Yeates, L., Kennerson, M., Donald, J. A., ... Semsarian, C. (2010). Mutations in Alpha-Actinin-2 Cause Hypertrophic Cardiomyopathy. A Genome-Wide Analysis. *Journal of the American College of Cardiology*, 55(11), 1127–1135. <http://doi.org/10.1016/j.jacc.2009.11.016>
- Chu, V. T., Weber, T., Wefers, B., Wurst, W., Sander, S., Rajewsky, K., & Kühn, R. (2015). Increasing the efficiency of homology-directed repair for CRISPR-Cas9-induced precise gene editing in mammalian cells. *Nature Biotechnology*, 33(5), 543–548. <http://doi.org/10.1038/nbt.3198>
- Cong, L., Ann Ran, F., Cox, D., Lin, S., Barretto, R., Habib, N., ... Zhang, F. (2013). Multiplex Genome Engineering Using CRISPR/Cas Systems. *Scienceexpress*, 339, 819–823. <http://doi.org/10.1038/nbt1319>
- Crilley, J. G., Boehm, E. A., Blair, E., Rajagopalan, B., Blamire, A. M., Styles, P., ... Watkins, H. (2003). Hypertrophic cardiomyopathy due to sarcomeric gene mutations is characterized by impaired energy metabolism irrespective of the degree of hypertrophy. *Journal of the American College of Cardiology*, 41(10), 1776–1782. [http://doi.org/10.1016/S0735-1097\(02\)03009-7](http://doi.org/10.1016/S0735-1097(02)03009-7)
- Dambrot, C., Braam, S. R., Tertoolen, L. G. J., Birket, M., Atsma, D. E., & Mummery, C. L. (2014). Serum supplemented culture medium masks hypertrophic phenotypes in human pluripotent stem cell derived cardiomyocytes. *Journal of Cellular and Molecular Medicine*, 18(8), 1509–1518. <http://doi.org/10.1111/jcmm.12356>
- Darwin, C. (1872). *The Origin of Species - 6th Edition*, 186–229.
- del Monte, F., Williams, E., Lebeche, D., Schmidt, U., Rosenzweig, A., Gwathmey, J. K., ... Hajjar, R. J. (2001). Improvement in



- survival and cardiac metabolism after gene transfer of sarcoplasmic reticulum Ca(2+)-ATPase in a rat model of heart failure. *Circulation*, 104, 1424–1429. <http://doi.org/10.1161/hc3601.095574>
- Denning, C., Borgdorff, V., Crutchley, J., Firth, K. S. A., George, V., Kalra, S., ... Young, L. E. (2016). Cardiomyocytes from human pluripotent stem cells: From laboratory curiosity to industrial biomedical platform. *Biochimica et Biophysica Acta - Molecular Cell Research*, 1863(7), 1728–1748. <http://doi.org/10.1016/j.bbamcr.2015.10.014>
- Devalla, H. D., Schwach, V., Ford, J. W., Milnes, J. T., El-Haou, S., Jackson, C., ... Passier, R. (2015). Atrial-like cardiomyocytes from human pluripotent stem cells are a robust preclinical model for assessing atrial-selective pharmacology. *EMBO Molecular Medicine*, 7(4), 394–410. <http://doi.org/10.15252/emmm.201404757>
- Dhandapany, P. S., Sadayappan, S., Xue, Y., Powell, G. T., Rani, D. S., Nallari, P., ... Thangaraj, K. (2009). A common MYBPC3 (cardiac myosin binding protein C) variant associated with cardiomyopathies in South Asia. *Nature Genetics*, 41(2), 187–191. <http://doi.org/10.1038/ng.309>
- Dixson, J. D., Forstner, M. R. J., & Garcia, D. M. (2002). The Alpha-actinin gene family: A revised classification. *Journal of Molecular Evolution*, 56(1), 1–10. <http://doi.org/10.1007/s00239-002-2374-5>
- Djinovic-Carugo, K., Gautel, M., Ylänne, J., & Young, P. (2002). The spectrin repeat: A structural platform for cytoskeletal protein assemblies. *FEBS Letters*, 513(1), 119–123. [http://doi.org/10.1016/S0014-5793\(01\)03304-X](http://doi.org/10.1016/S0014-5793(01)03304-X)
- Doetschman, T. C., Eistetter, H., Katz, M., Schmidt, W., & Kemler, R. (1985). The in vitro development of blastocyst-derived embryonic stem cell lines: formation of visceral yolk sac, blood islands and myocardium. *Journal of Embryology and Experimental Morphology*, 87, 27–45. <http://doi.org/10.1263/jbb.103.389>
- Doi, A., Park, I.-H., Wen, B., Murakami, P., Aryee, M. J., Irizarry, R., ... Feinberg, A. P. (2009). Differential methylation of tissue- and cancer-specific CpG island shores distinguishes human induced pluripotent stem cells, embryonic stem cells and fibroblasts. *Nature Genetics*, 41(12), 1350–1353. <http://doi.org/10.1038/ng.471>
- Doroudgar, S., Quijada, P., Konstandin, M., Ilves, K., Broughton, K., Khalafalla, F. G., ... Völkers, M. (2016). S100A4 protects the myocardium against ischemic stress. *Journal of Molecular and Cellular Cardiology*, 100, 54–63. <http://doi.org/10.1016/j.yjmcc.2016.10.001>
- Dürst, M., Gissmann, L., Ikenberg, H., & Hausen, H. Z. U. R. (1983). A papillomavirus , DNA- from a cervical carcinoma and-its -prevalence in cancer biopsy samples from different geographic regions. *Proceedings of the National Academy of Sciences of the United States of America*, 80, 3812–3815.
- Ebashi, S., & Ebashi, F. (1965). Alpha-Actinin, a New Structural Protein from Striated Muscle. *The Journal of Biochemistry*, 58(1), 7–12.
- Ebeling, A. H. (1922). A Ten Year Old Strain of Fibroblasts. *The Journal of Experimental Medicine*, 35(6), 755–759. <http://doi.org/10.1084/jem.35.6.755>
- Ebeling, A. H., & Fischer, A. (1922). Mixed Cultures of Pure Strains of Fibroblasts and Epithelial Cells. *The Journal of Experimental Medicine*, 36(3), 285–289. <http://doi.org/10.1084/jem.36.3.285>
- Ebert, A. D., Yu, J., Rose, F. F., Mattis, V. B., Lorson, C. L., Thomson, J. A., & Svendsen, C. N. (2009). Induced pluripotent stem cells from a spinal muscular atrophy patient. *Nature*, 457(7227), 277–280. <http://doi.org/10.1038/nature07677>
- Eiges, R., Urbach, A., Malcov, M., Frumkin, T., Schwartz, T., Amit, A., ... Ben-Yosef, D. (2007). Developmental Study of Fragile X Syndrome Using Human Embryonic Stem Cells Derived from Preimplantation Genetically Diagnosed Embryos. *Cell Stem Cell*, 1(5), 568–577. <http://doi.org/10.1016/j.stem.2007.09.001>
- Einstein, A. (1916). Näherungsweise Integration der Feldgleichungen der Gravitation. *Sitzungsber. K. Preuss. Akad. Wiss.* 1, 688 (1916), 99–108.
- Erdmann, J., Raible, J., Maki-Abadi, J., Hummel, M., Hammann, J., Wollnik, B., ... Regitz-Zagrosek, V. (2001). Spectrum of clinical phenotypes and gene variants in cardiac myosin-binding protein C mutation carriers with hypertrophic cardiomyopathy. *Journal of the American College of Cardiology*, 38(2), 322–30.
- Eschenhagen, T. (2010). Is ryanodine receptor phosphorylation key to the fight or flight response and heart failure? *The Journal of Clinical Investigation*, 120(12), 102–106. <http://doi.org/10.1172/JCI45251.node>
- Eschenhagen, T., Mummery, C., & Knollmann, B. C. (2015). Modelling sarcomeric cardiomyopathies in the dish: from human heart samples to iPSC cardiomyocytes. *Cardiovascular Research*, 105, 424–438.
- Evans, M. J., & Kaufmann, M. H. (1981). Establishment in culture of pluripotential cells from mouse embryos. *Nature*, 292, 154–156.
- Franzot, G., Sjöblom, B., Gautel, M., & Carugo, K. D. (2005). The crystal structure of the actin binding domain from  $\alpha$ -actinin in its closed conformation: Structural insight into phospholipid regulation of  $\alpha$ -actinin. *Journal of Molecular Biology*, 348(1), 151–165. <http://doi.org/10.1016/j.jmb.2005.01.002>
- Fraser, C. M., Gocayne, J. D., White, O., Adams, M. D., Clayton, R. a, Fleischmann, R. D., ... Venter, J. C. (1995). The Minimal Gene Complement of Mycoplasma genitalium. *Science*, 270(5235), 397–403.
- Freedman, L. P., Gibson, M. C., Ethier, S. P., Soule, H. R., Neve, R. M., & Reid, Y. A. (2015). Reproducibility: changing the policies and culture of cell line authentication. *Nature Methods*, 12(6), 493–497. <http://doi.org/10.1038/nmeth.3403>
- Frey, N., Luedde, M., & Katus, H. A. (2012). Mechanisms of disease: hypertrophic cardiomyopathy. *Nature Reviews Cardiology*, 9(2), 91–100. <http://doi.org/10.1038/nrcardio.2011.159>
- Friedrich, F. W., & Carrier, L. (2012). Genetics of hypertrophic and dilated cardiomyopathy. *Current Pharmaceutical*

*Biotechnology*, 13(13), 2467–76. <http://doi.org/10.2174/138920112804583041>

- Gautel, M., & Djinic-Carugo, K. (2016). The sarcomeric cytoskeleton: from molecules to motion. *Journal of Experimental Biology*, 219(2), 135–145. <http://doi.org/10.1242/jeb.124941>
- Gautel, M., Zuffardi, O., Freiburg, A., & Labeit, S. (1995). Phosphorylation switches specific for the cardiac isoform of myosin binding protein-C: a modulator of cardiac contraction? *The EMBO Journal*, 14(9), 1952–60.
- Gedicke-Hornung, C., Behrens-Gawlik, V., Reischmann, S., Geertz, B., Stimpel, D., Weinberger, F., ... Carrier, L. (2013). Rescue of cardiomyopathy through U7snRNA-mediated exon skipping in Mybpc3-targeted knock-in mice. *EMBO Molecular Medicine*, 5(7), 1060–77. <http://doi.org/10.1002/emmm.201202168>
- Geisterfer-Lowrance, A. A., Kass, S., Tanigawa, G., Vosberg, H. P., McKenna, W., Seidman, C. E., & Seidman, J. G. (1990). A molecular basis for familial hypertrophic cardiomyopathy: a beta cardiac myosin heavy chain gene missense mutation. *Cell*, 62(5), 999–1006. Retrieved from <http://www.ncbi.nlm.nih.gov/pubmed/1975517>
- Geisterfer-Lowrance, A. A. T., Christe, M., Conner, D. A., Ingwall, J. S., Schoen, F. J., Seidman, C. E., & Seidman, J. G. (1996). A Mouse Model of Familial Hypertrophic Cardiomyopathy. *Science*, 272, 731–734.
- Gersh, B. J., Maron, B. J., Bonow, R. O., Dearani, J. A., Fifer, M. A., Link, M. S., ... Yancy, C. W. (2011). 2011 ACCF/AHA Guideline for the Diagnosis and Treatment of Hypertrophic Cardiomyopathy: A Report of the American College of Cardiology Foundation/American Heart Association Task Force on Practice Guidelines Developed in Collaboration With the American Ass. *Journal of the American College of Cardiology*, 58(25), 212–260. <http://doi.org/10.1016/j.jacc.2011.06.011>
- Gershlak, J. R., Hernandez, S., Fontana, G., Perreault, L. R., Hansen, K. J., Larson, S. A., ... Gaudette, G. R. (2017). Crossing kingdoms: Using decellularized plants as perfusable tissue engineering scaffolds. *Biomaterials*, 125, 13–22. <http://doi.org/10.1016/j.biomaterials.2017.02.011>
- Geske, J. B., Ong, K. C., Siontis, K. C., Hebl, V. B., Ackerman, M. J., Hodge, D. O., ... Ommen, S. R. (2017). Women with hypertrophic cardiomyopathy have worse survival. *European Heart Journal*, (November), 1–9. <http://doi.org/10.1093/eurheartj/ehx527>
- Gest, H. (2004). The discovery of microorganisms by Robert Hooke and Antoni van Leeuwenhoek, Fellows of The Royal Society. *Notes and Records of the Royal Society*, 58(2), 187–201. <http://doi.org/10.1098/rsnr.2004.0055>
- Ghosh, Z., Wilson, K. D., Wu, Y., Hu, S., Quertermous, T., & Wu, J. C. (2010). Persistent donor cell gene expression among human induced pluripotent stem cells contributes to differences with human embryonic stem cells. *PLoS ONE*, 5(2), 1–10. <http://doi.org/10.1371/journal.pone.0008975>
- Gibson, D. G., Glass, J. I., Lartigue, C., Noskov, V. N., Chuang, R.-Y., Algire, M. A., ... Venter, J. C. (2010). Creation of a Bacterial Cell Controlled by a Chemically Synthesized Genome. *Science*, 329(5987), 52–56. <http://doi.org/10.1126/science.1190719>
- Gilbert, R., Cohen, J. A., Pardo, S., Basu, A., & Fischman, D. A. (1999). Identification of the A-band localization domain of myosin binding proteins C and H (MyBP-C, MyBP-H) in skeletal muscle. *Journal of Cell Science*, 112, 69–79.
- Ginn, S. L., Alexander, I. E., Edelstein, M. L., Abedi, M. R., & Wixon, J. (2013). Gene transfer into guinea pig cochlea using adeno-associated virus vectors. *The Journal of Gene Medicine*, 15, 65–77. <http://doi.org/10.1002/jgm>
- Girolami, F., Ho, C. Y., Semsarian, C., Baldi, M., Will, M. L., Baldini, K., ... Olivetto, I. (2010). Clinical Features and Outcome of Hypertrophic Cardiomyopathy Associated With Triple Sarcomere Protein Gene Mutations. *Journal of the American College of Cardiology*, 55(14), 1444–1453. <http://doi.org/10.1016/j.jacc.2009.11.062>
- Girolami, F., Iascone, M., Tomberli, B., Bardi, S., Benelli, M., Marseglia, G., ... Olivetto, I. (2014). Novel  $\alpha$ -actinin 2 variant associated with familial hypertrophic cardiomyopathy and juvenile atrial arrhythmias: A massively parallel sequencing study. *Circulation: Cardiovascular Genetics*, 7(6), 741–750. <http://doi.org/10.1161/CIRCGENETICS.113.000486>
- Greenberg, B., Butler, J., Felker, G. M., Ponikowski, P., Voors, A. A., Desai, A. S., ... Zsebo, K. M. (2016). Calcium upregulation by percutaneous administration of gene therapy in patients with cardiac disease (CUPID 2): A randomised, multinational, double-blind, placebo-controlled, phase 2b trial. *The Lancet*, 387(10024), 1178–1186. [http://doi.org/10.1016/S0140-6736\(16\)00082-9](http://doi.org/10.1016/S0140-6736(16)00082-9)
- Gruen, M., & Gautel, M. (1999). Mutations in beta-myosin S2 that cause familial hypertrophic cardiomyopathy (FHC) abolish the interaction with the regulatory domain of myosin-binding protein-C. *Journal of Molecular Biology*, 286(3), 933–49. <http://doi.org/10.1006/jmbi.1998.2522>
- Guo, Y., Vandusen, N. J., Zhang, L., Gu, W., Sethi, I., Guatimosim, S., ... Pu, W. T. (2017). Analysis of Cardiac Myocyte Maturation Using CASA AV, a Platform for Rapid Dissection of Cardiac Myocyte Gene Function in Vivo. *Circulation Research*, 120(12), 1874–1888. <http://doi.org/10.1161/CIRCRESAHA.116.310283>
- Haas, J., Frese, K. S., Peil, B., Kloos, W., Keller, A., Nietsch, R., ... Meder, B. (2015). Atlas of the clinical genetics of human dilated cardiomyopathy. *European Heart Journal*, 36(18), 1123–1135. <http://doi.org/10.1093/eurheartj/ehu301>
- Hamazaki, T., Iiboshi, Y., Oka, M., Papst, P. J., Meacham, A. M., Zon, L. I., & Terada, N. (2001). Hepatic maturation in differentiating embryonic stem cells in vitro. *FEBS Letters*, 497, 15–19.
- Hammond, S. M., & Wood, M. J. A. (2011). Genetic therapies for RNA mis-splicing diseases. *Trends in Genetics*, 27(5), 196–205. <http://doi.org/10.1016/j.tig.2011.02.004>
- Han, L., Li, Y., Tchao, J., Kaplan, A. D., Lin, B., Li, Y., ... Yang, L. (2014). Study familial hypertrophic cardiomyopathy using patient-specific induced pluripotent stem cells. *Cardiovascular Research*, 104(2), 258–269.

<http://doi.org/10.1093/cvr/cvu205>

- Hansen, A., Eder, A., Bönstrup, M., Flato, M., Mewe, M., Schaaf, S., ... Eschenhagen, T. (2010). Development of a drug screening platform based on engineered heart tissue. *Circulation Research*, *107*(1), 35–44. <http://doi.org/10.1161/CIRCRESAHA.109.211458>
- Harris, S. P. (2002). Hypertrophic Cardiomyopathy in Cardiac Myosin Binding Protein-C Knockout Mice. *Circulation Research*, *90*(5), 594–601. <http://doi.org/10.1161/01.RES.0000012222.70819.64>
- Harrison, R. G. (1907). Observations on the living Developing Nerve Fiber. *The Anatomical Record*, 116–128.
- Haywood, N. J., Wolny, M., Rogers, B., Trinh, C. H., Shuping, Y., Edwards, T. A., & Peckham, M. (2016). Hypertrophic cardiomyopathy mutations in the calponin-homology domain of ACTN2 affect actin binding and cardiomyocyte Z-disc incorporation. *Biochemical Journal*, *473*(16), 2485–2493. <http://doi.org/10.1042/BCJ20160421>
- Helms, A. S., Davis, F. M., Coleman, D., Bartolone, S. N., Glazier, A. A., Pagani, F., ... Day, S. M. (2014). Sarcomere mutation-specific expression patterns in human hypertrophic cardiomyopathy. *Circulation: Cardiovascular Genetics*, *7*(4), 434–443. <http://doi.org/10.1161/CIRCGENETICS.113.000448>
- Hescheler, J., Fleischmann, B. K., Lentini, S., Maltsev, V. a, Rohwedel, J., Wobus, a M., & Addicks, K. (1997). Embryonic stem cells: a model to study structural and functional properties in cardiomyogenesis. *Cardiovasc Res*, *36*(2), 149–162. <http://doi.org/S0008636397001934> [pii]
- Hinson, J. T., Chopra, A., Nafissi, N., Polacheck, W. J., Benson, C. C., Swist, S., ... Seidman, C. E. (2015). Titin mutations in iPS cells define sarcomere insufficiency as a cause of dilated cardiomyopathy. *Science*, *349*(6251), 982–986. <http://doi.org/10.1126/science.aaa5458>
- Ho, C. Y. (2010). Hypertrophic Cardiomyopathy. *Heart Failure Clinics*, *6*(2), 141–159. <http://doi.org/10.1016/j.hfc.2009.12.001>
- Ho, C. Y., Lever, H. M., DeSanctis, R., Farver, C. F., Seidman, J. G., & Seidman, C. E. (2000). Homozygous Mutation in Cardiac Troponin T: Implications for Hypertrophic Cardiomyopathy. *Circulation*, *102*(16), 1950–1955. <http://doi.org/10.1161/01.CIR.102.16.1950>
- Hockemeyer, D., & Jaenisch, R. (2016). Induced pluripotent stem cells meet genome editing. *Cell Stem Cell*, *18*(5), 573–586. <http://doi.org/10.1016/j.stem.2016.04.013>
- Hoedemaekers, Y. M., Caliskan, K., Michels, M., Frohn-Mulder, I., Van Der Smagt, J. J., Phefferkorn, J. E., ... Majoor-Krakauer, D. F. (2010). *The importance of genetic counseling, DNA diagnostics, and cardiologic family screening in left ventricular noncompaction cardiomyopathy.* *Circulation: Cardiovascular Genetics* (Vol. 3). <http://doi.org/10.1161/CIRCGENETICS.109.903898>
- Hsu, P. D., Lander, E. S., & Zhang, F. (2014). Development and applications of CRISPR-Cas9 for genome engineering. *Cell*, *157*(6), 1262–1278. <http://doi.org/10.1016/j.cell.2014.05.010>
- Hublin, J.-J., Ben-Ncer, A., Bailey, S. E., Freidline, S. E., Neubauer, S., Skinner, M. M., ... Gunz, P. (2017). New fossils from Jebel Irhoud, Morocco and the pan-African origin of Homo sapiens. *Nature*, *546*(7657), 289–292. <http://doi.org/10.1038/nature22336>
- Ingles, J., Doolan, A., Chiu, C., Seidman, J., Seidman, C., & Semsarian, C. (2005). Compound and double mutations in patients with hypertrophic cardiomyopathy: implications for genetic testing and counselling. *Journal of Medical Genetics*, *42*(10), 59–65. <http://doi.org/10.1136/jmg.2005.033886>
- Ingwall, J. S., & Weiss, R. G. (2004). Is the failing heart energy starved? On using chemical energy to support cardiac function. *Circulation Research*, *95*(2), 135–145. <http://doi.org/10.1161/01.RES.0000137170.41939.d9>
- Iyer, D., Gambardella, L., Bernard, W. G., Serrano, F., Mascetti, V. L., Pedersen, R. A., ... Talasila, A. (2015). Robust derivation of epicardium and its differentiated smooth muscle cell progeny from human pluripotent stem cells. *Development*, *143*(5), 904–904. <http://doi.org/10.1242/dev.136143>
- Jara-Avaca, M., Kempf, H., Rückert, M., Robles-Diaz, D., Franke, A., de la Roche, J., ... Zweigerdt, R. (2017). EBIO Does Not Induce Cardiomyogenesis in Human Pluripotent Stem Cells but Modulates Cardiac Subtype Enrichment by Lineage-Selective Survival. *Stem Cell Reports*, *8*(2), 305–317. <http://doi.org/10.1016/j.stemcr.2016.12.012>
- Jarcho, J. A., Anas, A., Toutouzas, P., Hospital, H., & El-, E. (1998). The New England Journal of Medicine MUTATIONS IN THE GENE FOR CARDIAC MYOSIN-BINDING PROTEIN C.
- Jessup, M., Greenberg, B., Mancini, D., Cappola, T., Pauly, D. F., Jaski, B., ... Hajjar, R. J. (2011). Calcium upregulation by percutaneous administration of gene therapy in cardiac disease (CUPID): A phase 2 trial of intracoronary gene therapy of sarcoplasmic reticulum Ca<sup>2+</sup>-ATPase in patients with advanced heart failure. *Circulation*, *124*(3), 304–313. <http://doi.org/10.1161/CIRCULATIONAHA.111.022889>
- Jiang, J., Wakimoto, H., Seidman, J. G., & Seidman, C. E. (2013). Allele-specific silencing of mutant Myh6 transcripts in mice suppresses hypertrophic cardiomyopathy. *Science (New York, N.Y.)*, *342*(6154), 111–114. <http://doi.org/10.1126/science.1236921>
- Jinek, M., Chylinski, K., Fonfara, I., Hauer, M., Doudna, J. A., & Charpentier, E. (2012). A Programmable Dual-RNA – Guided, *337*(August), 816–822. <http://doi.org/10.1126/science.1225829>
- Johansen, A. K., Molenaar, B., Versteeg, D., Leitoguinho, A. R., Demkes, C., Spanjaard, B., ... van Rooij, E. (2017). Postnatal Cardiac Gene Editing Using CRISPR/Cas9 With AAV9-Mediated Delivery of Short Guide RNAs Results in Mosaic Gene Disruption. *Circulation Research*, *121*(10), 1168–1181. <http://doi.org/10.1161/CIRCRESAHA.116.310370>
- Kang, X., He, W., Huang, Y., Yu, Q., Chen, Y., Gao, X., ... Fan, Y. (2016). Introducing precise genetic modifications into human

- 3PN embryos by CRISPR/Cas-mediated genome editing. *Journal of Assisted Reproduction and Genetics*, 34(7), 963. <http://doi.org/10.1007/s10815-017-0946-y>
- Kattman, S. J., Witty, A. D., Gagliardi, M., Dubois, N. C., Niapour, M., Hotta, A., ... Keller, G. (2011). Stage-specific optimization of activin/nodal and BMP signaling promotes cardiac differentiation of mouse and human pluripotent stem cell lines. *Cell Stem Cell*, 8(2), 228–240. <http://doi.org/10.1016/j.stem.2010.12.008>
- Kawasaki H, Mizuseki K, Nishikawa S, Kaneko S, Kuwana Y, Nakanishi S, Nishikawa SI, S. Y. (2000). Induction of midbrain dopaminergic neurons from ES cells by stromal cell derived inducing activity. *Neuron*, 28(1), 31–40.
- Kawase, Y., Ly, H. Q., Prunier, F., Lebeche, D., Shi, Y., Jin, H., ... Hajjar, R. J. (2008). Reversal of Cardiac Dysfunction After Long-Term Expression of SERCA2a by Gene Transfer in a Pre-Clinical Model of Heart Failure. *Journal of the American College of Cardiology*, 51(11), 1112–1119. <http://doi.org/10.1016/j.jacc.2007.12.014>
- Kensah, G., Lara, A. R., Dahlmann, J., Zweigerdt, R., Schwanke, K., Hegermann, J., ... Martin, U. (2013). Murine and human pluripotent stem cell-derived cardiac bodies form contractile myocardial tissue in vitro. *European Heart Journal*, 34(15), 1134–1146. <http://doi.org/10.1093/eurheartj/ehs349>
- Kilpinen, H., Goncalves, A., Leha, A., Afzal, V., Alasoo, K., Ashford, S., ... Gaffney, D. J. (2017). Common genetic variation drives molecular heterogeneity in human iPSCs. *Nature*, 546(7658), 370–375. <http://doi.org/10.1038/nature22403>
- Kim, C., Wong, J., Wen, J., Wang, S., Wang, C., Spiering, S., ... Chen, H. S. V. (2013). Studying arrhythmogenic right ventricular dysplasia with patient-specific iPSCs. *Nature*, 494(7435), 105–110. <http://doi.org/10.1038/nature11799>
- Kim, K., Doi, A., Wen, B., Ng, K., Zhao, R., Cahan, P., ... Daley, G. Q. (2010). Epigenetic memory in induced pluripotent stem cells. *Nature*, 467(7313), 285–290. <http://doi.org/10.1038/nature09342>
- Kim, S., Kim, D., Cho, S. W., Kim, J., & Kim, J.-S. (2014). Highly efficient RNA-guided genome editing in human cells via delivery of purified Cas9 ribonucleoproteins. *Genome Research*, 24, 1012–1019. <http://doi.org/10.1101/gr.171322.113>
- Kooij, V., Holewinski, R. J., Murphy, A. M., & Van Eyk, J. E. (2013). Characterization of the cardiac myosin binding protein-C phosphoproteome in healthy and failing human hearts. *Journal of Molecular and Cellular Cardiology*, 60(1), 116–120. <http://doi.org/10.1016/j.yjmcc.2013.04.012>
- Kulikovskaya, I., McClellan, G., Flavigny, J., Carrier, L., & Winegrad, S. (2003). Effect of MyBP-C Binding to Actin on Contractility in Heart Muscle. *The Journal of General Physiology*, 122(6), 761–774. <http://doi.org/10.1085/jgp.200308941>
- Kuppusamy, K. T., Jones, D. C., Sperber, H., Madan, A., Fischer, K. A., Rodriguez, M. L., ... Ruohola-Baker, H. (2015). Let-7 family of microRNA is required for maturation and adult-like metabolism in stem cell-derived cardiomyocytes. *Proceedings of the National Academy of Sciences*, 112(21), 2785–2794. <http://doi.org/10.1073/pnas.1424042112>
- Laflamme, M. A., Chen, K. Y., Naumova, A. V., Muskheli, V., Fugate, J. A., Dupras, S. K., ... Murry, C. E. (2007). Cardiomyocytes derived from human embryonic stem cells in pro-survival factors enhance function of infarcted rat hearts. *Nature Biotechnology*, 25(9), 1015–1024. <http://doi.org/10.1038/nbt1327>
- Lahti, A. L., Kujala, V. J., Chapman, H., Koivisto, A.-P., Pekkanen-Mattila, M., Kerkelä, E., ... Aalto-Setälä, K. (2012). Model for long QT syndrome type 2 using human iPSCs demonstrates arrhythmogenic characteristics in cell culture. *Disease Models & Mechanisms*, 5(2), 220–30. <http://doi.org/10.1242/dmm.008409>
- Lamke, G. T., Allen, R. D., Edwards, W. D., Tazelaar, H. D., & Danielson, G. K. (2003). Surgical pathology of subaortic septal myectomy not associated with hypertrophic cardiomyopathy: A study of 98 cases (1996-2000). *Cardiovascular Pathology*, 12(4), 207–215. [http://doi.org/10.1016/S1054-8807\(03\)00057-7](http://doi.org/10.1016/S1054-8807(03)00057-7)
- Lan, F., Lee, A. S., Liang, P., Sanchez-Freire, V., Nguyen, P. K., Wang, L., ... Wu, J. C. (2013). Abnormal calcium handling properties underlie familial hypertrophic cardiomyopathy pathology in patient-specific induced pluripotent stem cells. *Cell Stem Cell*, 12(1), 101–113. <http://doi.org/10.1016/j.stem.2012.10.010>
- Lee, G., Papapetrou, E. P., Kim, H., Chambers, S. M., Tomishima, M. J., Fasano, C. a., ... Studer, L. (2009). Modelling pathogenesis and treatment of familial dysautonomia using patient-specific iPSCs. *Nature*, 461(7262), 402–6. <http://doi.org/10.1038/nature08320>
- Lee, P., Klos, M., Bollensdorff, C., Hou, L., Ewart, P., Kamp, T. J., ... Herron, T. J. (2012). Simultaneous voltage and calcium mapping of genetically purified human induced pluripotent stem cell-derived cardiac myocyte monolayers. *Circulation Research*, 110(12), 1556–1563. <http://doi.org/10.1161/CIRCRESAHA.111.262535>
- Lekanne Deprez, R. H., Muurling-Vlietman, J. J., Hruda, J., Baars, M. J. H., Wijnaendts, L. C. D., Stolte-Dijkstra, I., ... van Hagen, J. M. (2006). Two cases of severe neonatal hypertrophic cardiomyopathy caused by compound heterozygous mutations in the MYBPC3 gene. *Journal of Medical Genetics*, 43(10), 829–32. <http://doi.org/10.1136/jmg.2005.040329>
- Lemoine, M. D., Mannhardt, I., Breckwoldt, K., Prondzynski, M., Flenner, F., Ulmer, B., ... Christ, T. (2017). Human iPSC-derived cardiomyocytes cultured in 3D engineered heart tissue show physiological upstroke velocity and sodium current density. *Scientific Reports*, 7(1). <http://doi.org/10.1038/s41598-017-05600-w>
- Lewis, W. H., & Lewis, M. R. (1912). The cultivation of sympathetic nerves from the intestine of chick embryos in saline solutions. *The Anatomical Record*, 6(1), 7–31. <http://doi.org/10.1002/ar.1090060103>
- Liang, P., Xu, Y., Zhang, X., Ding, C., Huang, R., Zhang, Z., ... Huang, J. (2015). CRISPR/Cas9-mediated gene editing in human tripronuclear zygotes. *Protein and Cell*, 6(5), 363–372. <http://doi.org/10.1007/s13238-015-0153-5>
- Lim, D., Lutucuta, S., Bachireddy, P., Youker, K., Evans, A., Entman, M., ... Marian, A. J. (2001). Angiotensin II Blockade Reverses Myocardial Fibrosis in a Transgenic Mouse Model of Human Hypertrophic Cardiomyopathy. *Circulation*, 789–792. <http://doi.org/10.1161/01.CIR.103.6.789>

- Lin, S., Staahl, B., Alla, R. K., & Doudna, J. A. (2014). Enhanced homology-directed human genome engineering by controlled timing of CRISPR / Cas9 delivery. *ELife*, 1–32. <http://doi.org/10.7554/eLife.04766>
- Lodola, F., Morone, D., Denegri, M., Bongianino, R., Nakahama, H., Rutigliano, L., ... Di Pasquale, E. (2016). Adeno-associated virus-mediated CASQ2 delivery rescues phenotypic alterations in a patient-specific model of recessive catecholaminergic polymorphic ventricular tachycardia. *Cell Death and Disease*, 7(10), e2393-10. <http://doi.org/10.1038/cddis.2016.304>
- Long, C., Amoasii, L., Mireault, A. A., McAnally, J. R., Li, H., Sanchez-Ortiz, E., ... Olson, E. N. (2016). Postnatal genome editing partially restores dystrophin expression in a mouse model of muscular dystrophy. *Science*, 351(6271), 400–403. <http://doi.org/10.1126/science.aad5725>
- Lu, L., Timofeyev, V., Li, N., Rafizadeh, S., Singapur, A., Harris, T. R., & Chiamvimonvat, N. (2009). Alpha-actinin2 cytoskeletal protein is required for the functional membrane localization of a Ca<sup>2+</sup>-activated K<sup>+</sup> channel (SK2 channel). *Proceedings of the National Academy of Sciences of the United States of America*, 106(43), 18402–18407. <http://doi.org/10.1073/pnas.0908207106>
- Lundy, S. D., Zhu, W.-Z., Regnier, M., & Laflamme, M. A. (2013). Structural and Functional Maturation of Cardiomyocytes Derived From Human Pluripotent Stem Cells. *Stem Cells and Development*, 22, 1991–2002.
- Luther, P. K., Bennett, P. M., Knupp, C., Craig, R., Padrón, R., Harris, S. P., ... Moss, R. L. (2008). Understanding the Organisation and Role of Myosin Binding Protein C in Normal Striated Muscle by Comparison with MyBP-C Knockout Cardiac Muscle. *Journal of Molecular Biology*, 384(1), 60–72. <http://doi.org/10.1016/j.jmb.2008.09.013>
- Ma, H., Marti-Gutierrez, N., Park, S.-W., Wu, J., Lee, Y., Suzuki, K., ... Mitalipov, S. (2017). Correction of a pathogenic gene mutation in human embryos. *Nature*. <http://doi.org/10.1038/nature23305>
- Ma, J., Guo, L., Fiene, S. J., Anson, B. D., Thomson, J. A., Kamp, T. J., ... Ct, J. (2011). High purity human-induced pluripotent stem cell-derived cardiomyocytes: electrophysiological properties of action potentials and ionic currents. *Am J Physiol Heart Circ Physiol*, 301(5), 2006–2017. <http://doi.org/10.1152/ajpheart.00694.2011>.
- Mali, P., Yang, L., Esvelt, K. M., Aach, J., Guell, M., DiCarlo, J. E., ... Church, G. M. (2013). RNA-Guided Human Genome Engineering via Cas9. *Science*, 339(6121), 823–826. <http://doi.org/10.1126/science.1232033>
- Mannhardt, I., Breckwoldt, K., Letuffe-Brenière, D., Schaaf, S., Schulz, H., Neuber, C., ... Hansen, A. (2016). Human Engineered Heart Tissue: Analysis of Contractile Force. *Stem Cell Reports*, 7(1), 29–42. <http://doi.org/10.1016/j.stemcr.2016.04.011>
- Mannhardt, I., Eder, A., Dumotier, B., Prondzynski, M., Kr-amer, E., Traebert, M., ... Hansen, A. (2017). Blinded contractility analysis in hiPSC-cardiomyocytes in engineered heart tissue format: Comparison with human atrial trabeculae. *Toxicological Sciences*, 158(1), 164–175. <http://doi.org/10.1093/toxsci/kfx081>
- Marchetto, M. C. N., Yeo, G. W., Kainohana, O., Marsala, M., Gage, F. H., & Muotri, A. R. (2009). Transcriptional signature and memory retention of human-induced pluripotent stem cells. *PLoS ONE*, 4(9), 1–12. <http://doi.org/10.1371/journal.pone.0007076>
- Marian, A. J. (2002). Modifier genes for hypertrophic cardiomyopathy. *Current Opinion Cardiology*, 17(3), 242–252. <http://doi.org/10.1016/j.jneumeth.2010.08.011>. Autogenic
- Marian, A. J. (2009). Contemporary treatment of hypertrophic cardiomyopathy. *Texas Heart Institute Journal / from the Texas Heart Institute of St. Luke's Episcopal Hospital, Texas Children's Hospital*, 36(3), 194–204. Retrieved from <http://www.pubmedcentral.nih.gov/articlerender.fcgi?artid=2696493&tool=pmcentrez&rendertype=abstract>
- Marian, A. J. (2010). Hypertrophic cardiomyopathy: from genetics to treatment. *European Journal of Clinical Investigation*, 40(4), 360–369. <http://doi.org/10.1111/j.1365-2362.2010.02268.x>
- Maron, B. J. (2002). Hypertrophic Cardiomyopathy. *Circulation*, 106(19), 2419–2421. <http://doi.org/10.1161/01.CIR.0000034170.83171.0B>
- Maron, B. J. (2010). Contemporary insights and strategies for risk stratification and prevention of sudden death in hypertrophic cardiomyopathy. *Circulation*, 121(3), 445–456. <http://doi.org/10.1161/CIRCULATIONAHA.109.878579>
- Maron, B. J., Gardin, J. M., Flack, J. ., Gidding, S. S., Kurosaki, T. T., & Bild, D. E. (1995). Prevalance of Hypertrophic Cardiomyopathy in a General Population of Young Adults: Echocardiographic analysis of 4111 Subjects in the Cardia Study. *Circulation*, 92(4), 835–841. <http://doi.org/10.1161/01.CIR.92.4.835>
- Maron, B. J., & Maron, M. S. (2012). Hypertrophic cardiomyopathy, 6736(12).
- Maron, B. J., & Maron, M. S. (2013). Hypertrophic cardiomyopathy. *Lancet*, 381(9862), 242–55. [http://doi.org/10.1016/S0140-6736\(12\)60397-3](http://doi.org/10.1016/S0140-6736(12)60397-3)
- Maron, B. J., & Maron, M. S. (2013). Hypertrophic cardiomyopathy. *The Lancet*, 381(9862), 242–255. [http://doi.org/10.1016/S0140-6736\(12\)60397-3](http://doi.org/10.1016/S0140-6736(12)60397-3)
- Maron, B. J., Olivotto, I., Spirito, P., Casey, S. a., Bellone, P., Gohman, T. E., ... Cecchi, F. (2000). Epidemiology of Hypertrophic Cardiomyopathy-Related Death: Revisited in a Large Non-Referral-Based Patient Population. *Circulation*, 102(8), 858–864. <http://doi.org/10.1161/01.CIR.102.8.858>
- Maron, B. J., Shirani, J., Poliac, L., Tathenge, R., Roberts, W. C., & Mueller, F. O. (1996). Sudden Death in Young Competitive Athletes. *Jama*, 273(3), 199–204. <http://doi.org/10.1001/jama.1996.03540030033028>
- Maron, M. S., Olivotto, I., Zenovich, A. G., Link, M. S., Pandian, N. G., Kuvin, J. T., ... Maron, B. J. (2006). Hypertrophic cardiomyopathy is predominantly a disease of left ventricular outflow tract obstruction. *Circulation*, 114(21), 2232–2239. <http://doi.org/10.1161/CIRCULATIONAHA.106.644682>

- Marraffini, L. A. (2015). CRISPR-Cas immunity in prokaryotes. *Nature*, 526(7571), 55–61. <http://doi.org/10.1038/nature15386>
- Marston, S., Copeland, O., Gehmlich, K., Schlossarek, S., & Carrier, L. (2012). How do MYBPC3 mutations cause hypertrophic cardiomyopathy? *Journal of Muscle Research and Cell Motility*, 33(1), 75–80. <http://doi.org/10.1007/s10974-011-9268-3>
- Marston, S., Copeland, O., Jacques, A., Livesey, K., Tsang, V., McKenna, W. J., ... Watkins, H. (2009). Evidence from human myectomy samples that MYBPC3 mutations cause hypertrophic cardiomyopathy through haploinsufficiency. *Circulation Research*, 105(3), 219–22. <http://doi.org/10.1161/CIRCRESAHA.109.202440>
- Martin, F., Sánchez-Hernández, S., Gutiérrez-Guerrero, A., Pinedo-Gomez, J., & Benabdellah, K. (2016). Biased and unbiased methods for the detection of off-target cleavage by CRISPR/Cas9: An overview. *International Journal of Molecular Sciences*, 17(9). <http://doi.org/10.3390/ijms17091507>
- Martin, G. R. (1981). Isolation of a pluripotent cell line from early mouse embryos cultured in medium conditioned by teratocarcinoma stem cells. *Proceedings of the National Academy of Sciences*, 78(12), 7634–7638. <http://doi.org/10.1073/pnas.78.12.7634>
- Martonosi, A. N. (2000). Animal electricity, Ca<sup>2+</sup> and muscle contraction. A brief history of muscle research. *Acta Biochimica Polonica*, 47(3), 493–516.
- Maruoka, N. D., Steele, D. F., Au, B. P. Y., Dan, P., Zhang, X., Moore, E. D. W., & Fedida, D. (2000).  $\alpha$ -Actinin-2 couples to cardiac Kv1.5 channels, regulating current density and channel localization in HEK cells. *FEBS Letters*, 473(2), 188–194. [http://doi.org/10.1016/S0014-5793\(00\)01521-0](http://doi.org/10.1016/S0014-5793(00)01521-0)
- Maysnar, Y., Ben-David, U., Lavon, N., Biancotti, J.-C., Yakir, B., Clark, A. T., ... Benvenisty, N. (2010). Identification and Classification of Chromosomal Aberrations in Human Induced Pluripotent Stem Cells. *Cell Stem Cell*, 7(4), 521–531. <http://doi.org/10.1016/j.stem.2010.07.017>
- McLeod, C. J., Ackerman, M. J., Nishimura, R. A., Tajik, A. J., Gersh, B. J., & Ommen, S. R. (2009). Outcome of Patients With Hypertrophic Cardiomyopathy and a Normal Electrocardiogram. *Journal of the American College of Cardiology*, 54(3), 229–233. <http://doi.org/10.1016/j.jacc.2009.02.071>
- Mearini, G., Stimpel, D., Geertz, B., Weinberger, F., Krämer, E., Schlossarek, S., ... Carrier, L. (2014). Mybpc3 gene therapy for neonatal cardiomyopathy enables long-term disease prevention in mice. *Nature Communications*, 5(May), 1–10. <http://doi.org/10.1038/ncomms6515>
- Mearini, G., Stimpel, D., Krämer, E., Geertz, B., Braren, I., Gedicke-Hornung, C., ... Carrier, L. (2013). Repair of Mybpc3 mRNA by 5'-trans-splicing in a Mouse Model of Hypertrophic Cardiomyopathy. *Molecular Therapy. Nucleic Acids*, 2, 1–9. <http://doi.org/10.1038/mtna.2013.31>
- Mills, M., Yang, N., Weinberger, R. P., Vander Woude, D. L., Beggs, A. H., Easteal, S., & North, K. N. (2001). Differential expression of the actin-binding proteins,  $\alpha$ -actinin-2 and -3, in different species: implications for the evolution of functional redundancy. *Human Molecular Genetics*, 10(13), 1335–1346. <http://doi.org/10.1093/hmg/10.13.1335>
- Mohapatra, B., Jimenez, S., Lin, J. H., Bowles, K. R., Coveler, K. J., Marx, J. G., ... Bowles, N. E. (2003). Mutations in the muscle LIM protein and  $\alpha$ -actinin-2 genes in dilated cardiomyopathy and endocardial fibroelastosis. *Molecular Genetics and Metabolism*, 80(1–2), 207–215. [http://doi.org/10.1016/S1096-7192\(03\)00142-2](http://doi.org/10.1016/S1096-7192(03)00142-2)
- Monteiro da Rocha, A., Guerrero-Serna, G., Helms, A., Luzod, C., Mironov, S., Russell, M., ... Herron, T. J. (2016). Deficient cMyBP-C protein expression during cardiomyocyte differentiation underlies human hypertrophic cardiomyopathy cellular phenotypes in disease specific human ES cell derived cardiomyocytes. *Journal of Molecular and Cellular Cardiology*, 99, 197–206. <http://doi.org/10.1016/j.jmcc.2016.09.004>
- Moolman, J. C., Corfield, V. a, Posen, B., Ngumbela, K., Seidman, C., Brink, P. a, & Watkins, H. (1997). Sudden death due to troponin T mutations. *Journal of the American College of Cardiology*, 29(3), 549–55. Retrieved from <http://www.ncbi.nlm.nih.gov/pubmed/15466629>
- Mooren, F. C., Viereck, J., Kruger, K., & Thum, T. (2014). Circulating micromRNAs as potential biomarkers of aerobic exercise capacity. *AJP: Heart and Circulatory Physiology*, 306(4), 557–563. <http://doi.org/10.1152/ajpheart.00711.2013>
- Moretti, A., Bellin, M., Welling, A., Jung, C. B., Lam, J. T., Bott-Flügel, L., ... Laugwitz, K. (2010). Patient-specific induced pluripotent stem-cell models for long-QT-syndrom. *The New England Journal of Medicine*, 363(15), 1397–1409. <http://doi.org/10.1056/NEJMoa0908679>
- Moretti, A., Bellin, M., Welling, A., Jung, C., Lam, J., Bott-Flügel, L., ... Laugwitz, K. (2010). Patient-Specific Induced Pluripotent Stem-Cell Models for Long-QT Syndrome. *New England Journal of Medicine*, 363(15), 123–134. <http://doi.org/10.1056/NEJMoa1603827>
- Moss, R. L., Fitzsimons, D. P., & Ralphe, J. C. (2015). Cardiac MyBP-C regulates the rate and force of contraction in mammalian myocardium. *Circulation Research*, 116(1), 183–192. <http://doi.org/10.1161/CIRCRESAHA.116.300561>
- Mullis, K. B., & Faloona, F. (1987). Specific Synthesis of DNA in Vitro via a Polymerase-Catalyzed Chain Reaction. *Methods In Enzymology*, 155, 335–350.
- Mummery, C. L., Zhang, J., Ng, E. S., Elliott, D. A., Elefanty, A. G., & Kamp, T. J. (2012). Differentiation of human embryonic stem cells and induced pluripotent stem cells to cardiomyocytes: A methods overview. *Circulation Research*, 111(3), 344–358. <http://doi.org/10.1161/CIRCRESAHA.110.227512>
- Murakami, U., & Uchida, K. (1976). Cardiac Purification Myosin from Pig Heart Ventricle. *J. Biol. Chem.*, 80(3), 611–619.
- Murphy, A. C. H., & Young, P. W. (2015). The actinin family of actin cross-linking proteins – a genetic perspective. *Cell & Bioscience*, 5(1), 49. <http://doi.org/10.1186/s13578-015-0029-7>

- Murry, C. E., & Keller, G. (2008). Differentiation of Embryonic Stem Cells to Clinically Relevant Populations: Lessons from Embryonic Development. *Cell*, 132(4), 661–680. <http://doi.org/10.1016/j.cell.2008.02.008>
- Nagy, E., & Maquat, L. E. (1998). A rule for termination-codon position within intron-containing genes: When nonsense affects RNA abundance. *Trends in Biochemical Sciences*, 23(6), 198–199. [http://doi.org/10.1016/S0968-0004\(98\)01208-0](http://doi.org/10.1016/S0968-0004(98)01208-0)
- Nakano, T., Kodama, H., & Honjo, T. (1994). Generation of lymphohematopoietic cells from embryonic stem cells in culture. *Science*, 265(June), 1098–1101. <http://doi.org/10.1126/science.8066449>
- Nanni, L., Pieroni, M., Chimenti, C., Simionati, B., Zimbello, R., Maseri, A., ... Lanfranchi, G. (2003). Hypertrophic cardiomyopathy: Two homozygous cases with “typical” hypertrophic cardiomyopathy and three new mutations in cases with progression to dilated cardiomyopathy. *Biochemical and Biophysical Research Communications*, 309(2), 391–398. <http://doi.org/10.1016/j.bbrc.2003.08.014>
- Nerbonne, J. M. (2004). Studying cardiac arrhythmias in the mouse—a reasonable model for probing mechanisms? *Trends in Cardiovascular Medicine*, 14(3), 83–93. <http://doi.org/10.1016/j.tcm.2003.12.006>
- Niimura, H., Bachinski, L. L., Sangwatanaroj, S., Watkins, H., Chudley, A. E., McKenna, W., ... Seidman, C. E. (1998). Mutations in the Gene for Cardiac Myosin-Binding Protein C and late-onset Familial Hypertrophic Cardiomyopathy. *The New England Journal of Medicine*, 338(18), 1248–1257.
- Nishikawa, S. I., Nishikawa, S., Hirashima, M., Matsuyoshi, N., & Kodama, H. (1998). Progressive lineage analysis by cell sorting and culture identifies FLK1+VE-cadherin+ cells at a diverging point of endothelial and hemopoietic lineages. *Development (Cambridge, England)*, 125(9), 1747–1757.
- Obergrossberger, A., Bruggemann, A., Goetze, T. A., Rapedius, M., Haarmann, C., Rinke, I., ... Fertig, N. (2016). Automated Patch Clamp Meets High-Throughput Screening: 384 Cells Recorded in Parallel on a Planar Patch Clamp Module. *Journal of Laboratory Automation*, 21(6), 779–793. <http://doi.org/10.1177/2211068215623209>
- Offer, G., Moos, C., & Starr, R. (1973). A new protein of the thick filaments of vertebrate skeletal myofibrils. Extraction, purification and characterization. *Journal of Molecular Biology*, 74, 653–676.
- Ojala, M., Prajapati, C., Pölonen, R. P., Rajala, K., Pekkanen-Mattila, M., Rasku, J., ... Aalto-Setälä, K. (2016). Mutation-specific phenotypes in hiPSC-derived cardiomyocytes carrying either myosin-binding protein C or  $\alpha$ -tropomyosin mutation for hypertrophic cardiomyopathy. *Stem Cells International*, 1–16. <http://doi.org/10.1155/2016/1684792>
- Okabe, S., Forsberg-Nilsson, K., Spiro, A. C., Segal, M., & McKay, R. D. G. (1996). Development of neuronal precursor cells and functional postmitotic neurons from embryonic stem cells in vitro. *Mechanisms of Development*, 59(1), 89–102. [http://doi.org/10.1016/0925-4773\(96\)00572-2](http://doi.org/10.1016/0925-4773(96)00572-2)
- Olivotto, I., Cecchi, F., Casey, S. A., Dolara, A., Traverse, J. H., & Maron, B. J. (2001). Impact of atrial fibrillation on the clinical course of apical hypertrophic cardiomyopathy. *Circulation*, 104(21), 2517–2524. <http://doi.org/10.1136/heartjnl-2016-310720>
- Olivotto, I., Maron, M. S., Adabag, A. S., Casey, S. A., Vargiu, D., Link, M. S., ... Maron, B. J. (2005). Gender-related differences in the clinical presentation and outcome of hypertrophic cardiomyopathy. *Journal of the American College of Cardiology*, 46(3), 480–487. <http://doi.org/10.1016/j.jacc.2005.04.043>
- Palpant, N. J., Pabon, L., Friedman, C. E., Roberts, M., Hadland, B., Zaunbrecher, R. J., ... Murry, C. E. (2016). Generating high-purity cardiac and endothelial derivatives from patterned mesoderm using human pluripotent stem cells. *Nature Protocols*, 12(1), 15–31. <http://doi.org/10.1038/nprot.2016.153>
- Perales-Clemente, E., Cook, A. N., Evans, J. M., Roellinger, S., Secreto, F., Emmanuele, V., ... Nelson, T. J. (2016). Natural underlying mtDNA heteroplasmy as a potential source of intra-person hiPSC variability. *The EMBO Journal*, 1–12. <http://doi.org/10.15252/embj.201694892>
- Pioner, J. M., Racca, A. W., Klaiman, J. M., Yang, K.-C., Guan, X., Pabon, L., ... Regnier, M. (2016). Isolation and Mechanical Measurements of Myofibrils from Human Induced Pluripotent Stem Cell-Derived Cardiomyocytes. *Stem Cell Reports*, 6(6), 885–896. <http://doi.org/10.1016/j.stemcr.2016.04.006>
- Pohlmann, L., Kröger, I., Vignier, N., Schlossarek, S., Krämer, E., Coirault, C., ... Carrier, L. (2007). Cardiac myosin-binding protein C is required for complete relaxation in intact myocytes. *Circulation Research*, 101(9), 928–938. <http://doi.org/10.1161/CIRCRESAHA.107.158774>
- Polo, J. M., Liu, S., Figueroa, M. E., Kulalart, W., Eminli, S., Tan, K. Y., ... Hochedlinger, K. (2010). Cell type of origin influences the molecular and functional properties of mouse induced pluripotent stem cells. *Nature Biotechnology*, 28(8), 848–855. <http://doi.org/10.1038/nbt.1667>
- Ponikowski, P., Voors, A. A., Anker, S. D., Bueno, H., Cleland, J. G. F., Coats, A. J. S., ... Van Der Meer, P. (2016). 2016 ESC Guidelines for the diagnosis and treatment of acute and chronic heart failure. *European Heart Journal*, 37(27), 2129–2200. <http://doi.org/10.1093/eurheartj/ehw128>
- Probst, S., Oechslin, E., Schuler, P., Greutmann, M., Boye, P., Knirsch, W., ... Klaassen, S. (2011). Sarcomere gene mutations in isolated left ventricular noncompaction cardiomyopathy do not predict clinical phenotype. *Circulation: Cardiovascular Genetics*, 4, 367–374. <http://doi.org/10.1161/CIRCGENETICS.110.959270>
- Prondzynski, M., Krämer, E., Laufer, S. D., Shibamiya, A., Pless, O., Flenner, F., ... Carrier, L. (2017). Evaluation of MYBPC3 trans-Splicing and Gene Replacement as Therapeutic Options in Human iPSC-Derived Cardiomyocytes. *Molecular Therapy - Nucleic Acids*, 7, 475–486. <http://doi.org/10.1016/j.omtn.2017.05.008>
- Prondzynski, M., Krämer, E., Laufer, S. D., Shibamiya, A., Pless, O., Flenner, F., ... Carrier, L. (2017). Evaluation of MYBPC3 trans-Splicing and Gene Replacement as Therapeutic Options in Human iPSC-Derived Cardiomyocytes. *Molecular*

- Therapy: Nucleic Acid*, 7, 475–486. <http://doi.org/10.1016/j.omtn.2017.05.008>
- Puri, M. C., & Nagy, A. (2012). Concise review: Embryonic stem cells versus induced pluripotent stem cells: The game is on. *Stem Cells*, 30(1), 10–14. <http://doi.org/10.1002/stem.788>
- Ran, F. A., Hsu, P. D., Wright, J., Agarwala, V., Scott, D. A., & Zhang, F. (2013). Genome engineering using the CRISPR-Cas9 system. *Nature Protocols*, 8(11), 2281–2308. <http://doi.org/10.1038/nprot.2013.143>
- Raper, S. E., Chirmule, N., Lee, F. S., Wivel, N. A., Bagg, A., Gao, G., ... Batshaw, M. L. (2003). Fatal systemic inflammatory response syndrome in a ornithine transcarbamylase deficient patient following adenoviral gene transfer. *Molecular Genetics and Metabolism*, 80(1–2), 148–158.
- Ribeiro, E. D. A., Pinotsis, N., Ghisleni, A., Salmazo, A., Konarev, P. V., Kostan, J., ... Djinović-Carugo, K. (2014). The structure and regulation of human muscle  $\alpha$ -Actinin. *Cell*, 159(6), 1447–1460. <http://doi.org/10.1016/j.cell.2014.10.056>
- Ribeiro, M. C., Tertoolen, L. G., Guadix, J. A., Bellin, M., Kosmidis, G., D'Aniello, C., ... Passier, R. (2015). Functional maturation of human pluripotent stem cell derived cardiomyocytes invitro - Correlation between contraction force and electrophysiology. *Biomaterials*, 51, 138–150. <http://doi.org/10.1016/j.biomaterials.2015.01.067>
- Richard, P., Charron, P., Carrier, L., Ledeuil, C., Cheav, T., Pichereau, C., ... Komajda, M. (2003). Hypertrophic cardiomyopathy: distribution of disease genes, spectrum of mutations, and implications for a molecular diagnosis strategy. *Circulation*, 107(17), 2227–32. <http://doi.org/10.1161/01.CIR.0000066323.15244.54>
- Richard, P., Villard, E., Charron, P., & Isnard, R. (2006a). The Genetic Bases of Cardiomyopathies. *Journal of the American College of Cardiology*, 48(9), 79–89. <http://doi.org/10.1016/j.jacc.2006.09.014>
- Richard, P., Villard, E., Charron, P., & Isnard, R. (2006b). The Genetic Bases of Cardiomyopathies. *Journal of the American College of Cardiology*, 48(9), A79–A89. <http://doi.org/10.1016/j.jacc.2006.09.014>
- Riegler, J., Tiburcy, M., Ebert, A., Tzatzalos, E., Raaz, U., Abilez, O. J., ... Wu, J. C. (2015). Human Engineered Heart Muscles Engraft and Survive Long Term in a Rodent Myocardial Infarction Model. *Circulation Research*, 117(8), 720–730. <http://doi.org/10.1161/CIRCRESAHA.115.306985>
- Robinton, D. A., & Daley, G. Q. (2012). The promise of induced pluripotent stem cells in research and therapy. *Nature*, 481(7381), 295–305. <http://doi.org/10.1038/nature10761>
- Robson, R. M., Goll, D. E., Arakawa, N., & Stromer, M. H. (1970). Purification and Properties of Alpha-Actinin from Rabbit Skeletal Muscle. *Biochimica et Biophysica Acta*, 200, 296–318.
- Rust, M. J., Bates, M., & Zhuang, X. (2006). Sub-diffraction-limit imaging by stochastic optical reconstruction microscopy (STORM). *Nature Methods*, 3(10), 793–796. <http://doi.org/10.1038/nmeth929>
- Sadayappan, S., & De Tombe, P. P. (2014). Cardiac myosin binding protein-C as a central target of cardiac sarcomere signaling: A special mini review series. *Pflügers Archiv European Journal of Physiology*, 466(2), 195–200. <http://doi.org/10.1007/s00424-013-1396-8>
- Sadayappan, S., Gulick, J., Klevitsky, R., Lorenz, J. N., Sargent, M., Molkentin, J. D., & Robbins, J. (2009). Cardiac myosin binding protein-C phosphorylation in a beta-myosin heavy chain background. *Circulation*, 119(9), 1253–1262. <http://doi.org/10.1161/CIRCULATIONAHA.108.798983>
- Sadayappan, S., Gulick, J., Osinska, H., Martin, L. a, Hahn, H. S., Dorn, G. W., ... Robbins, J. (2005). Cardiac myosin-binding protein-C phosphorylation and cardiac function. *Circulation Research*, 97(11), 1156–63. <http://doi.org/10.1161/01.RES.0000190605.79013.4d>
- Sadayappan, S., Osinska, H., Klevitsky, R., Lorenz, J. N., Sargent, M., Molkentin, J. D., ... Robbins, J. (2006). Cardiac myosin binding protein C phosphorylation is cardioprotective. *Proceedings of the National Academy of Sciences of the United States of America*, 103(45), 16918–23. <http://doi.org/10.1073/pnas.0607069103>
- Sadeghi, A., Doyle, A. D., & Johnson, B. D. (2002). Regulation of the cardiac L-type Ca<sup>2+</sup> channel by the actin-binding proteins alpha -actinin and dystrophin. *AJP: Cell Physiology*, 282(6), 1502–1511. <http://doi.org/10.1152/ajpcell.00435.2001>
- Sakata, S., Lebeche, D., Sakata, N., Sakata, Y., Chemaly, E. R., Liang, L. F., ... Hajjar, R. J. (2007). Restoration of mechanical and energetic function in failing aortic-banded rat hearts by gene transfer of calcium cycling proteins. *Journal of Molecular and Cellular Cardiology*, 42(4), 852–861. <http://doi.org/10.1016/j.yjmcc.2007.01.003>
- Sala, L., Bellin, M., & Mummery, C. L. (2016). Integrating cardiomyocytes from human pluripotent stem cells in safety pharmacology: Has the time come? *British Journal of Pharmacology*, 174, 3749–3765. <http://doi.org/10.1111/bph.13577>
- Sander, J. D., & Joung, J. K. (2014). CRISPR-Cas systems for editing, regulating and targeting genomes. *Nature Biotechnology*, 32(4), 347–350. <http://doi.org/10.1038/nbt.2842>
- Sanger F, C. A. (1975). A Rapid Method for Determining Sequences in DNA by Primed Synthesis with DNA Polymerase. *Journal of Molecular Biology*, 94, 441–448.
- Schaaf, S., Shibamiya, A., Mewe, M., Eder, A., Stöhr, A., Hirt, M. N., ... Hansen, A. (2011). Human engineered heart tissue as a versatile tool in basic research and preclinical toxicology. *PLoS ONE*, 6(10), 1–11. <http://doi.org/10.1371/journal.pone.0026397>
- Schlossarek, S., Mearini, G., & Carrier, L. (2011). Cardiac myosin-binding protein C in hypertrophic cardiomyopathy: mechanisms and therapeutic opportunities. *Journal of Molecular and Cellular Cardiology*, 50(4), 613–620. <http://doi.org/10.1016/j.yjmcc.2011.01.014>
- Sequeira, V., Wijnker, P. J. M., Nijenkamp, L. L. A. M., Kuster, D. W. D., Najafi, A., Witjas-Paalberends, E. R., ... Van Der



- Velden, J. (2013). Perturbed length-dependent activation in human hypertrophic cardiomyopathy with missense sarcomeric gene mutations. *Circulation Research*, 112(11), 1491–1505. <http://doi.org/10.1161/CIRCRESAHA.111.300436>
- Shadrin, I. Y., Allen, B. W., Qian, Y., Jackman, C. P., Carlson, A. L., Juhas, M. E., & Bursac, N. (2017). Cardiopatch platform enables maturation and scale-up of human pluripotent stem cell-derived engineered heart tissues. *Nature Communications*, 8(1825), 1–15. <http://doi.org/10.1038/s41467-017-01946-x>
- Shadrin, I. Y., Khodabukus, A., & Bursac, N. (2016). Striated muscle function, regeneration, and repair. *Cellular and Molecular Life Sciences*, 73(22), 4175–4202. <http://doi.org/10.1007/s00018-016-2285-z>
- Shirani, J., Maron, B. J., Ili, R. C., Shahin, S., & Roberts, W. C. (1993). Clinicopathologic Features of Hypertrophic Cardiomyopathy Managed by Cardiac Transplantation. *The American Journal of Cardiology*, 72, 434–440.
- Sjöblom, B., Salmazo, A., & Djinić-Carugo, K. (2008).  $\alpha$ -Actinin structure and regulation. *Cellular and Molecular Life Sciences*, 65(17), 2688–2701. <http://doi.org/10.1007/s00018-008-8080-8>
- Spirito, P., Seidman, C. E., McKenna, W. J., & Maron, B. J. (1997). The Management of Hypertrophic Cardiomyopathy. *New England Journal of Medicine*, 336(11), 775–785.
- Stelzer, J. E., Patel, J. R., & Moss, R. L. (2006). Protein kinase A-mediated acceleration of the stretch activation response in murine skinned myocardium is eliminated by ablation of cMyBP-C. *Circulation Research*, 99(8), 884–890. <http://doi.org/10.1161/01.RES.0000245191.34690.66>
- Stillitano, F., Turnbull, I. C., Karakikes, I., Nonnenmacher, M., Backeris, P., Hulot, J. S., ... Costa, K. D. (2016). Genomic correction of familial cardiomyopathy in human engineered cardiac tissues. *European Heart Journal*, 37(43), 3282–3284. <http://doi.org/10.1093/eurheartj/ehw307>
- Stoehr, A., Neuber, C., Baldauf, C., Vollert, I., Friedrich, F. W., Flenner, F., ... Hansen, A. (2014). Automated analysis of contractile force and Ca<sup>2+</sup> transients in engineered heart tissue. *AJP: Heart and Circulatory Physiology*, 306(9), 1353–1363. <http://doi.org/10.1152/ajpheart.00705.2013>
- Stöhr, A., Friedrich, F. W., Flenner, F., Geertz, B., Eder, A., Schaaf, S., ... Eschenhagen, T. (2013). Contractile abnormalities and altered drug response in engineered heart tissue from Mybpc3-targeted knock-in mice. *Journal of Molecular and Cellular Cardiology*, 63, 189–198. <http://doi.org/10.1016/j.yjmcc.2013.07.011>
- Strande, J. L. (2015). Haploinsufficiency MYBPC3 mutations: Another stress induced cardiomyopathy? Let's take a look! *Journal of Molecular and Cellular Cardiology*, 79, 284–286. <http://doi.org/10.1016/j.yjmcc.2014.12.008>
- Sugden, P. H. (2003). An overview of endothelin signaling in the cardiac myocyte. *Journal of Molecular and Cellular Cardiology*, 35(8), 871–886. [http://doi.org/10.1016/S0022-2828\(03\)00153-6](http://doi.org/10.1016/S0022-2828(03)00153-6)
- Synergren, J., Ameen, C., Jansson, A., & Sartipy, P. (2012). Global transcriptional profiling reveals similarities and differences between human stem cell-derived cardiomyocyte clusters and heart tissue. *Physiological Genomics*, 44(4), 245–258. <http://doi.org/10.1152/physiolgenomics.00118.2011>
- Taapken, S. M., Nisler, B. S., Newton, M. A., Sampson-Barron, T. L., Leonhard, K. A., McIntire, E. M., & Montgomery, K. D. (2011). Karyotypic abnormalities in human induced pluripotent stem cells and embryonic stem cells. *Nature Biotechnology*, 29(4), 313–314. <http://doi.org/10.1038/nbt.1835>
- Takahashi, K., Tanabe, K., Ohnuki, M., Narita, M., Ichisaka, T., Tomoda, K., & Yamanaka, S. (2007). Induction of pluripotent stem cells from adult human fibroblasts by defined factors. *Cell*, 131(5), 861–72. <http://doi.org/10.1016/j.cell.2007.11.019>
- Takahashi, K., & Yamanaka, S. (2006). Induction of pluripotent stem cells from mouse embryonic and adult fibroblast cultures by defined factors. *Cell*, 126(4), 663–76. <http://doi.org/10.1016/j.cell.2006.07.024>
- Takeda, N., & Manabe, I. (2011). Cellular Interplay between Cardiomyocytes and Nonmyocytes in Cardiac Remodeling. *International Journal of Inflammation*, 2011, 1–13. <http://doi.org/10.4061/2011/535241>
- Tanaka, A., Yuasa, S., Mearini, G., Egashira, T., Seki, T., Kodaira, M., ... Fukuda, K. (2014). Endothelin-1 induces myofibrillar disarray and contractile vector variability in hypertrophic cardiomyopathy-induced pluripotent stem cell-derived cardiomyocytes. *Journal of the American Heart Association*, 3(6), 1–26. <http://doi.org/10.1161/JAHA.114.001263>
- Tang, L., Zeng, Y., Du, H., Gong, M., Peng, J., Zhang, B., ... Liu, J. (2017). CRISPR/Cas9-mediated gene editing in human zygotes using Cas9 protein. *Molecular Genetics and Genomics*, 292(3), 525–533. <http://doi.org/10.1007/s00438-017-1299-z>
- Tardiff, J. C., Carrier, L., Bers, D. M., Poggesi, C., Ferrantini, C., Coppini, R., ... Van Der Velden, J. (2015). Targets for therapy in sarcomeric cardiomyopathies. *Cardiovascular Research*, 105(4), 457–470. <http://doi.org/10.1093/cvr/cvv023>
- Teerlink, J. R., Clarke, C. P., Saikali, K. G., Lee, J. H., Chen, M. M., Escandon, R. D., ... Wolff, A. A. (2011). Dose-dependent augmentation of cardiac systolic function with the selective cardiac myosin activator, omecamtiv mecarbil: A first-in-man study. *The Lancet*, 378(9792), 667–675. [http://doi.org/10.1016/S0140-6736\(11\)61219-1](http://doi.org/10.1016/S0140-6736(11)61219-1)
- Theis, J. L., Martijn Bos, J., Bartleson, V. B., Will, M. L., Binder, J., Vatta, M., ... Ackerman, M. J. (2006). Echocardiographic-determined septal morphology in Z-disc hypertrophic cardiomyopathy. *Biochemical and Biophysical Research Communications*, 351(4), 896–902. <http://doi.org/10.1016/j.bbrc.2006.10.119>
- Thomson, J., Itskovitz-Eldor, J., Shapiro, S. S., Waknitz, M. A., Swiergiel, J. J., Marshall, V. S., & Jones, J. M. (1998). Embryonic Stem Cell Lines Derived from Human Blastocysts. *Science*, 282(5391), 1145–1147. Retrieved from <papers://4a4d46d0-94f3-46c5-8455-299f3d52958c/Paper/p6900>
- Tiburcy, M., Hudson, J. E., Balfanz, P., Schlick, S., Meyer, T., Chang Liao, M.-L., ... Zimmermann, W.-H. (2017). Defined

- Engineered Human Myocardium with Advanced Maturation for Applications in Heart Failure Modelling and Repair. *Circulation*, 135(6), 1–32. <http://doi.org/10.1161/CIRCULATIONAHA.116.024145>
- Trounson, A., & McDonald, C. (2015). Stem Cell Therapies in Clinical Trials: Progress and Challenges. *Cell Stem Cell*, 17(1), 11–22. <http://doi.org/10.1016/j.stem.2015.06.007>
- Tulloch, N. L., Muskheli, V., Razumova, M. V., Korte, F. S., Regnier, M., Hauch, K. D., ... Murry, C. E. (2011). Growth of engineered human myocardium with mechanical loading and vascular coculture. *Circulation Research*, 109(1), 47–59. <http://doi.org/10.1161/CIRCRESAHA.110.237206>
- Turnbull, I. C., Karakikes, I., Serrao, G. W., Backeris, P., Lee, J. J., Xie, C., ... Costa, K. D. (2014). Advancing functional engineered cardiac tissues toward a preclinical model of human myocardium. *FASEB Journal*, 28(2), 644–654. <http://doi.org/10.1096/fj.13-228007>
- Uesugi, M., Ojima, A., Taniguchi, T., Miyamoto, N., & Sawada, K. (2014). Low-density plating is sufficient to induce cardiac hypertrophy and electrical remodeling in highly purified human iPS cell-derived cardiomyocytes. *Journal of Pharmacological and Toxicological Methods*, 69(2), 177–188. <http://doi.org/10.1016/j.vascn.2013.11.002>
- Uzun, A. U., Mannhardt, I., Breckwoldt, K., Horváth, A., Johannsen, S. S., Hansen, A., ... Christ, T. (2016). Ca<sup>2+</sup>-currents in human induced pluripotent stem cell-derived cardiomyocytes effects of two different culture conditions. *Frontiers in Pharmacology*, 7(300), 1–14. <http://doi.org/10.3389/fphar.2016.00300>
- van den Berg, C. W., Okawa, S., Chuva de Sousa Lopes, S. M., van Iperen, L., Passier, R., Braam, S. R., ... Mummery, C. L. (2015). Transcriptome of human foetal heart compared with cardiomyocytes from pluripotent stem cells. *Development*, 142(18), 3231–3238. <http://doi.org/10.1242/dev.123810>
- van Dijk, S. J., Dooijes, D., dos Remedios, C., Michels, M., Lamers, J. M. J., Winegrad, S., ... van der Velden, J. (2009). Cardiac myosin-binding protein C mutations and hypertrophic cardiomyopathy: haploinsufficiency, deranged phosphorylation, and cardiomyocyte dysfunction. *Circulation*, 119(11), 1473–1483. <http://doi.org/10.1161/CIRCULATIONAHA.108.838672>
- Veerman, C. C., Kosmidis, G., Mummery, C. L., Casini, S., Verkerk, A. O., & Bellin, M. (2015). Immaturity of Human Stem-Cell-Derived Cardiomyocytes in Culture: Fatal Flaw or Soluble Problem? *Stem Cells and Development*, 24(9), 1035–1052. <http://doi.org/10.1089/scd.2014.0533>
- Vignier, N., Schlossarek, S., Fraysse, B., Mearini, G., Krämer, E., Pointu, H., ... Carrier, L. (2009). Nonsense-mediated mRNA decay and ubiquitin-proteasome system regulate cardiac myosin-binding protein C mutant levels in cardiomyopathic mice. *Circulation Research*, 105(3), 239–248. <http://doi.org/10.1161/CIRCRESAHA.109.201251>
- Wally, V., Murauer, E. M., & Bauer, J. W. (2012). Spliceosome-mediated trans-splicing: the therapeutic cut and paste. *The Journal of Investigative Dermatology*, 132(8), 1959–66. <http://doi.org/10.1038/jid.2012.101>
- Wang, G., McCain, M. L., Yang, L., He, A., Pasqualini, F. S., Agarwal, A., ... Pu, W. T. (2014). Modeling the mitochondrial cardiomyopathy of Barth syndrome with induced pluripotent stem cell and heart-on-chip technologies. *Nature Medicine*, 20(6), 616–623. <http://doi.org/10.1038/nm.3545>
- Wang, L., Kryshnal, D. O., Kim, K., Parikh, S., Cadar, A. G., Bersell, K. R., ... Knollmann, B. C. (2017). Myofilament Calcium-Buffering Dependent Action Potential Triangulation in Human-Induced Pluripotent Stem Cell Model of Hypertrophic Cardiomyopathy. *Journal of the American College of Cardiology*, 70(20), 2600–2602. <http://doi.org/10.1016/j.jacc.2017.09.033>
- Wasserman, W. W., Palumbo, M., Thompson, W., Fickett, J. W., & Lawrence, C. E. (2000). Human-mouse genome comparisons to locate regulatory sites. *Nature Genetics*, 26(2), 225–228. <http://doi.org/10.1038/79965>
- Watkins, H., Ashrafian, B. M., & Redwood, C. (2011). Inherited cardiomyopathies. *New England Journal of Medicine*, 364(17), 2347–2356. <http://doi.org/DN/JST.JSTAGE/circj/CJ-14-0893> [pii]
- Watkins, H., Conner, D., Thierfelder, L., Jarcho, J. A., MacRae, C., McKenna, W. J., ... Seidman, C. E. (1995). Mutations in the cardiac myosin binding protein-C gene on chromosome 11 cause familial hypertrophic cardiomyopathy. *Nature Medicine*, 11, 434–437.
- Watson, J. D., & Crick, F. H. (1953). The structure of DNA. *Cold Spring Harbor Symposia on Quantitative Biology*, 18, 123–131. <http://doi.org/10.1101/SQB.1953.018.01.020>
- Weinberger, F., Breckwoldt, K., Pecha, S., Kelly, A., Geertz, B., Starbatty, J., ... Eschenhagen, T. (2016). Cardiac repair in guinea pigs with human engineered heart tissue from induced pluripotent stem cells. *Science Translational Medicine*, 8(363), 1–12. <http://doi.org/10.1126/scitranslmed.aaf8781>
- Weins, A., Schlondorff, J. S., Nakamura, F., Denker, B. M., Hartwig, J. H., Stossel, T. P., & Pollak, M. R. (2007). Disease-associated mutant alpha-actinin-4 reveals a mechanism for regulating its F-actin-binding affinity. *Proceedings of the National Academy of Sciences of the United States of America*, 104(41), 16080–16085. <http://doi.org/10.1073/pnas.0702451104>
- Werfel, S., Jungmann, A., Lehmann, L., Ksienzyk, J., Bekerredjian, R., Kaya, Z., ... Cancer, G. (2014). Rapid and highly efficient inducible cardiac gene knockout in adult mice using AAV-mediated expression of Cre recombinase. *Cardiovascular Research*, 104(1), 15–23.
- Wessels, M. W., Herkert, J. C., Frohn-Mulder, I. M., Dalinghaus, M., van den Wijngaard, A., de Krijger, R. R., ... Dooijes, D. (2015). Compound heterozygous or homozygous truncating MYBPC3 mutations cause lethal cardiomyopathy with features of noncompaction and septal defects. *European Journal of Human Genetics*, 23(7), 922–928. <http://doi.org/10.1038/ejhg.2014.211>

- Wijnker, P. J. M., Friedrich, F. W., Dutsch, A., Reischmann, S., Eder, A., Mannhardt, I., ... Carrier, L. (2016). Comparison of the effects of a truncating and a missense MYBPC3 mutation on contractile parameters of engineered heart tissue. *Journal of Molecular and Cellular Cardiology*, *97*, 82–92. <http://doi.org/10.1016/j.yjmcc.2016.03.003>
- Willig, K. I., Harke, B., Medda, R., & Hell, S. W. (2007). STED microscopy with continuous wave beams. *Nature Methods*, *4*(11), 915–918. <http://doi.org/10.1038/nmeth1108>
- Winegrad, S. (1999). Cardiac Myosin Binding Protein C. *Circulation Research*, *84*(10), 1117–1126. <http://doi.org/10.1161/01.RES.84.10.1117>
- Witjas-Paalberends, E. R., Ferrara, C., Scellini, B., Piroddi, N., Montag, J., Tesi, C., ... van der Velden, J. (2014). Faster cross-bridge detachment and increased tension cost in human hypertrophic cardiomyopathy with the R403Q MYH7 mutation. *The Journal of Physiology*, *592*(15), 3257–3272. <http://doi.org/10.1113/jphysiol.2014.274571>
- Witjas-Paalberends, E. R., Güclü, A., Germans, T., Knaapen, P., Harms, H. J., Vermeer, A. M. C., ... Van Der Velden, J. (2014). Gene-specific increase in the energetic cost of contraction in hypertrophic cardiomyopathy caused by thick filament mutations. *Cardiovascular Research*, *103*(2), 248–257. <http://doi.org/10.1093/cvr/cvu127>
- Witjas-Paalberends, E. R., Piroddi, N., Stam, K., Van Dijk, S. J., Oliviera, V. S., Ferrara, C., ... Van Der Velden, J. (2013). Mutations in MYH7 reduce the force generating capacity of sarcomeres in human familial hypertrophic cardiomyopathy. *Cardiovascular Research*, *99*(3), 432–441. <http://doi.org/10.1093/cvr/cvt119>
- Witty, A. D., Mihic, A., Tam, R. Y., Fisher, S. A., Mikryukov, A., Shoichet, M. S., ... Keller, G. (2014). Generation of the epicardial lineage from human pluripotent stem cells. *Nature Biotechnology*, *32*(10), 1026–1035. <http://doi.org/10.1038/nbt.3002>
- Wu, Y., Liang, D., Wang, Y., Bai, M., Tang, W., Bao, S., ... Li, J. (2013). Correction of a genetic disease in mouse via use of CRISPR-Cas9. *Cell Stem Cell*, *13*(6), 659–662. <http://doi.org/10.1016/j.stem.2013.10.016>
- Xie, C., Zhang, Y. P., Song, L., Luo, J., Qi, W., Hu, J., ... Yan, Y. (2016). Genome editing with CRISPR/Cas9 in postnatal mice corrects PRKAG2 cardiac syndrome. *Cell Research*, *26*(10), 1099–1111. <http://doi.org/10.1038/cr.2016.101>
- Xin, B., Puffenberger, E., Tumbush, J., Bockoven, J. R., & Wang, H. (2007). Homozygosity for a Novel Splice Site Mutation in the Cardiac Myosin-Binding Protein C Gene Causes Severe Neonatal Hypertrophic Cardiomyopathy. *American Journal of Medical Genetics*, *143*(18), 2106–2112. <http://doi.org/10.1002/ajmg.a>
- Yamamoto, K., & Moos, C. (1983). The C-proteins of rabbit red, white, and cardiac muscles. *Journal of Biological Chemistry*, *258*(13), 8395–8401.
- Yang, Q., Sanbe, A., Osinska, H., Hewett, T., Klevitsky, R., & Robbins, J. (1998). A Mouse Model of Myosin Binding Protein C Human Familial Hypertrophic Cardiomyopathy. *Journal of Clinical Investigation*, *102*(7), 1292–1300.
- Young, P., & Gautel, M. (2000). The interaction of titin and alpha-actinin is controlled by a phospholipid-regulated intramolecular pseudoligand mechanism. *The EMBO Journal*, *19*(23), 6331–40. <http://doi.org/10.1093/emboj/19.23.6331>
- Yu, M., Selvaraj, S. K., Liang-Chu, M. M. Y., Aghajani, S., Busse, M., Yuan, J., ... Neve, R. M. (2015). A resource for cell line authentication, annotation and quality control. *Nature*, *520*(7547), 307–311. <http://doi.org/10.1038/nature14397>
- Zaragoza, C., Gomez-Guerrero, C., Martin-Ventura, J. L., Blanco-Colio, L., Lavin, B., Mallavia, B., ... Egido, J. (2011). Animal Models of Cardiovascular Diseases. *Journal of Biomedicine and Biotechnology*, *2011*, 1–13. <http://doi.org/10.1155/2011/497841>
- Zhang, D., Shadrin, I. Y., Lam, J., Xian, H. Q., Snodgrass, H. R., & Bursac, N. (2013). Tissue-engineered cardiac patch for advanced functional maturation of human ESC-derived cardiomyocytes. *Biomaterials*, *34*(23), 5813–5820. <http://doi.org/10.1016/j.biomaterials.2013.04.026>
- Zhang, X., Azhar, G., Chai, J., Sheridan, P., Nagano, K., Brown, T., ... Wei, J. Y. (2001). Cardiomyopathy in transgenic mice with cardiac-specific overexpression of serum response factor. *Am J Physiol Heart Circ Physiol*, *280*(4), 1782–1792.
- Ziane, R., Huang, H., Moghadaszadeh, B., Beggs, A. H., Levesque, G., & Chahine, M. (2010). Cell membrane expression of cardiac sodium channel Nav1.5 is modulated by  $\alpha$ -actinin-2 interaction. *Biochemistry*, *49*(1), 166–178. <http://doi.org/10.1021/bi901086v>
- Zsebo, K., Yaroshinsky, A., Rudy, J. J., Wagner, K., Greenberg, B., Jessup, M., & Hajjar, R. J. (2014). Long-term effects of AAV1/SERCA2a gene transfer in patients with severe heart failure: Analysis of recurrent cardiovascular events and mortality. *Circulation Research*, *114*(1), 101–108. <http://doi.org/10.1161/CIRCRESAHA.113.302421>

## 7. Appendix

### 7.1 Materials

#### 7.1.1 Antibodies

##### 7.1.1.1 Antibodies used for immunofluorescence staining

Investigated protein	Primary Antibody	Company	Dilution	Secondary Antibody	Company	Dilution
$\alpha$ -Actinin 2	Clone EA-53; monoclonal	Sigma	1:800	anti-mouse IgG, Alexa Fluor-488	Molecular Probes	1:800

#### 7.1.2 Bacterial strains

Bacterial strain	Manufacturer
One Shot® TOP10 Chemically Competent <i>E. coli</i>	Invitrogen

#### 7.1.3 Chemicals

Product	Manufacturer
Ampicilline trihydrate	Serva
Accutase	Gibco
Dulbecco's modified Eagle medium (DMEM)	Biochrom
Fetal calf serum	Biochrom
Geltrex™ LDEV-Free	Gibco
Histofix®	Roth
Hoechst 33342	Thermo Scientific
Insulin	Sigma
Milk powder	Roth
Matrigel	Corning
Penicillin/streptomycin	Gibco
Phosphate buffered saline (PBS)	Biochrom
Triton X-100	Sigma

#### 7.1.4 Consumable materials

Product	Manufacturer
Culture plates (24-well)	Nunc
Culture plates (96-well micro-clear bottom)	Greiner

#### 7.1.5 Kits

Kit	Manufacturer
CloneJET PCR Cloning Kit	ThermoFisher Scientific
Primary Cell 4D-Nucleofector® X Kit	Lonza

### 7.1.6 Laboratory equipment

Product	Manufacturer
Confocal microscope (LSM800, Airyscan) with a 40x-oil objective	Zeiss
Amaya Nucleofector™	Lonza
FACSAria™ III	BD Bioscience

### 7.1.7 Enzymes

Restriction enzyme with supplied buffer	Manufacturer
AmpliTaq Gold® DNA Polymerase	Applied Biosystems
PrimeStar® HS DNA Polymerase	Clontech

### 7.1.8 Oligonucleotides

*ACTN2* primers were designed according to the NCBI gene accession number NG\_009081.1. All primers were designed using SnapGene and purchased from the MWG Biotech AG.

#### 7.1.8.1 *ACTN2* primer sequences for PCR and sequencing

Primers	Sequence (5' to 3')
Forward	GGCCCATGAAACACAGAAAT
Reverse	AGGGCCATTCTTCCTCAAGG

#### 7.1.8.2 Off-target primer sequences for PCR and sequencing

Primers	Forward (5' to 3')	Reverse (5' to 3')
NG_029480	ggggtgatggtgttcttg	ggcaggaggacatggttg
NM_016642	ctttgcttctggtggct	gtctcctctggacagtctgc
NG_013304	ggaagagaagacactgggct	gactgagtgtgtgcagctgg
NG_029938	ccaaggttcagagaagggc	cccggaagatgatggtgtct
NM_000827	ttgtttgatcccacagcaa	ggtctccatctgctccagtt
NG_009061	agggtgcttgagttgatcct	tgttggtggcagtgga
NM_025268	ccgcagaagatgatgctgta	ggctgcagctccagtgatag
NC_018924	ttctgggtcaagccatcct	aagctcactgaaaggaaaggt
NC_018930	cttccagtcagagcaagtg	cagtcaaatacccagctctgc
NC_018931	tcagtttctacggccactgt	tgaaacctctctctgccgt
NC_018919	agtgggtgctgcagagtaa	acaggtgtgagccatgtacc
NC_018916	tctgcactgtgtaggtcatgt	tgatgagaaaacgggaggca
NC_018929	gcaagggcatccacgaatagt	gctatttggggcactttggt

### 7.1.8.3 Sequence of the ssODN repair template

---

ssODN	Sequence (5' to 3')
Repair template	ACCCACACTGCCACCTTGCCTGCCCCCTGACCAGTCTCTCCA TGGGGTAGCCAACAGCAGGGCGTGACATGTGGGTGGGGTGTG CAGCAGGTCCTAGCACTTGGCTGGTTCCACACA

## 7.2 List of abbreviations

°C	Degree Celsius	EHT	Engineered heart tissue
µg	Micrograms	ESC	Embryonic stem cell
µL	Microliter	e.g.	<i>Exempli gratia</i> (for example)
µm	Micrometer	et al.	<i>Et alii</i> (and others)
µM	Micromolar	FACS	Fluorescence-activated cell sorting
2D	Two-dimensional	FCS	Fetal calf serum
3D	Three-dimensional	Fig.	Figure
<b>ACTN2</b>	α-Actinin 2	FTDA	bFGF, TGFβ1, dorsomorphin and activin A based hiPSC medium
<b>Anova</b>	Analysis of variance	g	gram
<b>AON</b>	Antisense oligonucleotide	gRNA	Guide RNA
<b>AP</b>	Action potential	HBSS	Hank's Balanced Salt Solution
<b>APD</b>	Action potential duration	HCM	Hypertrophic cardiomyopathy
<b>ATP</b>	Adenosine 5'-triphosphate	HDR	Homology-directed repair
<b>BB</b>	Backbone	hESC	Human embryonic stem cell
<b>bFGF</b>	Basic fibroblast growth factor	hiPSC	Human induced pluripotent stem cell
<b>BMP4</b>	Bone-morphogenetic protein 4	hiPSC-CM	Human iPSC-derived cardiac myocyte
<b>bp</b>	Base pairs	Hz	Hertz
<b>β-MHC</b>	Beta-myosin heavy chain	i.e.	<i>Id est</i> (that is)
<b>cAMP</b>	Ca <sup>2+</sup> /calmodulin-dependent protein kinase II	iPSC	Induced pluripotent stem cell
<b>CM</b>	Cardiac myocyte	iPSC-CM	Human iPSC-derived cardiac myocyte
<b>cMyBP-C</b>	Cardiac myosin-binding protein C (Protein)	kb	Kilobase
<b>Cas</b>	CRISPR-associated protein	kDa	Kilodalton
<b>Cas9n</b>	CRISPR-associated protein 9 nickase	KI	Knock-in
<b>CASQ2</b>	Calsequestrin 2	KO	Knock-out
<b>cDNA</b>	Complementary deoxyribonucleic acid	LTCC	Long lasting-type calcium channel
<b>EB</b>	Embryoid body	LV	Left ventricle
<b>CM</b>	Cardiomyocyte	M	Molar
<b>cm</b>	Centimeter	min	Minutes
<b>CRISPR</b>	Clustered Regularly Interspaced Short Palindromic Repeats	MOI	Multiplicity of infection
<b>cTNC</b>	Cardiac troponin C	mRNA	Messenger ribonucleic acid
<b>cTNI</b>	Cardiac troponin I	mm	Millimeter
<b>cTNT</b>	Cardiac troponin T	mM	Millimolar
<b>d</b>	days	<b>MYBPC3</b>	Cardiac myosin-binding protein C (Gene)
<b>DCM</b>	Dilated Cardiomyopathy	<b>MYH7</b>	Beta (β)-myosin heavy chain
<b>DMEM</b>	Dulbecco's modified Eagle medium	<b>NaOH</b>	Sodium hydroxide
<b>DNA</b>	Deoxyribonucleic acid	<b>NCBI</b>	National Center for Biotechnology Information
<b>DSB</b>	Double strand break	<b>NCX</b>	Sodium-calcium exchanger
<b>ECC</b>	Excitation-contraction coupling	<b>NHEJ</b>	Non-homologous end joining
<b>ECG</b>	Electrocardiograph	<b>ns</b>	not significant
<b>EDTA</b>	Ethylendiaminetetraacetic acid	<b>nt</b>	Nucleotide

<b>PAM</b>	Protospacer adjacent motif
<b>PBS</b>	Phosphate-buffered saline
<b>PCR</b>	Polymerase chain reaction
<b>PTC</b>	Premature termination codon
<b>PLN</b>	Phospholamban
<b>RNA</b>	Ribonucleic acid
<b>ROS</b>	Reactive oxygen species
<b>RYR2</b>	Ryanodin receptor 2
<b>sec</b>	Seconds
<b>SEM</b>	Standard error of mean
<b>SERCA2a</b>	Sarcoplasmic-endoplasmatic reticulum calcium ATPase 2a
<b>sgRNA</b>	Single guide RNA
<b>SNP</b>	Single nucleotide polymorphism
<b>ssODN</b>	Single-stranded donor oligonucleotide
<b>T1</b>	Contraction time
<b>T2</b>	Relaxation time
<b>TAE</b>	Tris acetate EDTA
<b>Talen</b>	Transcription activator-like effector nucleases
<b>TBS</b>	Tris buffered saline
<b>TBS-T</b>	Tris buffered saline with Tween 20
<b>TGF-<math>\beta</math></b>	Transforming growth factor- $\beta$
<b>TNNT2</b>	Titin (Gene)
<b>TRIS</b>	tris-(hydroxymethyl)-aminoethane
<b>V</b>	Volt
<b>vs.</b>	Versus
<b>WT</b>	Wild-type



## Abstract

Induced pluripotent stem cells (iPSCs) and their ability to differentiate into any kind of cell offers an exceptional human disease model as patient-derived iPSC lines can be generated with disease-relevant mutations. This constitutes a unique chance in understanding molecular pathophysiology and for evaluation of new therapeutic options in genetic diseases, such as Hypertrophic cardiomyopathy (HCM). HCM is an autosomal-dominant disease, characterized by myocardial disarray, left ventricular hypertrophy and diastolic dysfunction. Molecular links between genetics and clinical outcome are still elusive and no curative treatment is available up to date. Therefore the aim of this study was to evaluate human iPSC-derived cardiomyocytes (hiPSC-CMs) as a tool to model HCM and for assessment of *trans*-splicing, gene replacement (GR) and CRISPR/Cas9 genome editing as molecular-based interventions. Three different iPSC lines were provided: one control cell line derived from a healthy individual and two cell lines derived from HCM patients identified with novel mutations in the *MYBPC3* (c.1358dupC; p.Val454CysFsX21) or the *ACTN2* (c.740C>T; p.Thr247Met) gene at the heterozygous state. For generation of hiPSC-CMs a new differentiation protocol was developed, which is embryoid body-based, cost-effective and generates high purity of hiPSC-CMs. This protocol was successfully applied to all investigated cell lines in this thesis. *MYBPC3* mutant hiPSC-CMs showed higher mRNA levels of proteins associated with hypertrophy, lower mRNA levels of proteins involved in calcium handling, haploinsufficiency and larger cell size, all hallmarks of HCM. Additionally, successful *trans*-splicing was observed using control hiPSC-CMs, although with low efficiency. Treatment with GR using the full-length *MYBPC3* cDNA resulted in 2.5-fold higher *MYBPC3* mRNA levels in *MYBPC3* mutant hiPSC-CMs and control hiPSC-CMs. This restored the cMyBP-C level to 81% of the control level, suppressed hypertrophy, and partially restored gene expression to control level in HCM cells. CRISPR/Cas9 genome editing was used for the generation of an isogenic control cell line repairing the *ACTN2* mutation. Evaluation of the *ACTN2* mutant hiPSC-CMs revealed 1.8-fold higher cell areas in 2D and a significantly higher force and prolongation time in engineered heart tissues (EHT), when compared to isogenic control hiPSC-CMs. This work provides evidence for successful disease modeling of HCM and the application of molecular-based interventions in hiPSC-CMs.

## Zusammenfassung

Induziert pluripotente Stammzellen (iPSC) und ihre Fähigkeit in alle Zellarten zu differenzieren ermöglicht eine neue Art und Weise humane Krankheiten zu modellieren. Dies eröffnet die Chance neue Einblicke in pathophysiologische Mechanismen zu gewinnen und neue Therapien in genetischen Krankheiten, wie der Hypertrophen Kardiomyopathie (HCM), zu testen. HCM ist eine autosomal dominant vererbte Krankheit, welche durch die chaotische Orientierung von Kardiomyozyten (CMs), einer Verdickung der linken Herzkammer und einer diastolischen Dysfunktion charakterisiert ist. Bis heute sind die molekularen Mechanismen zwischen genetischer Grundlage und klinischem Ausgang in der HCM nicht klar. Zusätzlich wurde noch keine heilende Therapie beschrieben. Deshalb war das Ziel dieser Arbeit mit CMs aus human induziert pluripotenten Stammzellen (hiPSC-CMs) HCM zu modellieren und Gentherapie zu testen. Dafür wurden drei Zelllinien zur Verfügung gestellt: Eine Kontrollzelllinie, von einem gesunden Individuum und zwei Zelllinien von Patienten die mit HCM diagnostiziert wurden, aufgrund jeweils einer Mutation im *MYBPC3* Gen (c.1358dupC; p.Val454CysFsX21) und im *ACTN2* Gen (c.740C>T; p.Thr247Met). Für die Herstellung von hiPSC-CMs wurde ein neues Differenzierungsprotokoll entwickelt, welches auf der Formation von Embryoid-Körpern basiert, preiswert ist und hohe Reinheiten an hiPSC-CMs aufweist. Dieses Protokoll wurde erfolgreich für alle in dieser Arbeit untersuchten Zelllinien verwendet. Die *MYBPC3* mutierten hiPSC-CMs zeigten ein verändertes Genexpression-Profil (GP), Haploinsuffizienz und erhöhte Zellgrößen, alles Kennzeichen der HCM. Zusätzlich wurde erfolgreich *Trans*-Splicing in den Kontroll (Ktl) hiPSC-CMs getestet, jedoch mit einer geringen Effizienz. Behandlung mit GR unter der Verwendung der vollständigen *MYBPC3* Sequenz resultierte in 2,5-fach höheren *MYBPC3* Transkripten und das cMyBP-C Level wurde wieder auf 81% der Ktl gehoben, Hypertrophy unterdrückt und teilweise wurde das GP wieder dem der Ktl angepasst. CRISPR/Cas9 wurde verwendet um die vorliegende *ACTN2* Mutation zu reparieren und somit eine isogene Ktl-Zelllinie herzustellen. Untersuchung von *ACTN2* mutierten hiPSC-CMs zeigte 1,8-fach erhöhte Zellgrößen in 2D und eine signifikant höhere Kraft und Relaxationszeit in künstlich hergestelltem Herzgewebe im Vergleich zur isogenen Ktl-Zelllinie. Diese Arbeit liefert Beweise für das erfolgreiche modellieren der HCM und die Anwendung von neuen Therapien in hiPSC-CMs.

## Acknowledgments

As already implied in the beginning science is a journey, as was my PhD. In this part I would like to acknowledge everybody who contributed to my understanding of science and gave me the possibility to do research under their supervision.

I would like first to thank Prof. Dr. Lucie Carrier, who listened and argued about theories and scientific findings that I brought into our lab meetings, trusted my judgement, and created a safe environment for exchanging ideas.

Thanks to Prof. Dr. Carrier and Prof. Dr. Eschenhagen, with whom I felt supported in my decisions as a scientist and most importantly in fulfilling my dreams in respect to high-end technology equipment.

I would also like to thank Prof. Dr. Thomas Dobner for the revision of my thesis.

I would like to thank the AG Carrier, including Dr. Giulia Mearini, Dr. Saskia Schlossarek, Dr. Felix Friedrich, Dr. Frederik Flenner, Dr. Sonia Singh, Dr. Doreen Stimpel, Birgit Geertz, Silke Reischmann-Düsener for their support, as the many students I got to know that kept me entertained and lifted my spirit.

A very important thanks goes to Elisabeth Krämer, with whom I shared all my ups and downs and who became a close friend to me.

I also want to thank Antonia Zech for her support, organizational skills and overall having my back. Our common projects are inspiring, fascinating and scientifically challenging. I am happy to share this with her.

A tremendous work effort was and still is accomplished by everybody, who is involved in the cardiac differentiation and the HEXT iPS core facility. Therefore, I would like to thank Arne Hansen, Anika Knaust, Marta Lemme, Mirja Schulze, Ingra Mannhardt, Thomas Schulze, Tessa Werner, Birgit Klampe, Bärbel Ulmer, Umber Saleem, Pierre Bobin, Marina Reinsch, Sandra Laufer, Christine Neuber and Aya Shibamiya.

For scientific inspiration, I want to thank Prof. Dr. Frederike Cuello, Dr. Ingke Braren, Dr. Torsten Christ, and most importantly Dr. Marc Lemoine. Discussions with Marc were always very fruitful, and sometimes, it was more challenging to convince him of my theories than I expected. Probably, he is still not convinced.

Special thanks goes to Steven Schulz and Bernado Dolce for spending time on other topics than science, whereby we also talked a lot about science.

I also would like to thank Anna Steenpaß, Agnez Diaz, Jutta Starbatty for spending time with me apart from the lab inspiring me to travel, eat and visit cultural events.

I would also like to thank the Fraunhofer ScreeningPort including Dr. Philip Gribbon, Dr. Carsten Claussen, Oliver Keminer and Dr. Ole Pless for supporting me on my path with counsel and scientific expertise. A very special role goes to Dr. Pless. He laid the foundation for my scientific understanding and perception, and left me with a skill- and mindset ready to analyze and understand science and more.

Finally, I would like to thank the most important women in my life starting with Sue Lopes. She helped me through this journey with visual contribution to all my scientific endeavors, an unbelievable enthusiasm for science and her presence in my life. In a way, she does research with my heart; therefore, I hope that our journey will continue together. Moreover, I want to thank my grandmother. She taught me how to respect and cherish nature and how to look for the beauty within details that are often hidden from us. Finally, I want to thank my mum, who helped me to become who I am now. Without her I would have not written this thesis.

This work was supported by Deutsches Zentrum für Herz-Kreislauf-Forschung (DZHK, Standort Hamburg/Kiel/Lübeck).

# English language certification



Fraunhofer IME-SP | Schnackenburgallee 114 | 22525 Hamburg

Fraunhofer-Institut für Molekularbiologie  
und Angewandte Oekologie IME

Institutsleiter  
Prof. Dr. Dr. Gerd Geisslinger  
(geschäftsführend)  
Prof. Dr. Stefan Schillberg  
Prof. Dr. Christoph Schäfers

Abteilung ScreeningPort  
Leitung Prof. Dr. Carsten Claussen

Dr. Philip Gribbon  
Assistant Head of Department  
Durchwahl +49 40 303764-271  
Philip.gribbon@ime.fraunhofer.de

Hamburg, 18<sup>th</sup> December 2017

## English language thesis certification

To whom it may concern:

Mr Kamill Maksymilian Prondzynski is submitting his thesis entitled "Modeling of hypertrophic cardiomyopathy and assessment of gene therapy in human iPSC-derived cardiomyocytes" in English. As a native speaker and experienced drug discovery scientist, I have reviewed the thesis for the quality of the English used in expressing the scientific concepts and findings therein. I am happy to confirm that the thesis reaches an appropriate standard of English for submission.

Yours sincerely,

A handwritten signature in black ink, appearing to read 'Philip Gribbon'.

Dr Philip Gribbon,

Fraunhofer IME ScreeningPort,

Coordinator of EU-OPENSREEN (the European Infrastructure for Chemical Biology)

Fraunhofer-Gesellschaft zur Förderung der angewandten Forschung e. V., München  
Vorstand  
Prof. Dr.-Ing. habil. Prof. E. h. Dr.-Ing. E. h. mult. Dr. h. c. mult. Reimund Neugebauer, Präsident  
Prof. (Univ. Stellenbosch) Dr. rer. pol. Alfred Gossner  
Prof. Dr. rer. publ. ass. iur. Alexander Kurz  
Prof. Dr. rer. nat. Georg Rosenfeld

Bankverbindung Deutsche Bank, München  
Konto 752193300 BLZ 700 700 10  
IBAN DE86 7007 0010 0752 1933 00  
BIC (SWIFT-Code) DEUTDEMM  
UST-IdNr. DE129515865  
Steuernummer 143/215/20392

## Authorship contribution



Universitätsklinikum  
Hamburg-Eppendorf

Department of Experimental  
Pharmacology and Toxicology

Lucie Carrier, Ph.D.

Prof. Dr.

Director of Research CNRS

Team Leader

Martinistraße 52

20246 Hamburg

Germany

Phone: +49-40-7410-57208

Fax: +49-40-7410-55925

Email: l.carrier@uke.de

Universitätsklinikum Hamburg-Eppendorf Martinistraße 52 20246 Hamburg

September 27, 2018

## Authorship contribution

To whom it may concern:

Mr. Kamill Maksymilian Prondzynski is submitting his cumulative dissertation with the title “Modeling of hypertrophic cardiomyopathy and assessment of gene therapy in human iPSC-derived cardiomyocytes”.

Hereby I confirm his participation in the manuscript entitled “Evaluation of *MYBPC3* *trans*-splicing and gene replacement as therapeutic options in human iPSC-derived cardiomyocytes”. Mr. Kamill Maksymilian Prondzynski was involved in conceptualization, methodology, investigation, formal analysis, visualization, project administration and writing of the original manuscript and response to reviewers.

Mit freundlichen Grüßen,

Frau Prof. Carrier



Universitätsklinikum  
Hamburg-Eppendorf

Universitätsklinikum  
Hamburg-Eppendorf  
Institut für Experimentelle  
Pharmakologie und Toxikologie  
Haus N30  
Martinistraße 52  
20246 Hamburg  
Gebäude N30

Prof. Dr. Arne Hansen  
Telefon: +49 (0) 40 7410-57207  
ar.hansen@uke.de  
www.uke.de

### **Authorship contribution**

September 27, 2018

#### **To whom it may concern:**

Mr. Kamill Maksymilian Prondzynski is submitting his cumulative dissertation with the title “Modeling of hypertrophic cardiomyopathy and assessment of gene therapy in human iPSC-derived cardiomyocytes”.

Hereby I confirm his participation in the manuscript entitled “Differentiation of cardiomyocytes and generation of human engineered heart tissue”. Mr. Kamill Maksymilian Prondzynski was involved in the development and validation of the protocol.

Mit freundlichen Grüßen,

Prof. Dr. Arne Hansen

## **Eidesstattliche Erklärung**

Hiermit bestätige ich, Kamill Maksymilian Prondzynski, dass die vorliegende Arbeit von mir selbständig verfasst wurde und ich keine anderen als die angegebenen Hilfsmittel – insbesondere keine im Quellenverzeichnis nicht benannten Internet-Quellen – benutzt habe und die Arbeit von mir vorher nicht in einem anderen Prüfungsverfahren eingereicht wurde.

Hamburg, den 21. Dezember 2017

---

Kamill Maksymilian Prondzynski



